2011

Delivery accuracy of image guided radiation therapy using Elekta Infinity's on-board imaging

Matthew William Sutton
Louisiana State University and Agricultural and Mechanical College, mws5003@gmail.com

DELIVERY ACCURACY OF IMAGE GUIDED RADIATION THERAPY USING ELEKTA INFINITY'S ON-BOARD IMAGING

A Thesis

Submitted to the Graduate Faculty of the
Louisiana State University and
Agricultural and Mechanical College
in partial fulfillment of the
requirements for the degree of
Master of Science

in

The Department of Physics and Astronomy

by
Matthew William Sutton
B.S., Pennsylvania State University, 2008
August 2011

ACKNOWLEDGMENT

I thank my committee chair, Kip Matthews, for his help throughout the entire research process and in preparation of this thesis. I also thank James Payne, Elekta Field Service Engineer, and the therapists at Mary Bird Perkins Cancer Center for assisting me with the use and operation of the Elekta system during the research. I thank Frank Apollo, MBPCC dosimetrist, who aided me with treatment planning for my project. Additionally I thank my supervisory committee: Kenneth Hogstrom, Brent Parker, Polad Shikhaliev, Maurice King, and Shane Stadler for their time, knowledge, and assistance on this project. This research was supported by a research grant from Elekta Inc. to Mary Bird Perkins Cancer Center; LSU providedg assistantships for my first two years in graduate school. Finally, I thank my family and friends for their support and perspective to help keep me focused throughout graduate school.

TABLE OF CONTENTS

LIST OF TABLES

LIST OF FIGURES

ABSTRACT

Purpose: Using the technique developed by Vinci *et al.* (2007), this project quantified the accuracy and precision of the Elekta Infinity using an end-to-end test for the entire image guided radiation therapy (IGRT) treatment process. The IGRT capabilities of the on-board imaging systems for megavoltage (MV) planar imaging and kilovoltage cone beam computed tomography (kVCBCT) were both evaluated. The accuracy of the on-board imaging systems will impact the size of planning treatment margins.

Method and Materials: A CIRS radiosurgery head phantom with a Gafchromic EBT^2 film dosimetry block insert was used to measure the dose distributions in the three orthogonal planes. A coplanar, isocentric, seven-field treatment plan was created for a cylindrical target volume located at the center of the film cube. The phantom was manually positioned on the treatment couch, either correctly aligned to the room lasers or with intentional misalignments of ±5 mm in three directions of couch motion. Prior to treatment, one of the IGRT modalities was utilized to identify misalignment; the calculated realignment values were used to shift the phantom prior to treatment delivery. After treatment, the delivered dose distributions were analyzed and compared to the calculated planar dose distributions. Two metrics were analyzed from the film: positional alignment error of the 70% isodose line and comparison of spatial shifts of the 80% dose points. Positional alignment error quantified displacement between the midpoints of the measured and calculated dose profiles; shifts at the 80% dose points indicated distortions in the profiles.

Results and Conclusions: Investigation of the accuracy of the couch motion revealed a systematic 1 mm error at fixed locations along the longitudinal axis. Using a non-invasive immobilization device and on-board image guidance, setup margins on the Elekta Infinity should be set to 2 mm using kVCBCT and 3 mm using MV planar imaging. To use the Elekta Infinity

for high precision deliveries with minimal planning target volumes would require tighter tolerances in couch motion; a couch with rotational as well as translational motion seems advisable. For high precision deliveries, image guidance using kVCBCT is recommended over MV planar image guidance.

CHAPTER 1. INTRODUCTION

1.1 International Committee on Radiation Units and Measurements

The International Committee on Radiation Units and Measurements (ICRU) provides guidelines and recommendations on a variety of topics relevant to working with radiation. ICRU Reports 50 and 62 provide specific information for guiding radiation treatments. These recommendations suggest various volume definitions for use in planning radiation treatments. It is important that clear, well-defined, and unambiguous concepts and parameters are used for reporting purposes to ensure a common language between different cancer centers around the world. ICRU Report 62 provides recommendations on the volumes and absorbed doses that are important in prescribing, recording, and reporting photon beam therapy.

Figure 1.1 illustrates the volume definitions defined by ICRU 62. The primary volume that is first created during treatment planning is the gross tumor volume (GTV). The GTV is defined as the gross palpable or visible/demonstrable extent and location of the malignant growth (Wambersie and Landberg, 1999). The GTV is the physical manifestation of what can be seen via computed tomography (CT), magnetic resonance imaging (MRI) and angiography.

Surrounding the GTV, the ICRU defined the clinical target volume (CTV). The CTV contains the GTV as well as any subclinical microscopic malignant disease, which needs to be eliminated (Wambersie and Landberg, 1999). The subclinical involvement margin may contain tissue adjacent to the GTV that is believed to contain undetected microscopic cancer cells. The CTV may also encompass any lymph nodes in the region about the GTV.

The internal target volume (ITV) contains the CTV and includes a margin to account for physiological patient movements that cannot be accommodated or eliminated during treatment. The margin used for creating an ITV is known as the internal margin. The internal margins

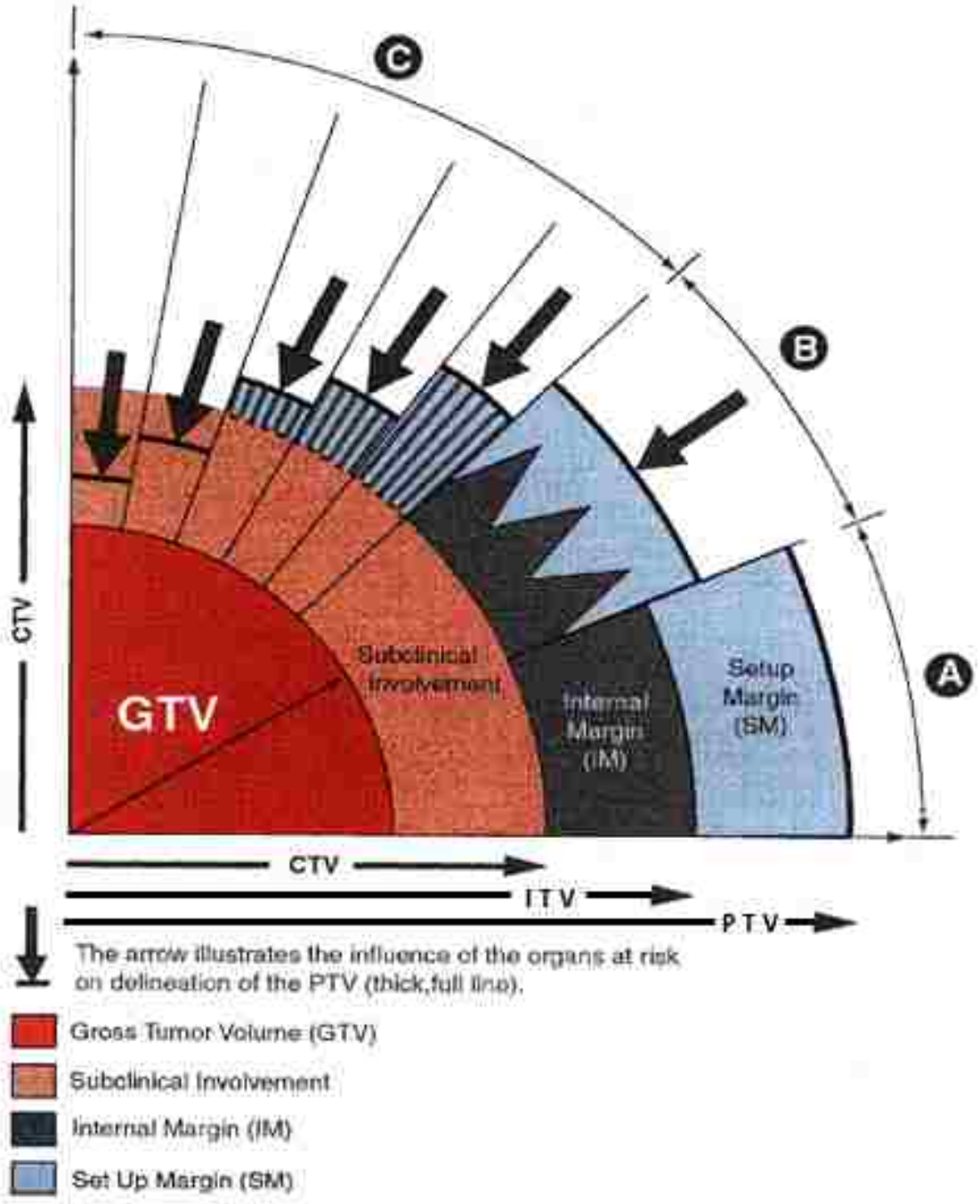

Figure 1.1: Target volume definitions defined by ICRU 62 (from Wambersie and Landberg, 1999). The areas in red (GTV) and orange (CTV) represent the cancerous volume that requires treatment. To treat 100% of these areas, one creates internal margins (dark grey) and setup margins (blue) in the healthy adjacent tissue. Setting internal and setup margins consequently requires irradiating healthy adjacent tissue.

compensate for expected physiologic movements and variations in size, shape, and position of the CTV during therapy. These physiologic motions can occur when the CTV position changes on a day-to-day basis and is mainly associated with organs that are part of or adjacent to the respiratory or digestive system. Changes in the patient's condition, such as weight gain or loss, can also affect the relative position of the CTV.

The volume that surrounds the ITV is the planning target volume (PTV). The PTV is an expansion from the ITV that is necessary to account for external treatment inaccuracies (Wambersie and Landberg, 1999). The margin used to create a PTV is known as the setup margin, and it considers the net effect of all variations and inaccuracies to ensure that the prescribed dose is actually absorbed throughout the ITV. The setup margin accounts for any uncertainties related to patient positioning, for mechanical uncertainties of the equipment, and for dosimetric uncertainties.

1.2 Image Guided Radiation Therapy

Image guided radiation therapy (IGRT) procedures use imaging technology to identify and correct errors arising from inter- and intra-fractional variations in patient setup and anatomy. IGRT is used to verify the location, shapes, and volumes of treatment targets, organs at risk, and surrounding normal tissues. IGRT can be used at various stages of the radiation therapy process including patient data acquisition, treatment planning, treatment simulation, patient setup, and target localization. Modern treatment techniques such as 3D conformal radiotherapy (3D-CRT) and intensity modulated radiotherapy (IMRT) conform the dose distribution to complex PTV shapes. Consequently, the accuracy requirements of PTV localization and its dosimetric coverage during treatment become increasingly demanding. These requirements have propelled advances in the area of dynamic targeting of PTVs and visualization of surrounding anatomy

before and during treatments (Letourneau *et al.*, 2007; Letourneau *et al.*, 2009; Rowbottom and Jaffray, 2004; Webster *et al.*, 2009).

Until recently this past decade, image guidance typically was achieved using megavoltage (MV) x-ray portal films, but now is typically achieved using both MV and kilovoltage (kV) x-ray imaging systems. IGRT modalities can be divided into two groups: planar image-based and CT-based. The imaging systems can be physically separate from the linac or can be mounted directly on the gantry; the latter are known as on-board imagers (OBIs).

1.2.1 Planar Image-Based IGRT

Two types of planar imaging systems are available for use with modern linacs: (a) a kV x-ray imager consisting of a conventional x-ray tube(s) with an opposing flat-panel detector(s) and (b) an MV imager consisting of a flat-panel detector and the linac's MV x-ray source. The flat panel detectors in these systems are frequently called electronic imaging devices (EIDs). Since kV x-rays attenuate in matter more than MV x-rays, kV imaging provides higher contrast than MV imaging. The MV and kV imagers can either be gantry-mounted (e.g. Varian Trilogy, Elekta Synergy, and Siemens ONCOR) or positioned independent of the gantry (e.g. BrainLab Novalis ExacTrac system). Prior to treatment, planar images are acquired and compared to digitally reconstructed radiographs (DRR) generated from the planning CT scan by the treatment planning system. From this comparison, misalignment of the patient's anatomy parallel to the image plane is identified; however, misalignment perpendicular to the image plane cannot be identified from a single image. Using images from two or more perspectives (e.g. orthogonal), misalignments can be identified in 3D and the patient's position is shifted in 3D to match the planned setup. Another drawback of planar images is the superposition of anatomy in the projection images, potentially obscuring shifts of the anatomy of interest.

1.2.2 CT-Based IGRT

CT provides tomographic 3D image data, without the confounding superposition of anatomy found with planar images. CT images also typically provide better spatial resolution. An in-room CT scanner makes it feasible to obtain CT images directly prior to each treatment; the CT scanner and the linac typically share a common patient bed so that the patient does not move between imaging and treatment. As with planar imaging systems, the CT system can be stand-alone or mounted on the linac gantry. Examples of gantry-mounted CT-based IGRT systems include cone-beam MVCT (Siemens), cone-beam kVCT (Varian Trilogy, Elekta Infinity, Siemens ARTISTE) and serial fan beam MVCT (Tomotherapy). An example of a stand-alone CT is CT Vision which has a CT on rails (Siemens).

Previously mentioned, some linacs are able to acquire kilovoltage cone-beam computed tomographies (kVCBCT). KVCBCT utilizes the same flat panel imagers that are used to acquire kV planar images. As the gantry rotates, planar projection images from multiple directions are acquired by the flat panel detector. Three-dimensional volumetric images are reconstructed from these multiple radiographs, which utilizes a filtered back-projection algorithm. Due to the geometry of kVCBCT imaging, the radiation beam in kVCBCT is conical in shape (Figure 1.2) with a beam size limited by the size of the EID; as a consequence, some peripheral anatomy might not be present in the field for all gantry angles. This makes kVCBCT typically adequate for head and neck regions but inadequate for the pelvis or other regions that are larger than the x-ray beam (Khan, 2010)

The quality of cone-beam CT reconstructed images can suffer from poor contrast, mis-registration, and artifacts. These problems arise from gravity-induced flex in the support arms of the x-ray tube and detector, sagging and slipping of the accelerator gantry during rotation, and the combined effects of beam hardening and x-ray scatter. Center of rotation corrections on the

order of 2 mm are required to compensate for gravity-induced flex of the support arm and gantry (Jaffray *et al.*, 2002). Beam hardening and x-ray scatter cause inaccurate CT numbers, contrast reduction, and cupping artifacts. These effects are minimized by algorithmic corrections in the reconstruction software. Scatter can be reduced by using antiscatter grids (Khan, 2010).

With proper corrections, it is possible to obtain cone-beam images with good contrast and sub-millimeter spatial resolution. The typical resolution employed in the clinical implementation of kVCBCT is about 1 mm voxel size at isocenter. Because kV x-rays are used, the images show reasonably good soft-tissue contrast, which is helpful in delineating the gross tumor volume (GTV). Due to the relatively low energy range of the photons, a single kVCBCT scan contributes approximately 1.5 cGy to the center of the patient (Khan, 2010).

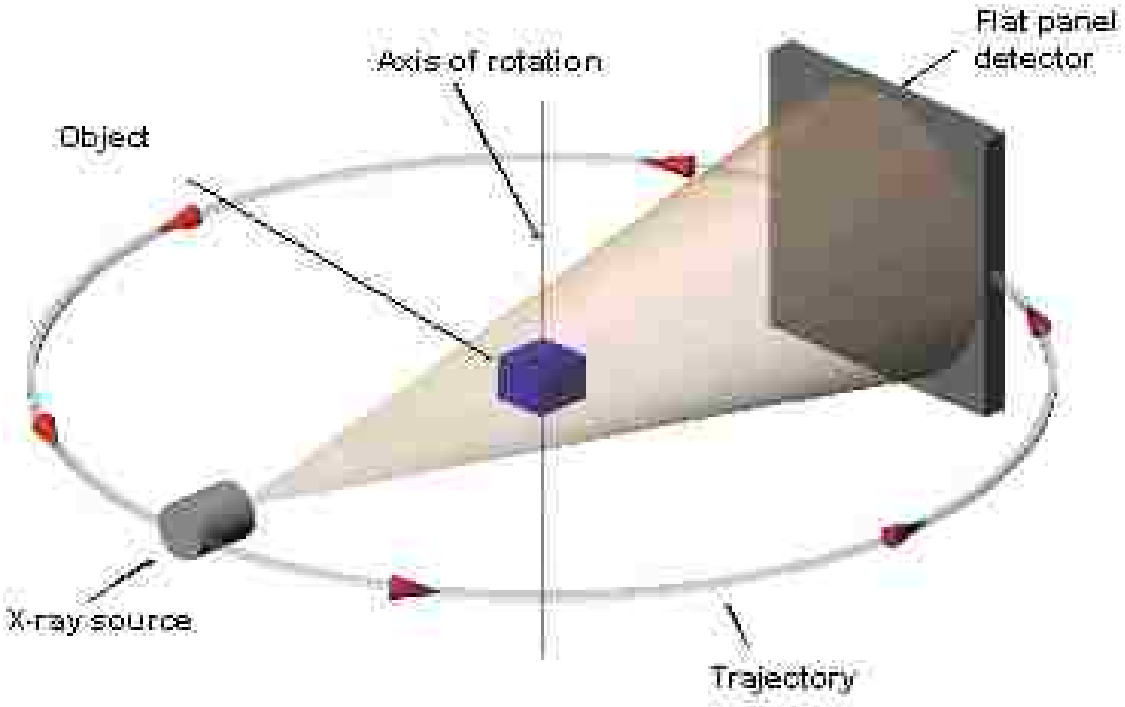

Figure 1.2: Sketch of the process of Cone Beam Computed Tomography (Simon and Sauerwein, 2000). A conical beam from an x-ray source penetrates the object. The transmitted radiation is measured by the flat panel detector. The x-ray source and flat panel detector are simultaneously rotated around the object to measure a set of projections. The 3D structure of the object is reconstructed from the projections.

1.3 Elekta Infinity

The Elekta Infinity system is equipped with both a kV x-ray imager and a MV imager (Elekta, 2006), as shown in Figure 1.3. These OBIs allow the user to know the location of the patient anatomy in space in relation to the linac isocenter. Both systems use flat panel image detectors; the MV imager uses the linac's MV x-ray beam while the kV imager uses a gantry-mounted kV x-ray tube.

Figure 1.3: Photograph of the Elekta Infinity system with (a) the MV x-ray beam source (linac head), (b) the kV x-ray source, (c) the MV flat panel detector, and (d) the kV flat panel detector.

The EIDs on the Elekta Infinity each consists of a matrix of 256x256 solid state amorphous silicon photodiodes. Both flat panels are 425 x 425 mm^2 but only have an active

imaging region of 409.6 x 409.6 mm^2. Radiation absorbed by the detector induces a charge that is integrated over the image acquisition time. The photodiode matrix is connected to readout electronics that measure the accumulated charge from each diode. Because the signal in each photodiode is proportional to the energy deposited by the radiation, the signal can be represented as pixel gray scale values to generate an image.

Although kV planar images have better contrast than MV planar images from the EIDs, neither has sufficiently good quality to visualize soft-tissue targets in their entirety. However, the OBIs are useful in determining the planned target position in relation to bony landmarks and/or radio-opaque markers (fiducials) implanted in the target tissues. In addition, the kV imager on the Elekta Infinity can be used in both radiographic and fluoroscopic modes to check patient setup before each treatment or to track the movement of fiducial markers due to respiratory motion. The MV imager can provide portal verification before each treatment as well as on-line monitoring of target position during treatment delivery.

The kV OBI of the Elekta Infinity is also capable of cone-beam CT (kVCBCT). The kV OBI is mounted at 90 degrees with respect to the central axis of the linear accelerator beam and shares the same isocenter as the linac as the gantry rotates. The kV OBI system can be retracted after use so as not to interfere with treatment delivery. Image acquisition with the kV OBI as the gantry rotates provides the CT image data. By using a small field of view setting to acquire kVCBCT, one can obtain a field size of 276.7 x 276.7 mm^2 with a pixel resolution of 1.08 mm.

1.3.1 Daily QA of the IG Systems on the Elekta Infinity

At Mary Bird Perkins Cancer Center, radiation therapists are responsible for the daily warm-up and accelerator quality assurance, including the coincidence of the MV planar imaging

and kVCBCT systems. The IG systems on the Elekta Infinity are monitored using a Penta-Guide cube phantom (Quasar, London, ON), shown in Figure 1.4.

This phantom is marked with crosshairs that are aligned with the room lasers. Next, the linac is set up to perform a kVCBCT on the Penta-Guide cube phantom. Once the kVCBCT has been acquired, auto image registration using Grey-value is used to register the kVCBCT of the cube with its original CT (Figure 1.5)

Figure 1.4: Image of the Penta-Guide phantom placed on the Elekta Infinity treatment couch. The phantom is initially setup to the crosshairs that are offset from the center of the cube.

The position error should be 1.0 ± 2.0 mm in the lateral, -1.4 ± 2.0 mm in the longitudinal, and -1.2 ± 2.0 mm in the vertical directions. The 2 mm uncertainties are a result of the inherent accuracy of positioning the treatment couch. The phantom's misalignment is then corrected for using the automated couch adjustments. The kVCBCT is repeated to determine

any residual error. The residual error for all three axes should be ≤ 1 mm. The results are indicated in the Morning Warm-Up Log Book.

Without moving the phantom, the gantry is set to 0 degrees, and a MV port film is acquired with the aid of a graticule (Figure 1.6). In this image of the phantom projection, each sphere should be in the center of its corresponding ring. Also, the central axis BB on the port film graticule should be in the center of the central axis sphere. This process is repeated using a gantry position of 270 degrees. The results are indicated in the Morning Warm-Up Log Book.

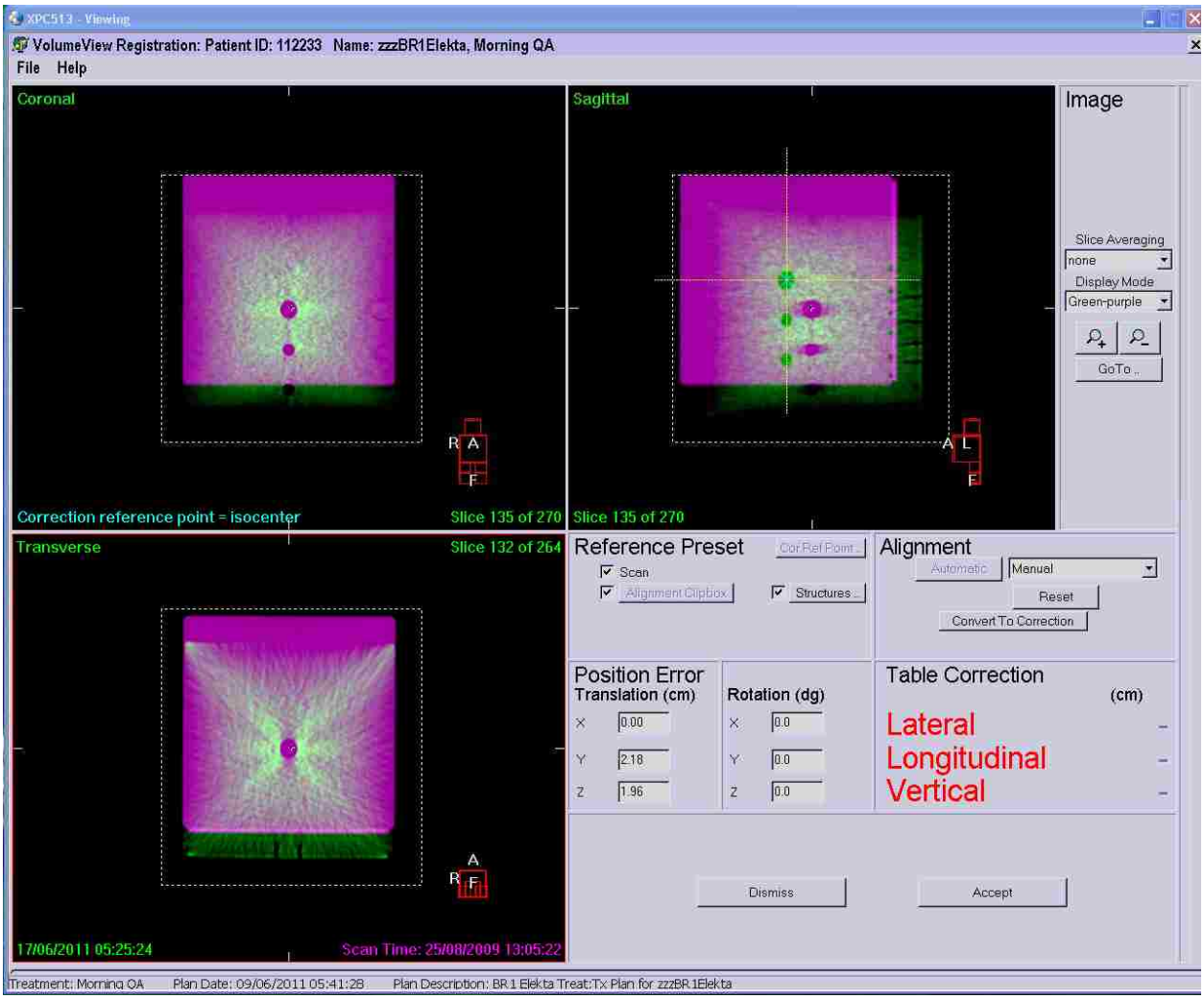

Figure 1.5: Screen capture of the registration tool in the Elekta Infinity software. The translations required to correct for the misalignment in the cube were obtained by moving the planning CT (purple) to overlap the kVCBCT data (green).

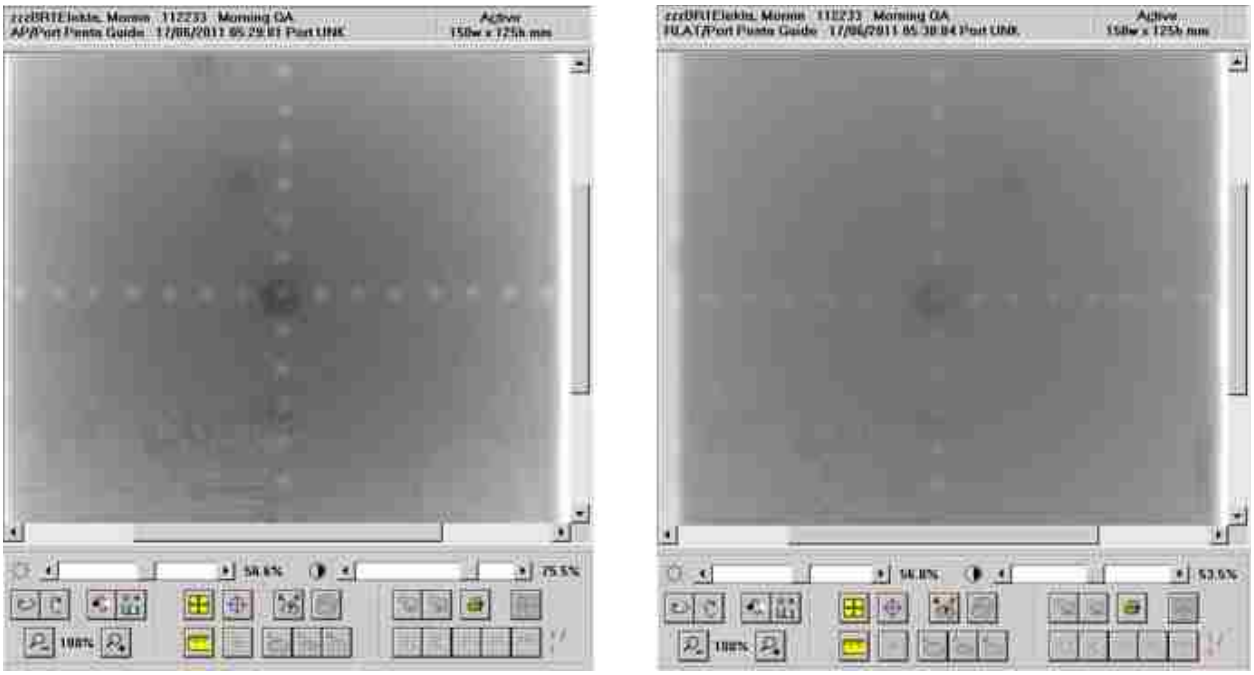

Figure 1.6: (Left) Screen capture of the AP MV planar image of the Penta-Guide phantom. (Right) Screen capture of the Right-Lateral MV planar image of the Penta-Guide phantom. Each sphere should be in the center of its corresponding ring.

1.3.2 Patient Setup on the Elekta Infinity

When a patient is initially setup on the Elekta treatment couch, the therapists align him or her with a combination of the room lasers and crosshairs that are drawn onto the patient after his or her initial CT. The use of immobilization devices like the Aquaplast mask and Vac-Lock bags (CIVCO Medical Solutions, Orange City, IA) aid in reproducing the patient setup process. Once set up with the room lasers, one of the IG procedures is implemented – usually kVCBCT. Depending on the location of the treatment target, one of the automatic kVCBCT registration algorithms is implemented – either bony registration or grey-value registration. During bony registration, the program uses an algorithm to match the bony anatomy of the kVCBCT with the patient's original CT. During gray-value registration, the program uses an algorithm to match various regions of similarly-shaded tissue of both images. Once the automatic registration is completed, the therapists will review the match, making small adjustments if needed. Once the

shifts have been accepted, the therapists can remotely move the treatment couch from outside of the vault in order to properly align the patient. As long as the patient remains immobilized, the radiation treatment plan is finally delivered. Conventional patient setup and treatments typically take about ten minutes to implement.

1.4 Motivation for Research

Ideally, one would only want to treat the GTV as well as any subclinical involvement located in the CTV. However, due to uncertainties with the positioning of the patient and inaccuracies of the treatment system, one needs to define ITVs and PTVs to guarantee full coverage of the CTV. This requires irradiating adjacent healthy tissue, with the amount determined by the size of the ITV and PTV margins; however, implementing IGRT can reduce the size of the internal margin and setup margin, lessening the irradiation of surrounding healthy tissue. Variability in daily patient setup is reduced by using a thermoplastic immobilization mask, which is custom fit to each patient. Using image guidance, inter- and intra-fraction error may be reduced even further, decreasing the required size of the PTV and reducing the volume of healthy tissue irradiated.

Margin reduction provides benefits to the patient; however, target positioning and dose delivery must be evaluated for the treatment system being used to confirm the level of accuracy that can be obtained. Similar work was completed by Murphy and Cox in verifying the positional and dose localization accuracy of the Cyberknife using IGRT (Murphy and Cox, 1996). Their results showed that the Cyberknife system achieved the same level of targeting precision as conventional frame-based radiosurgery.

1.5 Hypothesis and Specific Aims

This study focused on quantifying the accuracy and precision of both target positioning and dose delivery for an intracranial target delivered with the Elekta Infinity system using a non-invasive immobilization device. Quantifying the positional and dose accuracy of the entire IGRT system will aid in determining the minimum size of setup margins needed for intracranial treatments. The hypothesis of this project was that intracranial treatment delivery using the IGRT features of the Elekta Infinity system at Mary Bird Perkins Cancer Center will result in a positional accuracy within ±1mm. Two aims were completed to test this hypothesis:

Aim 1: Evaluate the positioning accuracy and precision from the Elekta Infinity imaging guidance modalities using a geometric and anthropomorphic phantom.

Sub-Aim 1a: Evaluate kVCBCT positional accuracy and precision.

Sub-Aim 1b: Evaluate MV planar imaging positional accuracy and precision.

Aim 2: Evaluate the dose localization accuracy and precision from the Elekta Infinity imaging guidance modalities using an anthropomorphic phantom.

Sub-Aim 2a: Evaluate the kVCBCT dose localization accuracy and precision.

Sub-Aim 2b: Evaluate the MV planar imaging dose localization accuracy and precision

CHAPTER 2. METHODS AND MATERIALS

To assess the delivery accuracy of the Elekta Infinity, a treatment plan was developed and delivered multiple times to a phantom. The phantom was intentionally misaligned along the three major orthogonal anatomical axes, and image guidance was used to identify and correct the misalignment prior to each delivery using the same procedure used in the MBPCC clinic. Positional and delivery accuracy was assessed by comparing the planned dose to the delivered dose measured using film. The following sections, which describe the experimental setup, the measurement process, and comparison of the delivered dose distributions to the planned distribution, are similar to those used in a previous study of a different imaging system and linac at MBPCC (Vinci, 2007; Vinci *et al.*, 2008).

2.1 Phantom and Treatment Planning

A treatment plan was developed for irradiation of an intracranial target in a head phantom. The treatment plan used intensity modulated delivery techniques to deliver the desired dose distribution. The phantom and the treatment planning process are detailed here.

2.1.1 Anthropomorphic Head Phantom

To acquire the most useful data, the phantom required specific characteristics. The phantom needed to be anthropomorphic with realistic internal structure to mimic the complex anatomy of the human head. The ability to accurately position and reposition the phantom on the treatment couch was essential. The capability to measure dose in the three orthogonal anatomical planes (transaxial, sagittal and coronal), if not in 3D, was necessary.

The CIRS® (Computerized Imaging Reference Systems; Norfolk, VA) Model 605 radiosurgery head phantom (Figure 2.1) provided the appropriate features for this work. This

anthropomorphic head phantom allows for 3D dose verification in a large cranial volume. It is fabricated from tissue-equivalent materials that mimic brain, bone, spinal cord, vertebral disks, and soft tissue. The linear attenuation coefficients of the tissues are reportedly within 1% of actual x-ray attenuation coefficients from 50 keV to 25 MeV (CIRS, 2010). A soft-tissue equivalent plastic cube fits inside a cavity in the brain. This segmented block holds pieces of film; by inserting the block in different orientations within the cavity, the plane of the film could be oriented in the transverse, sagittal and coronal planes.

Figure 2.1: (Left) CIRS Model 605 Radiosurgery head phantom. (Right) 6.35x6.35x6.35 cm^3 plastic block to hold up to 2 pieces of x-ray film; Figure 2.13 illustrates the placement of the film within the block.

2.1.2 Phantom CT Scans

CT imaging data of the phantom was required for treatment planning. The CT images of the head phantom were acquired using a GE Lightspeed CT Scanner (General Electric Healthcare, Waukesha, WI). Phantom setup for CT followed the procedure established by Vinci *et al.* and used by Batte *et al.* (Batte, 2010; Vinci *et al.*, 2008). Prior to imaging, an S-frame system (Med-Tec, Orange City, IA) with a Model-F head rest was fastened onto the CT couch. The phantom was positioned on the head rest with the transaxial film plane parallel to the CT

imaging plane; achieving proper alignment required scanning the phantom multiple times and adjusting the phantom position until the transaxial film plane was contained within a single CT slice. Position adjustment was facilitated by wedging two Styrofoam boards between the couch and superior edge of the S-frame to tilt the phantom, as well as by shifting the S-frame on the CT couch. Once the phantom was properly aligned, it was immobilized with a thermoplastic mask. Spherical radiopaque markers were then placed on the anterior and lateral surfaces of the thermoplastic mask at the three laser crosshairs. The superior edge of the S-frame was marked on the Styrofoam boards to facilitate reproducible positioning on the treatment couch (Batte, 2010). The bottom portion of the S-frame was weighted with three slabs of plastic water (5 cm thickness each) to ensure that it did not shift during scanning. The resulting setup is seen in Figure 2.2.

Figure 2.2: Head-phantom setup on the CT couch. In order to get the axial film plane parallel to the CT imaging plane, the head-phantom needed to be tilted upwards using the Styrofoam boards. Radiopaque BB's were placed at the laser crosshairs so setup could be mimicked on the treatment couch.

The treatment planning CT was acquired using the established clinical protocol for stereotactic radiosurgery (Table 2.1) at Mary Bird Perkins Cancer Center (MBPCC). However, for this study, the field of view was changed from 30 cm to 36 cm to fully encompass the head phantom and the large headrest. The treatment planning CT was acquired with the film plane in the transaxial anatomic plane.

Table 2.1: CT scanning parameters for the SRS clinical protocol at MBPCC.

Parameter	Value
Slice thickness	1.25 mm
Matrix size	512 x 512
mA	380
Field of view (FOV)	30 cm
kVp	140

2.1.3 Treatment Plan Design

The treatment planning CT was transferred to the Pinnacle^3 Treatment Planning System (Philips Healthcare, Andover, MA). A PTV was drawn to represent a centrally located cranial lesion. An approximate 2 cm diameter x 2 cm long cylindrical PTV was contoured and centered within the film block, with the long axis in the superior-inferior direction. Additional regions of interest were contoured to represent normal anatomy; the chosen regions were recommended for this plan by a MBPCC dosimetrist. The dose constraints for regions pictured in Figure 2.3 are summarized in Table 2.2. The "Normal tissue" structure was specified as dose-limiting structures in the plan to prevent overexposure of adjacent healthy tissue.

Prior to planning the treatment, the isocenter of the phantom CT was determined by demarcating the intersection point on the CT slice where the spherical radiopaque markers (defined by the CT lasers) were visible. The treatment isocenter was established in the treatment plan at the center of the cylindrical PTV. A seven-field IMRT plan was constructed with beams approximately equally spaced (every 51°) and focused on the treatment isocenter (Figure 2.4).

To minimize irradiating critical structures and creating hot and cold spots, the beams were set up with equal angular spacing around the phantom, starting with a true anterior beam (0°, 51°, 102°, 154°, 205°, 257°, 308°).

Table 2.2: Dose Constraints for treatment planning structures identified on the CT images.

Structure	Color (in Figure 2.3)	Dose Constraints (cGy)	Weight (%)	Objective Value
PTV	Red	D_{max} = 6038 D_{min} = 5992 DVH_{max} = 6000 (to 50% Volume) DVH_{min} = 6000 (to 100% Volume)	60 15 50 75	0.0000 0.0002 0.0015 0.0000
Spinal cord	Yellow	D_{max} = 450	5	0.0000
Eyes	Light Blue (right) and Pink (left)	D_{max} = 450	1	0.0000
Lenses	Dark Blue (right) and Purple (left)	D_{max} = 100	1	0.0000
Optic nerves	Green (right) and Orange (left)	D_{max} = 500	1	0.0000
Optic chiasm	Green	D_{max} = 500	1	0.0000
Brain stem	Dark Yellow	D_{max} = 500	1	0.0000
Normal tissue	-	DVH_{max} = 3000 (to 50%Volume)	25	0.0000

Dose prescription for the PTV was 300 cGy per fraction for 20 fractions. Dose constraints, shown in Table 2.2, were set for the remaining regions of interest to avoid overexposing these structures. This prescription was chosen to represent a typical fraction dose for multiple deliveries of the planned treatment. The fraction dose of 300 cGy was chosen to result in an optical density near the center of the dose range of Gafchromic EBT^2 film (see section 2.2). For each beam arrangement, the field size was set to a 4 x 4 cm^2 shape, and the multi-leaf collimators (MLC) were set to 0° having the leaves travel along the superior-inferior axis. The MLC positions for each beam were optimized by inverse planning in order to cover the whole target with 94% isodose, having put 100% equal to 300 cGy, the prescribed dose at the

isocenter. Inverse planning also allows the optimization algorithm to determine the best method of accurately irradiating the PTV to the prescribed dose while minimizing to irradiate the surrounding critical structures. The method of creating the treatment plan deviated from Coscia *et al.* and Vinci *et al.* who implemented forward planning techniques (Coscia *et al.*, 2009; Vinci, 2007). The weighting values and objective values for this treatment plan are shown in Table 2.2. The inverse plan was optimized with Direct Machine Parameter Optimization. The parameters used for MLC configuration and positioning are shown in Table 2.3. Once optimized, the treatment plan was reviewed and approved by a MBPCC dosimetrist. The isodose plots of the final treatment plan are shown in Figure 2.5, 2.6, and 2.7.

Table 2.3: Optimization parameters implemented for the treatment plan

Maximum Segment Value for Treatment	35
Minimum Segment Area	2 cm^2
Minimum Segment MU	2
Leaf/Field Edge Overlap	2 cm

2.1.4 Planar Dose Export

The 2D dose planes corresponding to the three film planes in the phantom were exported from the treatment plan's 3D dose matrix using the export feature available in Pinnacle^3. To use this feature, one first selected the desired anatomic plane. Next, the field size and dose grid resolution were selected. Because the isocenter of the treatment plan was placed at the center of the film cube, a 6x6 cm^2 planar export grid was centered over isocenter; the dose grid resolution was 0.1 mm, slightly less than the 0.178 mm scanning resolution of the Vidar film scanner resolution (see section 2.4). Three planar dose files were exported from the treatment plan – one in each of the transaxial, coronal, and sagittal planes.

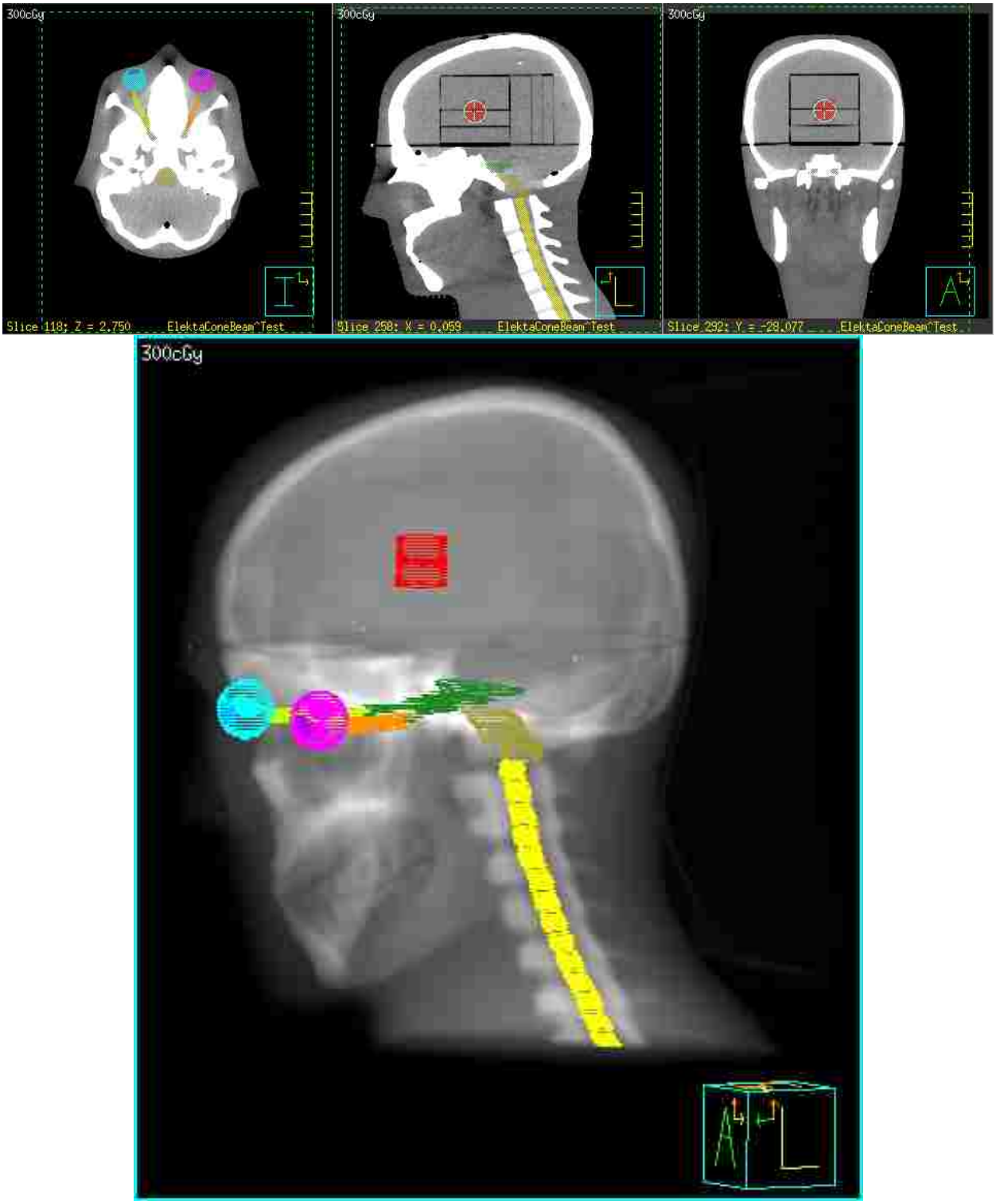

Figure 2.3: (Top) Transaxial (Left), sagittal (Middle), and coronal (Right) planes showing the regions of interest for treatment planning. (Bottom) DRR of the head phantom from a left-anterior oblique perspective showing all regions of interest. The structures and corresponding colors are identified in Table 2.2.

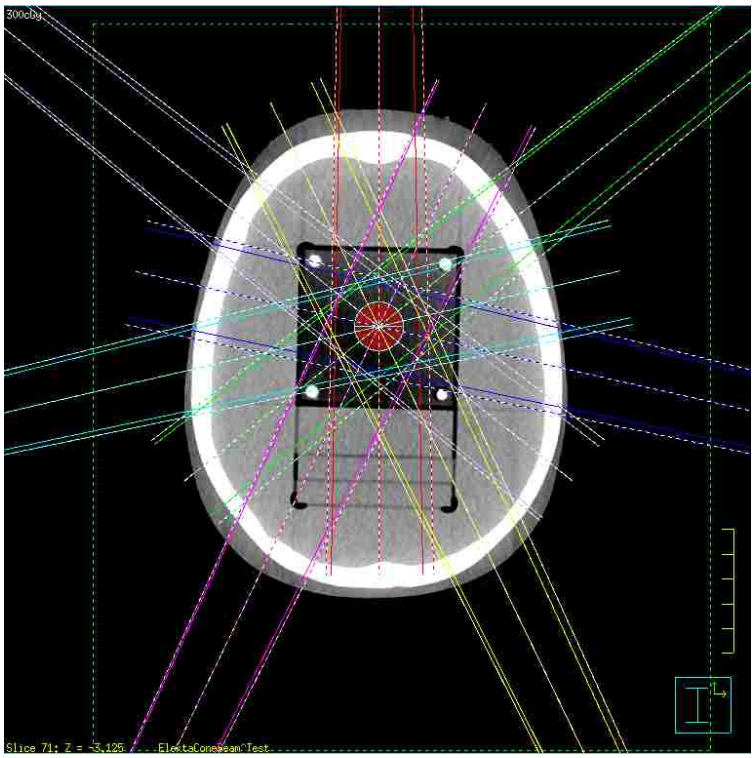

Figure 2.4: Transaxial view of the 7-beam isocentric treatment plan for the cylindrical PTV. The PTV appears as a red circle in this image plane.

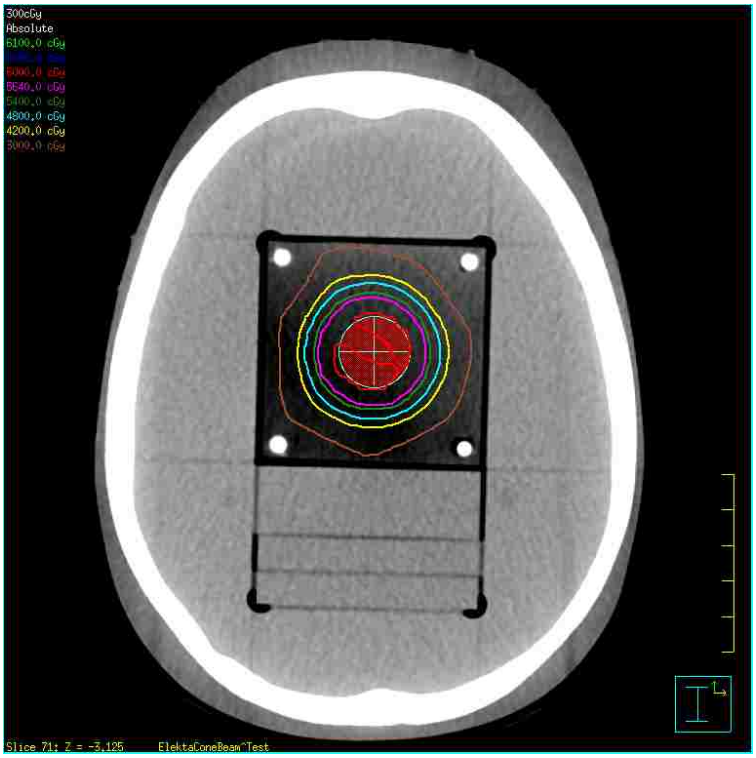

Figure 2.5: Isodose plot of the treatment plan in the axial orientation. The PTV is highlighted in red.

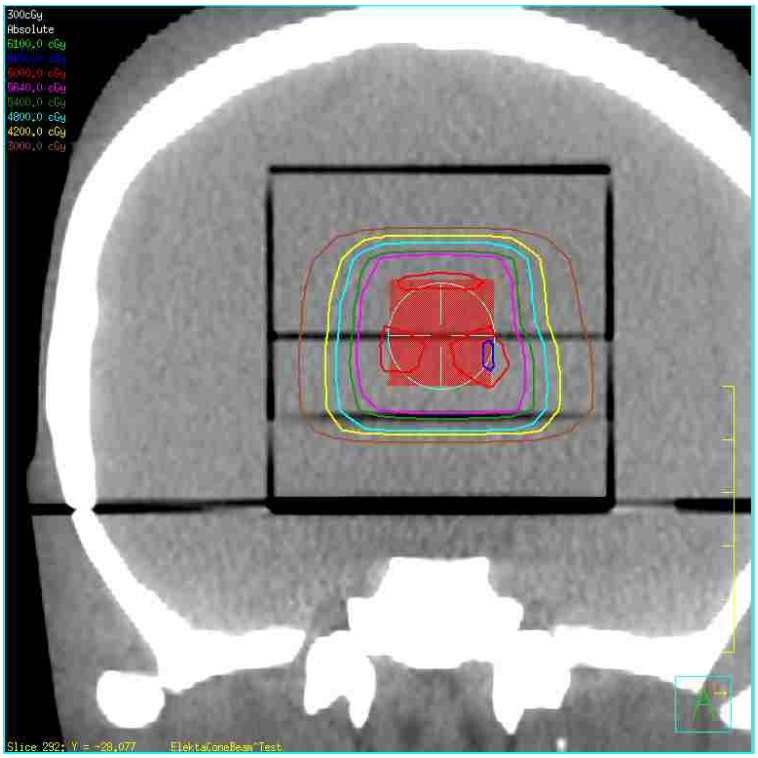

Figure 2.6: Isodose plot of the treatment plan in the coronal orientation. The PTV is highlighted in red.

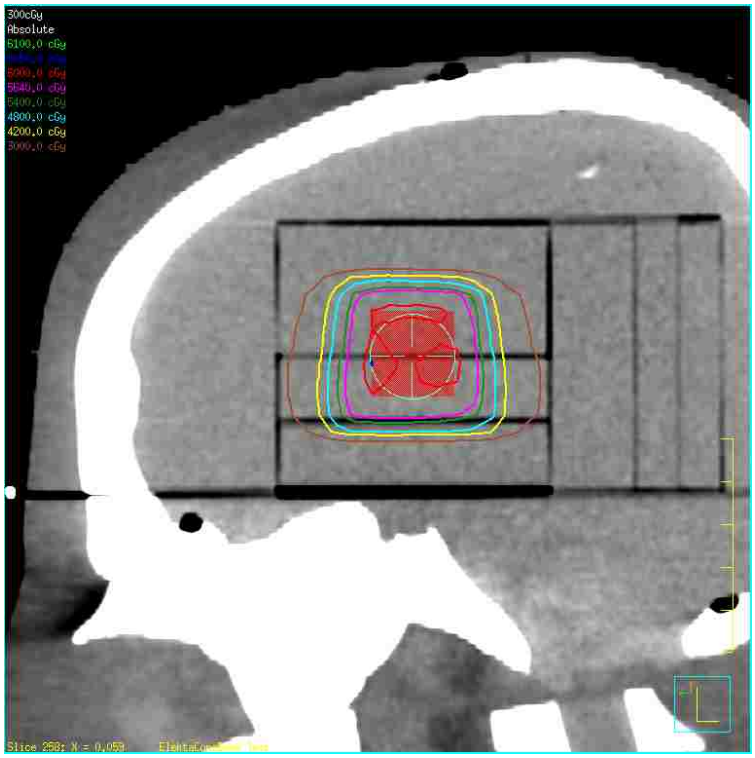

Figure 2.7: Isodose plot of the treatment plan in the sagittal orientation. The PTV is highlighted in red.

2.2 Film Dosimetry

To assess positional accuracy, a dosimeter capable of measuring 2D planar dose distributions inside of the phantom was needed. Film was selected for this project because it acquires a planar dose distribution from which one-dimensional dose profiles can be extracted. The small fields and steep dose gradients used to treat brain lesions required a dosimeter with high spatial resolution, which could also be achieved with film. Radiochromic film was selected over radiographic film because its relative insensitivity to room lights simplified the cutting of film pieces and assembling the film block inside the anthropomorphic head phantom. The suitability of radiochromic film has been reported previously for measurements in cone beam CT-based stereotactic radiosurgery (Jin *et al.*, 2009).

ISP Gafchromic EBT^2 film (International Specialty Products, Wayne, NJ) was used for this study because its extended dose range (1 cGy – 1000 cGy) matches well to realistic treatment dose fractions for conventional radiotherapy procedures (200 – 300 cGy). Gafchromic EBT^2 film is near tissue equivalent and provides at least 100 μm spatial resolution. As noted, its insensitivity to indoor light expedites phantom preparation. Finally, Gafchromic EBT^2 film is self-developing, avoiding the need for wet chemical processing (ISP, 2009b).

The film layer of EBT^2 Gafchromic film consists of a polyester overlaminate, an adhesive layer, the topcoat, the active layer, and a polyester substrate (Figure 2.8). The film is asymmetrical in its cross section; it is 80 μm from one surface and 175 μm from the other. Because the center of the active layer is not in the center of the film (±50 μm), film orientation during exposure and readout can affect results. The manufacturer marks EBT^2 film with a slit to provide orientation. Holding a film in landscape orientation with the slit at the right side of the top edge of the film indicates that the side facing the user is the side with the 50 μm polyester laminate (Figure 2.9).

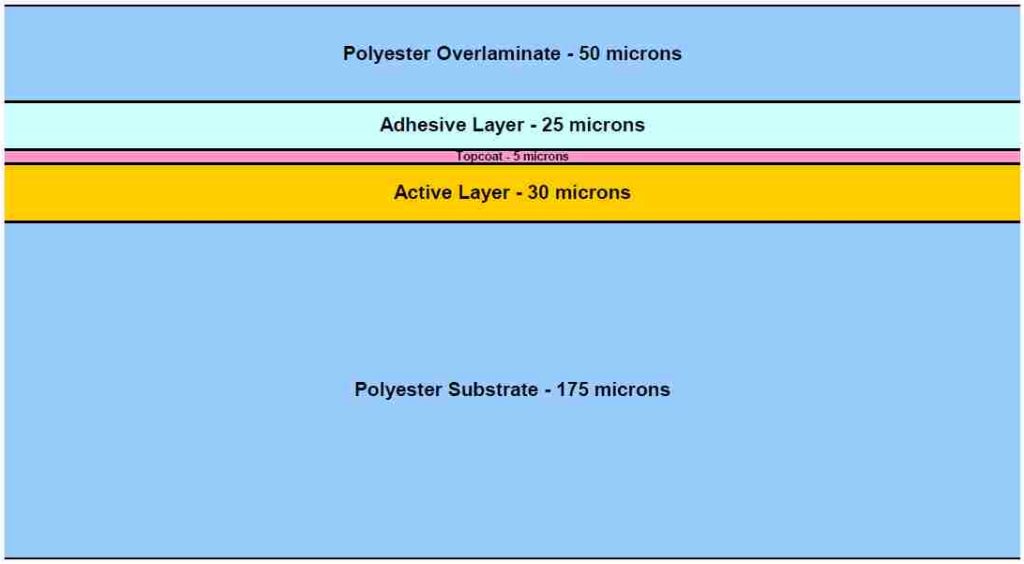

Figure 2.8: Illustration of the asymmetrical layering of Gafchromic EBT^2 film (ISP, 2009b).

Figure 2.9: (Left) Gafchromic EBT^2 film shown in the landscape orientation. (Right) Enlarged view of upper right corner (red box) showing the slit which distinguishes which side of the film to use.

2.2.1 Film Preparation

Accurate film dosimetry can be problematic due to variation in film response between different batches of film, time between exposure and processing, and processing conditions (Pai *et al.*, 2007; Niroomand-Rad *et al.*, 1998). For this work, all films came from the same batch;

calibration and test film measurements were made for each measurement session and all films were read out at the same time.

The response of Gafchromic EBT^2 film in scanning is dependent on whether the film is scanned in portrait or landscape orientation (ISP, 2009a). The variations in response are from anisotropic light scattering. The active component in Gafchromic EBT^2 film is in the form of needle-like particles approximately 1-2 μm in diameter and 15 – 25 μm in length (ISP, 2009b). The particles tend to align with the long axes parallel to the coating direction, thus scattering light differently in the two orthogonal directions (ISP, 2009b). Therefore, film orientation must be maintained throughout the readout process.

To prepare the film for use in the phantom, a single sheet of 8" x 10" Gafchromic EBT^2 film was cut into 3 strips (≈ 6.3 cm x 25.4 cm) using a paper cutter (Figure 2.10). Each strip was then cut into smaller pieces (≈ 6.3 cm x 6.3 cm) using the paper cutter. Each film piece was marked in the upper right hand corner to maintain the same orientation for all films during exposure and scanning. The accuracy of cutting the film only required that its edge did not protrude from the film block and that four holes at the fiducial rod locations described below could be drilled.

Once the film pieces were cut, each piece was prepared for use in the CIRS® radiosurgery head phantom using a custom aluminum film cutting template developed by Vinci *et al*. (Vinci *et al.*, 2008) and also used by Batte *et al. (Batte, 2010)* (Figure 2.11). Each film was individually loaded into the template and compressed and secured using two screws. Holes were drilled in the film using a drill and the template's machined holes as a guide. The holes in the film corresponded to the placement of the four fiducial rods that bolt together the pieces of the

phantom's film block. All film squares were placed in the cutting template in the same orientation for consistency.

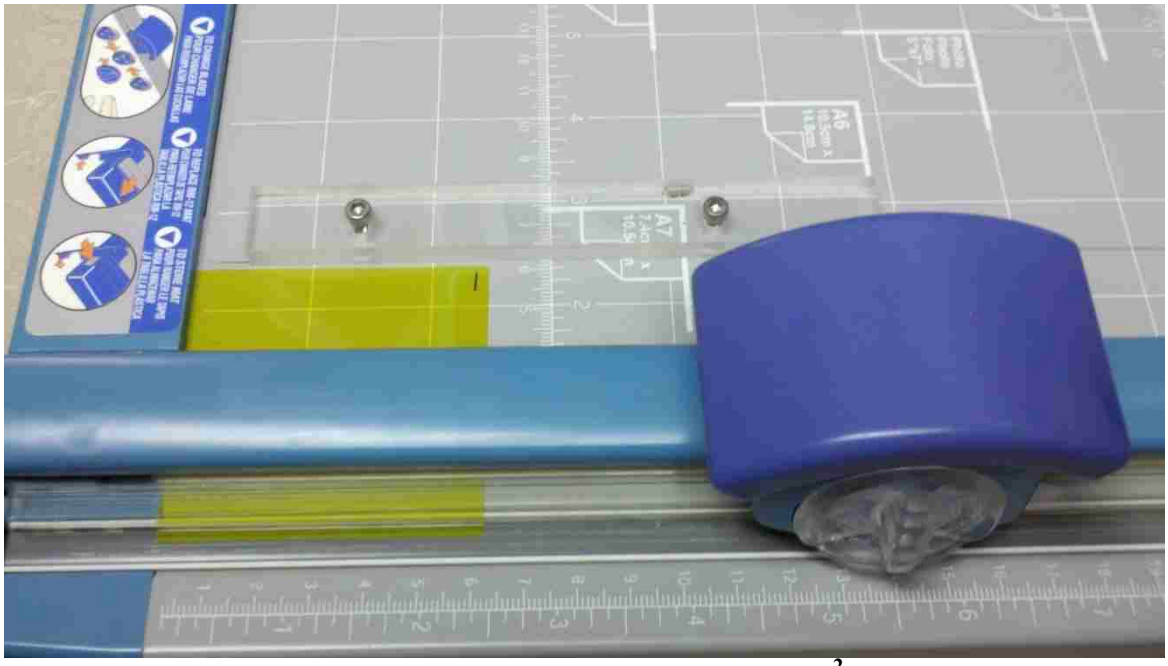

Figure 2.10: Photo of the film cutter used to make 6.3 x 6.3 cm^2 film pieces. The top right corner was marked to maintain consistent film orientation.

Figure 2.11: Holes were punched in the film so it could be placed in the film block. (Left) Film was placed in the film template, top removed. (Center) Once the top was attached, a drill was used to make four holes in the film. (Right) Resulting film, ready to be placed in the film block.

2.2.2 Film Calibration

Film calibration followed the guidelines from the TG-55 protocol on radiochromic film, as well as the Gafchromic EBT^2 Technical Brief (ISP, 2009a; Niroomand-Rad *et al.*, 1998). Various monitor unit (MU) values of radiation from a 6 MV photon beam with a 10 cm x 10 cm field size were delivered individually to twelve un-irradiated film squares using the Elekta Infinity. Each film square was placed in plastic water (Computerized Imaging Reference Systems, Inc., Norfolk, VA) at 100 cm source-to-axis distance (SAD) at a depth of 10 cm with 5 cm backscatter. Each film square was prescribed a percentage of the maximum dose of the treatment plan (10%, 20%, 30%… 110%, 120%); a thirteenth film square provided an unirradiated background dose point.

The absolute dose output (in cGy/MU) was determined with a Model TN30006 PTW Farmer Chamber (Freiburg, Germany) using the MBPCC protocol for monthly beam output checks. Output was measured for the 6 MV photon beam with a 10 cm x 10 cm field size at 100 cm SAD using the Elekta Infinity. The chamber was placed at a 10 cm depth in plastic water with 5 cm backscatter. The chamber received 100 MU of radiation, and the reading was recorded from the Keithley M614 electrometer (Keithley Instruments, Inc.; Cleveland, OH; Serial #: 350953). The measurement was repeated three times to determine an average reading. Using the TG-51 formalism to determine the photon dose, the daily output (cGy/MU) for 6MV photons was recorded (Almond *et al.*, 1999). Absolute dose output was measured at the same time as film calibration.

Each calibration film was scanned with a Vidar DosimetryPRO Advantage(RED) 16-bit film digitizer (Herndon, VA) and RIT113 (Radiological Imaging Technology Inc., Colorado Springs, CO) film dosimetry software (v5.2). The calibration films were scanned with the same geometry as the films used to measure delivered dose (see section 2.4). A region of interest

(ROI) was designated at the center of each film, including the un-irradiated background film. From the ROI of each film square, the scanner signal value was acquired. The scanner signal value was converted to optical density values (OD) using the formula:

$$OD = \log\left(\frac{I_0}{I}\right) \quad (1)$$

where **I** is the scanner signal value for a specific film, and $\mathbf{I_0}$ is the background scanner signal value.

A third order polynomial was fit to the OD data, generating a film calibration curve. The calibration curve was used to convert scanner signal values to dose on the films used to measure delivered dose. A new set of irradiated calibration films and calibration curve were created for each day's measurements. Scanned films were saved as a RIT image file (file extension *.rv4). A typical calibration curve is plotted in Figure 2.12.

2.3 Phantom Irradiation

2.3.1 Initial Phantom Setup

Prior to each film irradiation, a piece of unexposed Gafchromic EBT^2 film was placed inside the film block. The film was placed with its orientation mark to the right of the orientation arrow on the outside of the film block (Figure 2.13). The film block was then inserted into the phantom head cap. Figure 2.14 illustrates the three possible orientations of the film block, and thus the film itself, relative to the phantom anatomy for each of the measurement planes.

Once the film block was inserted in the head phantom, the phantom was reassembled and taped along its seam to ensure the pieces did not separate. The phantom was set up on the Elekta treatment couch using the same positioning and immobilization system used for CT scanning. The phantom was positioned such that the radiopaque markers on the lateral and anterior aspects

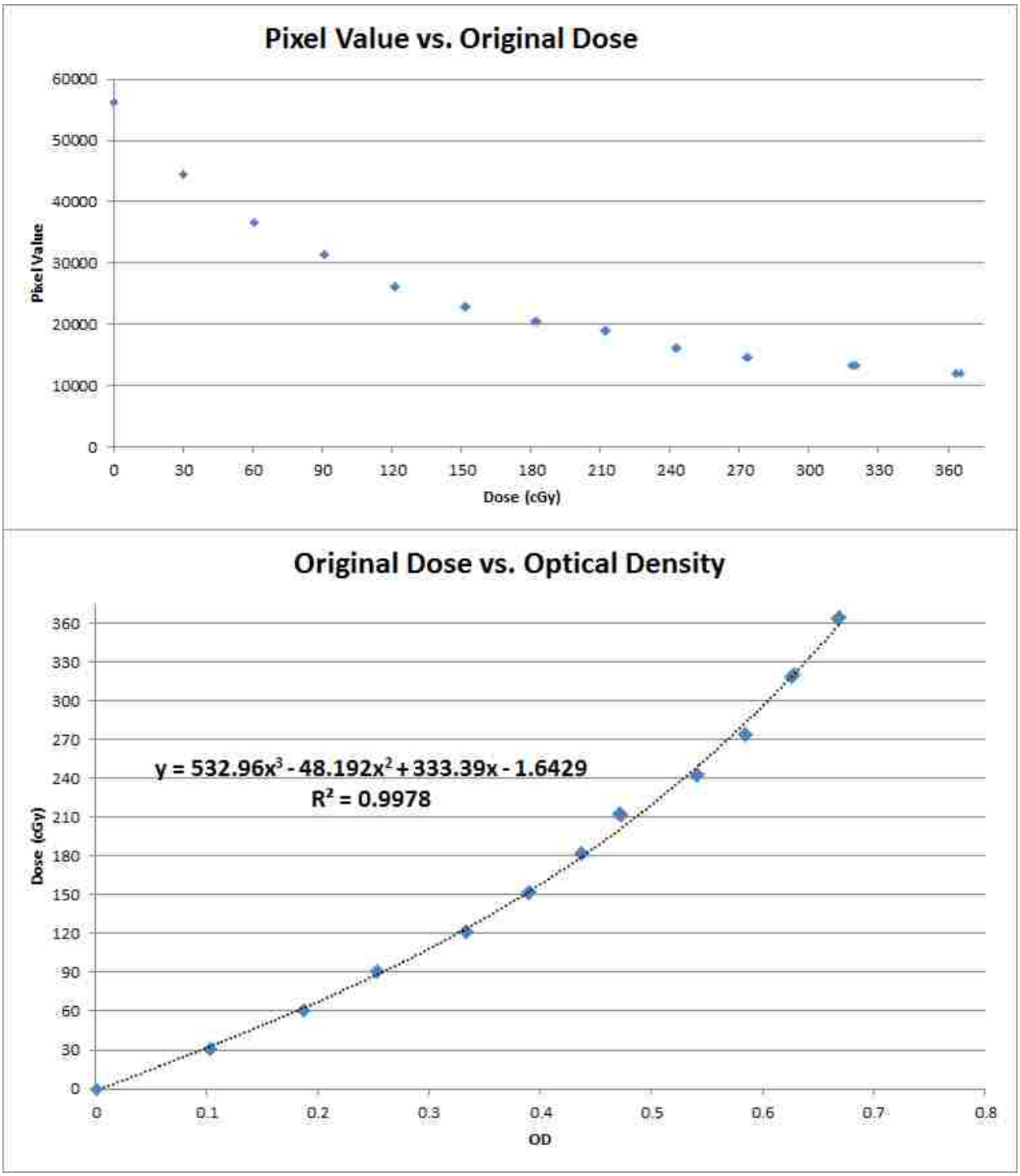

Figure 2.12: (Top) Plot of acquired scanner values with respect to dose for each calibration film. (Bottom) Plot of the calibration curve used on films that measured delivered dose. The calibration plot used 13 separate pieces of Gafchromic film.

of the immobilization mask coincided with the in-room setup lasers. For typical patient setup for intracranial treatments, the patient is placed on the S-frame, which is attached to the couch via an

Exact Bar (Medical Intelligence, Schwabmünchen, Germany). To mimic CT setup of the head phantom, the S-frame was tilted upwards with Styrofoam boards, negating the ability to use the Exact Bar. In lieu of the Exact Bar, the bottom portion of the S-frame was weighted with three slabs of plastic water (5 cm thickness each) to ensure that it did not shift during scanning or treatment.

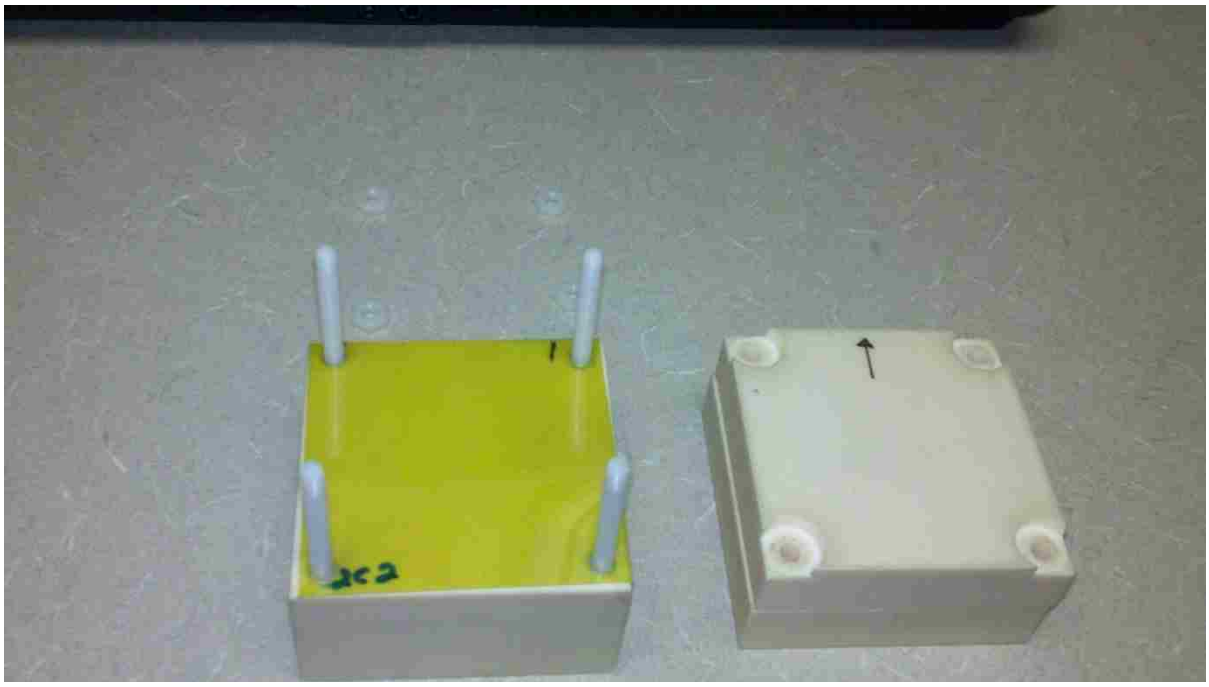

Figure 2.13: Film inserted into the film block. The arrow on the outside of the block indicates the film block orientation. The black mark on the top right of the film indicates the film orientation; the mark was always placed to the right of the orientation arrow. Each film was marked with a code in the bottom left corner to record its irradiation conditions.

Once the phantom was positioned on the treatment couch, an initial kVCBCT scan was acquired. The kVCBCT was automatically registered, using the soft tissue (gray scale) technique available in the Elekta linac control software. This initial kVCBCT checked for any rotational shift of the head phantom; because the Elekta couch cannot correct for rotational misalignments, any rotational errors were manually corrected. This kVCBCT also verified the

alignment of the phantom to the machine isocenter, which was then taken as the nominal (unshifted) position of the phantom. Once the phantom was set up to the machine isocenter, rulers were taped onto the couch in the 3 anatomic directions to mark the couch positions separately from the Elekta Infinity's digital position readout (Figure 2.15).

Figure 2.14: The three film cube orientations relative to the phantom anatomy. Shown are the orientations for the transaxial (Left), coronal (Middle), and sagittal (Right) anatomic planes.

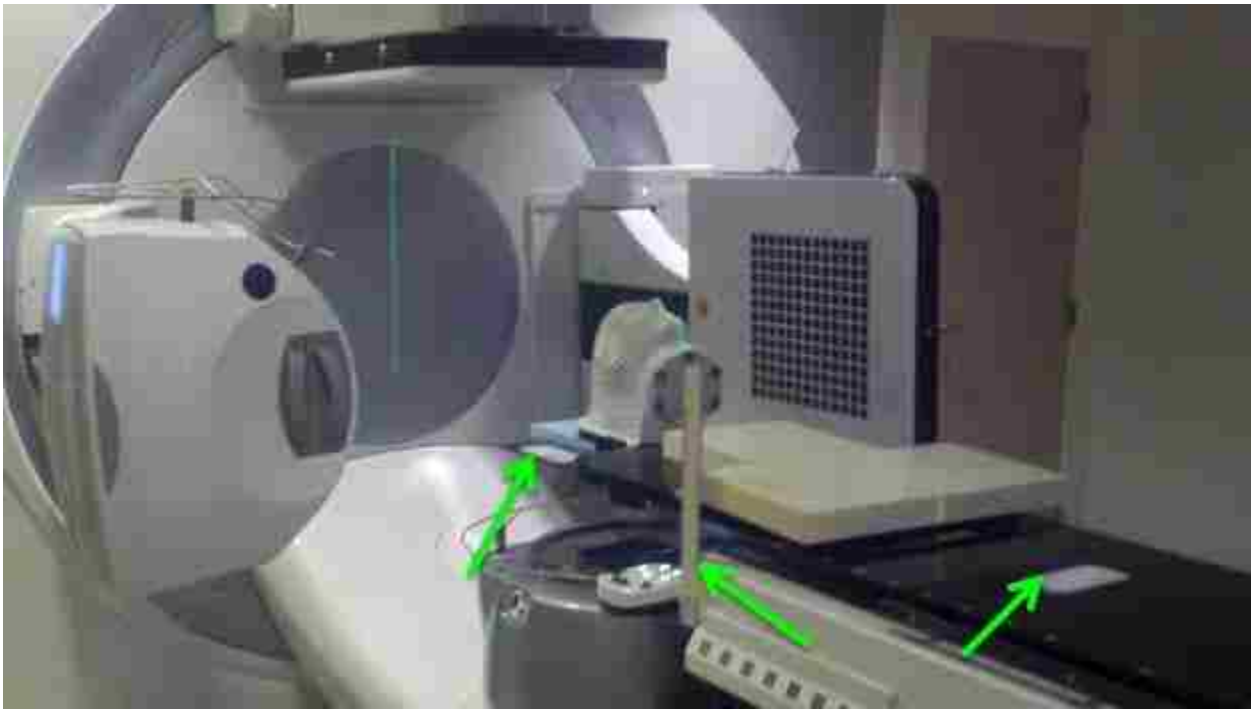

Figure 2.15: Photo of the head phantom in place for irradiation on the Elekta Infinity. Three rulers (green arrows) were used along with the room alignment lasers to set the intentional misalignments of the phantom.

2.3.2 Sample Space

To determine the ability of IGRT to identify and correct for misalignments, a series of intentional offsets were applied to the position of the phantom on the treatment couch ± 5 mm in the lateral, longitudinal, and vertical directions by manually moving the couch. Shifts were measured with the lasers and rulers, independent from the digital position readout on the Elekta gantry controls.

Delivered doses were measured in each of the three anatomic planes for nine measurement points: the nominal position with no offset and eight offset points that formed the vertices of a cube about the nominal position, illustrated in Figure 2.16. Table 2.4 lists the displacements of each point from the nominal position illustrated in Figure 2.16.

Table 2.4: Sample Space Points (distance from nominal position in mm).

Point	Lateral (Right - Left)	Longitudinal (Inferior - Superior)	Vertical (Anterior - Posterior)
0	0	0	0
1	5	5	-5
2	5	-5	5
3	5	-5	-5
4	5	5	5
5	-5	5	5
6	-5	-5	-5
7	-5	-5	5
8	-5	5	-5

2.3.3 Phantom Dose Delivery

Prior to film irradiation, an image guidance procedure that mimicked that in the clinic was used to identify misalignment and determine the necessary correction shift. Both kVCBCT and MV planar imaging were evaluated for each session as separate modalities.

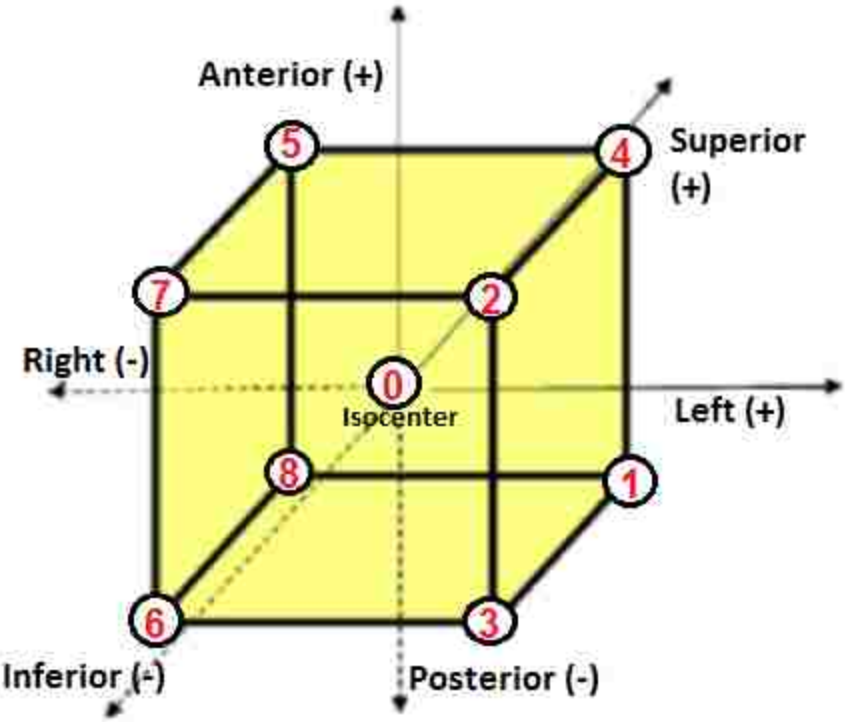

Figure 2.16: Spatial relationship of the intentional misalignments defined by translations in the lateral (right-left), longitudinal (inferior-superior), and vertical (anterior-posterior) directions (from Vinci, 2004). Offset coordinates are listed in Table 2.4.

2.3.3.1 kVCBCT Verification

Once the appropriate phantom position offset was applied, a kVCBCT was acquired with the "S20 Head and Neck" protocol. This protocol acquires a cone-beam with a small FOV with a 1.03 mm pixel resolution, kV tube potential of 100 kV, and current of 10 mA. Mimicking real patient setup, the kVCBCT was registered to the planning CT using automatic gray-value registration. The resulting translations required to shift the phantom to the correct location were determined from the registration of the two data sets. The registration was visually evaluated using a dual-color dual-image system (Figure 2.17) where the purple image represented the initial CT and the green image represented the kVCBCT. Almost every automatic gray-value registration produced a quality match between the kVCBCT and the CT; it was very rare that an additional slight manual correction was required.

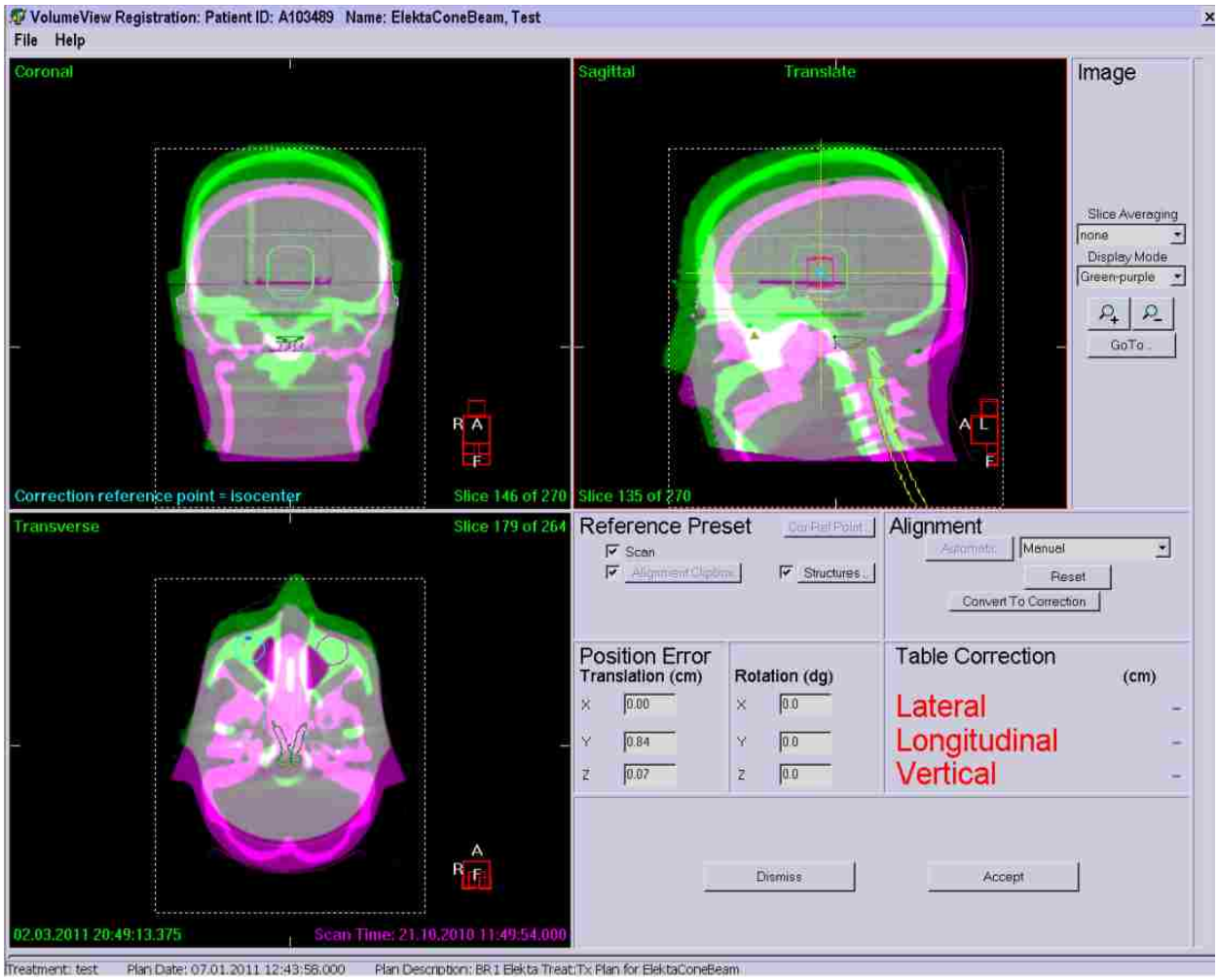

Figure 2.17: Screen capture of the registration tool in the Elekta Infinity software. The translations required to correct for misalignment were obtained by moving the planning CT (purple) to overlap the kVCBCT data (green).

These suggested translation values were noted and applied; the Elekta Infinity software automatically translated the couch by the specified amounts. Subsequently, the treatment plan was delivered to the phantom. After treatment the film was removed, stored in a light-proof container (recommended to protect from fluorescent light), and allowed to self-develop for 24 hours. This procedure was repeated with the film block in each of the three orientations for each of the nine sample space points.

2.3.3.2 MV Planar Imaging Verification

To correct for misalignment of the head phantom using MV port films, two DRRs were generated from the planning CT by Pinnacle[3]. The DRRs for the Anterior and Right-Lateral projections were used for comparison to the MV port films acquired by the MV EID of the Elekta Infinity.

With the phantom in position on the treatment couch, an open-air graticule was attached to the linac head. The graticule projected 1 cm demarcations, measured at isocenter, in the horizontal and vertical image directions onto the resulting MV images. Next, an Anterior view and a Right-Lateral view were acquired with the 6 MV beam using an open 20x20 cm^2 field size and 5 monitor unit prescription. A MBPCC radiation oncologist viewed the setup images with the 1 cm marks, compared them to the DRRs for each orientation, and determined the values for proper alignment. The Anterior view provided corrections for Inferior-Superior and Left-Right misalignments (Figure 2.18) while the Right-Lateral view provided the correction for Anterior-Posterior misalignment (Figure 2.19), as well as an additional measurement of Inferior-Superior misalignment. The oncologist determined the correct realignment shifts for all MV images that were analyzed. Shifts using MV planar imaging can only be implemented by entering the treatment room and using the couch digital readout to manually move the treatment couch into its proper position.

2.4 Data Analysis

2.4.1 Film Digitization

A template developed by Vinci *et al.* (2008) was used to hold the film pieces for scanning (Figure 2.20). The template consisted of a 14" x 17" blank piece of developed unexposed Kodak (Rochester, NY) EDR2 film in which the film pieces could be inserted. The films were digitized

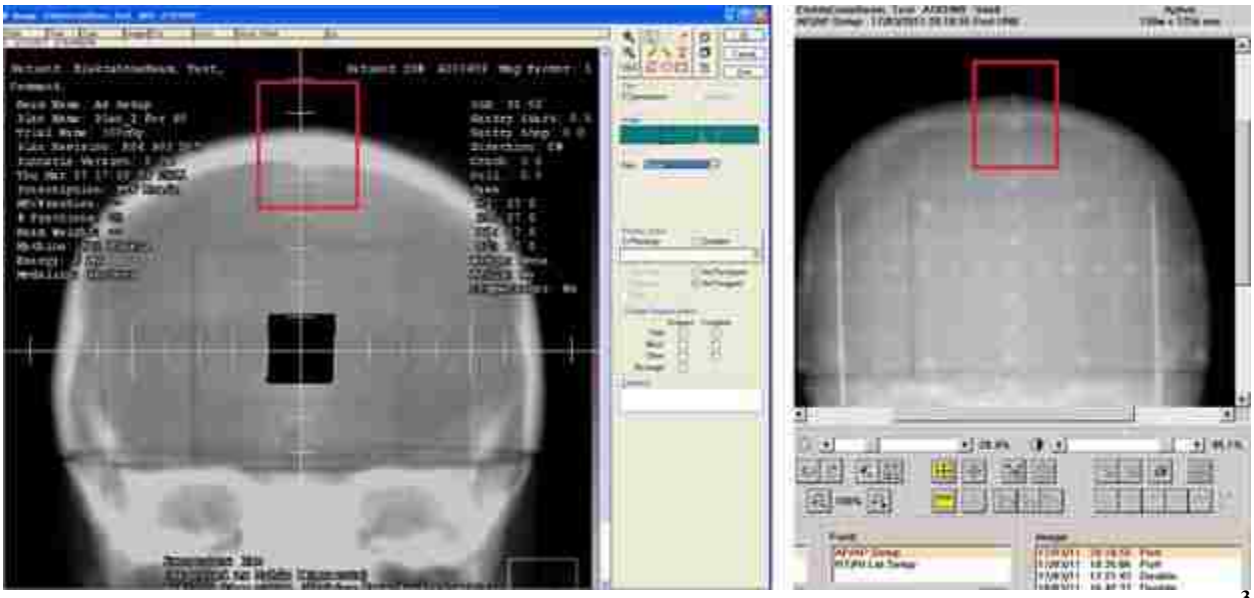

Figure 2.18: (Left) Screen capture of the Anterior DRR acquired from the Pinnacle[3] treatment plan; the tick marks on the horizontal and vertical axes represent 1 cm intervals in the plane of isocenter. (Right) Screen capture of the corresponding MV port film. The white dots denote 1 cm intervals in the plane of isocenter.

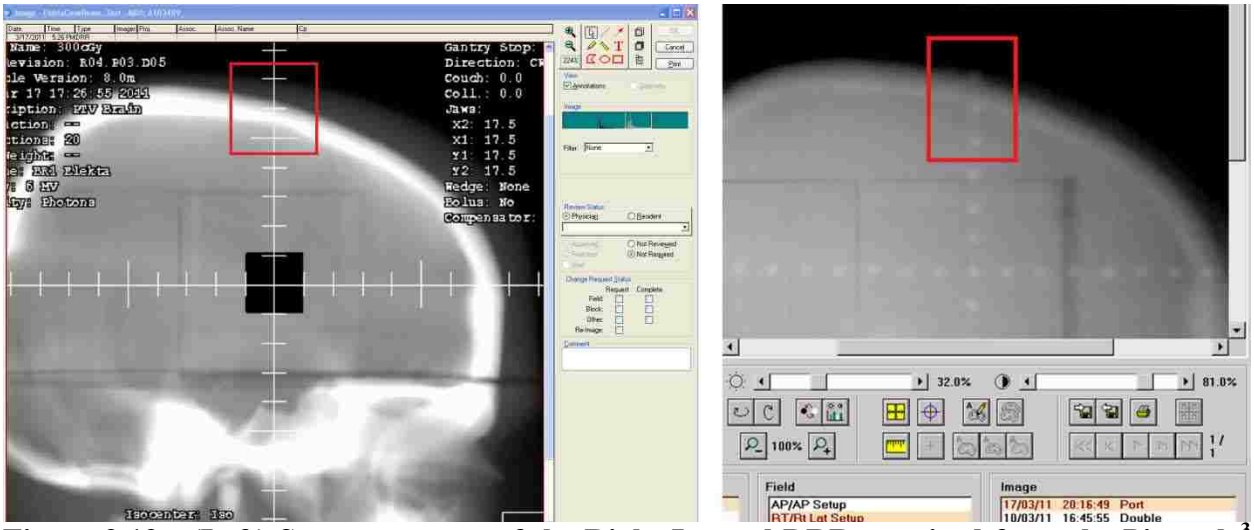

Figure 2.19: (Left) Screen capture of the Right-Lateral DRR acquired from the Pinnacle[3] treatment plan; the tick marks on the horizontal and vertical axes represent 1 cm intervals in the plane of isocenter. (Right) Screen capture of the corresponding MV port film. The white dots denote 1 cm intervals in the plane of isocenter.

with a resolution of 0.178 mm using a Vidar DosimetryPRO Advantage(RED) 16-bit film scanner (Herndon, VA), which utilizes a red-spectrum light. The intensity of the light transmitted through the film was measured as a 16-bit A/D value from a linear array of CCD

detector elements. All films were scanned against the left edge of the film scanner due to non-uniformities in scanner response across the scanning bed (Batte, 2010; Vinci, 2007).

Once the film was scanned, RIT113 (Radiological Imaging Technology Inc., Colorado Springs, CO) film dosimetry software (v5.2) was used for all data analysis. Each film piece was scanned with a region of interest (ROI) that enclosed the entire film square. The scanned image of each film was saved as a unique file with an embedded calibration file.

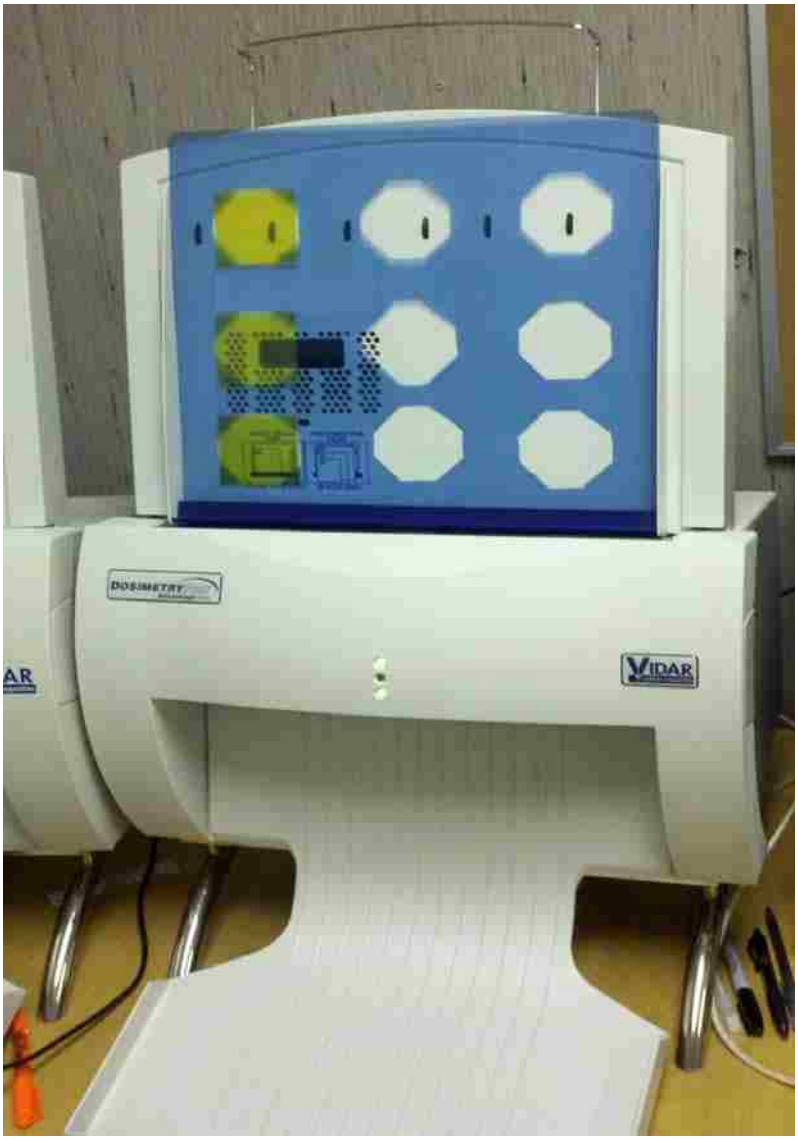

Figure 2.20: Photo of the Vidar DosimetryPRO Advantage(RED) film digitizer and the scanning template used to hold the film squares. Three film pieces (yellow squares) are in place on the template.

2.4.2 Registration of Film and Planar Doses

To register the measured dose distributions with the Pinnacle^3 calculated planar dose distributions, a registration template was created in RIT with the coordinates for the fiducial rods. The center of each fiducial rod was identified in the planning CT for the slice that contained the film plane. Using the measurement tools in Pinnacle^3 and the planning CT with the film plane in the axial direction, the cursor was manually placed over the center of each rod to determine the coordinates of the centers of the four fiducial rods with respect to the treatment isocenter (Figure 2.21). It was assumed that because isocenter was set to the center of the film cube, the same coordinates applied to the coronal and sagittal orientations. This varied from Vinci *et al.* who acquired CT scans in the three orientations of the film block. The template recorded the coordinates of the fiducial rods in terms of isocenter.

Once the registration template was applied to the exported planar dose data, a region surrounding a hole (corresponding to a fiducial rod) on each digitized film image was selected (Figure 2.22). In a magnified view, the cursor was manually positioned at the center of the hole and this coordinate was recorded. After repeating for the remaining three holes, the film image was registered to the planar dose grid using RIT's point-based rigid body registration tool.

2.4.3 Analysis Metrics

Film cross-profiles along the three orthogonal major axes (vertical axis and two horizontal axes) through the treatment isocenter were used to compare the planned and delivered dose distributions. For each 1-D film profile, five sample lines were acquired - one that went through the treatment isocenter along with four sample lines that traveled adjacent to the isocenter. From these five profile lines, the average pixel value was determined for each spatial coordinate, and the third order calibration curve was applied to convert the pixel values into

dose. The delivered dose profiles were then normalized to 300 cGy along the central centimeter of measurements. For all cases, absolute dose was analyzed. The analysis metrics evaluate both the position and shape of the measured distribution compared to the calculated distribution (Batte, 2010; Vinci, 2007).

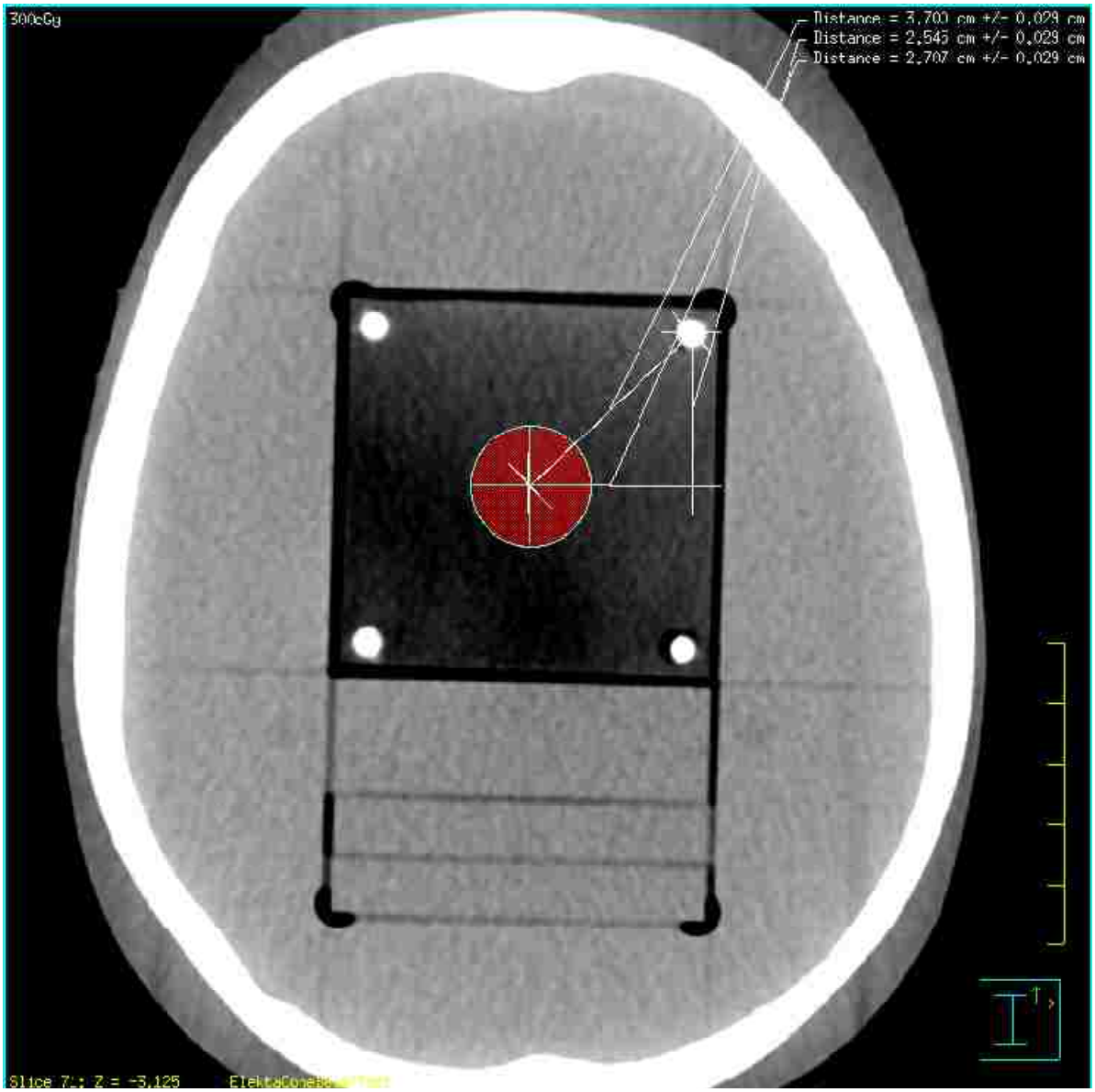

Figure 2.21: Enlarged transaxial view of the planning CT in the film plane. Measurement tools in Pinnacle[3] were used to determine the coordinates of the centers of the fiducial rods (white circles) with respect to isocenter (the center of the red PTV).

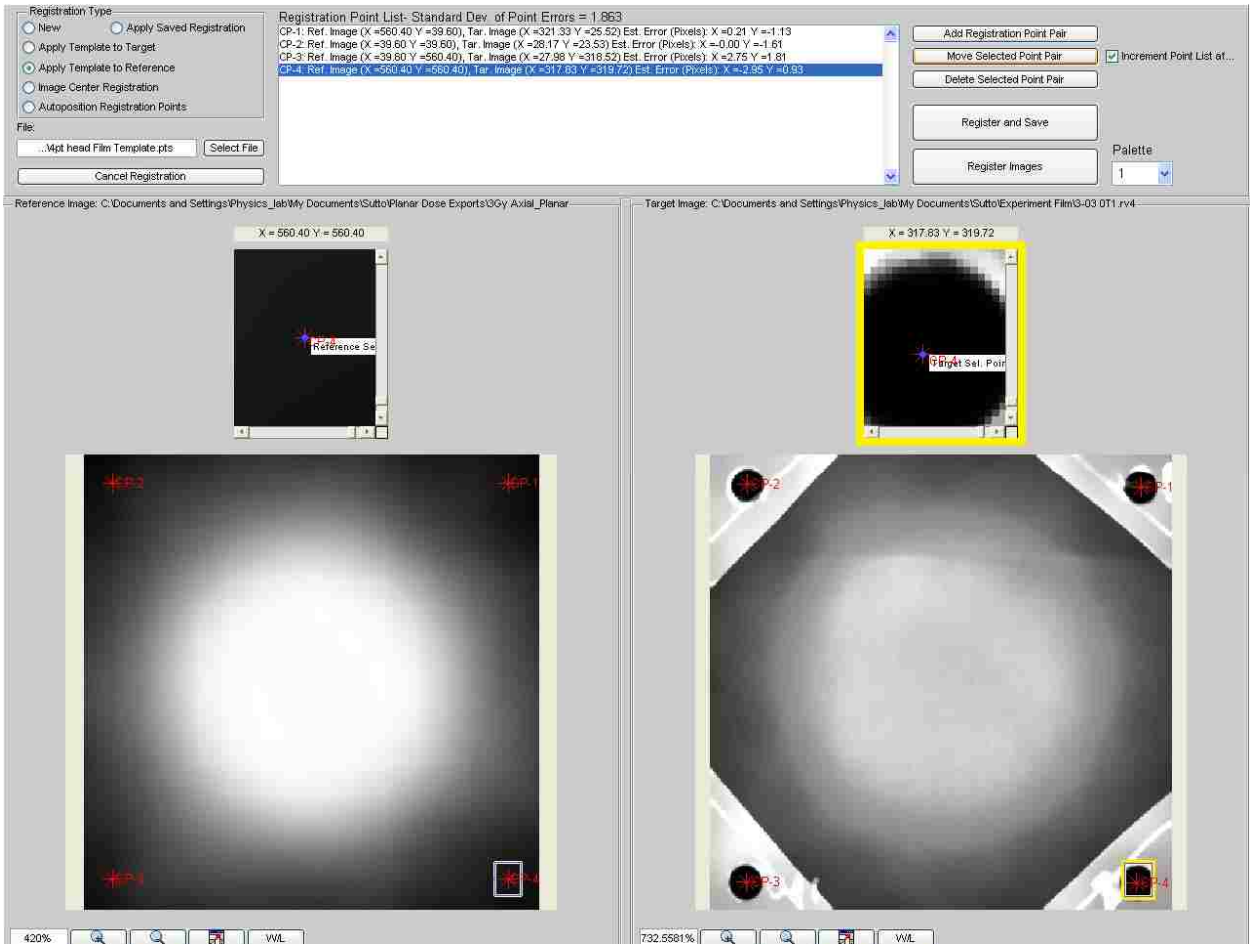

Figure 2.22: Screenshot of the RIT software displaying a scanned film (Right) and the corresponding Pinnacle calculated planar dose distribution (Left). The yellow box highlighted enlarged views of a hole that was used to determine the center of the hole.

The positional alignment error (Δc) was defined as the displacement between the midpoints of the calculated and measured profiles at the 70% dose level:

$$\Delta c = \tfrac{1}{2}\left(X_{70\%,Film+} + X_{70\%,Film-}\right) - \tfrac{1}{2}\left(X_{70\%,TPS+} + X_{70\%,TPS-}\right) \qquad (2)$$

where $X_{70\%}$ refers to the position of the 70% dose point. Subscripts (+) and (-) refer to the slopes of the profile, respectively while moving across the profile from negative to positive. Because the 100% dose refers to an absolute dose of 300 cGy, the 70% dose corresponds to an absolute dose of 210 cGy. The 70% dose level was selected because it is close to the location of the steepest dose gradient. The Δc metric is a measure of the alignment error in a particular

measurement. Positive values of Δc indicated that the measured profile was shifted to the left, posterior, or inferior direction of the measured profile from the treatment plan. Negative values of Δc indicated that the measured profile was shifted to the right, anterior, or superior direction of the measured profile from the treatment plan. The standard deviation of Δc is a measure of the reproducibility of alignment to the planning CT using kVCBCT image guidance (Batte, 2010).

Shifts in the 80% dose points (Δ80) represented the asymmetric deviations in the 80% isodose lines within the profiles. The 80% dose point shifts were defined as:

$$\Delta 80_{Anterior} = 80\%_{TPS,\,A} - 80\%_{Film,\,A} \quad (3)$$

$$\Delta 80_{Posterior} = 80\%_{Film,\,P} - 80\%_{TPS,\,P} \quad (4)$$

$$\Delta 80_{Right} = 80\%_{TPS,\,R} - 80\%_{Film,\,R} \quad (5)$$

$$\Delta 80_{Left} = 80\%_{Film,\,L} - 80\%_{TPS,\,L} \quad (6)$$

$$\Delta 80_{Superior} = 80\%_{TPS,\,S} - 80\%_{Film,\,S} \quad (7)$$

$$\Delta 80_{Inferior} = 80\%_{Film,\,I} - 80\%_{TPS,\,I} \quad (8)$$

The subscripts A, P, S, I, L, and R denote the anterior, posterior, superior, inferior, left, and right sides of the profile, respectively. Because the 100% dose refers to an absolute dose of 300 cGy, the 80% dose corresponds to an absolute dose of 240 cGy. The subscripts Film and TPS denote whether the reported 80% value was obtained from the film profile or planning system profile, respectively. Positive values of Δ80 indicated that the position of the measured 80% isodose point fell outside the calculated (planned) 80% isodose line. Conversely, negative values of Δ80 indicated that the measured 80% isodose point was inside the calculated (planned) 80% isodose line. Figure 2.23 illustrates the measurement directions that were obtained from each film orientation. Figure 2.24 shows the various film metrics that can be analyzed from each film.

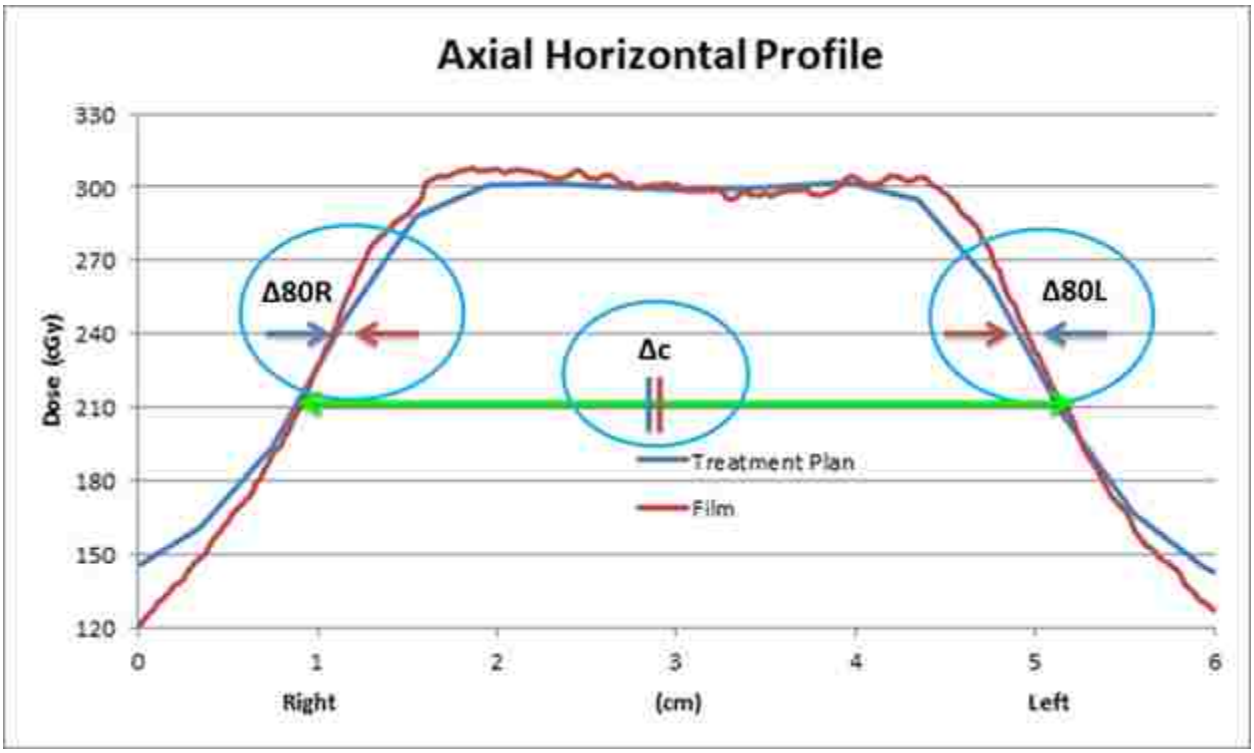

Figure 2.23: This graph shows the overlay of two profiles to illustrate the definitions of positional alignment error (Δc) and 80% dose shifts (Δ80).

2.4.4 Uncertainty in Analysis Metrics

The procedure to calculate uncertainty in the analysis metrics was derived from Vinci *et al.* (2008) and Batte (2010). To determine the uncertainty in the manual IGRT realignment process, the head phantom was first aligned to its isocenter. Next, the kVCBCT image guidance procedure was applied. The required shifts to re-align the phantom in each principle direction were determined. The process was repeated ten times without moving the phantom. Because identical distributions were being registered, all of the metrics should ideally have means and standard deviations of zero. Deviations from zero indicated the inherent error in the manual registration of the phantom with the planning CT data.

To determine the uncertainty introduced by the use of the RIT film analysis software, the same film was registered ten times to its corresponding calculated planar dose distribution. From this repeated registration, the analysis metrics were determined. This procedure was completed

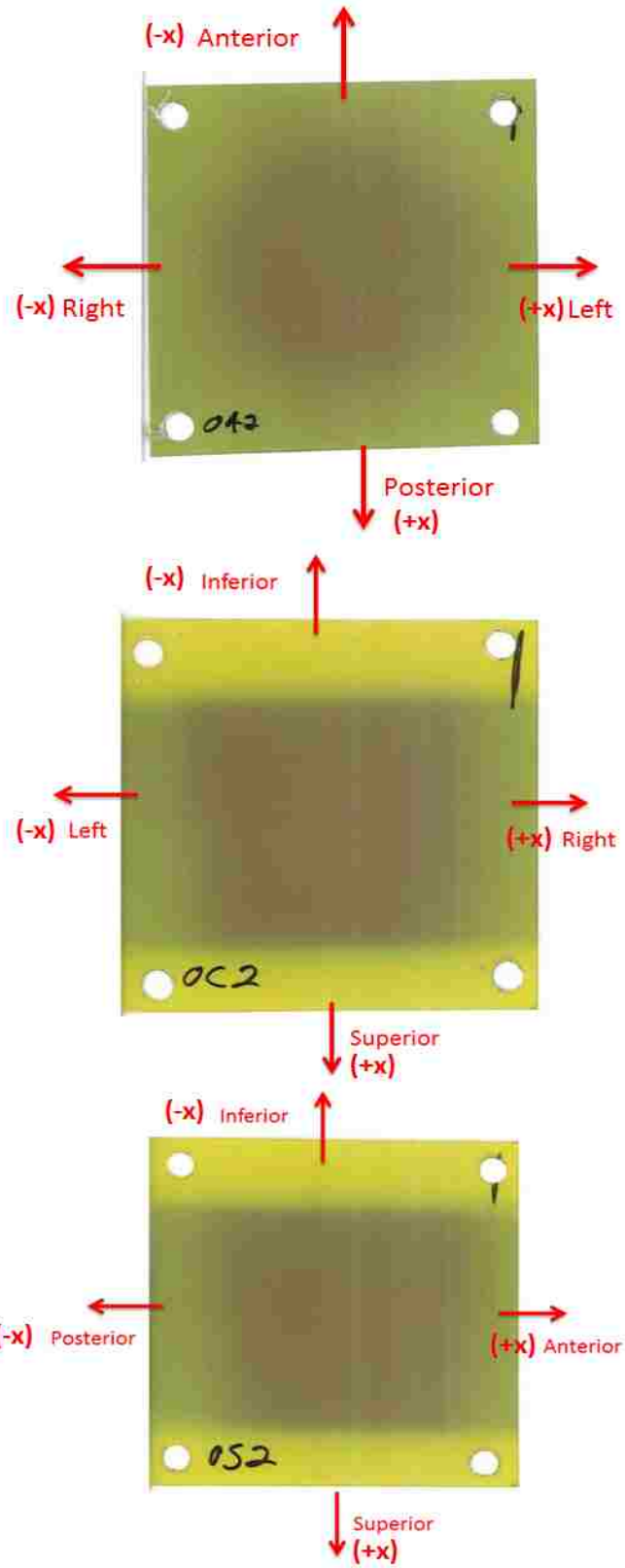

Figure 2.24: Illustration of the film metrics that can be analyzed from films acquired in the axial (Top), coronal (Middle), and sagittal (Bottom) planes.

for a film in each of the three principal planes. The standard deviations and standard errors of the metrics were calculated, representing the minimum uncertainty achievable in the analysis process.

2.4.5 Assessing Statistical Quality of Analysis Metrics

Ideally, each analyzed metric should have a mean value of zero. Student's T-Test was used to determine how well the measured values agreed with the expected value:

$$\boldsymbol{t = \frac{|x_{measured} - x_{expected}|}{SE}} \quad \textbf{(8)}$$

where **t** is the number of standard deviations by which the measured value differs from the expected value, $\mathbf{x_{measured}}$ is the mean of the several measurements used to determine a metric, $\mathbf{x_{expected}}$ is the expected value (0), and **SE** is the standard error of $x_{measured}$. If the t-value for a specific measurement is less than 1.96 SE (95% confidence), then the measurement should usually be judged as within agreement with the expected value. If the discrepancy is greater than 2.5 SE, then the measurements are usually judged as not in agreement with the expected value. For this work, t-values less than 1.9 SE were interpreted as insignificantly different than the expected value, t-values greater than 2.6 SE were considered significantly different than the expected value, and measurements with t-values in the range of 1.9 – 2.6 SE were inconclusive.

CHAPTER 3. RESULTS AND DISCUSSION

3.1 Uncertainty in Analysis Metrics

Table 3.1 shows the results of implementing kVCBCT and repeatedly registering the phantom to its planning CT ten consecutive times. Ideally, all of the translation values for realignment would be 0.00 mm, since the isocenter of the linac, as determined by use of the room lasers, was set to match that of the phantom. The mean values did not match the expected mean of 0.00 mm. This error likely was due to a mismatch between the linac isocenter and the isocenter as marked by the room lasers. Perfect coincidence would place the patient isocenter (based on alignment with the room lasers) at the linac isocenter. According to standard protocol set from the Task Group #142 report on quality assurance of medical accelerators, during linac maintenance, the laser isocenter is set as the best estimate of the center point of a virtual sphere created by the central ray of the radiation beam delivered under varying table and gantry angles (Klein *et al.*, 2009). The finite size of this sphere results from mechanical variability of the linac, due to gantry sag, gantry wobble, and table or collimator rotational wobble (sometimes referred to as "walkout"). Over time, lasers that are mounted on the walls of a vault may drift out of alignment. The combination of drift and mechanical inaccuracies means the lasers may not intersect at the true center of the sphere. Consequently, patient setup may exhibit a small amount of positional error with respect to the delivered radiation, even when the patient is carefully aligned to the room lasers.

Table 3.1: Mean, Standard Deviation, and Standard Error derived from repeating kVCBCT registration on phantom and initial CT

	Mean and Standard Error (mm) [N=10]	**Standard Deviation (mm)**
x-Lateral	0.20 ± 0.27	0.85
y-Longitudinal	0.34 ± 0.13	0.42
z-Vertical	-0.26 ± 0.02	0.07

Table 3.2 shows the results of registering a single film ten times to its corresponding calculated planar dose distribution and evaluating the analysis metrics as previously described. Ideally, the standard deviations (σ) of the repeated film-planar dose registrations should equal 0.00 mm. Each value in Table 3.2 had a standard deviation that is less than the film scanning resolution of 0.178 mm. These indicate that the manual registration technique and extraction of the analysis metrics was limited by the pixel resolution of the film.

Table 3.2: Results from registering the same film ten times with its corresponding calculated planar dose. Standard Errors (N=10) are in parentheses. All measurements are in mm.

Axial Film: 0A1	Coronal Film: 1C2	Sagittal Film: 7S1
$\sigma_{\Delta c\ L\text{-}R}$ = 0.04 (0.01)	$\sigma_{\Delta c\ L\text{-}R}$ = 0.05 (0.02)	$\sigma_{\Delta c\ A\text{-}P}$ = 0.07 (0.02)
$\sigma_{\Delta 80\ R}$ = 0.02 (0.01)	$\sigma_{\Delta 80\ L}$ = 0.07 (0.02)	$\sigma_{\Delta 80\ P}$ = 0.08 (0.03)
$\sigma_{\Delta 80\ L}$ = 0.06 (0.02)	$\sigma_{\Delta 80\ R}$ = 0.05 (0.02)	$\sigma_{\Delta 80\ A}$ = 0.09 (0.03)
$\sigma_{\Delta c\ A\text{-}P}$ = 0.04 (0.01)	$\sigma_{\Delta c\ I\text{-}S}$ = 0.04 (0.01)	$\sigma_{\Delta c\ I\text{-}S}$ = 0.06 (0.02)
$\sigma_{\Delta 80\ A}$ = 0.05 (0.02)	$\sigma_{\Delta 80\ I}$ = 0.05 (0.01)	$\sigma_{\Delta 80\ I}$ = 0.07 (0.02)
$\sigma_{\Delta 80\ P}$ = 0.04 (0.01)	$\sigma_{\Delta 80\ S}$ = 0.06 (0.02)	$\sigma_{\Delta 80\ S}$ = 0.07 (0.02)

3.2 Results of Phantom Irradiations

The phantom irradiation occurred over six sessions. The first three sessions irradiated the film with the aid of kVCBCT image guidance, and the last three sessions used MV planar image guidance prior to irradiation. Each session irradiated multiple orientation-specific films at the nine locations described in Table 2.4 in Section 2.3.2. For three orientations, this resulted in acquiring 27 films during each session and a total of 81 films for each image guidance modality. Figures 3.1, 3.2, and 3.3 show the images of the exposed films overlaid with their respective planar dose profile, along with their overlaid isodose plots. The figures collected in Appendix A provide one-dimensional profiles acquired for each film orientation, each of the nine sample space points, and for both image guidance modalities.

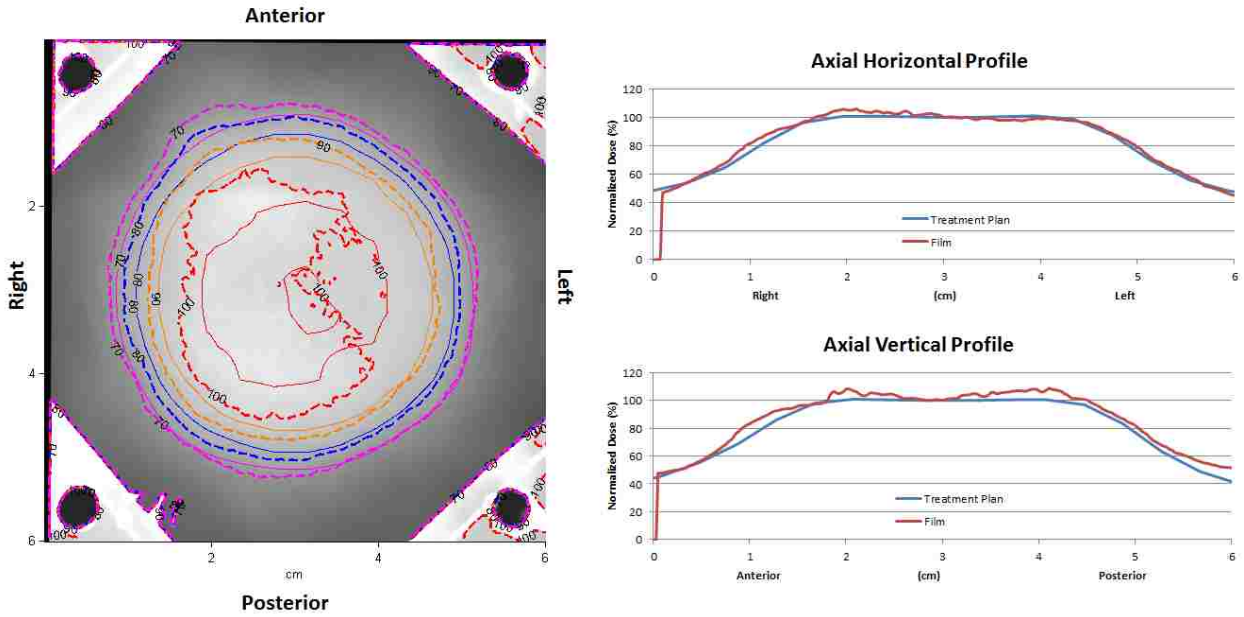

Figure 3.1: (Left) Overlay of an exposed film in the axial orientation with its corresponding planar dose profile. (Right) 1-D horizontal and vertical axial profiles.

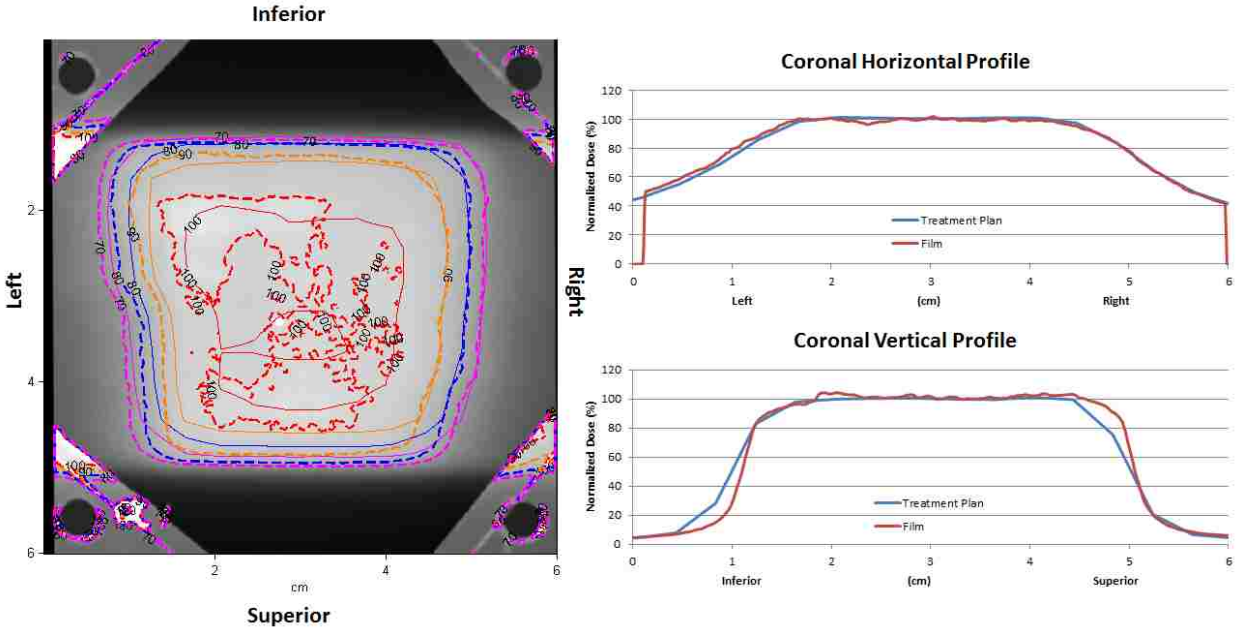

Figure 3.2: (Left) Overlay of an exposed film in the coronal orientation with its corresponding planar dose profile. (Right) 1-D horizontal and vertical coronal profiles.

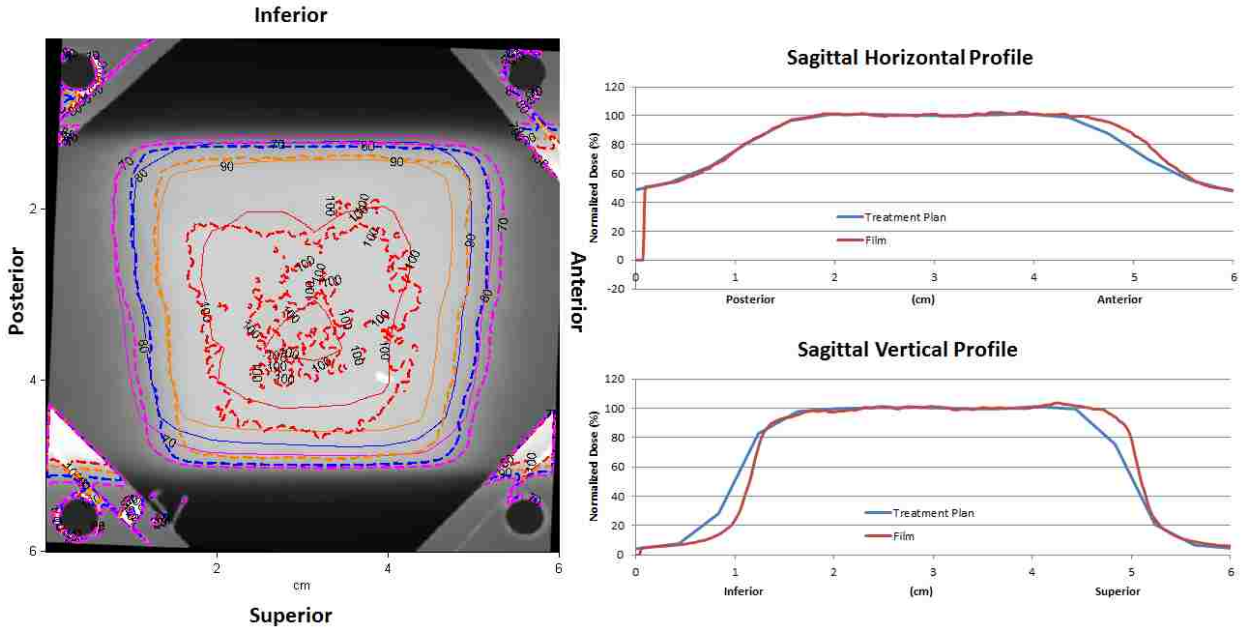

Figure 3.3: (Left) Overlay of an exposed film in the sagittal orientation with its corresponding planar dose profile. (Right) 1-D horizontal and vertical sagittal profiles.

3.2.1 kVCBCT Results

Table 3.3 summarizes the kVCBCT results for the Δc and Δ80 analysis metrics; the means, standard deviations (σ), ranges, and standard errors (SE) are all in millimeters. (Tables A.1, A.2, and A.3 provide all of the measurement results.) The meanings of positive and negative values of Δc and Δ80 were described in Section 2.4.3.

Table 3.3: Summary of Δc and Δ80 analysis metrics for kVCBCT image guidance.

Direction	Mean ± SE [N=54] (mm)	Range (mm)	σ (mm)	t-value
Δc				
Right-Left	-0.17 ± 0.09	-1.90 to 1.42	0.67	1.9
Anterior-Posterior	0.05 ± 0.13	-1.63 to 1.63	0.96	0.4
Superior-Inferior	1.27 ± 0.16	-1.80 to 4.05	1.21	7.7
Δ80				
Right	0.13 ± 0.08	-1.04 to 2.23	0.61	1.6
Left	0.43 ± 0.12	-1.98 to 2.37	0.91	3.4
Anterior	1.20 ± 0.08	0.08 to 2.31	0.56	15.6
Posterior	-0.69 ± 0.10	-2.37 to 1.01	0.74	6.9
Inferior	-1.02 ± 0.17	-3.63 to 2.08	1.25	6.0
Superior	2.13 ± 0.16	-0.88 to 5.06	1.19	13.2

Figure 3.4 plots the mean positional alignment errors Δc, with error bars representing ± one standard deviation. The results of Student's t-test showed that the Δc metrics consistently agreed with the planned dose distribution in the Right – Left and the Anterior – Posterior directions (t = 1.9 and 0.4 respectively); the mean Δc values were also close to zero for these directions.

The Inferior-Superior direction exhibited significantly less agreement between the measured and planned dose distributions (mean = 1.27 mm, t = 7.7). Subsequently, it was observed that the couch did not rigidly lock in its set position during intentional misalignment – the couch had a slight give to it in the longitudinal direction. When the couch was manually set to its misalignment position, the couch would slightly shake along its longitudinal axis. An attempt was made to quantitatively assess the table motion (See Section 3.3)

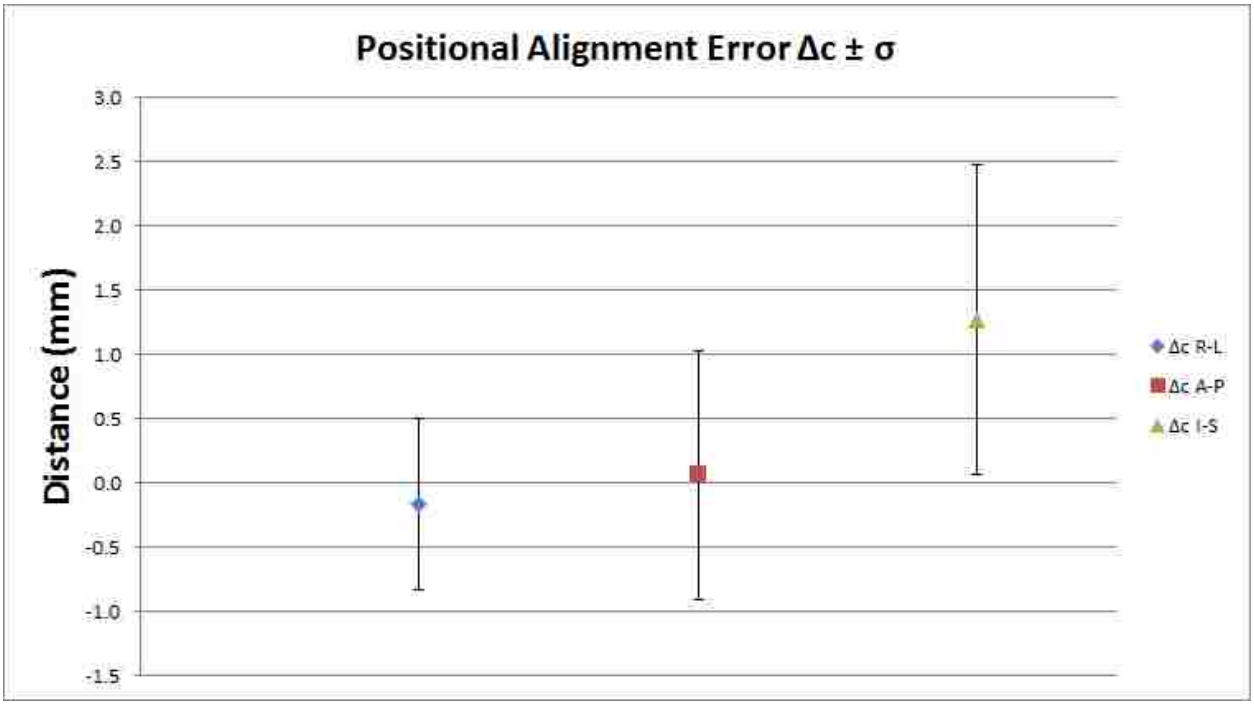

Figure 3.4: Plot of positional alignment errors when using kVCBCT image guidance. The data points are the mean values, and the error bars represent ± 1 standard deviation.

Some of the observed error in any direction can be attributed to the phantom not being able to be perfectly aligned for every setup. The radiopaque BB's on the aquaplast mask provide a close approximation to where the head phantom should be positioned, but they cannot provide sub-millimeter accuracy. The head phantom is also capable of making small rotational shifts inside the aquaplast mask every time it is placed back on the treatment couch. Reasonable effort was made to reduce the magnitude of the angular displacements to within ±1°. The current treatment couch is not capable of correcting for angular misalignments.

Figure 3.5 displays the mean and standard deviation for the displacement of the measured 80% dose point and the calculated 80% dose point for each direction. Similar to the positional alignment error data, the Δ80 values in the Right direction produced statistically acceptable agreement (t = 1.6).

Figure 3.5: Plot of the Δ80 results using kVCBCT image guidance. The data points are the mean values, and the error bars represent ± 1 standard deviation.

As with Δc, the large magnitudes for Δ80 occurred along the Inferior and Superior directions (t = 6.0 and 13.2 respectively). Previously stated, this variation may have stemmed from two sources. There could potentially be a rotational offset due to constantly repeating the entire process of removing the head phantom from its treatment position in order to replace the film. Another source of uncertainty may be caused by the slack in the couch along the longitudinal axis.

3.2.2 MV Planar Imaging Results

Table 3.4 summarizes the MV planar results for the Δc and Δ80 analysis metrics; the means, standard deviations (σ), ranges, and standard errors (SE) are all in millimeters. The meanings of positive and negative values of Δc and Δ80 were described in Section 2.4.3.

Table 3.4: Summary of Δc and Δ80 analysis metrics for MV planar image guidance.

Direction	Mean ± SE [N=18] (mm)	Range (mm)	σ (mm)	t-value
Δc				
Right-Left	-0.10 ± 0.15	-1.62 to 1.17	0.62	0.7
Anterior-Posterior	0.03 ± 0.25	-1.46 to 1.62	1.08	0.1
Superior-Inferior	1.75 ± 0.22	-0.02 to 3.42	0.95	7.8
Δ80				
Right	0.11 ± 0.16	-1.36 to 0.85	0.67	0.7
Left	0.69 ± 0.11	-0.35 to 1.68	0.48	6.0
Anterior	1.47 ± 0.11	0.74 to 2.20	0.46	13.5
Posterior	-0.93 ± 0.10	-1.39 to -0.16	0.41	9.7
Inferior	-1.54 ± 0.22	-3.14 to 0.09	0.93	7.0
Superior	2.56 ± 0.23	-0.76 to 4.29	0.98	11.1

Figure 3.6 plots the mean positional alignment errors Δc, with error bars representing standard deviation. The results of Student's t-test showed that the Δc metrics consistently agreed with the planned dose distribution in the Right – Left and the Anterior – Posterior directions (t = 0.7 and 0.1 respectively); the mean Δc values were also close to zero for these directions.

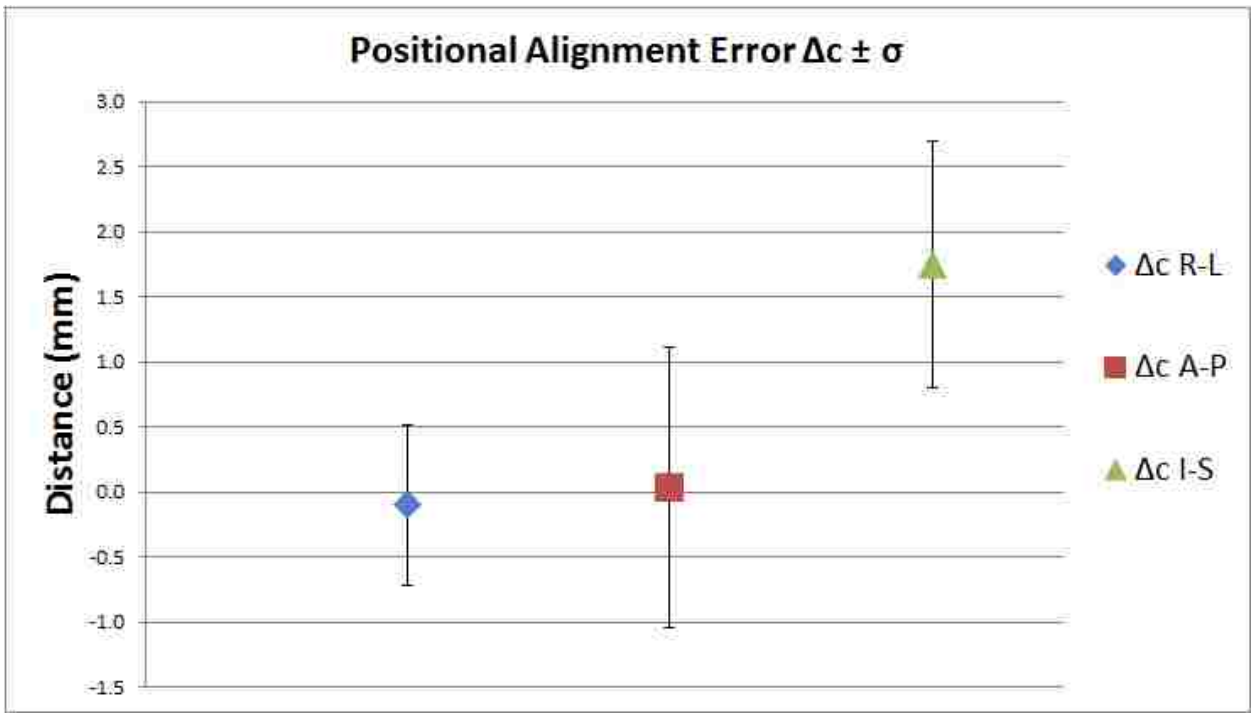

Figure 3.6: Mean positional alignment error values using MV planar image guidance. The data points shown are the mean values, and the error bars show a range of ± 1 standard deviation.

The Inferior-Superior direction exhibited significantly less agreement between the measured and planned dose distributions (mean = 1.75 mm, t = 7.8). It was observed that the couch did not rigidly lock in its set position during intentional misalignment – the couch had a slight give to it in the longitudinal direction. When the couch was manually set to its misalignment position, the couch would slightly shake along its longitudinal axis. An attempt was made to quantitatively assess the table motion (See Section 3.3)

Some of the observed error in any direction can be attributed to the phantom not being able to be perfectly aligned for every setup. The radiopaque BB's on the aquaplast mask provide a close approximation to where the head phantom should be positioned, but they cannot provide sub-millimeter accuracy. The head phantom is also capable of making small rotational shifts inside the aquaplast mask every time it is placed back on the treatment couch. Reasonable effort

was made to reduce the magnitude of the angular displacements to within ±1°. The current treatment couch is not capable of correcting for angular misalignments.

Image guidance using MV port films required using a graticule which contains radiopaque markers that are spaced 1 cm apart at isocenter. The graticules appeared to be useful for correcting centimeter-scale misalignments, but the large radiopaque markers made it difficult to make adjustments on the millimeter scale. MV port films are also limited in their ability to identify rotational misalignments.

Figure 3.7 displays the mean and standard deviation for the displacement of the measured 80% dose point and the calculated 80% dose point for each direction. All Δ80 metrics produced very large t-values which indicated unacceptable and potentially systematic errors. Previously stated, this variation may have stemmed from two sources. There could potentially be a

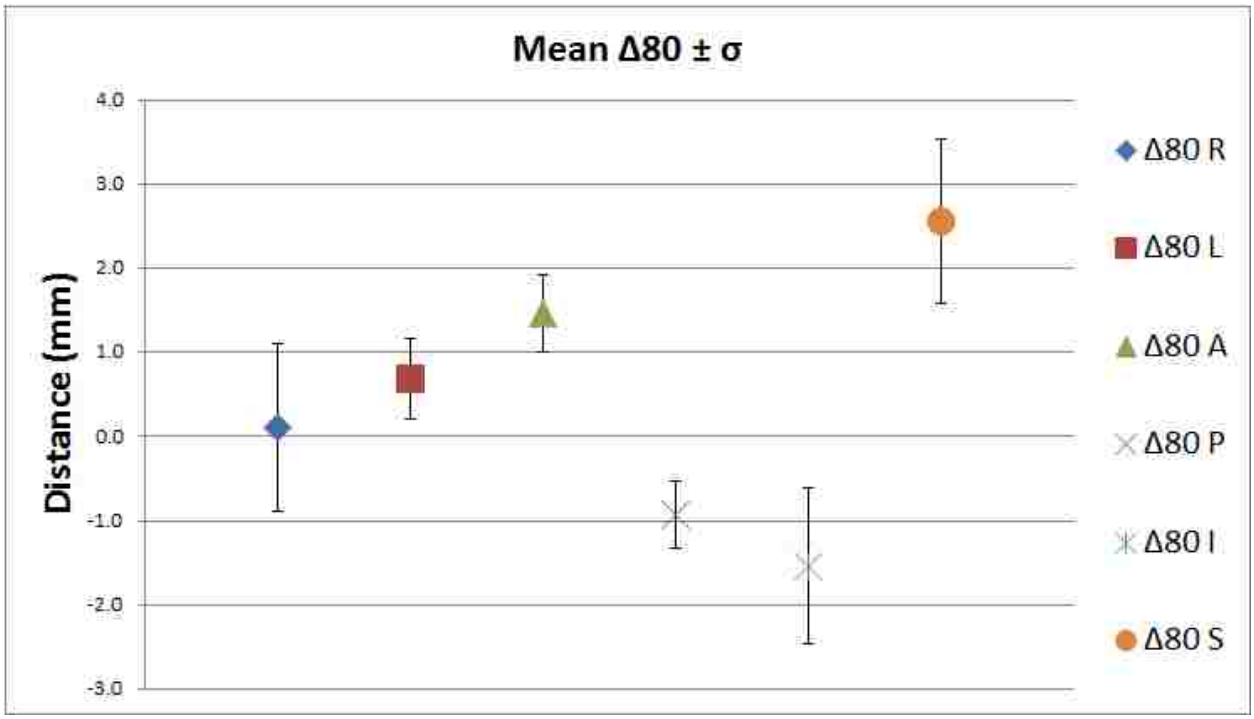

Figure 3.7: Total 80% Dose Shift values using MV planar image guidance. The data points shown are the mean values, and the error bars show a range of ± 1 standard deviation.

rotational offset due to constantly repeating the entire process of removing the head phantom from its treatment position in order to replace the film. Another source of uncertainty may be caused by the slack in the couch along the longitudinal axis.

The treatment process of the head phantom was modeled on conventional "real patient" setup. Once the phantom was misaligned using the rulers, the MV port films were analyzed to determine the shift corrections. Once determined, the corrections were manually applied using the digital readout on the linac gantry. The digital couch readouts only offer millimeter-degree accuracy, even though the couch is capable of sub-millimeter movements. Unfortunately, these small couch movements are not detected by the digital readout.

3.3 Error in Couch Motion

To further investigate the cause of the relatively high positional uncertainties (Δc) in the Superior-Inferior direction, the residual motion in the couch and the backlash in the couch were both investigated.

3.3.1 Residual Shift in the kVCBCT

The residual shift in the couch is defined as the additional translational distance (in each of the three anatomic directions) the kVCBCT recommends the couch needs to move in order to properly align a patient. To perform this test, the head phantom was aligned on the couch in the treatment position. The radiopaque BB's and room lasers were used to set up the phantom. From the nominal position, a kVCBCT was acquired to determine any necessary shifts. The phantom was aligned using the automated couch adjustments. From this new position, a second cone-beam was run to determine if any residual misalignment was still present. These secondary shifts are the residual shifts. This process was repeated for the "Point 1" position (5 mm Left, 5

mm Out, and 5 mm Up from the nominal position). The results of this test indicated the precision with which the couch can move to correct for misalignments.

Table 3.5 shows the residual shifts starting from the nominal position (Point 0) and Point 1 (left, out, up 5 mm). Previously stated, the kVCBCT registration algorithm is capable of identifying sub-millimeter shifts, but the treatment couch is only capable of millimeter adjustments. All of the acquired residual shifts were less than 1 mm. If the recommended shifts rounded up to 0.1 cm, then the couch has the option to move 1 mm in that direction. However, 1 mm shifts are judged as acceptable and are not required to be executed. This data shows that there are no significant residual shifts that the treatment couch needs to correct for.

Table 3.5: Data acquired from the residual shift tests

					What the Couch can Displace		
	x- Lateral (cm)	**y- Longitudinal (cm)**	**z- Vertical (cm)**		**x (cm)**	**y (cm)**	**z (cm)**
Primary Shifts (Point 0)	-0.15	-0.18	-0.07		**-0.2**	**-0.2**	**-0.1**
After Second kVCBCT; Residual Shifts	-0.06	-0.05	0.04		**-0.1**	**-0.1**	**0**
Primary Shifts (Point 1)	0.51	0.52	-0.52		**0.5**	**0.5**	**-0.5**
After Second kVCBCT; Residual Shifts	0.05	0.07	0.08		**0.1**	**0.1**	**0.1**

3.3.2 Couch Backlash Tests

In Section 3.2, the tendency of the couch to shake slightly along its longitudinal (Superior – Inferior) direction was noted. While MBPCC checks for couch slack on a monthly basis, a

more detailed test is required to check if there are variations in the couch positions at certain absolute coordinates. (Table A.4 provides the full measurement results.)

For this test, a meter stick was aligned with the room lasers and taped onto the couch. Once taped to the couch, starting at one end of the meter stick, the couch was moved in 3 cm intervals in one direction all the way to the other end. The couch position was verified by using the specific room lasers for that direction of motion. At every 3 cm interval, the digital couch position readout was noted. Once the room lasers reached one end of the meter stick, the same process was repeated in the reverse direction. This was repeated for each of the three directions of couch motion.

Table 3.6 shows the data acquired from moving the couch in 3 cm intervals. It is noted that the lateral and vertical couch movements globally agree with the digital couch readouts of the absolute coordinates. However, there appeared to be a systematic shift of the couch position along the longitudinal direction. Observations showed a 1 mm discrepancy at certain absolute couch positions. According to the full results, over 45 cm of longitudinal couch positioning acquired an error of 2 mm. When the couch reversed direction, the same 1 mm discrepancies appeared around the same absolute coordinates of the couch. In summary, a systematic position error of 1 mm occurred at fixed, repeatedly locations along the longitudinal direction of motion. This test was unable to determine if the systematic error is due to software or to hardware error.

In addition, backlash in the couch motion was investigated to determine if there was any directional dependence in the reproducibility of couch motion. This test had the same setup as the previous, only that the couch was moved in intervals of 5 cm forward and 3 cm backwards. (Table A.5 provides the full measurement results.)

Table 3.7 shows some of the values from the backlash test moving the couch in 5 cm forward and 3 cm backward intervals. Like the previous backlash test, the lateral and vertical couch movements produced no systematic direction-dependent errors, although some random fluctuations at non-reproducible positions were observed. For the longitudinal direction, systematic errors were again observed at the previously noted absolute coordinates as well as random variations in other locations. In any case, movements in alternating directions resulted in the expected displacements. Thus, the couch did not appear to exhibit position errors due to backlash. The head phantom was repeatedly positioned around the same location on the table, which coincided with one of the positions that exhibited the 1 mm systematic motion error; this likely explains larger position inaccuracies that were observed in the superior-inferior direction. Note that this table location near one end of the couch is generally where one would expect patients to be setup for treatment.

Table 3.6: Portions of data acquired from the first couch backlash test (3 cm intervals). Values in red indicate a discrepancy between the physical displacement and digital readout.

	LONGITUDINAL		LATERAL		VERTICAL	
Ruler (cm)	Digital (cm)	Difference (cm)	Digital (cm)	Difference (cm)	Digital (cm)	Difference (cm)
0	13.9		-22.4		17.1	
3	17.0	**3.1**	-19.4	3	14.1	3
6	20.0	3	-16.5	**2.9**	11.1	3
9	23.0	3	-13.4	**3.1**	8.1	3
12	26.0	3	-10.5	**2.9**	5.1	3
15	29.0	3	-7.5	3	2.1	3
18	32.0	3	-4.4	**3.1**	-0.9	3
21	35.0	3	-1.5	**2.9**	-4.0	**3.1**
24	38.0	3	1.5	3	-6.9	**2.9**
27	41.1	**3.1**	4.5	3	-9.9	3

Table 3.7: Portions of data acquired from the second couch backlash test (5 cm forward; 3 cm backward intervals). Values in red indicate a discrepancy between the physical displacement and digital readout.

	LONGITUDINAL		LATERAL		VERTICAL	
Ruler (cm)	Digital (cm)	Difference (cm)	Digital (cm)	Difference (cm)	Digital (cm)	Difference (cm)
35	55.0	5	9.5	5	14.1	5
32	57.9	**2.9**	6.5	3	17.1	3
37	52.9	5	11.5	5	12.1	5
34	56.0	**3.1**	8.5	3	15.1	3
39	50.9	**5.1**	13.5	5	10.1	5
36	53.9	3	10.5	3	13.1	3
41	48.8	**5.1**	15.5	5	8.1	5
38	51.9	**3.1**	12.5	3	11.1	3
43	46.9	5	17.4	**4.9**	6.1	5
40	49.9	3	14.5	**2.9**	9.1	3
45	44.9	5	19.5	5	4.2	**4.9**
42	47.9	3	16.4	**3.1**	7.1	**2.9**
47	42.9	5	21.4	5	2.1	5
44	45.8	**2.9**	18.5	**2.9**	5.1	3
49	40.9	**4.9**	23.5	5	0.1	5
46	43.9	3	20.5	3	3.1	3
51	38.8	**5.1**	25.4	**4.9**	-1.9	5

CHAPTER 4. CONCLUSIONS

4.1 Summary of Results

Tables 3.3 and 3.4 provide the overall results of the metrics obtained from using kVCBCT image guidance and MV planar image guidance. These values were determined by first creating intentional misalignments of 5 mm from the isocenter in a combination of the right – left, anterior – posterior, and inferior – superior directions. Most of these errors occurred in the Inferior – Superior axis, believed largely due to slack in the couch along this axis as the table would slightly shake along its axis during misalignment. The next step was to quantify the reason for the poor values. Upon further study, the couch was observed to have a discrepancy between its physical longitudinal position (using the rulers) and its corresponding digital readout. The rulers were not used as a second check because in the clinic, adjustments are made according the Elekta couch readout scale. Similar discrepancies have been determined in previous work (Ploquin *et al.*, 2008). The couch is also incapable of correcting for slight errors in unintentional rotational misalignments. MV planar image was worse than kVCBCT at correcting for misalignment; in addition, MV planar imaging is not able to identify rotational misalignments.

4.2 Evaluation of Hypothesis

The purpose of this project was to quantify the accuracy and precision of the IGRT treatment process for the Elekta Infinity's kV Cone-Beam CT and MV Planar imaging using a comprehensive phantom-based quality assurance procedure, with a goal of determining the minimum size of setup margin needed for treatment planning. The hypothesis of this project was that treatment delivery using the IG features of the Elekta Infinity will result in a positional accuracy within ±1mm for a cranial PTV in an anthropomorphic head phantom. This was not

proven to be true, as many of the measured alignment and dose coverage metrics were greater than 1 mm.

4.3 Clinical Recommendations

When using the image guidance methods on the Elekta Infinity, intracranial PTVs should use setup margins of at least 2 mm around the ITV when using kVCBCT and at least 3 mm when MV planar imaging is used. There are three recommendations that can be made to potentially reduce positional errors.

The first recommendation is that therapists should consider positioning patients longitudinally between the locations where the systematic 1 mm positional errors occur. The second recommendation is to request Elekta to provide a finer graticule for MV planar image guidance. The large radiopaque markers on 1 cm spacing are not conducive in correcting for small millimeter scale misalignments.

The kVCBCT potentially provides sub-millimeter correction shifts in the axial, lateral, and longitudinal directions. However, the couch digital readout reports movements only in 1 mm increments, which does not take the full advantage of kVCBCT. Therefore, the third recommendation is replacing the digital readout with one that provides sub-millimeter display. A sub-recommendation is to install a couch that can provide rotational corrections. Some research has already been completed in the area of using a hexapod couch (Meyer *et al.*, 2007).

4.4 Future Work

The data obtained in the research was dependent on the phantom being properly positioned on the couch. However, further research showed that there were certain longitudinal locations on the couch where there was a 1 mm disagreement between the physical positioning of the couch and the couch digital readout. The current work was done with the phantom placed

on the table in the region where one would expect to treat patients with intracranial lesions. A reevaluation of positional accuracy with the phantom could be made to confirm the capabilities of the Elekta Infinity if another location on the table was used. However, in clinical practice positioning a patient on a different part of the table for intracranial treatments may be problematic if the table interferes with treatment delivery.

Currently, this work only assessed IMRT treatment deliveries. Because of the availability of volumetric modulated arc therapy (VMAT) on the Elekta Infinity, an assessment of positional accuracy with image guidance as it relates to VMAT delivery could be assessed.

REFERENCES

Almond P R, Biggs P J, Coursey B M, Hanson W F, Huq M S, Nath R and Rogers D W 1999 AAPM's TG-51 protocol for clinical reference dosimetry of high-energy photon and electron beams *Medical Physics* **26** 1847-70

Batte C 2010 Accuracy of SRS Dose Delivery Using the Tomotherapy Hi-Art System. In: *MS in Medical Physics and Health Physics, Department of Physics and Astronomy,* (Baton Rouge, LA: Louisiana State University)

CIRS 2010 CT & X-Ray Phantoms. In: *Radiosurgery Head Phantom - For Evaluation of Treatment Accuracy,* (http://www.cirsinc.com/605_ct_xray.html)

Coscia G, Vaccara E, Corvisiero R, Cavazzani P, Ruggieri F G and Taccini G 2009 Fractionated stereotactic radiotherapy: a method to evaluate geometric and dosimetric uncertainties using radiochromic films *Med Phys* **36** 2870-80

Elekta 2006 *Elekta User Manual*

ISP 2009a EBT2 Product Specification Sheet.

ISP 2009b EBT2 White Paper. In: *GAFCHROMIC EBT2 Dosimetry Film,* (Wayne, NJ: International Specialty Products)

Jaffray D A, Siewerdsen J H, Wong J W and Martinez A A 2002 Flat-panel cone-beam computed tomography for image-guided radiation therapy *Int J Radiat Oncol Biol Phys* **53** 1337-49

Jin H, Huh S, Toramatsu C, Li Z and Malyapa R 2009 Dosimetric Verification of Ultra Small Fields of Image-Guided Linac-Based Stereotactic Radiosurgery *Medical Physics* **36** 2430

Khan F M 2010 *The Physics of Radiation Therapy* (Philadelphia: Lippincott Williams & Wilkins)

Klein E E, Hanley J, Bayouth J, Yin F F, Simon W, Dresser S, Serago C, Aguirre F, Ma L, Arjomandy B, Liu C, Sandin C and Holmes T 2009 Task Group 142 report: quality assurance of medical accelerators *Med Phys* **36** 4197-212

Letourneau D, Keller H, Sharpe M B and Jaffray D A 2007 Integral test phantom for dosimetric quality assurance of image guided and intensity modulated stereotactic radiotherapy *Med Phys* **34** 1842-9

Letourneau D, Publicover J, Kozelka J, Moseley D J and Jaffray D A 2009 Novel dosimetric phantom for quality assurance of volumetric modulated arc therapy *Med Phys* **36** 1813-21

Meyer J, Wilbert J, Baier K, Guckenberger M, Richter A, Sauer O and Flentje M 2007 Positioning accuracy of cone-beam computed tomography in combination with a HexaPOD robot treatment table *Int J Radiat Oncol Biol Phys* **67** 1220-8

Murphy M J and Cox R S 1996 The accuracy of dose localization for an image-guided frameless radiosurgery system *Med Phys* **23** 2043-9

Niroomand-Rad A, Blackwell C R, Coursey B M, Gall K P, Galvin J M, McLaughlin W L, Meigooni A S, Nath R, Rodgers J E and Soares C G 1998 TG-55: Radiochromic Film Dosimetry *Medical Physics* **25**

Pai S, Das I J, Dempsey J F, Lam K L, Losasso T J, Olch A J, Palta J R, Reinstein L E, Ritt D and Wilcox E E 2007 TG-69: Radiographic Film for Megavoltage Beam Dosimetry *Medical Physics* **34** 2228-58

Ploquin N, Rangel A and Dunscombe P 2008 Phantom evaluation of a commercially available three modality image guided radiation therapy system *Med Phys* **35** 5303-11

Rowbottom C G and Jaffray D A 2004 Development of an integral system test for image-guided radiotherapy *Med Phys* **31** 3500-5

Simon M and Sauerwein C 2000 Quality control of Light Metal Castings by 3D Computed Tomography. (Meersburg, Germany) http://www.ndt.net/article/wcndt00/papers/idn730/idn730.htm (Hans Wälischmiller GmbH)

Vinci J 2007 Accuracy of Cranial Coplanar Beam Therapy With Brainlab Exactrac Image Guidance. In: *MS in Medical Physics and Health Physics, Department of Physics and Astronomy,* (Baton Rouge, LA: Louisiana State University)

Vinci J P, Hogstrom K R and Neck D W 2008 Accuracy of cranial coplanar beam therapy using an oblique, stereoscopic x-ray image guidance system *Med Phys* **35** 3809-19

Wambersie A and Landberg T 1999 ICRU 62: Prescribing, Recording and Reporting Photon Beam Therapy (Supplement to ICRU Report 50). In: *International Commission on Radiation Units and Measurements,*

Webster G J, Rowbottom C G and Mackay R I 2009 Accuracy and precision of an IGRT solution *Med Dosim* **34** 99-106

APPENDIX. GRAPHS AND TABLES

The graphs and tables in this appendix collate all experimental data acquired during this project. Figures A.1 through A.33 show measured, mean, and treatment planning profiles for all points in sample space when using kVCBCT image guidance.

Tables A.1, A.2, and A.3 provide the results for all the treatments delivered with kVCBCT image guidance. Positive values of Δc indicated that the measured profile was shifted to the left, posterior, or inferior direction with respect to the calculated profile from the treatment plan. Positive values of $\Delta 80$ indicated that the measured 80% isodose line was outside the calculated (planned) 80% isodose line. Conversely, negative values of $\Delta 80$ indicated that the measured 80% isodose line was inside the calculated (planned) 80% isodose line. The means, standard deviations (σ) and the standard errors (SE) are all in millimeters.

Figures A.34 through A.66 show measured, mean, and treatment planning profiles for all points in sample space when using kVCBCT image guidance.

Tables A.4 and A.5 collate the couch movement measurements to assess the accuracy of couch motion.

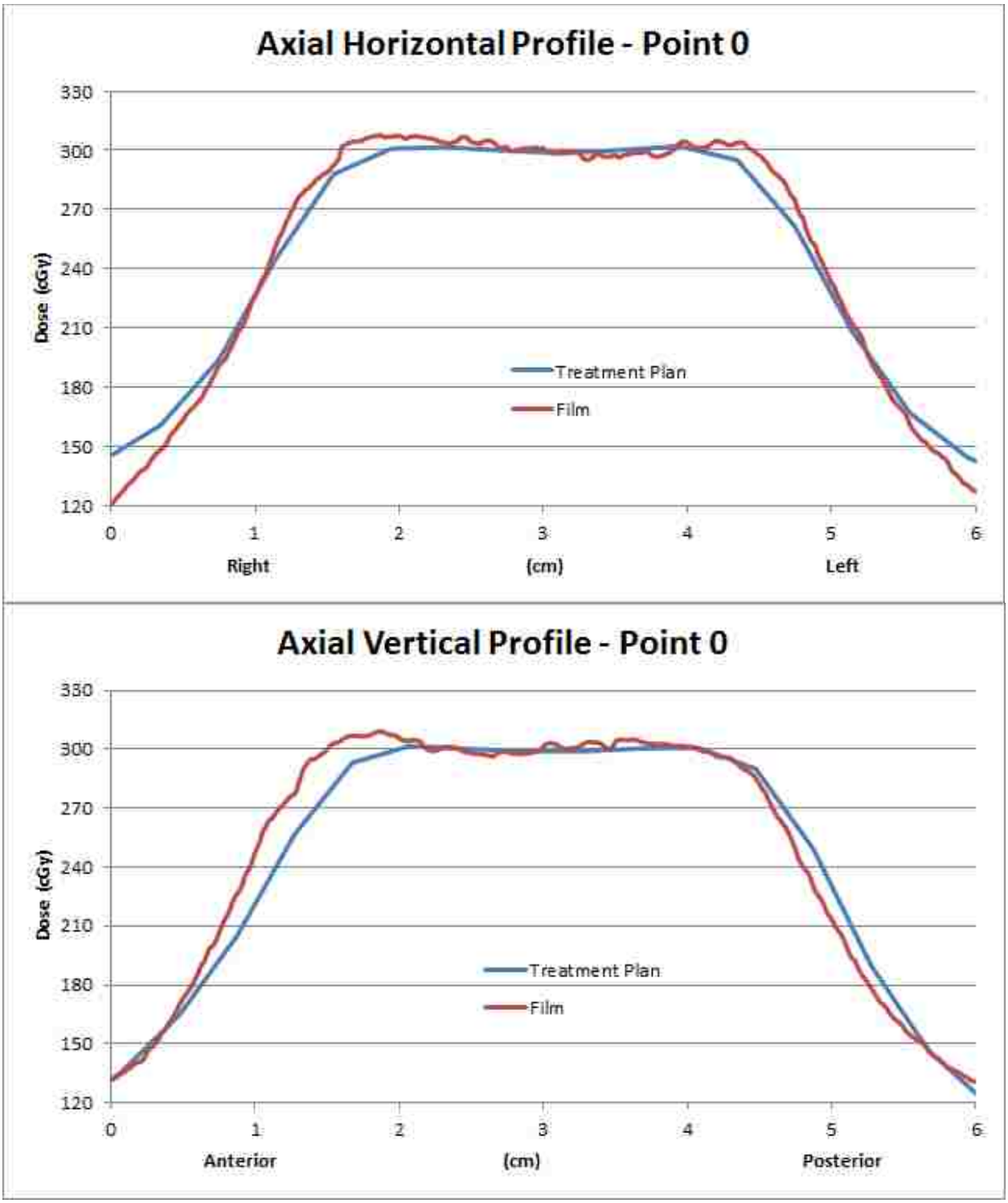

Figure A.1: Horizontal and vertical profiles for the axial image plane resulting from kVCBCT image guidance when the phantom was initially positioned at sample point 0.

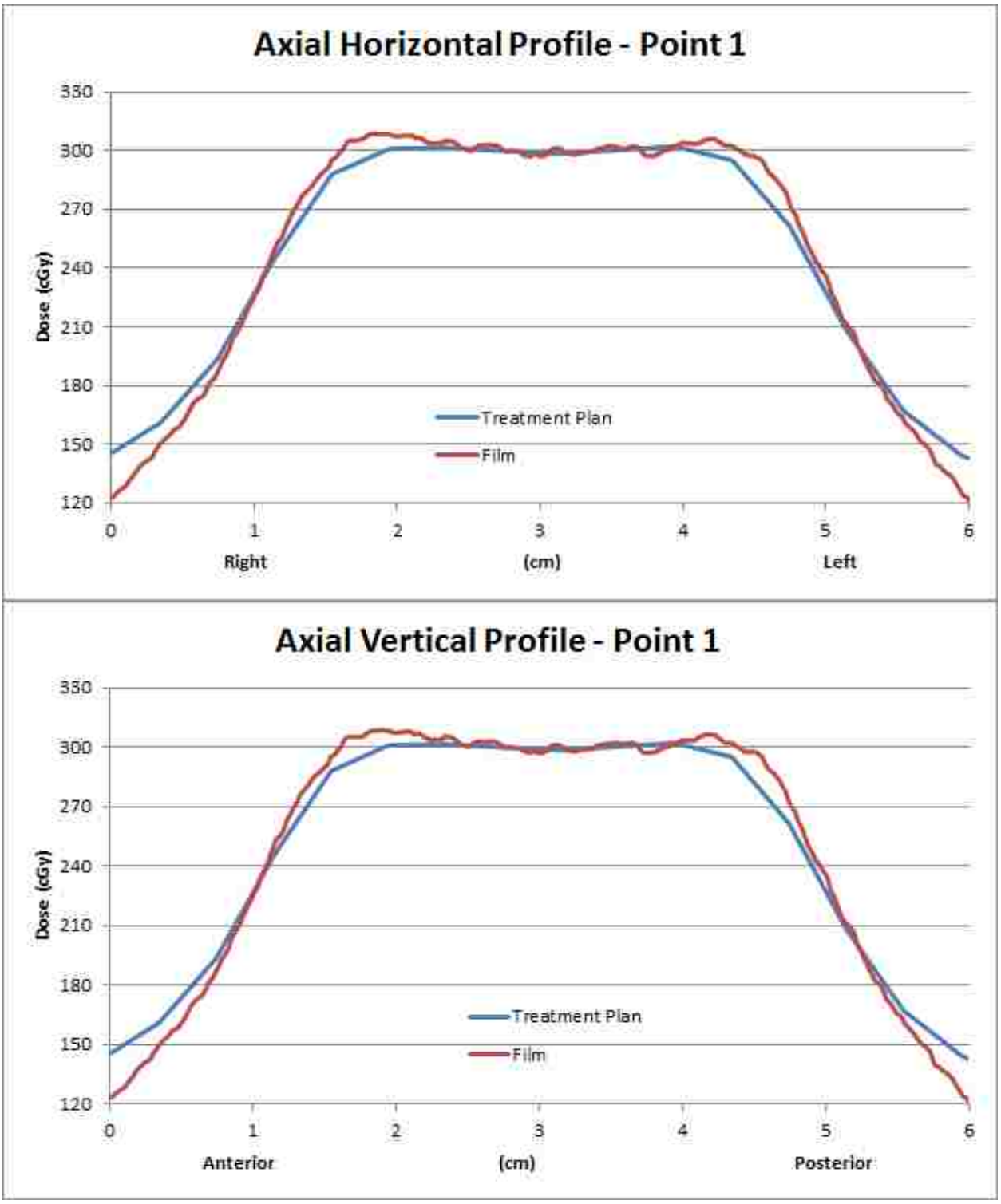

Figure A.2: Horizontal and vertical profiles for the axial image plane resulting from kVCBCT image guidance when the phantom was initially positioned at sample point 1.

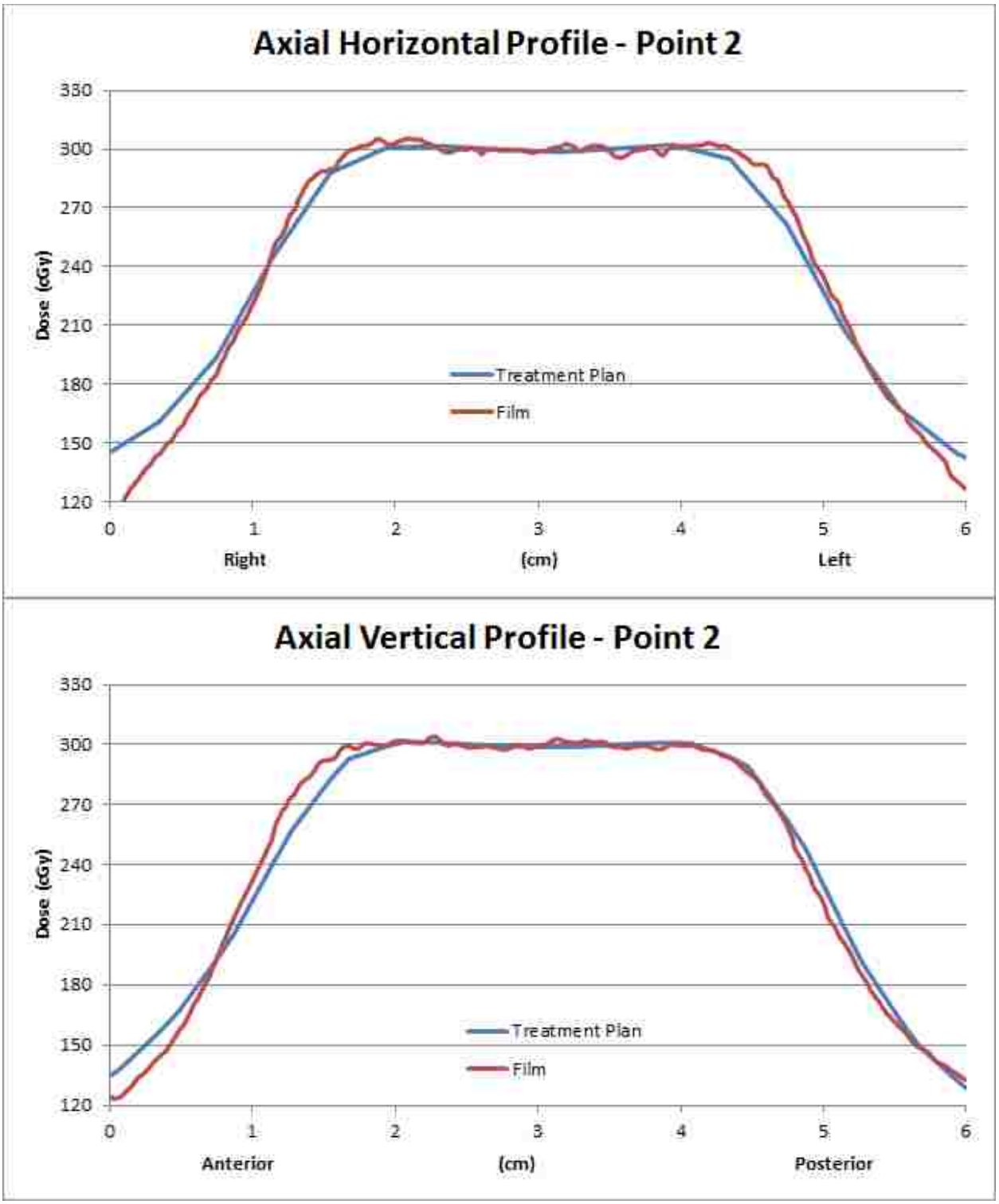

Figure A.3: Horizontal and vertical profiles for the axial image plane resulting from kVCBCT image guidance when the phantom was initially positioned at sample point 2.

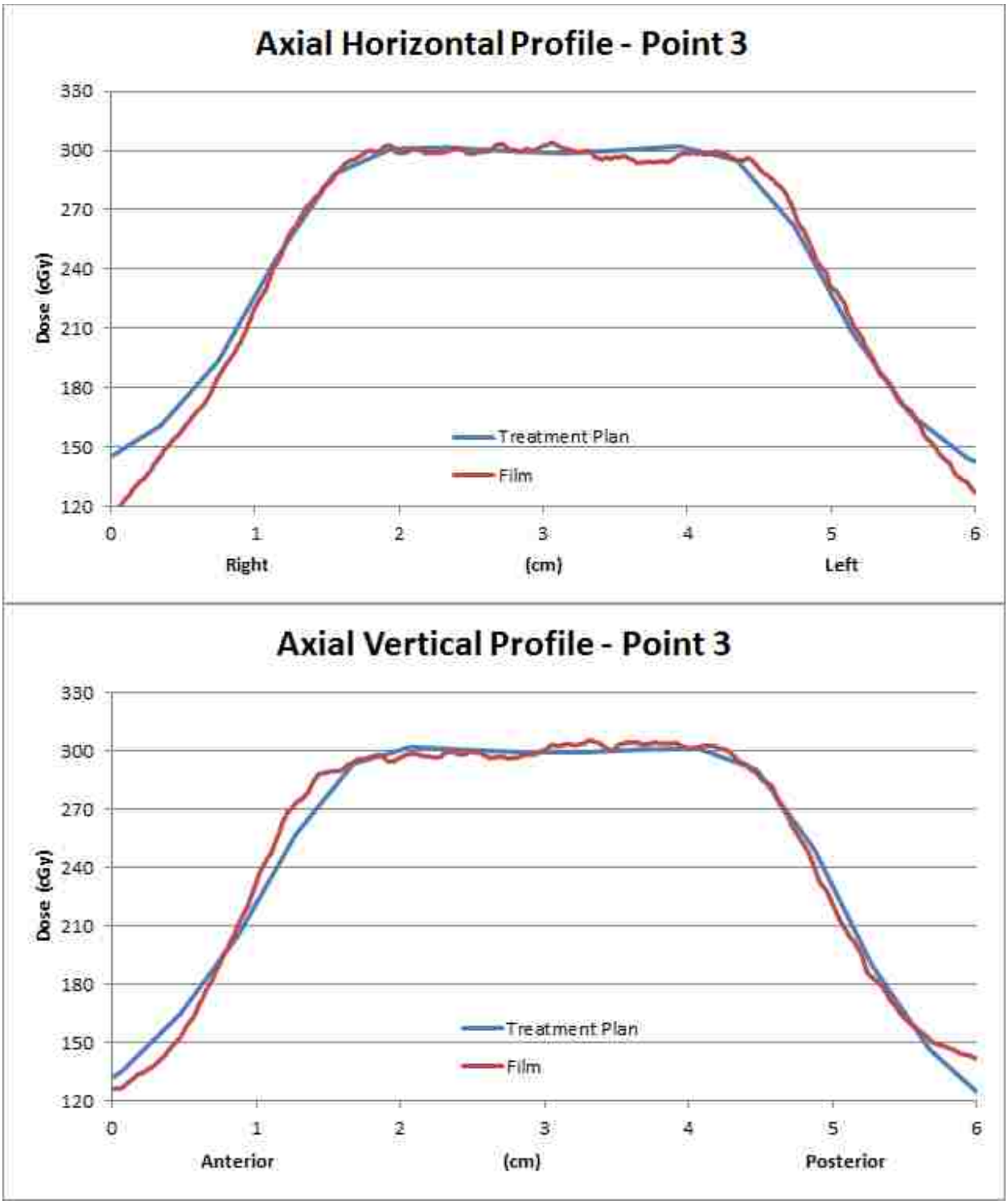

Figure A.4: Horizontal and vertical profiles for the axial image plane resulting from kVCBCT image guidance when the phantom was initially positioned at sample point 3.

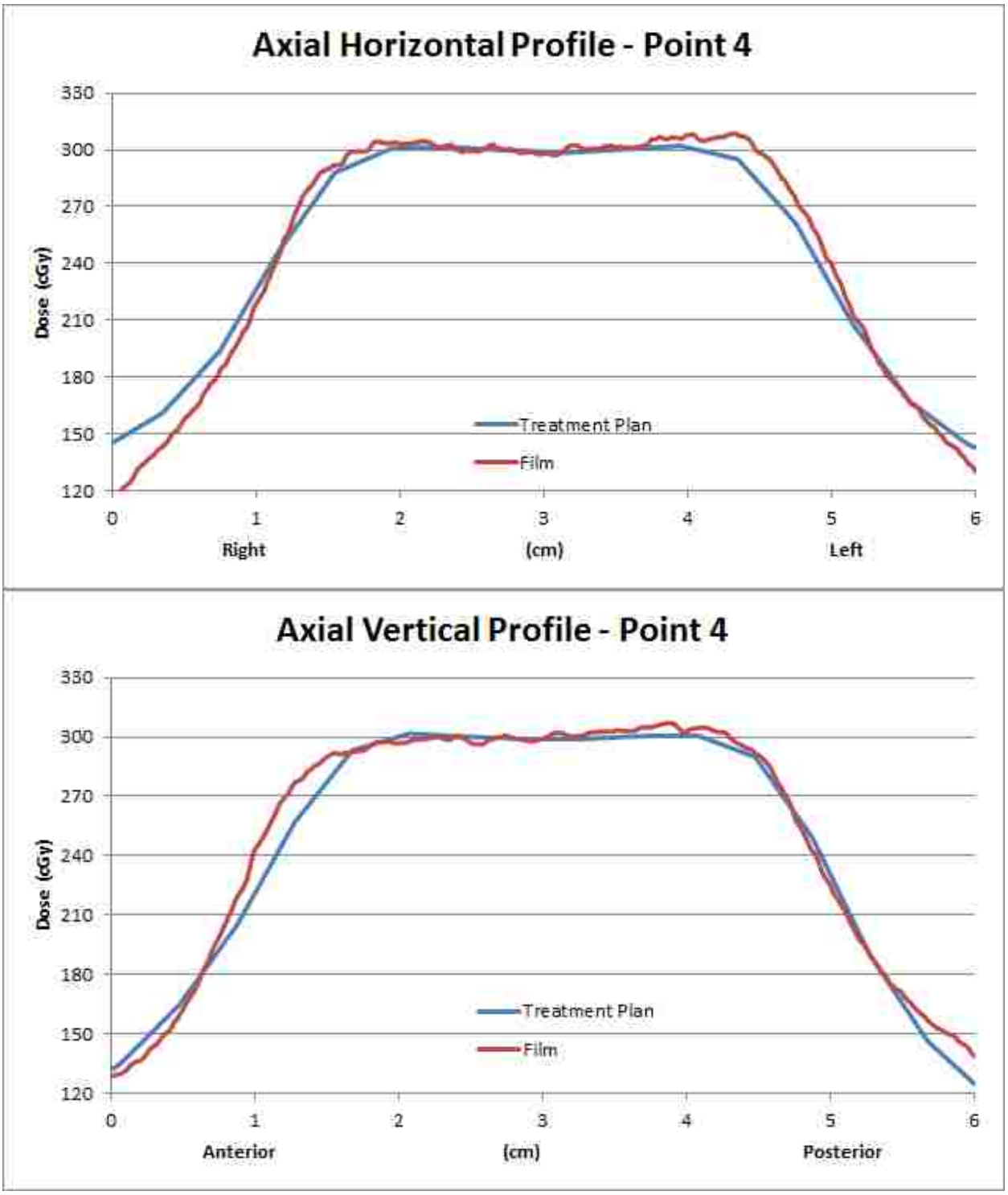

Figure A.5: Horizontal and vertical profiles for the axial image plane resulting from kVCBCT image guidance when the phantom was initially positioned at sample point 4.

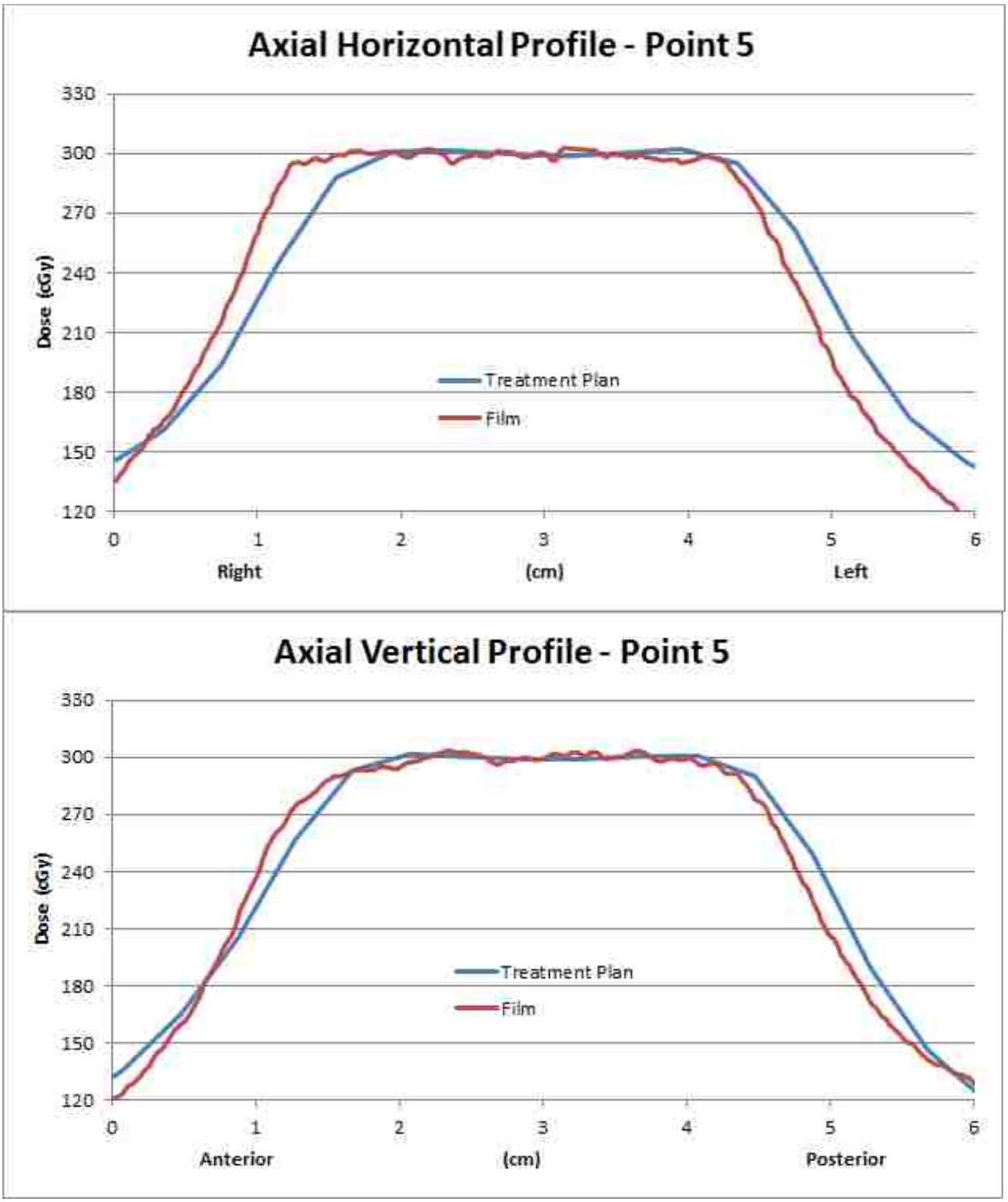

Figure A.6: Horizontal and vertical profiles for the axial image plane resulting from kVCBCT image guidance when the phantom was initially positioned at sample point 5.

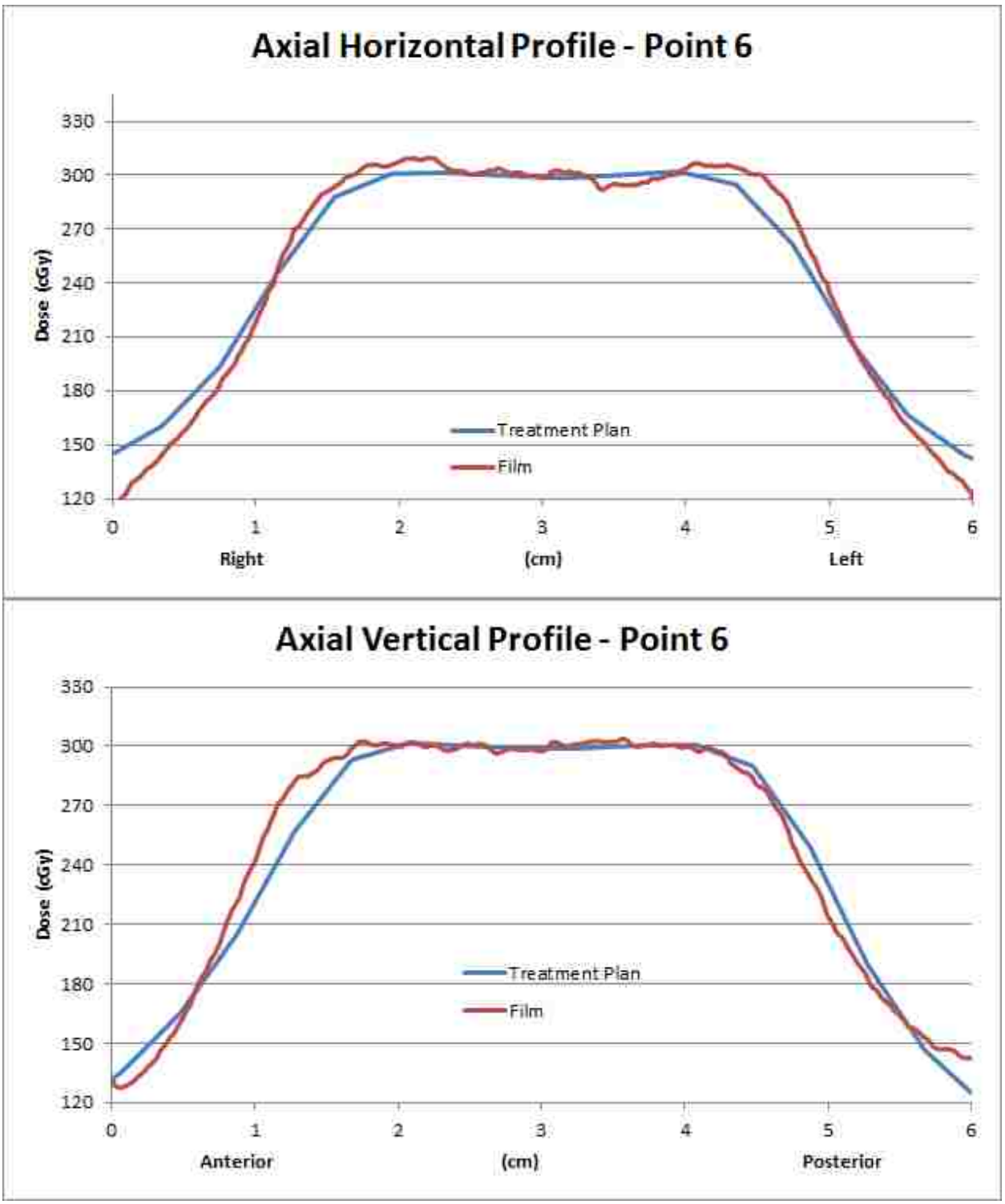

Figure A.7: Horizontal and vertical profiles for the axial image plane resulting from kVCBCT image guidance when the phantom was initially positioned at sample point 6.

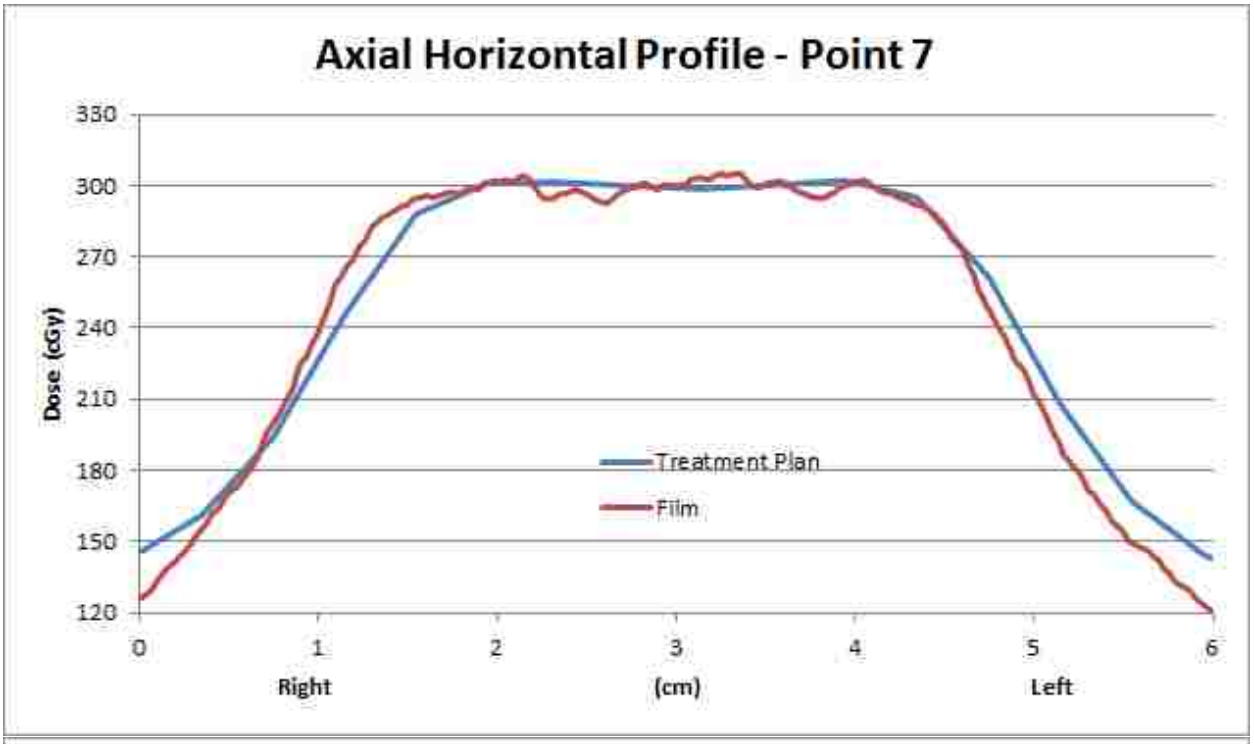

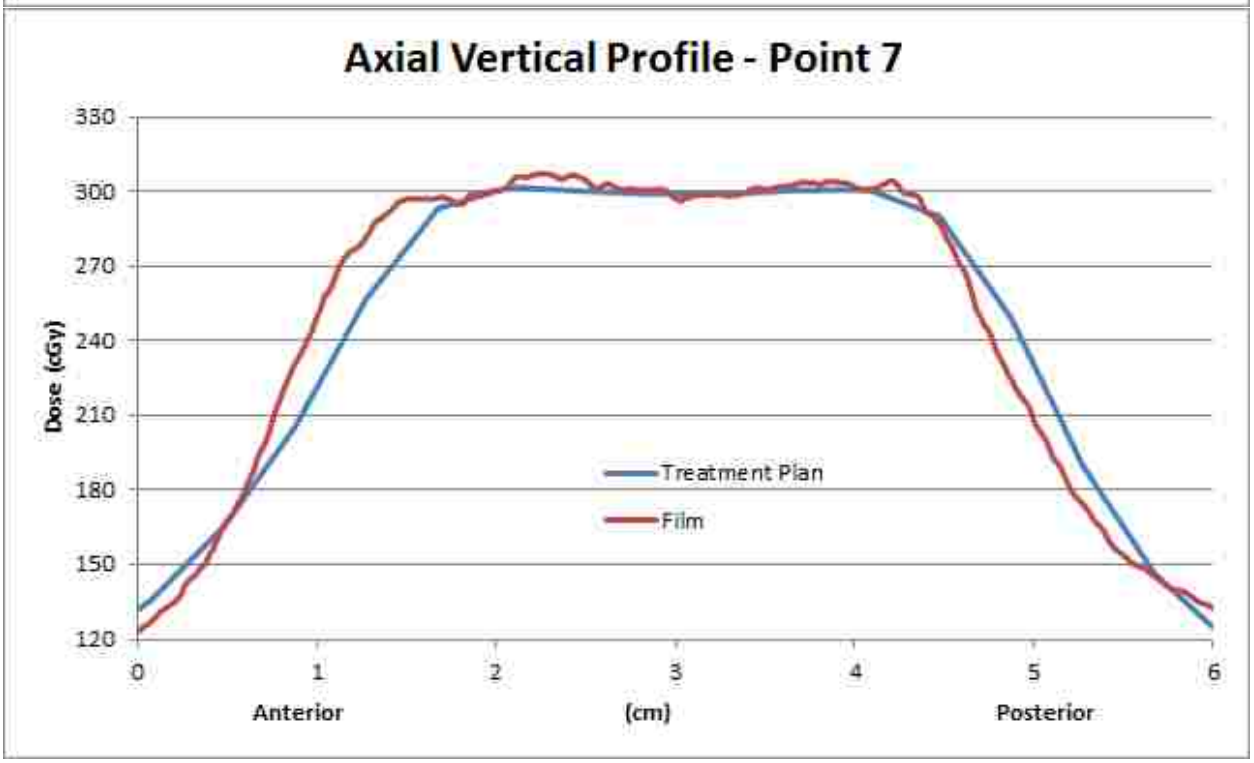

Figure A.8: Horizontal and vertical profiles for the axial image plane resulting from kVCBCT image guidance when the phantom was initially positioned at sample point 7.

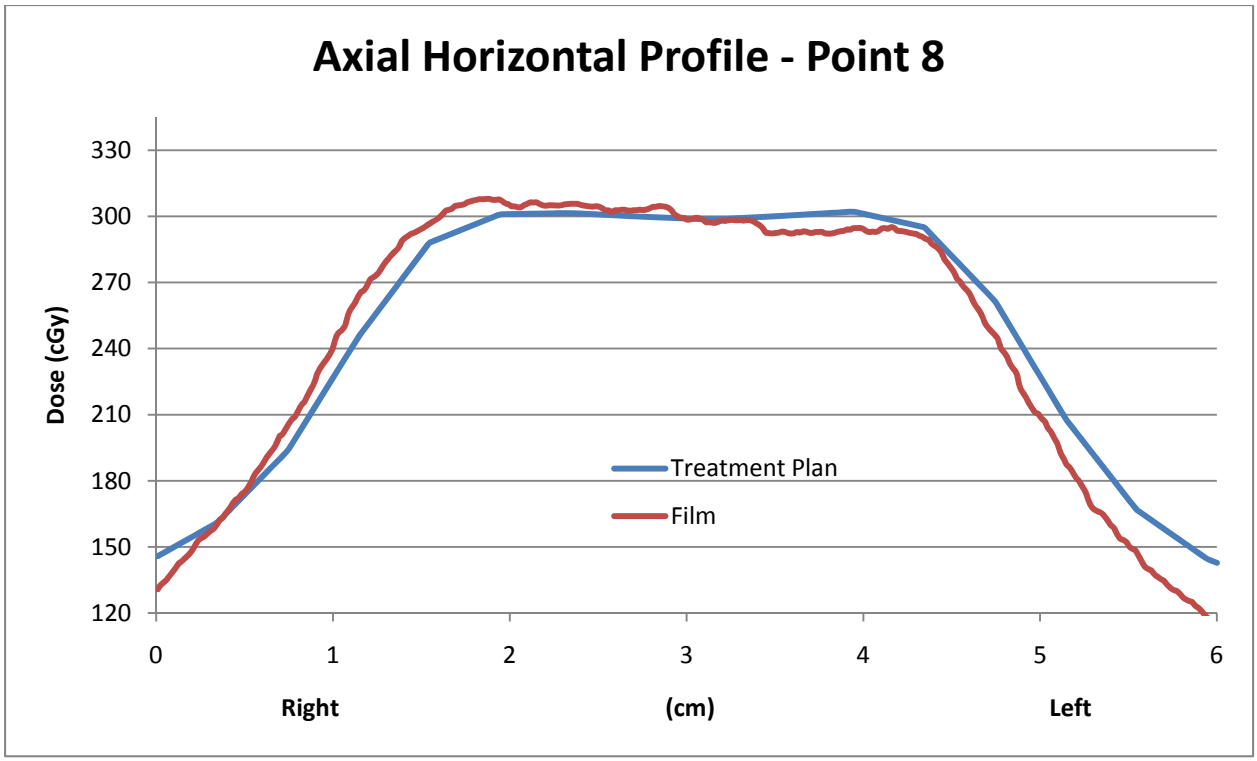

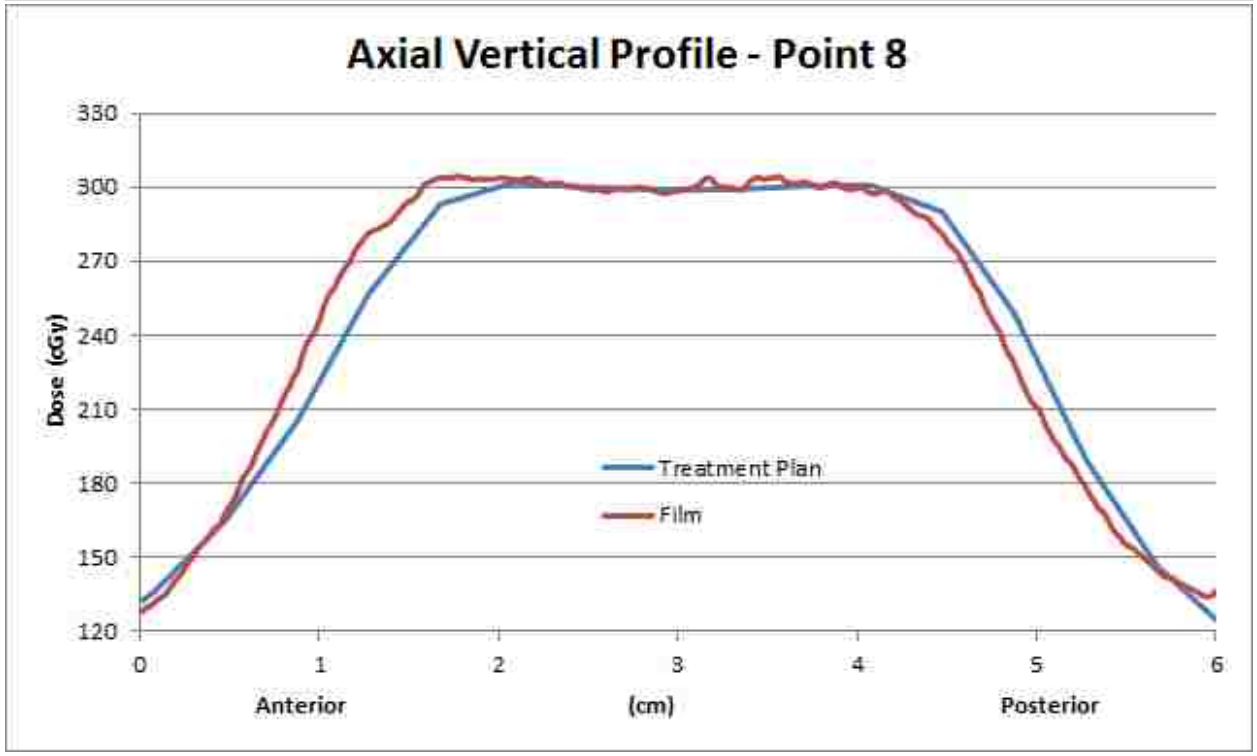

Figure A.9: Horizontal and vertical profiles for the axial image plane resulting from kVCBCT image guidance when the phantom was initially positioned at sample point 8.

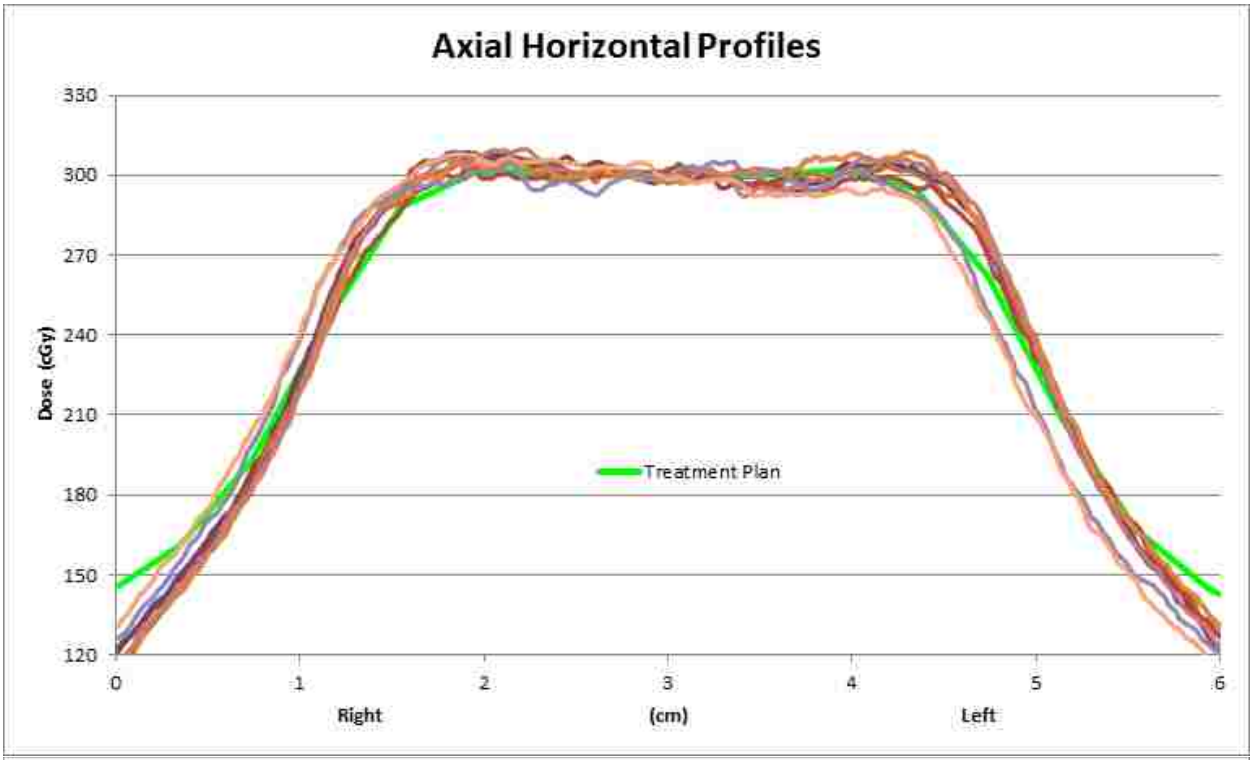

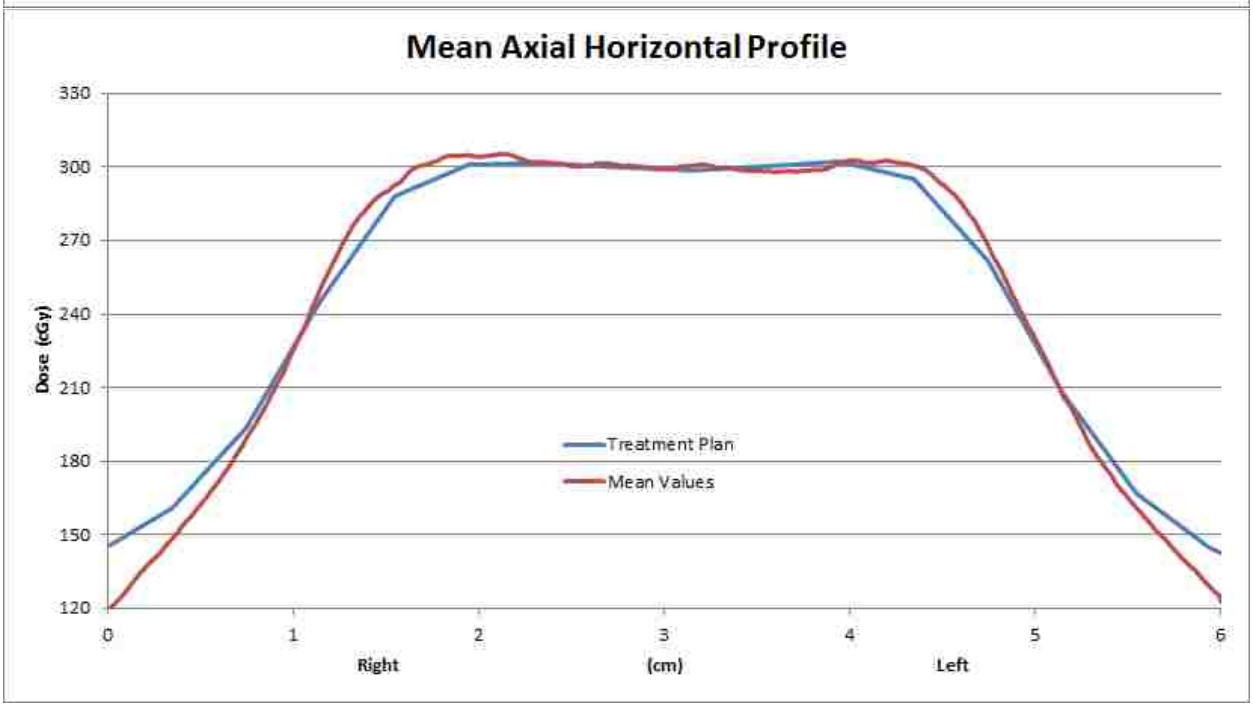

Figure A.10: (top) All horizontal profiles for the axial image plane resulting from kVCBCT image guidance. (bottom) Comparison of the mean axial horizontal profile with the profile from the treatment plan.

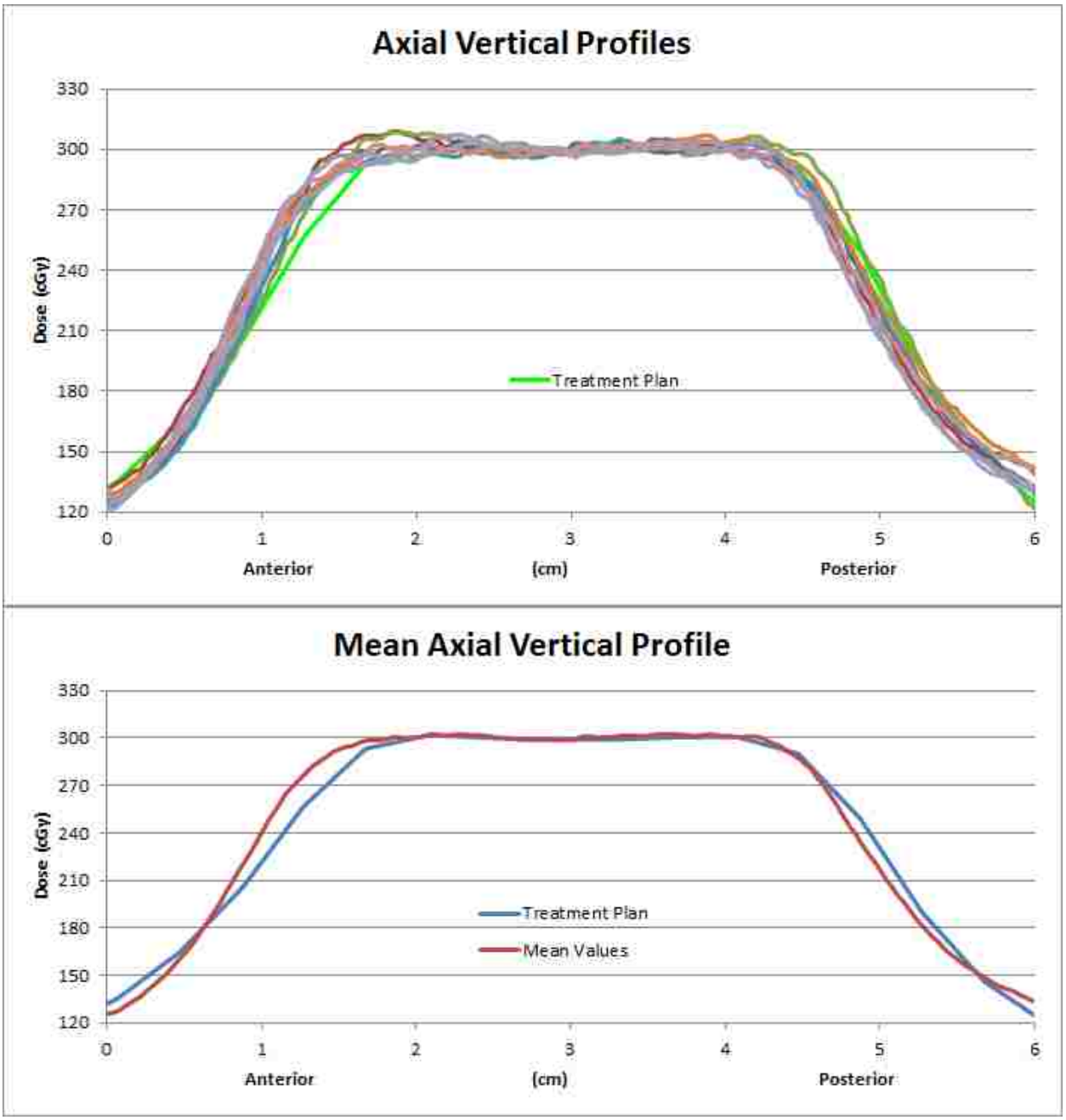

Figure A.11: (top) All vertical profiles for the axial image plane resulting from kVCBCT image guidance. (bottom) Comparison of the mean axial vertical profile with the profile from the treatment plan.

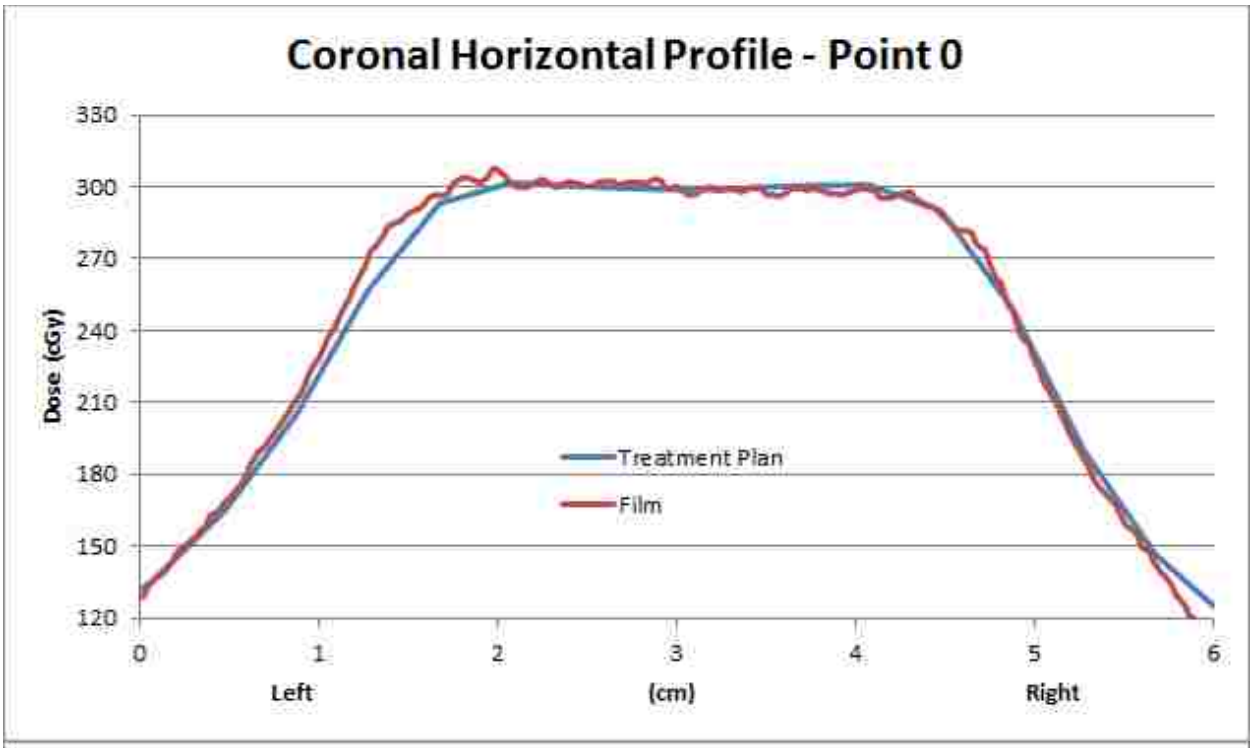

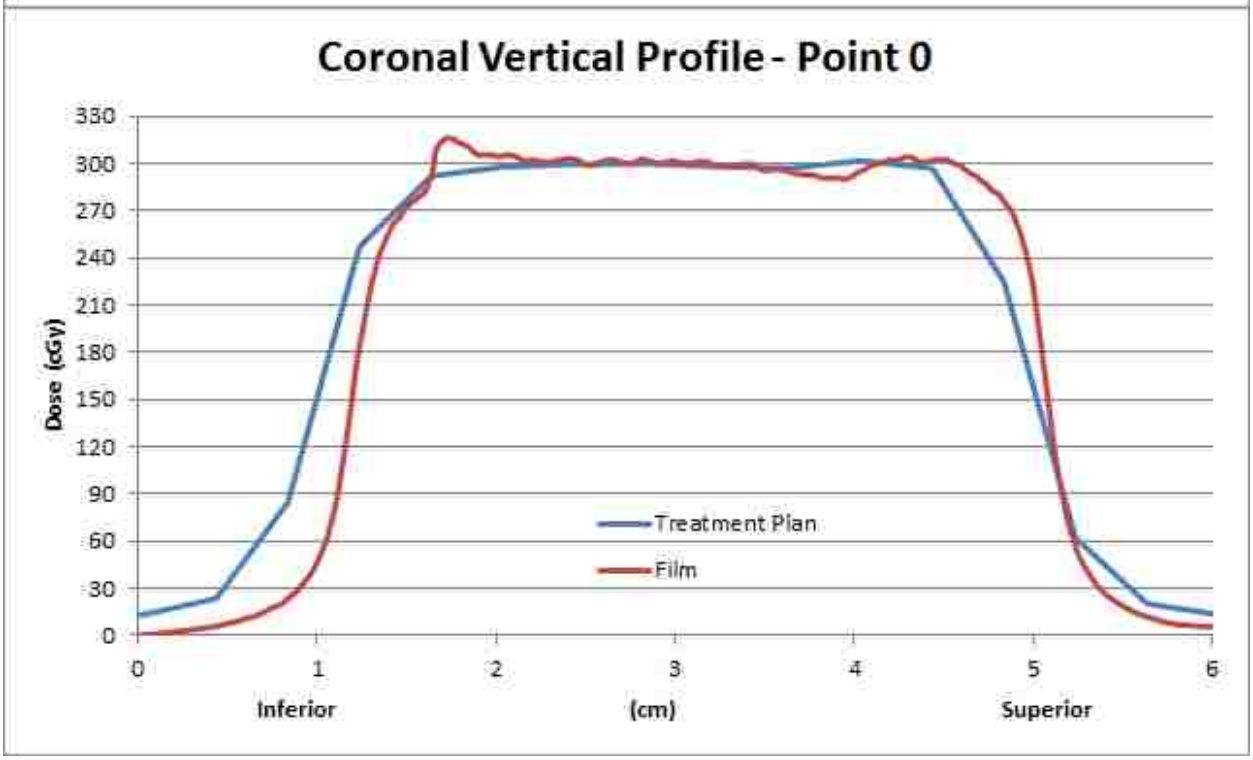

Figure A.12: Horizontal and vertical profiles for the coronal image plane resulting from kVCBCT image guidance when the phantom was initially positioned at sample point 0.

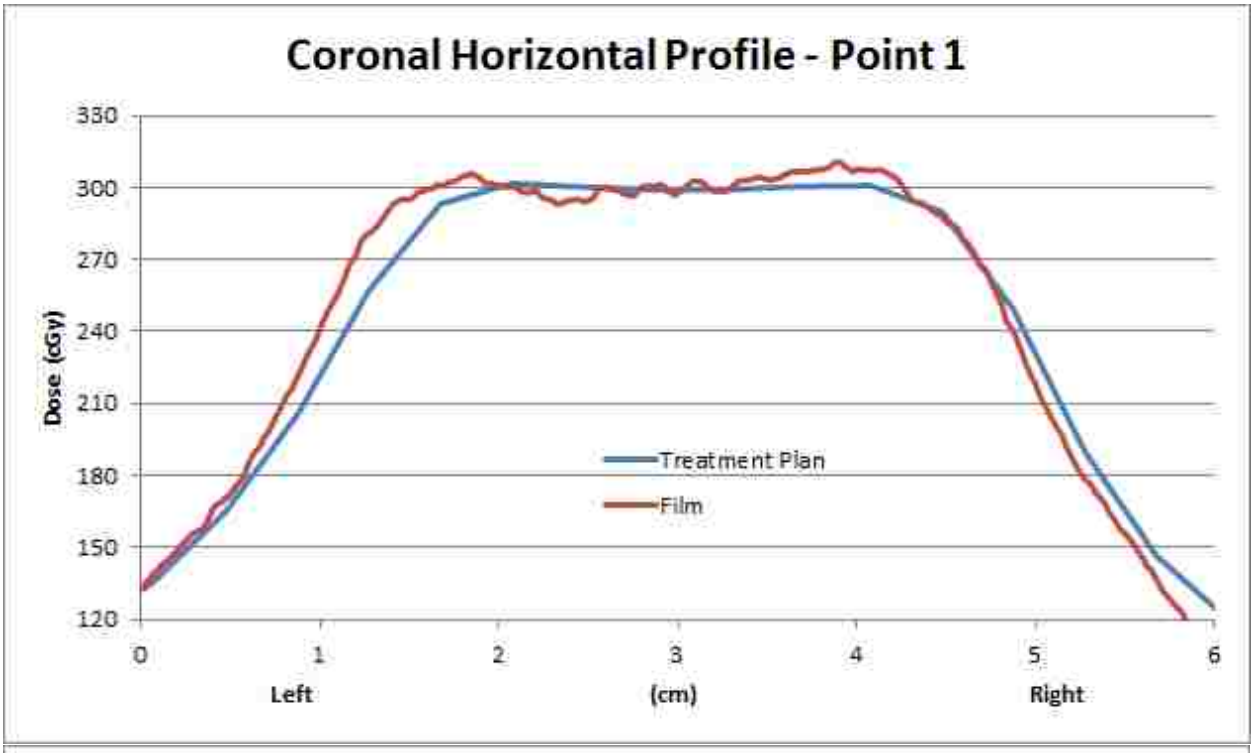

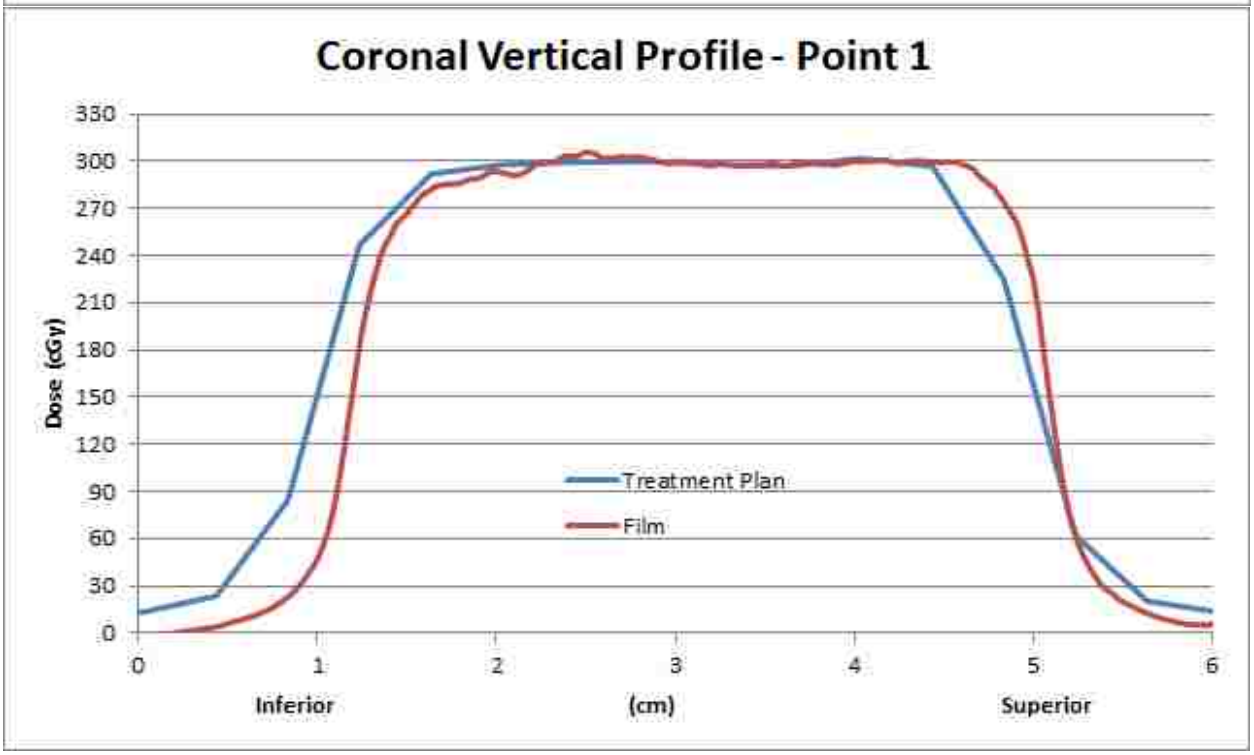

Figure A.13: Horizontal and vertical profiles for the coronal image plane resulting from kVCBCT image guidance when the phantom was initially positioned at sample point 1.

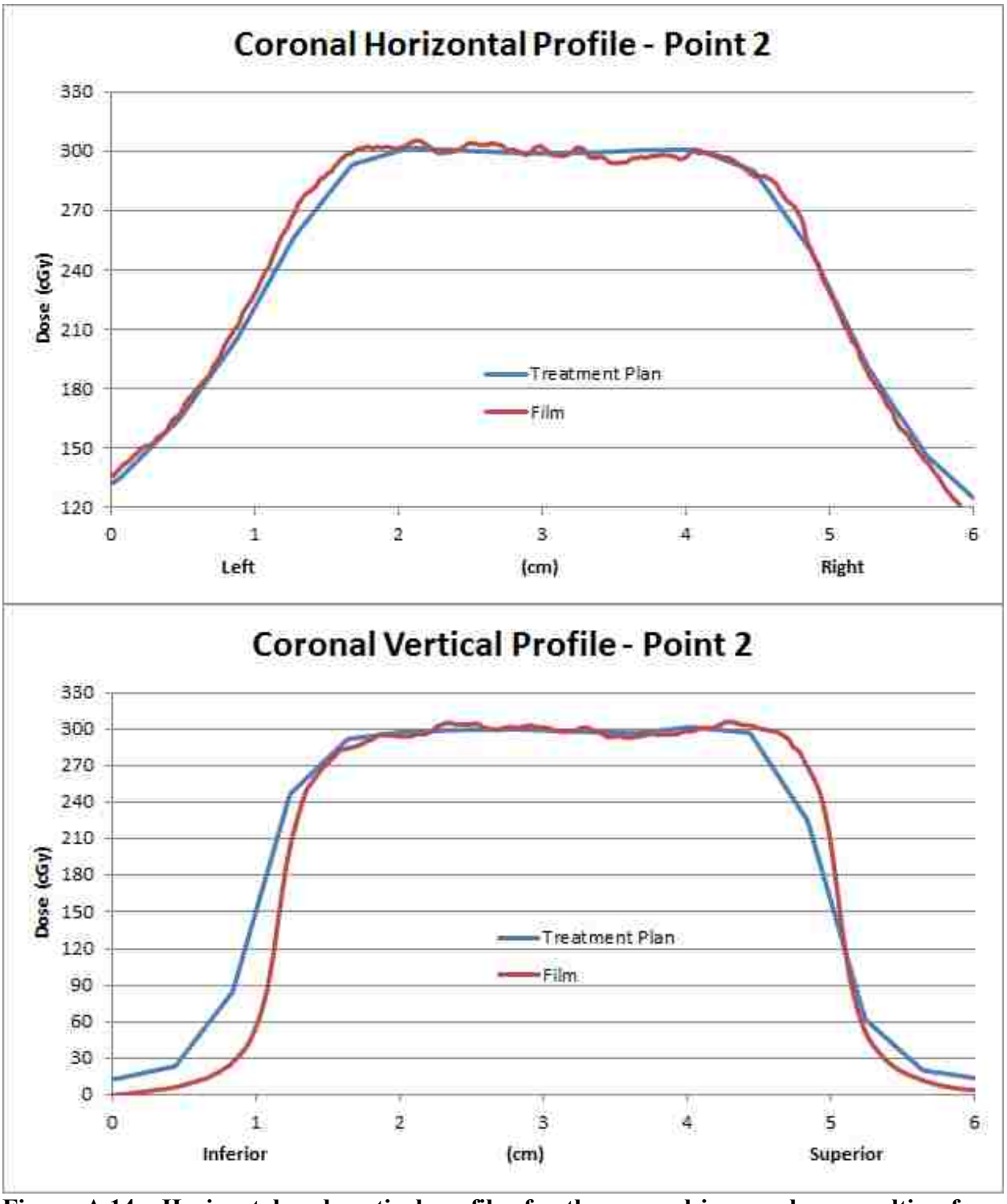

Figure A.14: Horizontal and vertical profiles for the coronal image plane resulting from kVCBCT image guidance when the phantom was initially positioned at sample point 2.

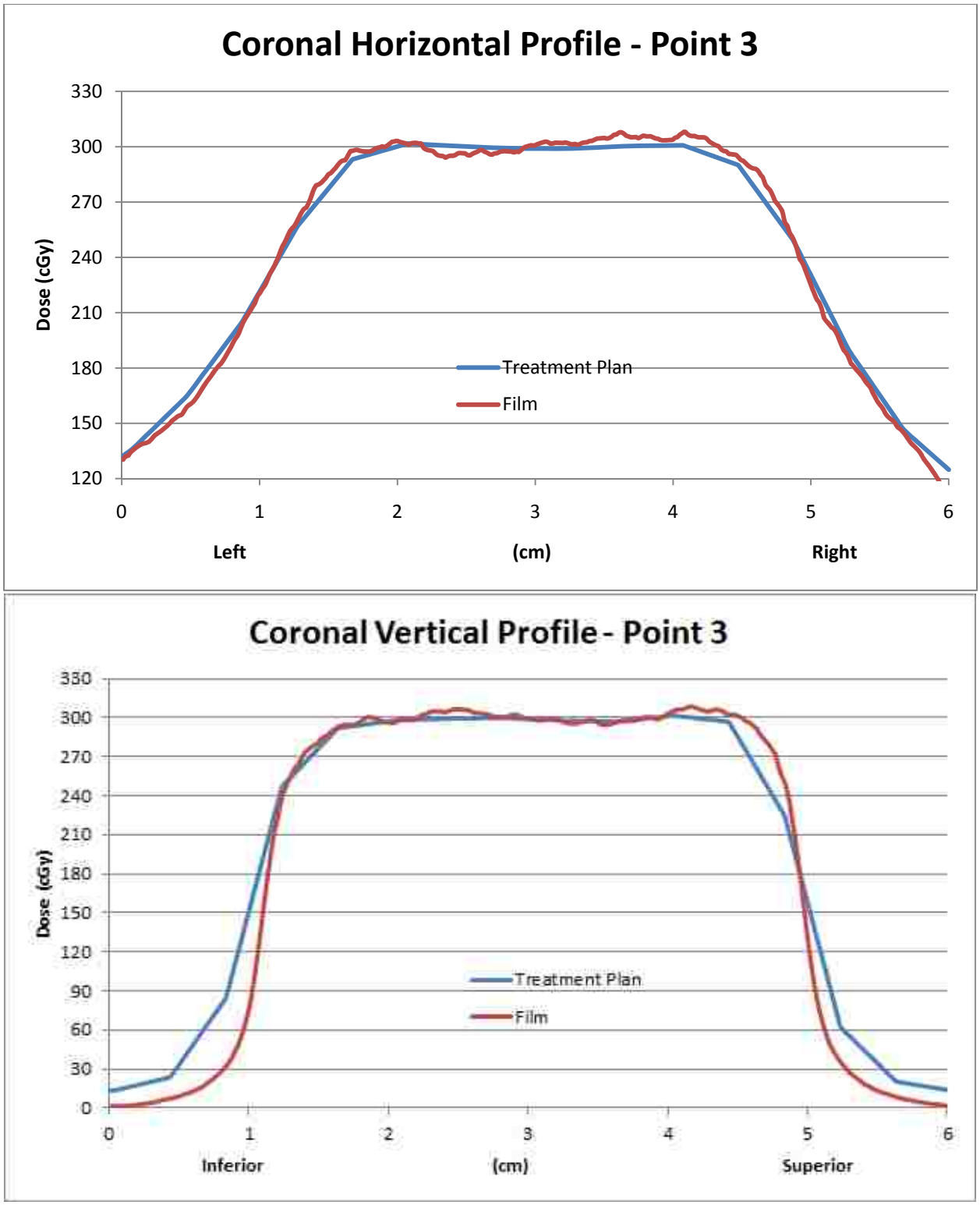

Figure A.15: Horizontal and vertical profiles for the coronal image plane resulting from kVCBCT image guidance when the phantom was initially positioned at sample point 3.

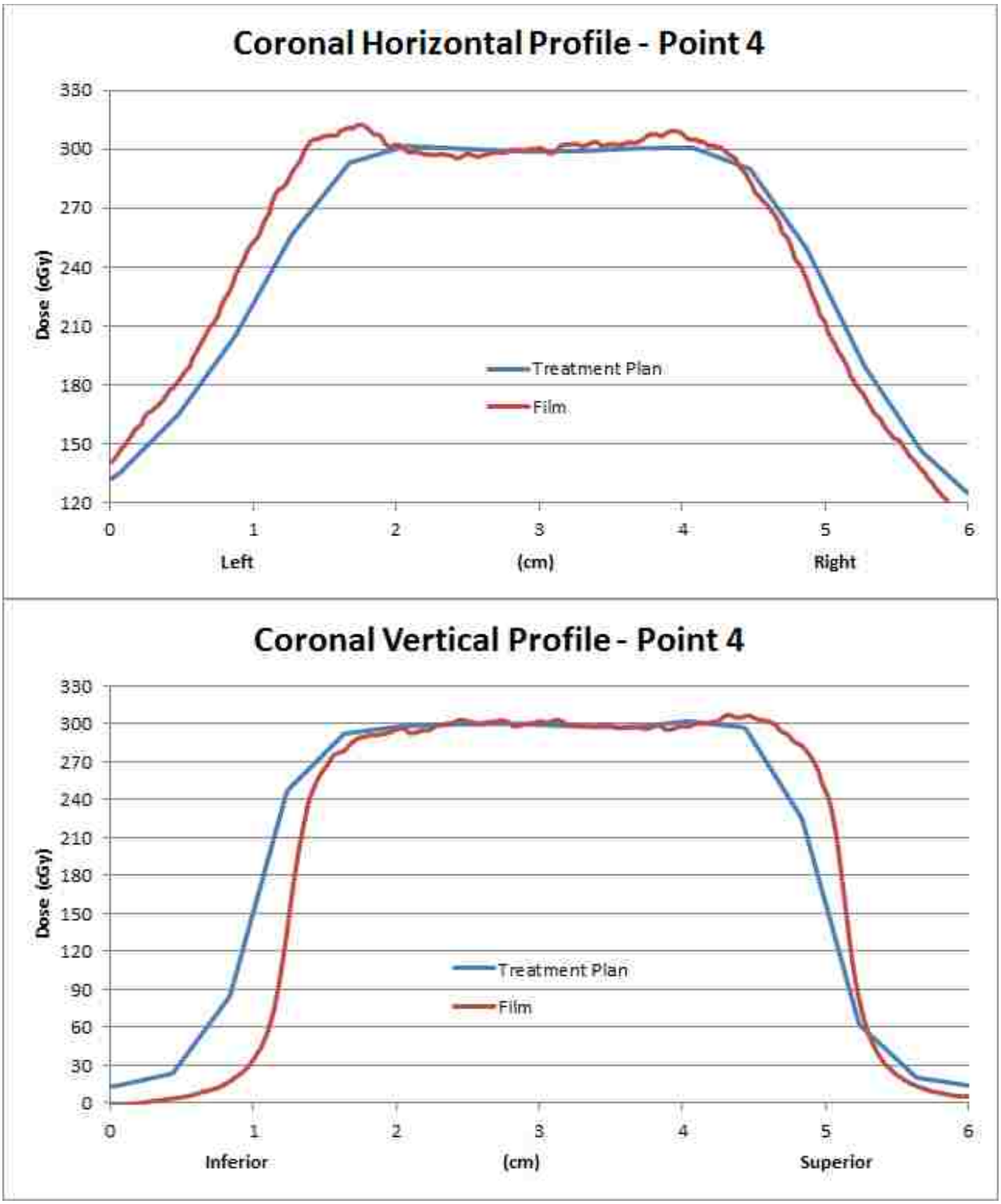

Figure A.16: Horizontal and vertical profiles for the coronal image plane resulting from kVCBCT image guidance when the phantom was initially positioned at sample point 4.

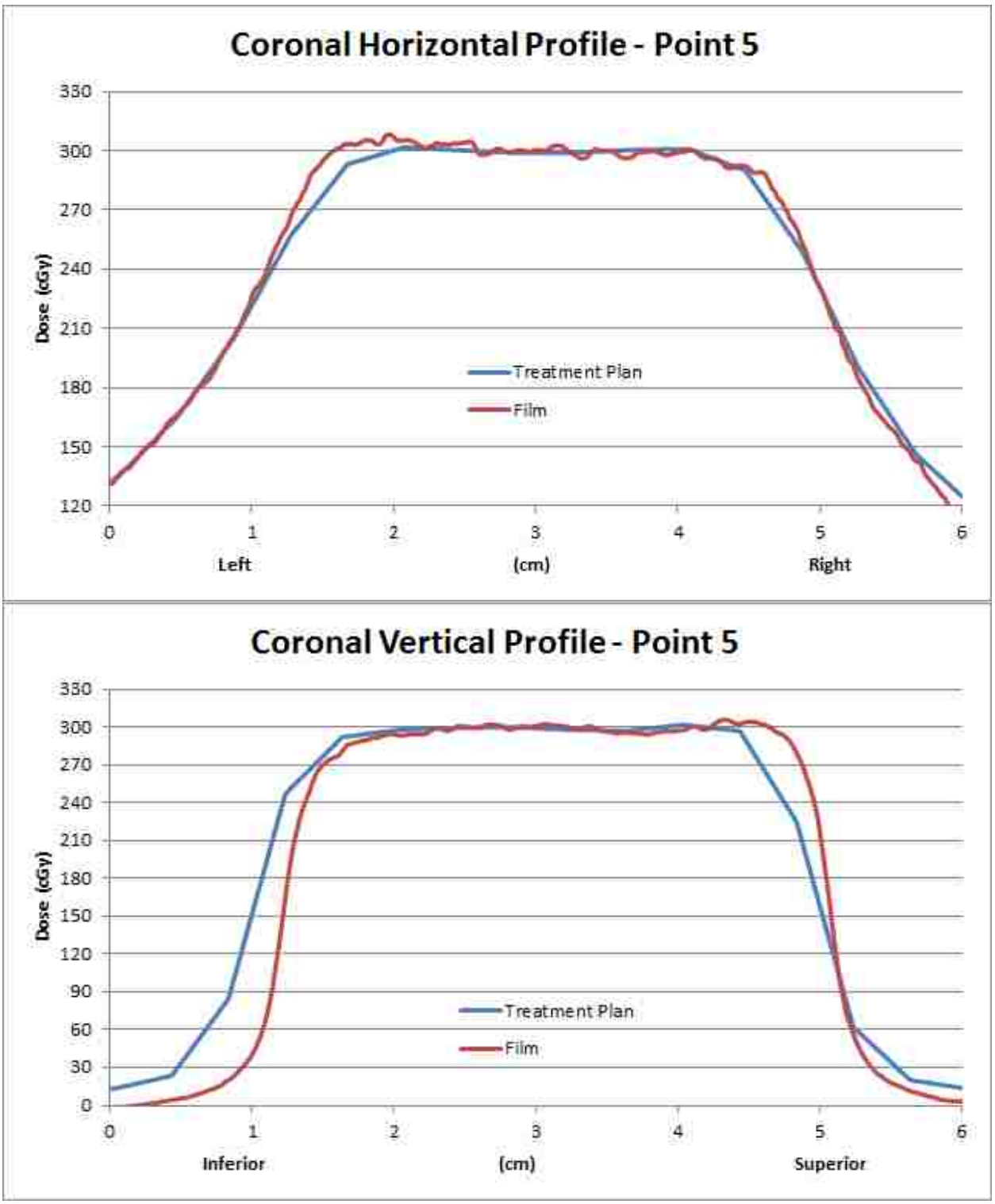

Figure A.17: Horizontal and vertical profiles for the coronal image plane resulting from kVCBCT image guidance when the phantom was initially positioned at sample point 5.

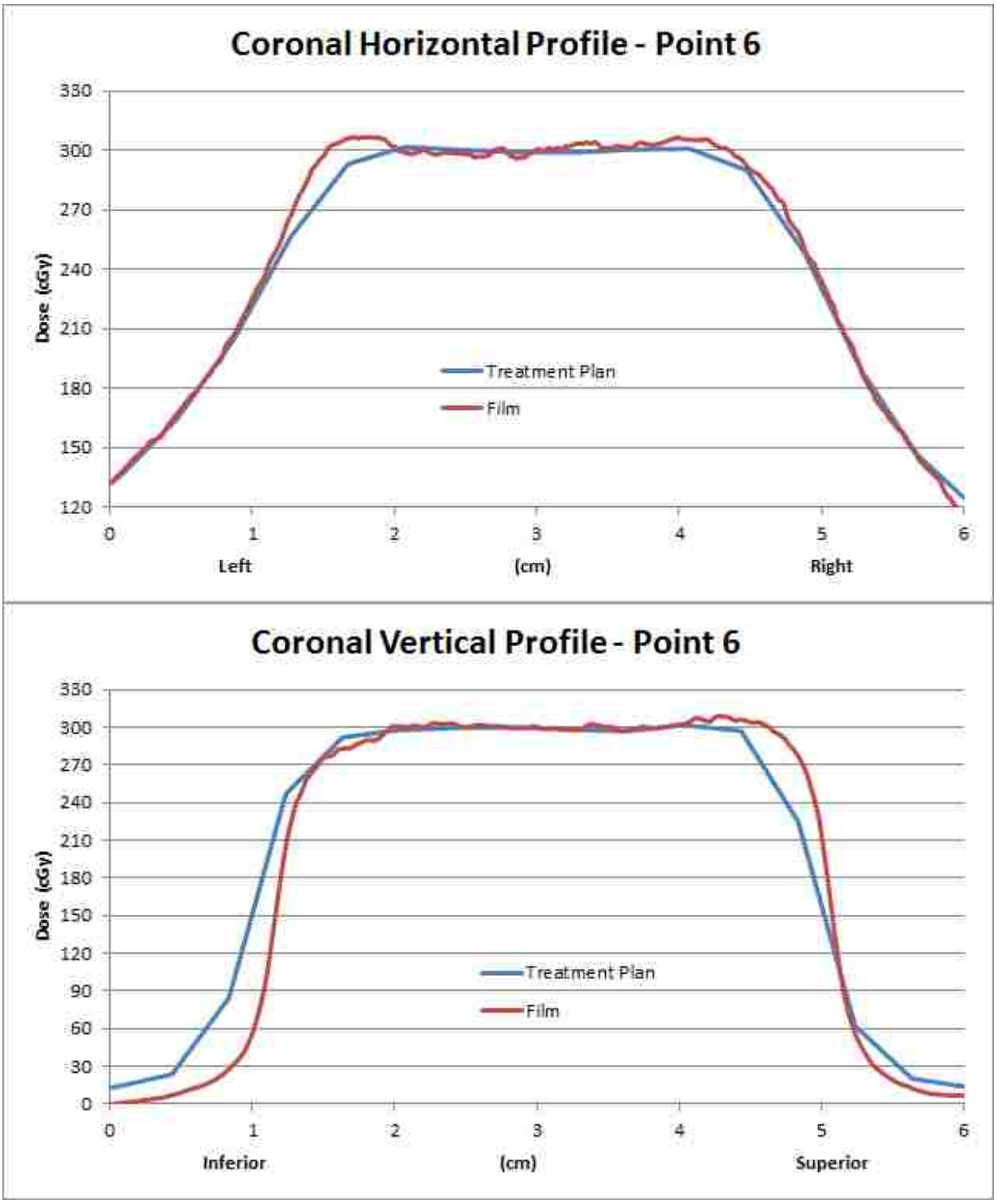

Figure A.18: Horizontal and vertical profiles for the coronal image plane resulting from kVCBCT image guidance when the phantom was initially positioned at sample point 6.

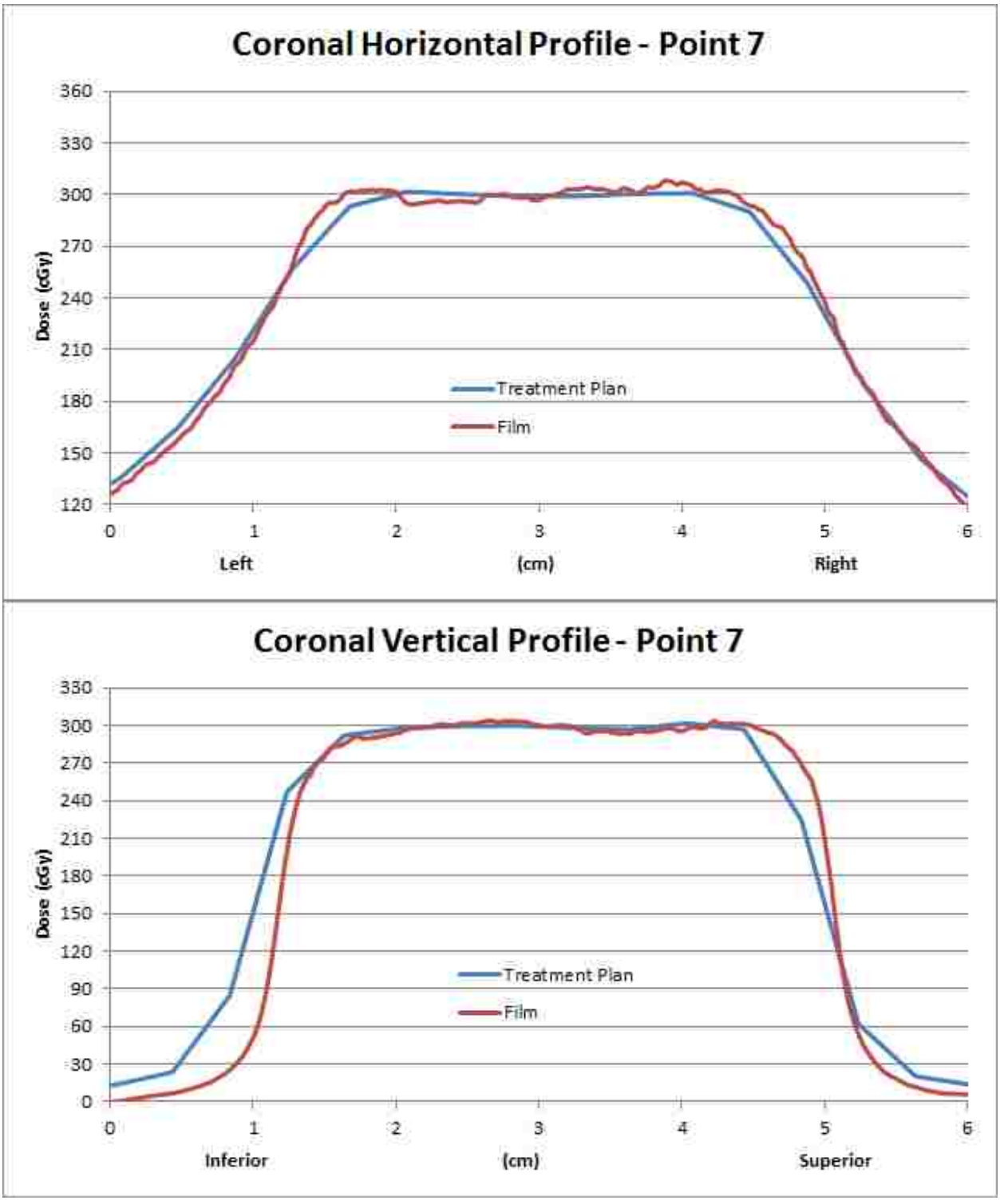

Figure A.19: Horizontal and vertical profiles for the coronal image plane resulting from kVCBCT image guidance when the phantom was initially positioned at sample point 7.

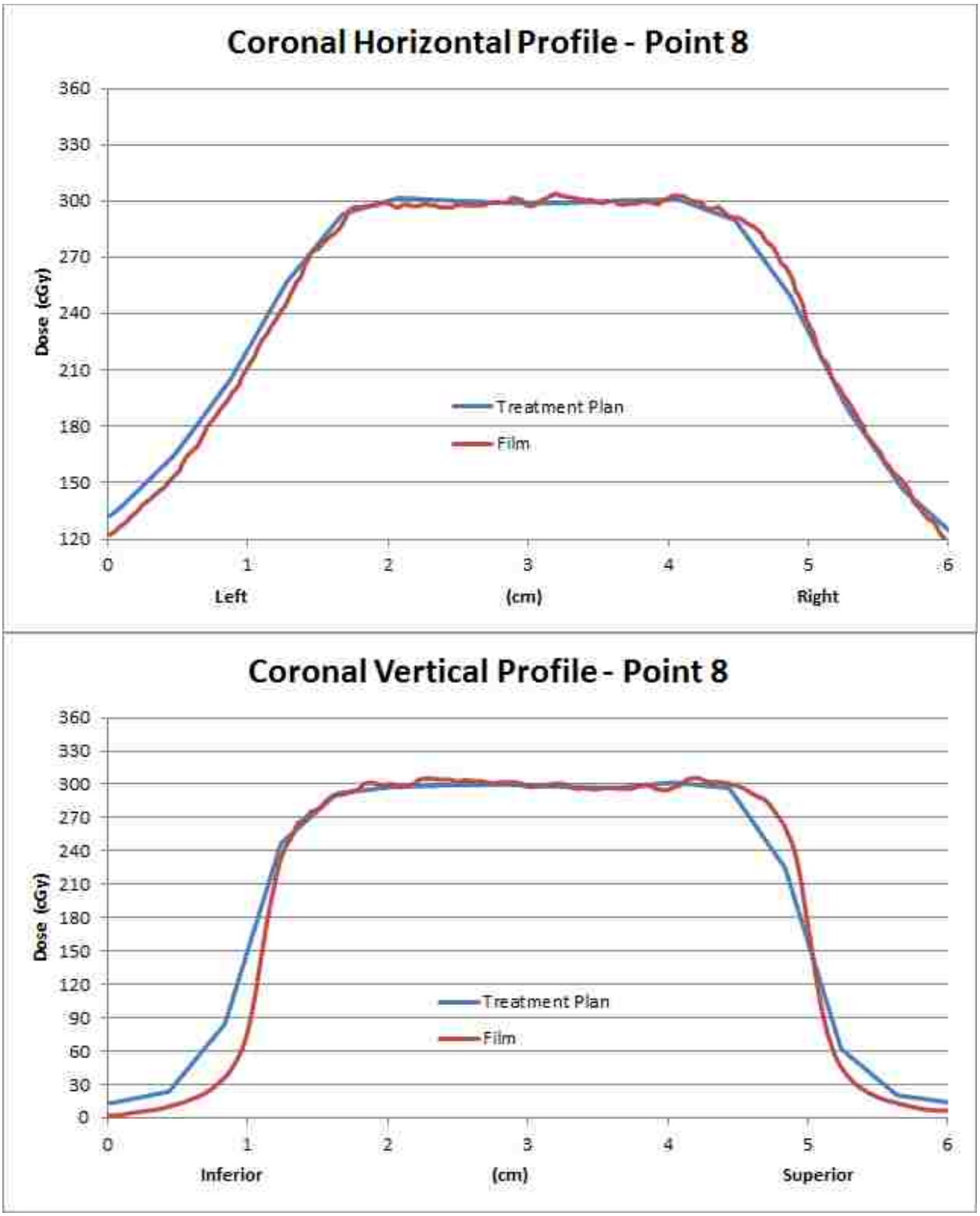

Figure A.20: Horizontal and vertical profiles for the coronal image plane resulting from kVCBCT image guidance when the phantom was initially positioned at sample point 8.

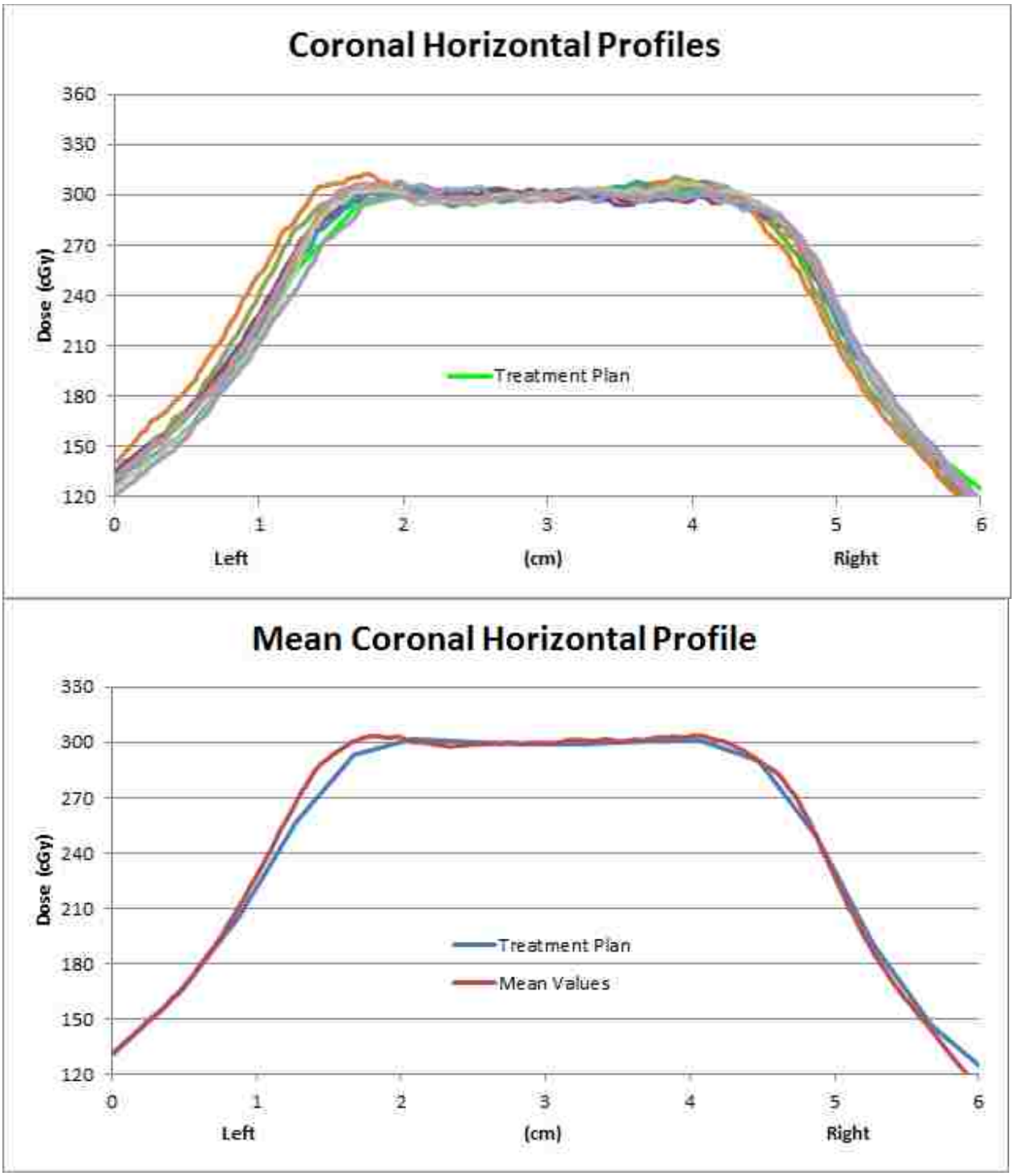

Figure A.21: (top) All horizontal profiles for the coronal image plane resulting from kVCBCT image guidance. (bottom) Comparison of the mean coronal horizontal profile with the profile from the treatment plan.

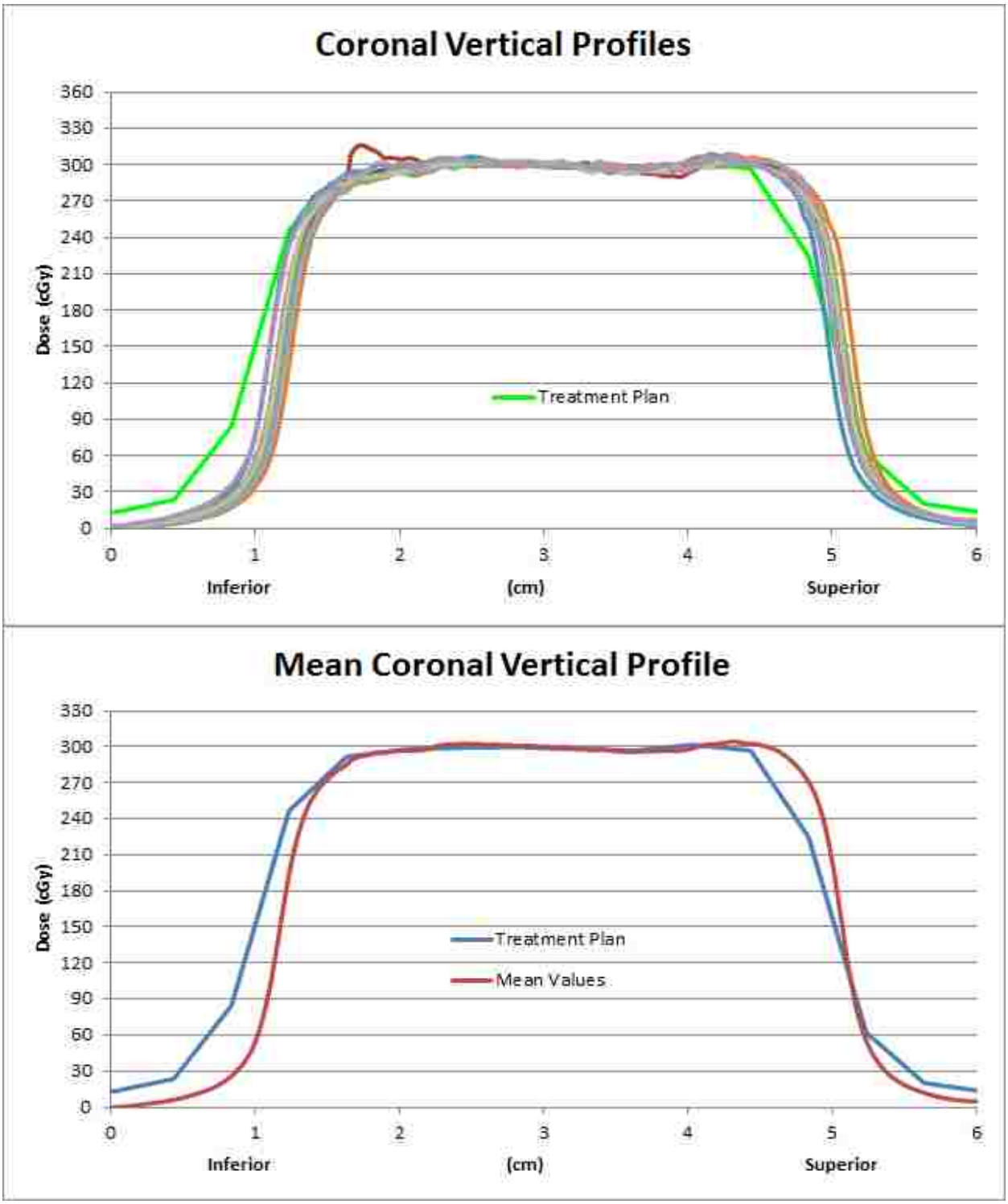

Figure A.22: (top) All vertical profiles for the coronal image plane resulting from kVCBCT image guidance. (bottom) Comparison of the mean coronal vertical profile with the profile from the treatment plan.

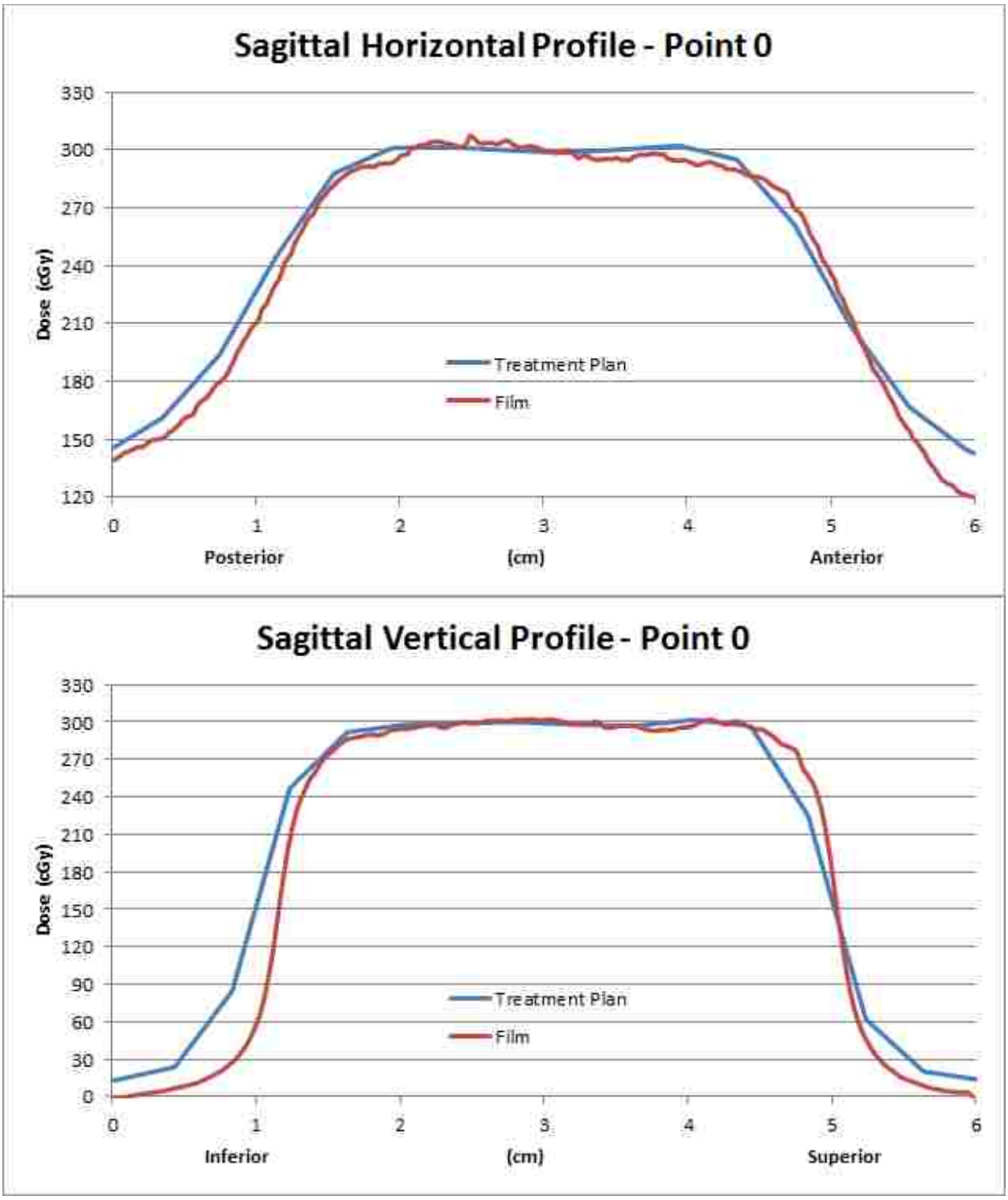

Figure A.23: Horizontal and vertical profiles for the sagittal image plane resulting from kVCBCT image guidance when the phantom was initially positioned at sample point 0.

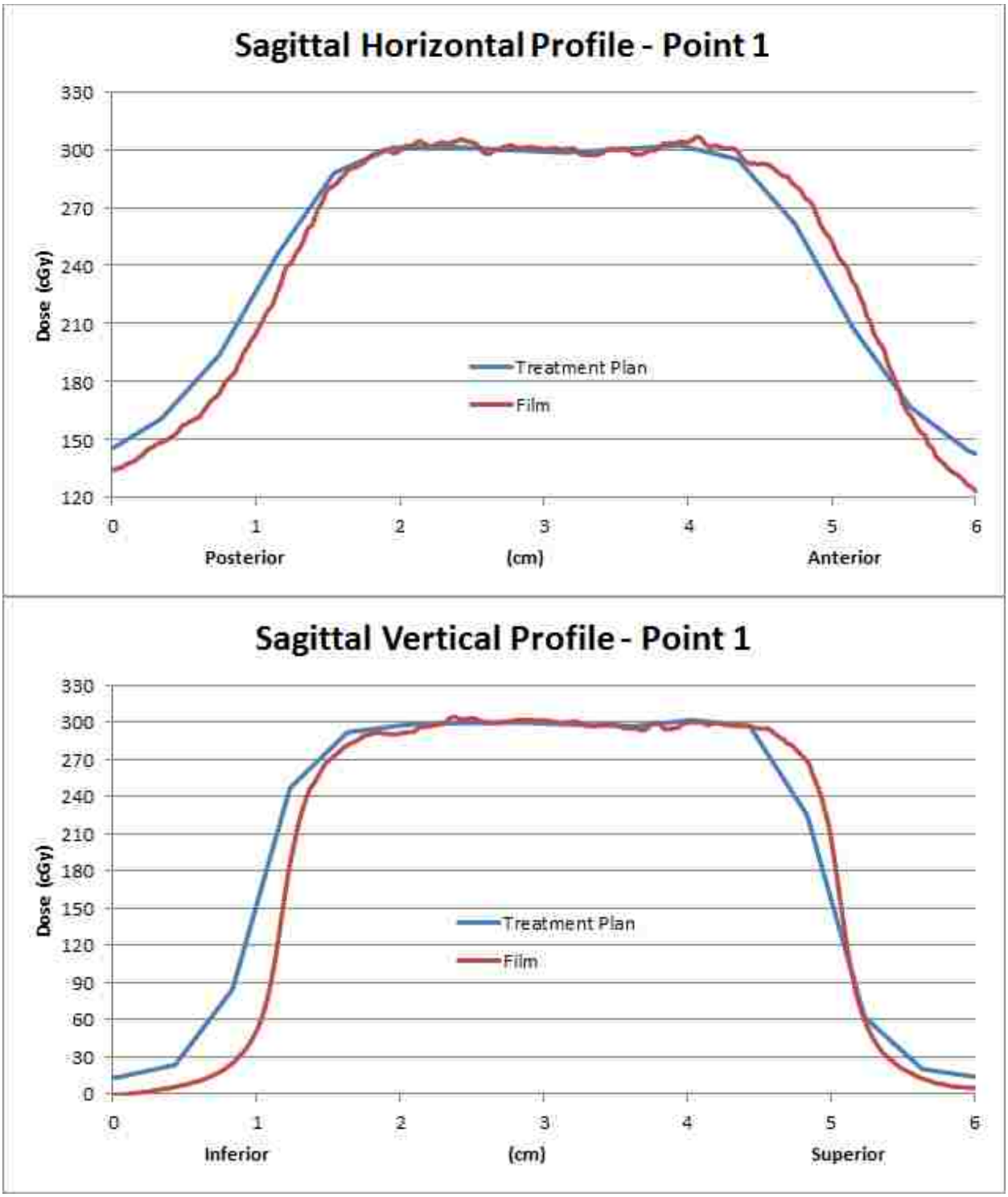

Figure A.24: Horizontal and vertical profiles for the sagittal image plane resulting from kVCBCT image guidance when the phantom was initially positioned at sample point 1.

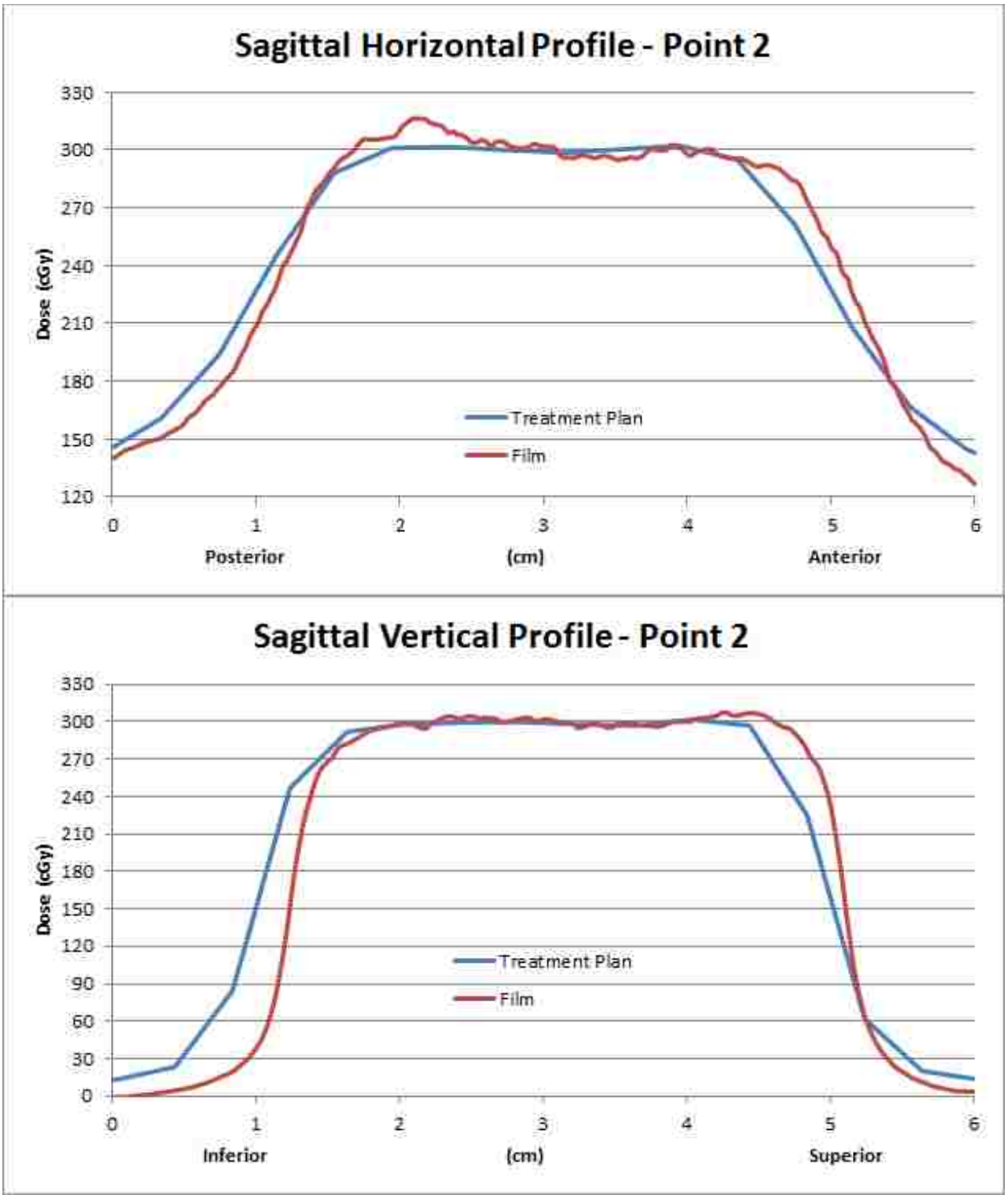

Figure A.25: Horizontal and vertical profiles for the sagittal image plane resulting from kVCBCT image guidance when the phantom was initially positioned at sample point 2.

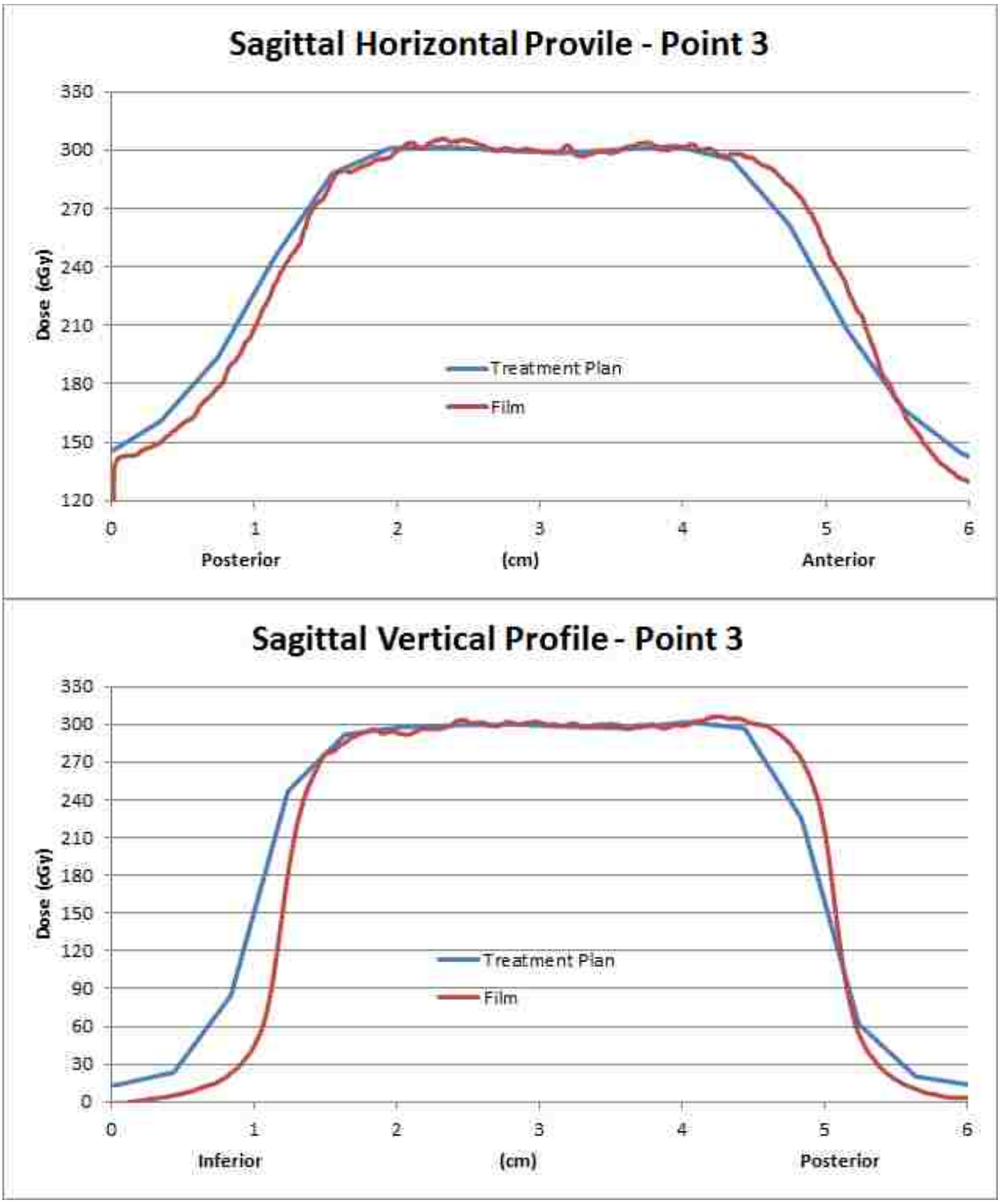

Figure A.26: Horizontal and vertical profiles for the sagittal image plane resulting from kVCBCT image guidance when the phantom was initially positioned at sample point 3.

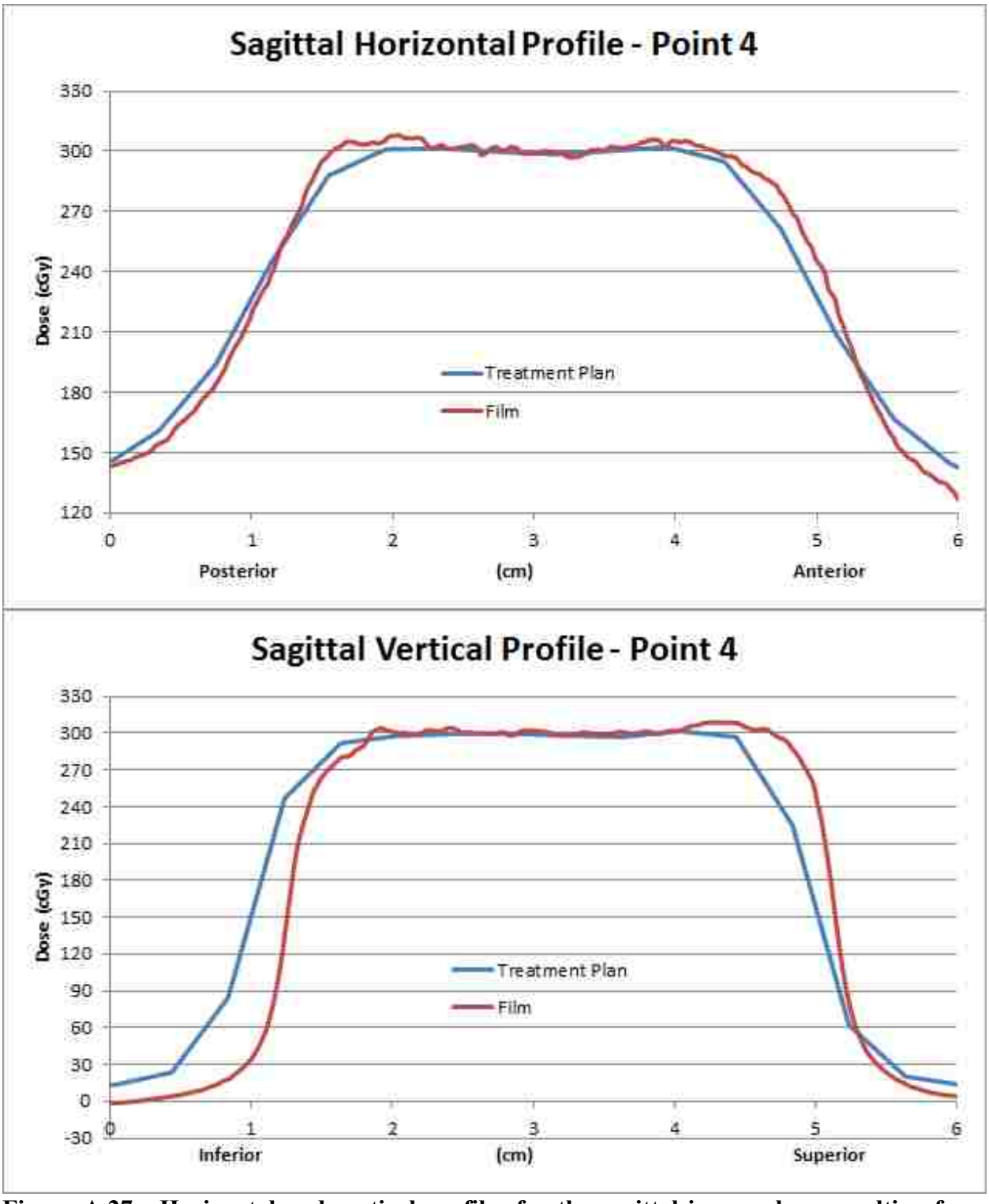

Figure A.27: Horizontal and vertical profiles for the sagittal image plane resulting from kVCBCT image guidance when the phantom was initially positioned at sample point 4.

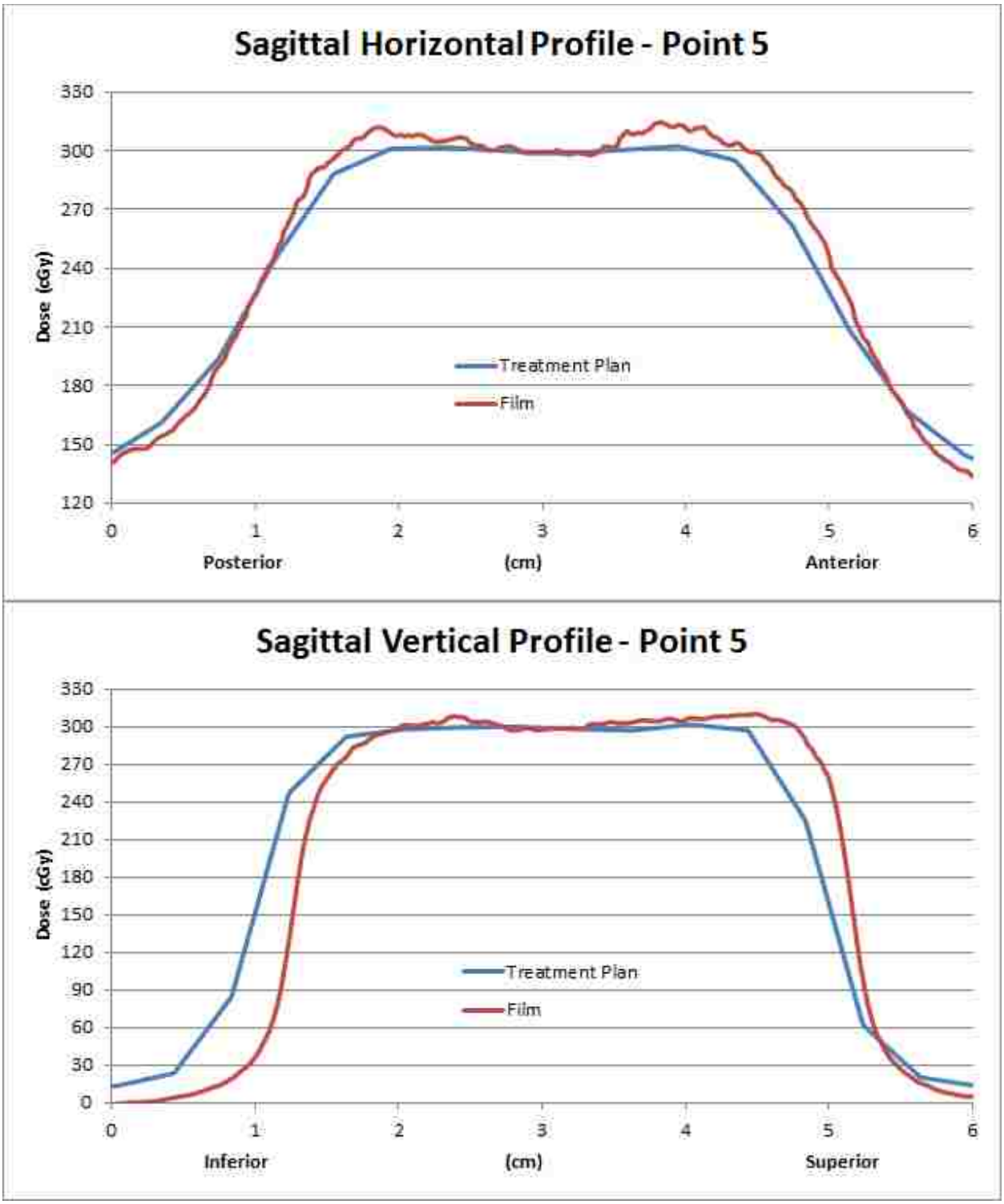

Figure A.28: Horizontal and vertical profiles for the sagittal image plane resulting from kVCBCT image guidance when the phantom was initially positioned at sample point 5.

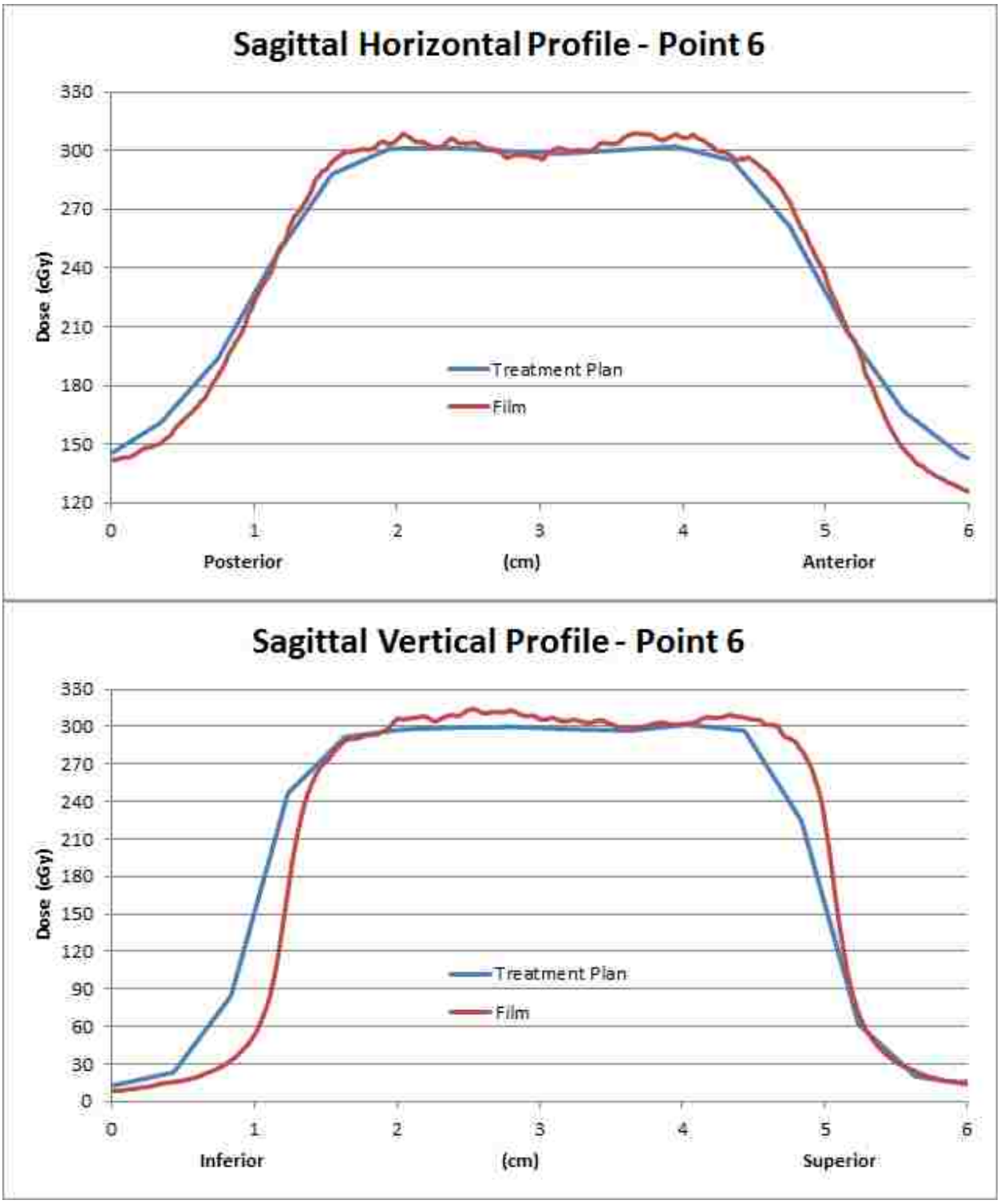

Figure A.29: Horizontal and vertical profiles for the sagittal image plane resulting from kVCBCT image guidance when the phantom was initially positioned at sample point 6.

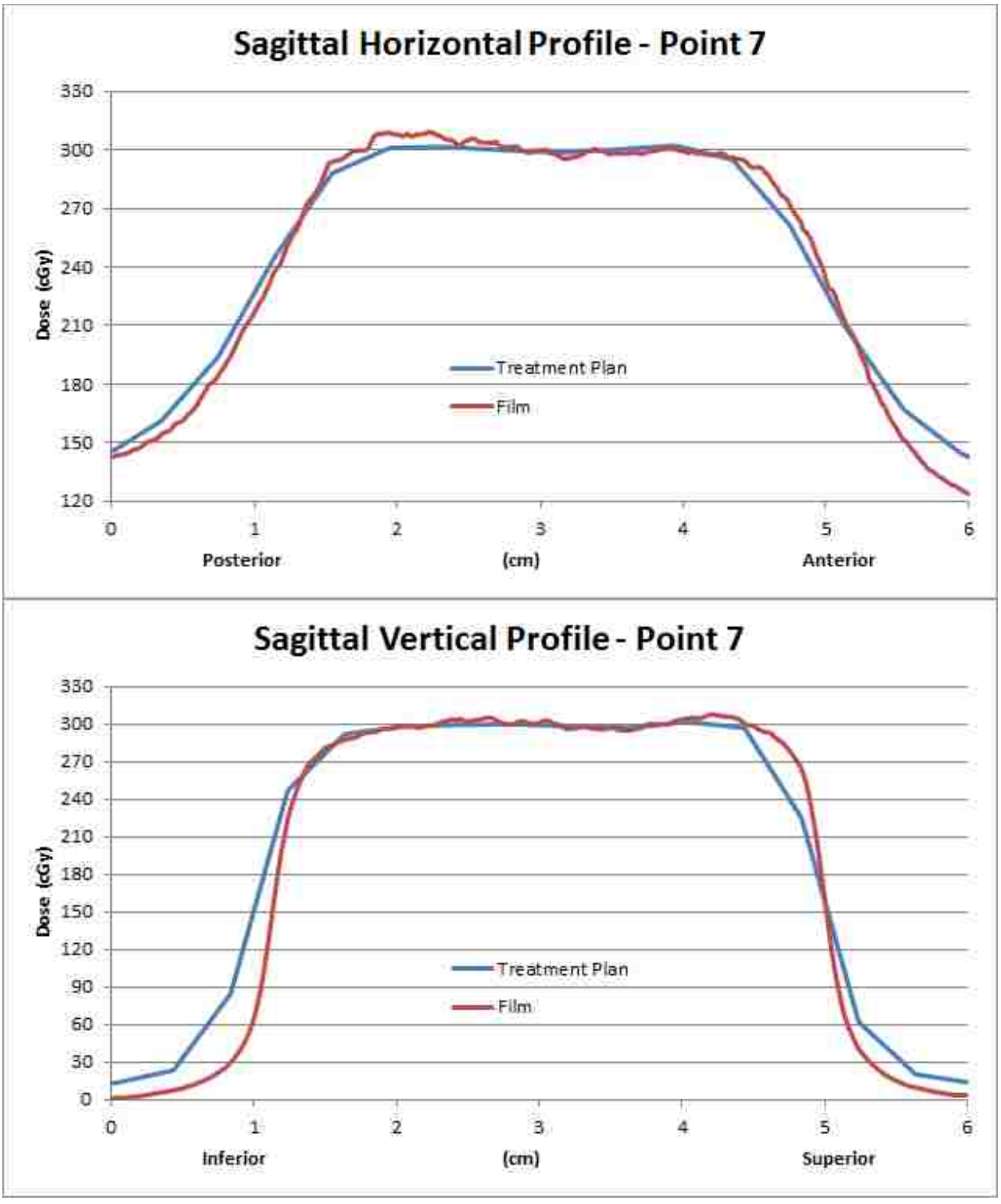

Figure A.30: Horizontal and vertical profiles for the sagittal image plane resulting from kVCBCT image guidance when the phantom was initially positioned at sample point 7.

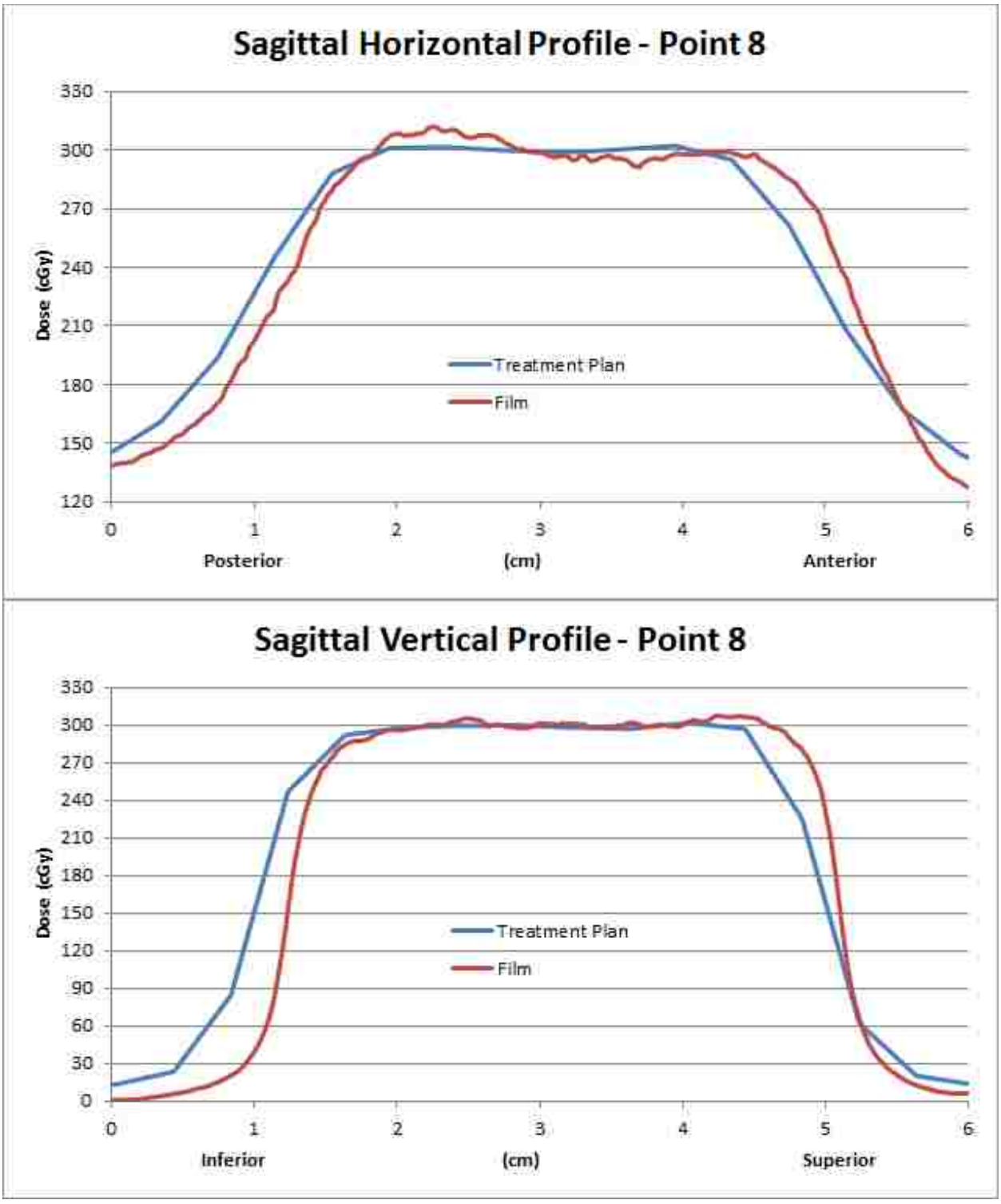

Figure A.31: Horizontal and vertical profiles for the sagittal image plane resulting from kVCBCT image guidance when the phantom was initially positioned at sample point 8.

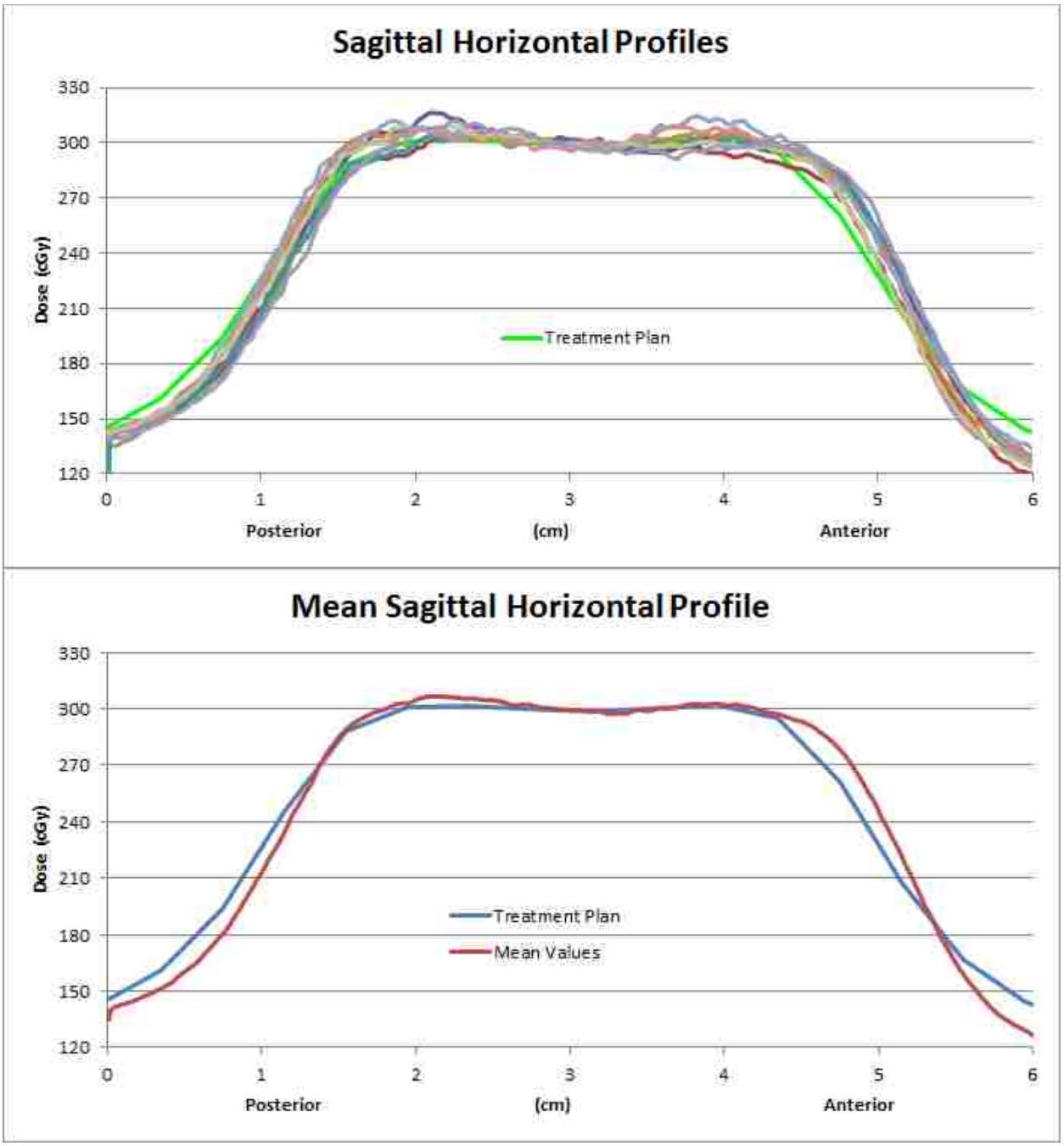

Figure A.32: (top) All horizontal profiles for the sagittal image plane resulting from kVCBCT image guidance. (bottom) Comparison of the mean sagittal horizontal profile with the profile from the treatment plan.

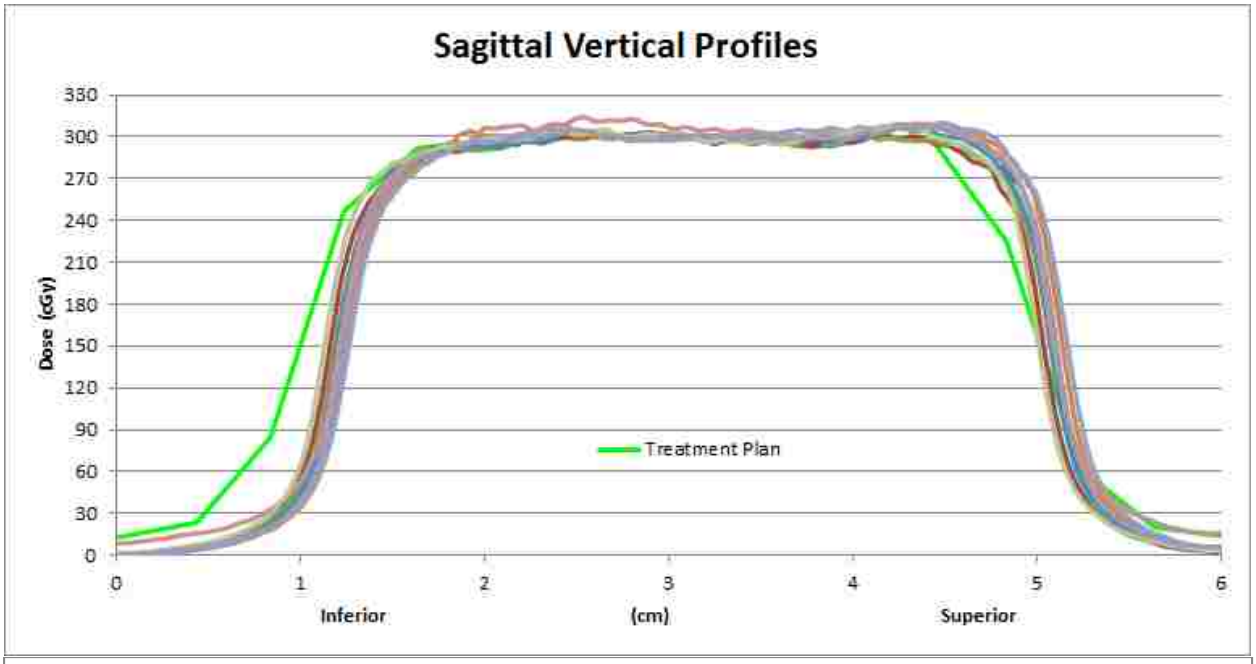

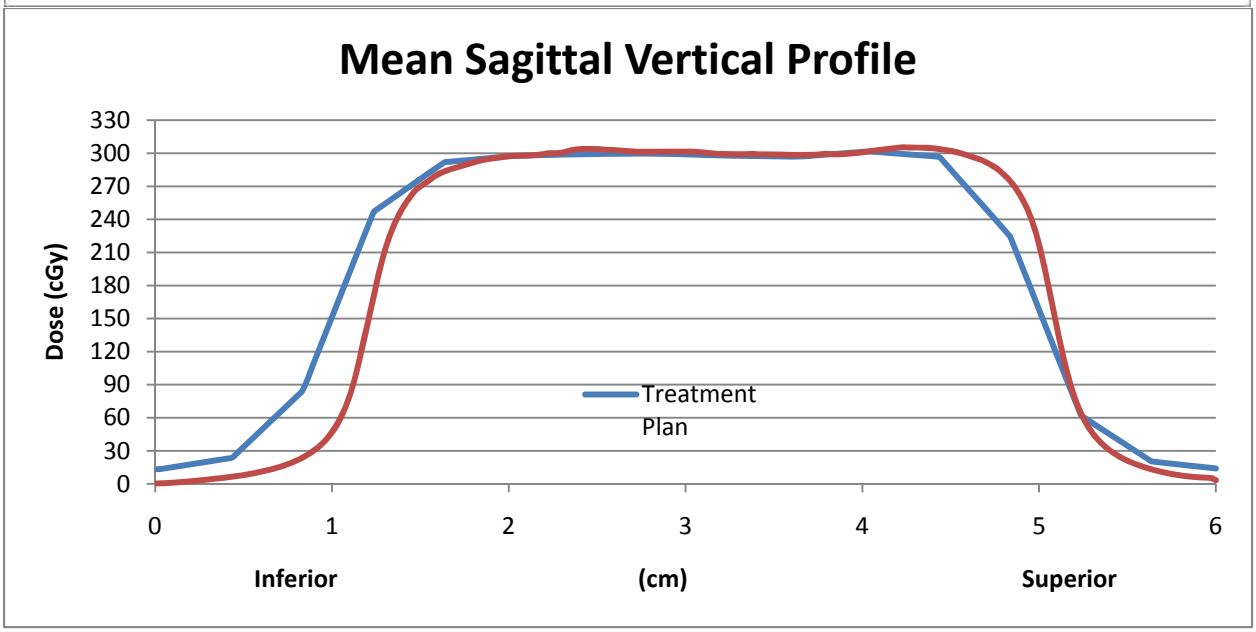

Figure A.33: (top) All vertical profiles for the sagittal image plane resulting from kVCBCT image guidance. (bottom) Comparison of the mean sagittal vertical profile with the profile from the treatment plan.

Table A.1: Metrics for measurements of axial-oriented film. Means, standard deviations, and standard errors (N = 3) are all in mm.

Point	Offset Coordinates	Δc_{R-L}	$\sigma_{\Delta c\ R-L}$	$SE_{\Delta c\ R-L}$	$\Delta 80_R$	$\sigma_{\Delta 80\ R}$	$SE_{\Delta 80\ R}$	$\Delta 80_L$	$\sigma_{\Delta 80\ L}$	$SE_{\Delta 80\ L}$
0	(0, 0, 0)	0.04	0.27	0.15	0.27	0.12	0.07	0.36	0.13	0.08
1	(5, 5, -5)	0.01	0.55	0.32	0.32	0.46	0.27	0.26	0.59	0.34
2	(5, -5, 5)	0.08	0.33	0.19	0.39	0.35	0.20	0.20	0.26	0.15
3	(5, -5, -5)	0.42	0.28	0.16	0.04	0.34	0.20	0.49	0.47	0.27
4	(5, 5, 5)	0.43	0.54	0.31	0.10	0.47	0.27	0.94	0.65	0.37
5	(-5, 5, 5)	-1.01	1.33	0.77	1.28	1.49	0.86	-1.09	1.00	0.57
6	(-5, -5, -5)	0.57	0.19	0.11	-0.12	0.40	0.23	1.07	0.33	0.19
7	(-5, -5, 5)	-0.09	0.70	0.40	0.24	0.62	0.36	-0.23	0.81	0.47
8	(-5, 5, -5)	-0.16	0.81	0.47	0.28	0.67	0.39	-0.33	0.89	0.51

Point	Offset Coordinates	Δc_{A-P}	$\sigma_{\Delta c\ A-P}$	$SE_{\Delta c\ A-P}$	$\Delta 80_A$	$\sigma_{\Delta 80\ A}$	$SE_{\Delta 80\ A}$	$\Delta 80_P$	$\sigma_{\Delta 80\ P}$	$SE_{\Delta 80\ P}$
0	(0, 0, 0)	-1.09	0.49	0.28	1.43	0.70	0.41	-1.23	0.42	0.24
1	(5, 5, -5)	-0.30	0.67	0.39	0.78	0.81	0.47	-0.06	0.58	0.34
2	(5, -5, 5)	-0.66	0.51	0.29	1.06	0.43	0.25	-0.73	0.58	0.33
3	(5, -5, -5)	-0.85	0.67	0.39	1.36	0.55	0.31	-0.72	0.67	0.39
4	(5, 5, 5)	-0.73	0.47	0.27	2.07	0.39	0.23	-0.10	0.99	0.57
5	(-5, 5, 5)	-0.35	0.76	0.44	0.91	0.38	0.22	-0.39	1.10	0.63
6	(-5, -5, -5)	-0.61	0.50	0.29	1.31	0.23	0.13	-0.48	0.68	0.39
7	(-5, -5, 5)	-1.21	0.61	0.35	1.61	0.54	0.31	-1.18	0.86	0.50
8	(-5, 5, -5)	-0.65	0.62	0.36	1.02	0.83	0.48	-0.77	0.50	0.29

Table A.2: Metrics for measurements of coronal-oriented film. Means, standard deviations, and standard errors (N = 3) are all in mm.

Point	Offset Coordinates	Δc_{L-R}	$\sigma_{\Delta c\ L-R}$	$SE_{\Delta c\ L-R}$	$\Delta 80_{L}$	$\sigma_{\Delta 80\ L}$	$SE_{\Delta 80\ L}$	$\Delta 80_{R}$	$\sigma_{\Delta 80\ R}$	$SE_{\Delta 80\ R}$
0	(0, 0, 0)	-0.51	0.13	0.07	0.63	0.14	0.08	-0.36	0.30	0.17
1	(5, 5, -5)	-0.57	0.46	0.26	1.05	0.51	0.29	-0.30	0.28	0.16
2	(5, -5, 5)	-0.52	0.15	0.09	1.06	0.42	0.25	0.00	0.08	0.05
3	(5, -5, -5)	-0.63	0.42	0.24	1.11	1.00	0.58	-0.24	0.09	0.05
4	(5, 5, 5)	-0.86	0.74	0.43	1.53	0.80	0.46	-0.17	0.76	0.44
5	(-5, 5, 5)	-0.14	0.61	0.35	0.29	1.47	0.85	0.02	0.29	0.17
6	(-5, -5, -5)	-0.25	0.44	0.26	0.68	1.29	0.75	-0.04	0.48	0.28
7	(-5, -5, 5)	0.31	1.06	0.61	-0.29	1.04	0.60	0.59	0.94	0.54
8	(-5, 5, -5)	-0.23	0.58	0.33	-0.05	0.68	0.39	0.00	0.41	0.24

Point	Offset Coordinates	Δc_{I-S}	$\sigma_{\Delta c\ I-S}$	$SE_{\Delta c\ I-S}$	$\Delta 80_{I}$	$\sigma_{\Delta 80\ I}$	$SE_{\Delta 80\ I}$	$\Delta 80_{S}$	$\sigma_{\Delta 80\ S}$	$SE_{\Delta 80\ S}$
0	(0, 0, 0)	1.28	0.48	0.28	-1.09	0.69	0.40	2.12	0.33	0.19
1	(5, 5, -5)	1.59	0.52	0.30	-1.40	0.59	0.34	2.38	0.49	0.28
2	(5, -5, 5)	1.51	0.34	0.20	-1.21	0.19	0.11	2.42	0.47	0.27
3	(5, -5, -5)	1.62	1.25	0.72	-1.34	1.14	0.66	2.52	1.37	0.79
4	(5, 5, 5)	2.29	0.83	0.48	-2.04	0.97	0.56	3.12	0.81	0.47
5	(-5, 5, 5)	1.50	2.30	1.33	-1.29	2.36	1.36	2.36	2.22	1.28
6	(-5, -5, -5)	0.88	2.56	1.48	-0.64	2.48	1.43	1.80	2.57	1.48
7	(-5, -5, 5)	0.95	0.31	0.18	-0.65	0.38	0.22	1.83	0.24	0.14
8	(-5, 5, -5)	0.65	0.39	0.22	-0.36	0.31	0.18	1.54	0.38	0.22

Table A.3: Metrics for measurements of sagittal-oriented film. Means, standard deviations, and standard errors (N = 3) are all in mm.

Point	Offset Coordinates	Δc_{P-A}	$\sigma_{\Delta c\ P-A}$	$SE_{\Delta c\ P-A}$	$\Delta 80_{P}$	$\sigma_{\Delta 80\ P}$	$SE_{\Delta 80\ P}$	$\Delta 80_{A}$	$\sigma_{\Delta 80\ A}$	$SE_{\Delta 80\ A}$
0	(0, 0, 0)	0.79	0.18	0.11	-0.74	0.41	0.24	0.98	0.45	0.26
1	(5, 5, -5)	1.25	0.48	0.28	-1.39	0.90	0.52	1.31	0.53	0.30
2	(5, -5, 5)	0.80	0.84	0.48	-0.52	0.90	0.52	1.26	0.73	0.42
3	(5, -5, -5)	0.91	0.66	0.38	-0.87	0.33	0.19	1.18	0.65	0.38
4	(5, 5, 5)	1.28	0.49	0.28	-1.18	0.67	0.39	1.58	0.47	0.27
5	(-5, 5, 5)	0.48	0.40	0.23	-0.21	0.91	0.52	0.84	0.31	0.18
6	(-5, -5, -5)	0.43	0.52	0.30	-0.34	0.89	0.52	0.76	0.15	0.09
7	(-5, -5, 5)	0.73	0.78	0.45	-0.76	0.82	0.47	0.88	0.47	0.27
8	(-5, 5, -5)	0.73	0.79	0.45	-0.77	0.99	0.57	1.21	0.71	0.41

Point	Offset Coordinates	Δc_{I-S}	$\sigma_{\Delta c\ I-S}$	$SE_{\Delta c\ I-S}$	$\Delta 80_{I}$	$\sigma_{\Delta 80\ I}$	$SE_{\Delta 80\ I}$	$\Delta 80_{S}$	$\sigma_{\Delta 80\ S}$	$SE_{\Delta 80\ S}$
0	(0, 0, 0)	1.04	0.10	0.06	-0.93	0.12	0.07	1.78	0.31	0.18
1	(5, 5, -5)	0.31	1.64	0.95	-0.14	1.92	1.11	1.06	1.43	0.83
2	(5, -5, 5)	1.55	0.09	0.05	-1.25	0.32	0.18	2.42	0.10	0.06
3	(5, -5, -5)	1.00	0.41	0.24	-0.67	0.61	0.35	1.90	0.25	0.14
4	(5, 5, 5)	1.68	1.68	0.97	-1.48	1.82	1.05	2.55	1.52	0.88
5	(-5, 5, 5)	1.77	2.45	1.42	-1.40	2.61	1.51	2.80	2.30	1.33
6	(-5, -5, -5)	1.59	2.24	1.29	-1.35	2.21	1.28	2.43	2.35	1.36
7	(-5, -5, 5)	0.42	0.43	0.25	-0.13	0.54	0.31	1.32	0.38	0.22
8	(-5, 5, -5)	1.13	0.47	0.27	-0.93	0.64	0.37	1.97	0.32	0.18

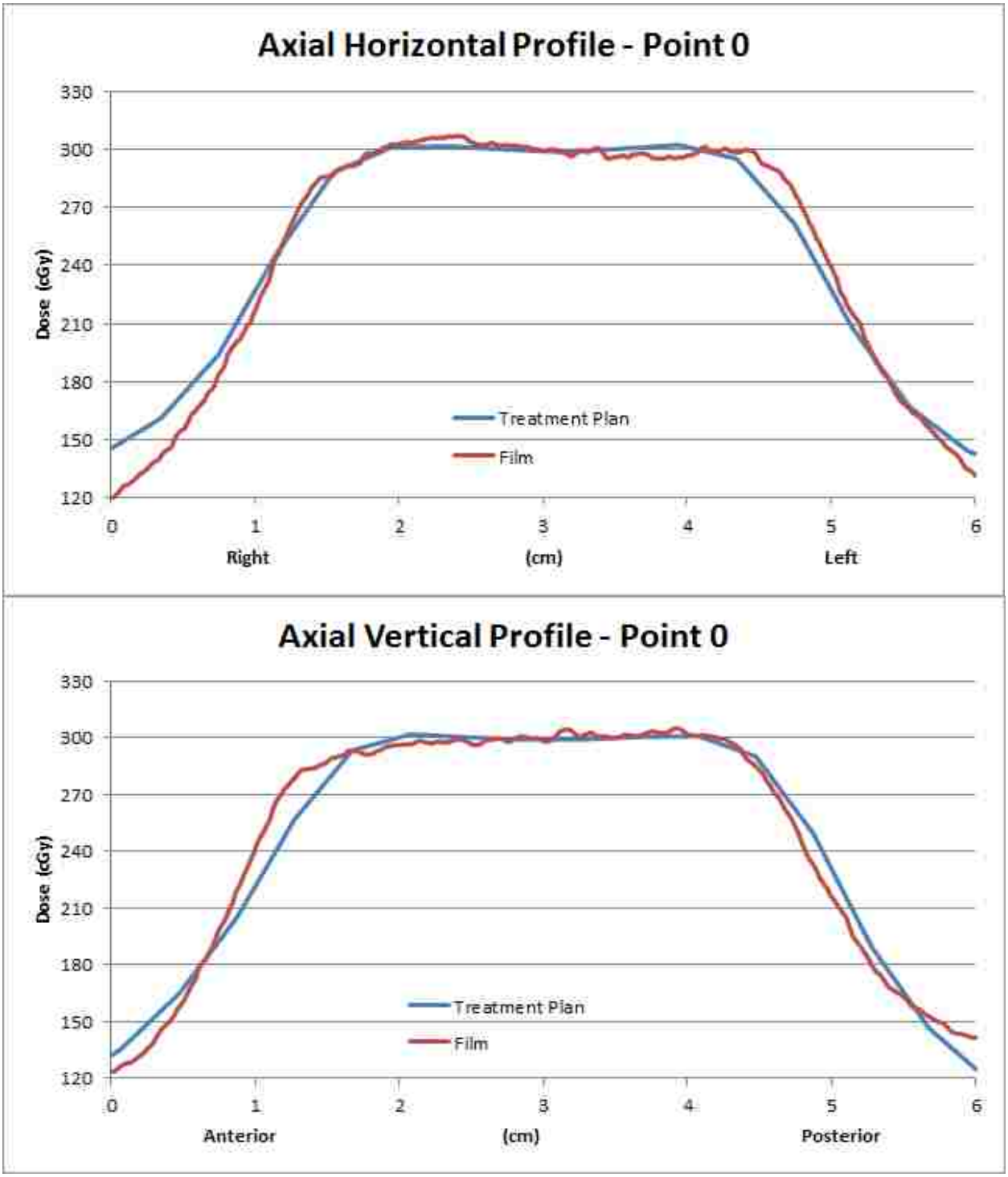

Figure A.34: Horizontal and vertical profiles for the axial image plane resulting from MV planar image guidance when the phantom was initially positioned at sample point 0.

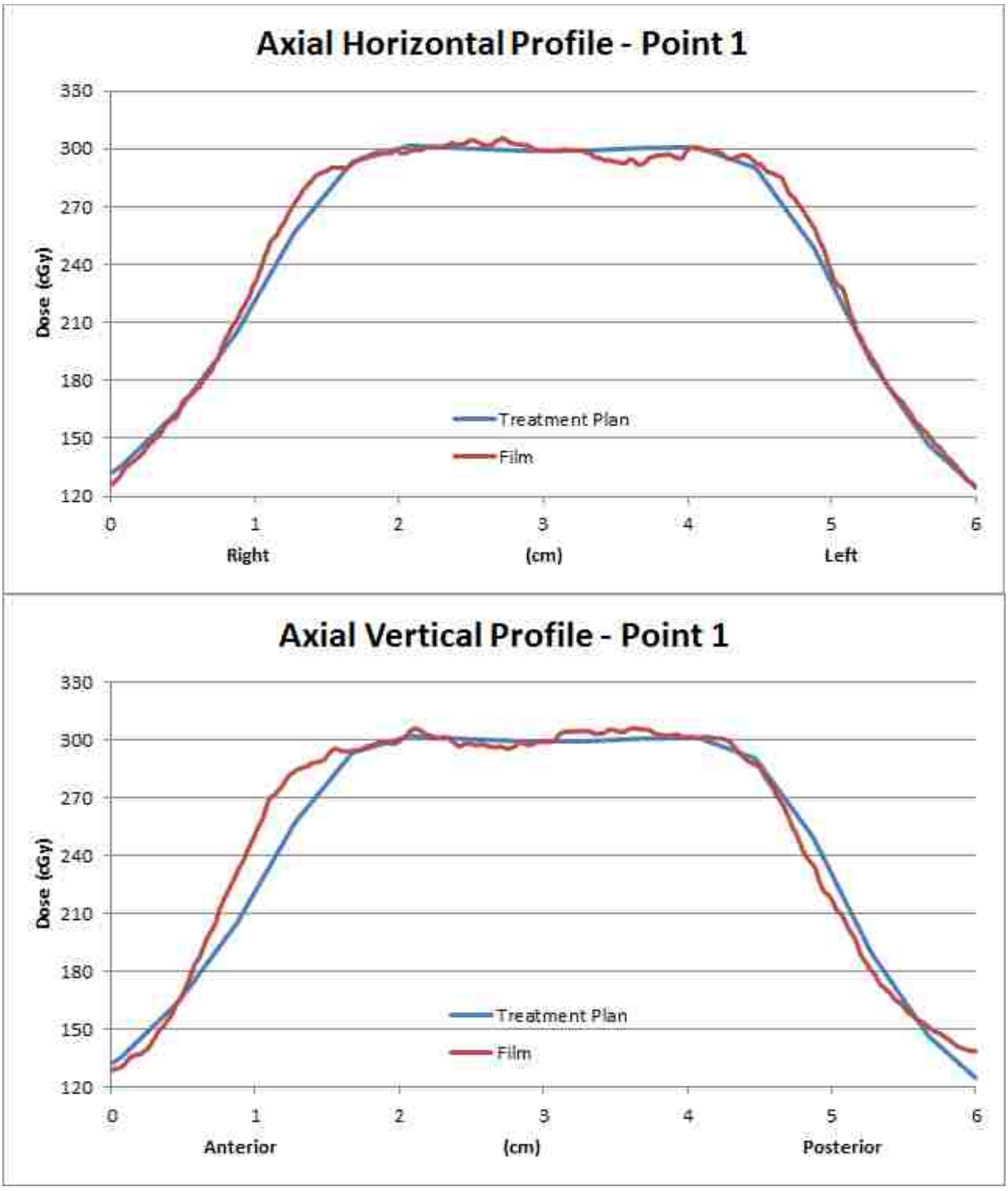

Figure A.35: Horizontal and vertical profiles for the axial image plane resulting from MV planar image guidance when the phantom was initially positioned at sample point 1.

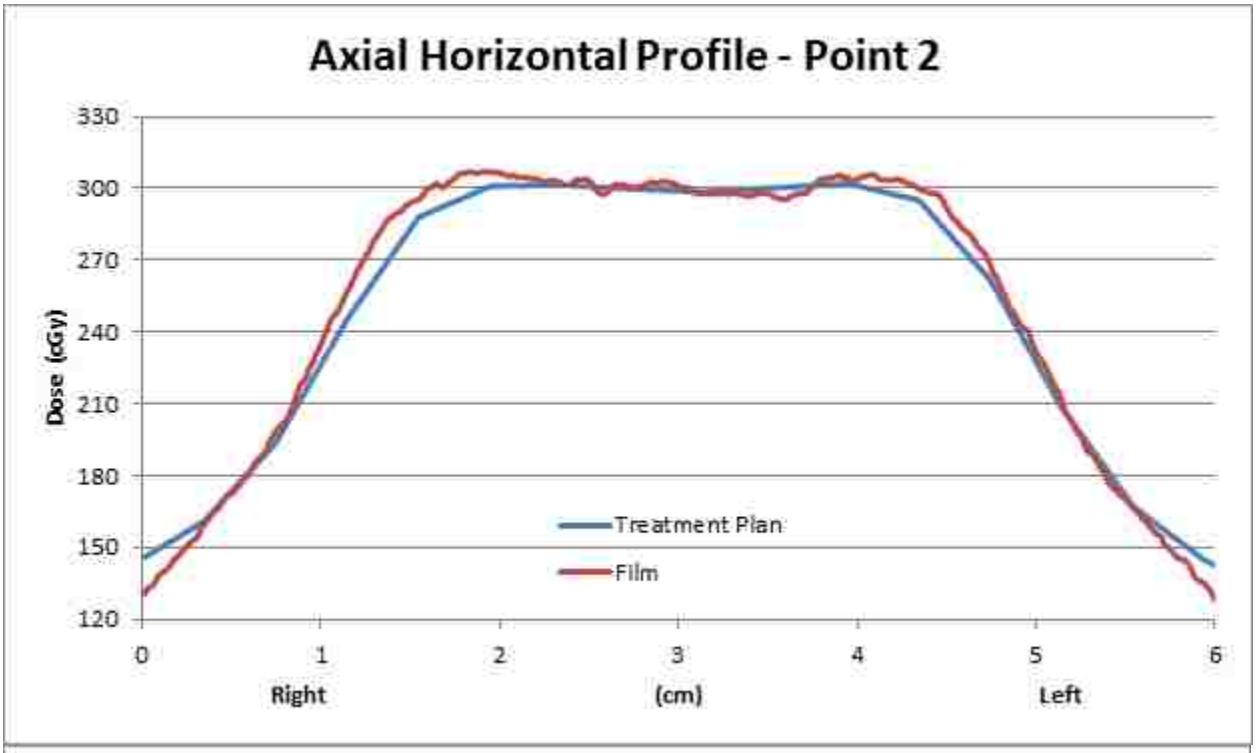

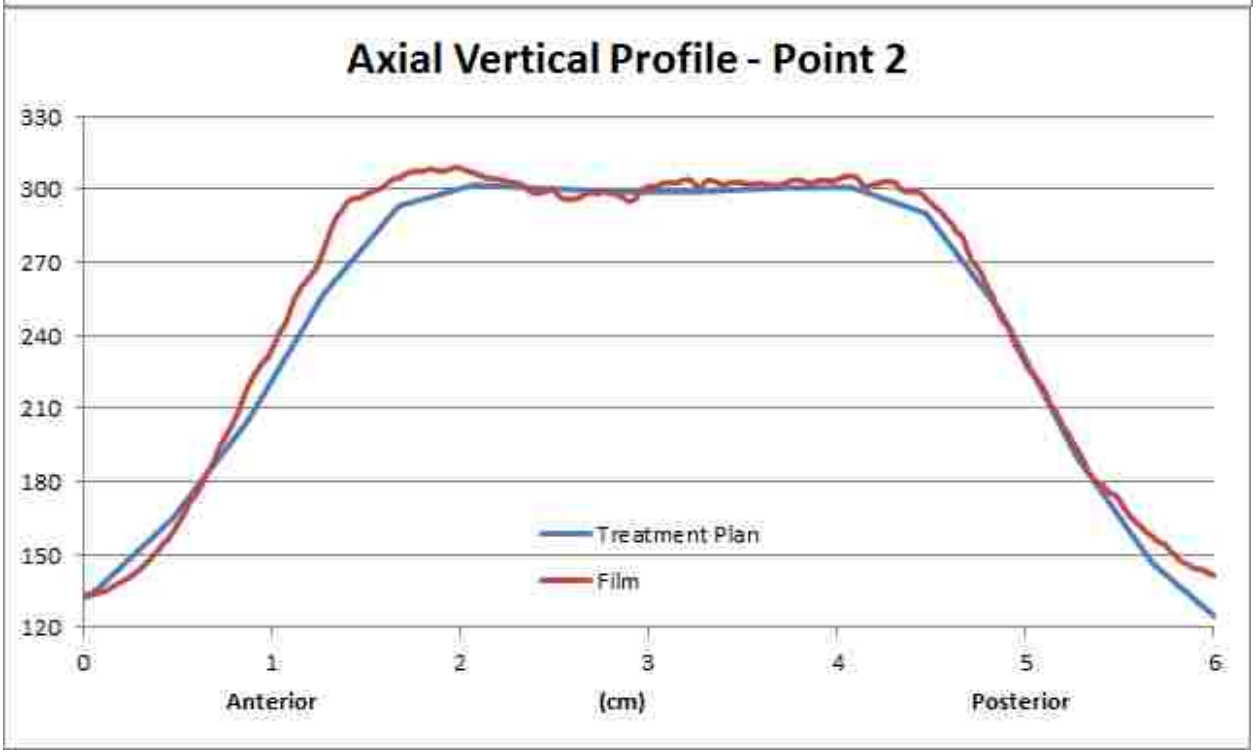

Figure A.36: Horizontal and vertical profiles for the axial image plane resulting from MV planar image guidance when the phantom was initially positioned at sample point 2.

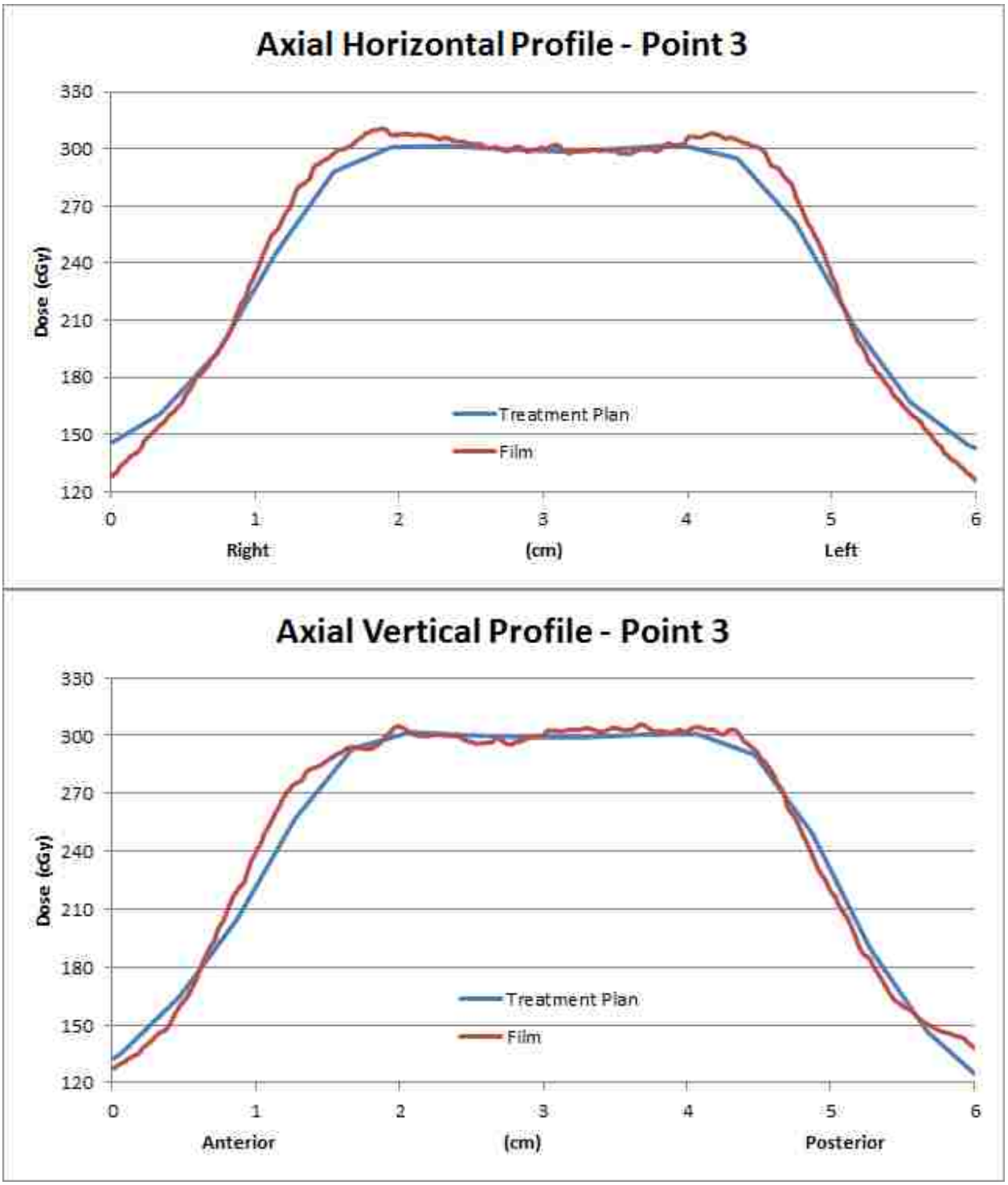

Figure A.37: Horizontal and vertical profiles for the axial image plane resulting from MV planar image guidance when the phantom was initially positioned at sample point 3.

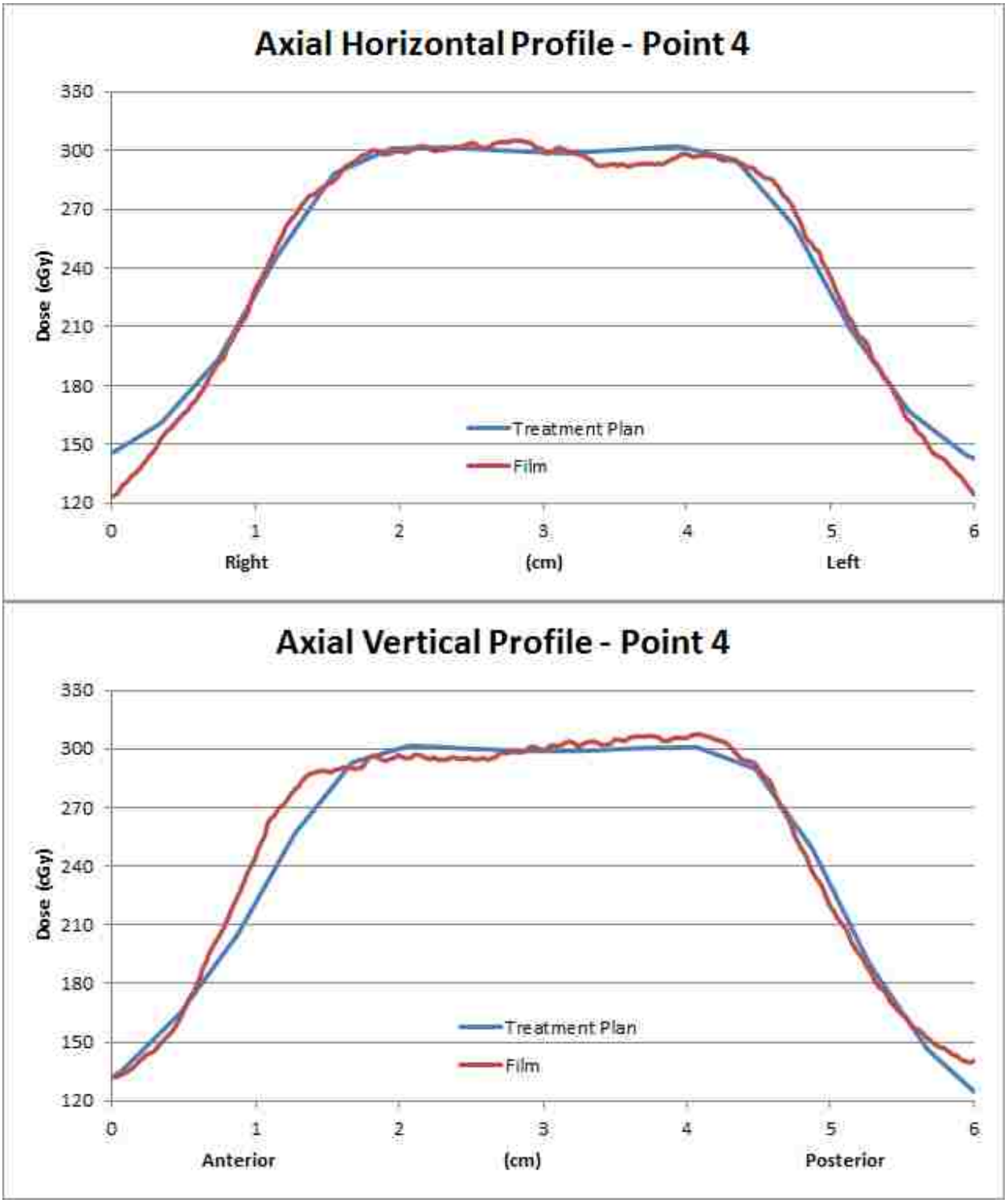

Figure A.38: Horizontal and vertical profiles for the axial image plane resulting from MV planar image guidance when the phantom was initially positioned at sample point 4.

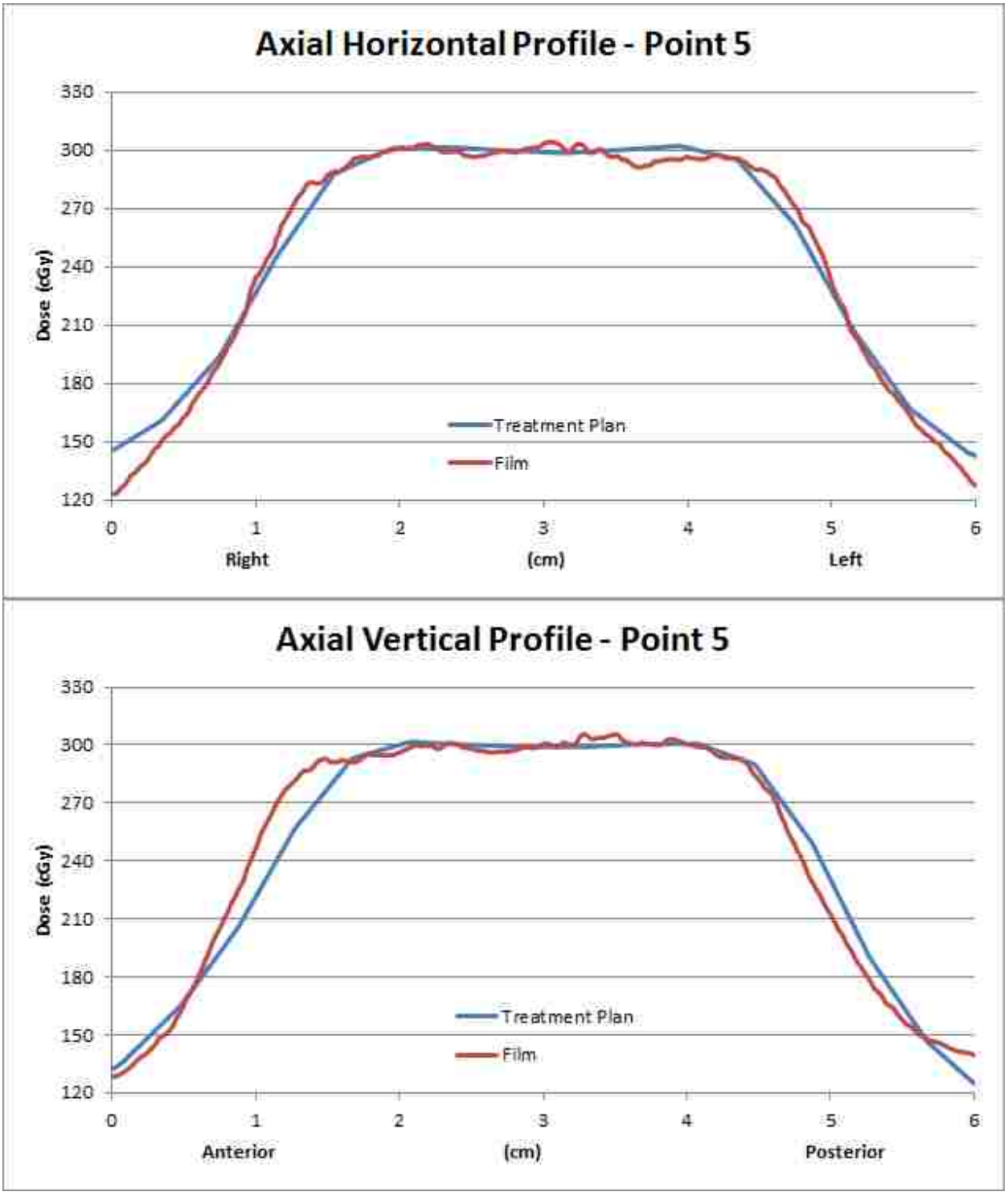

Figure A.39: Horizontal and vertical profiles for the axial image plane resulting from MV planar image guidance when the phantom was initially positioned at sample point 5.

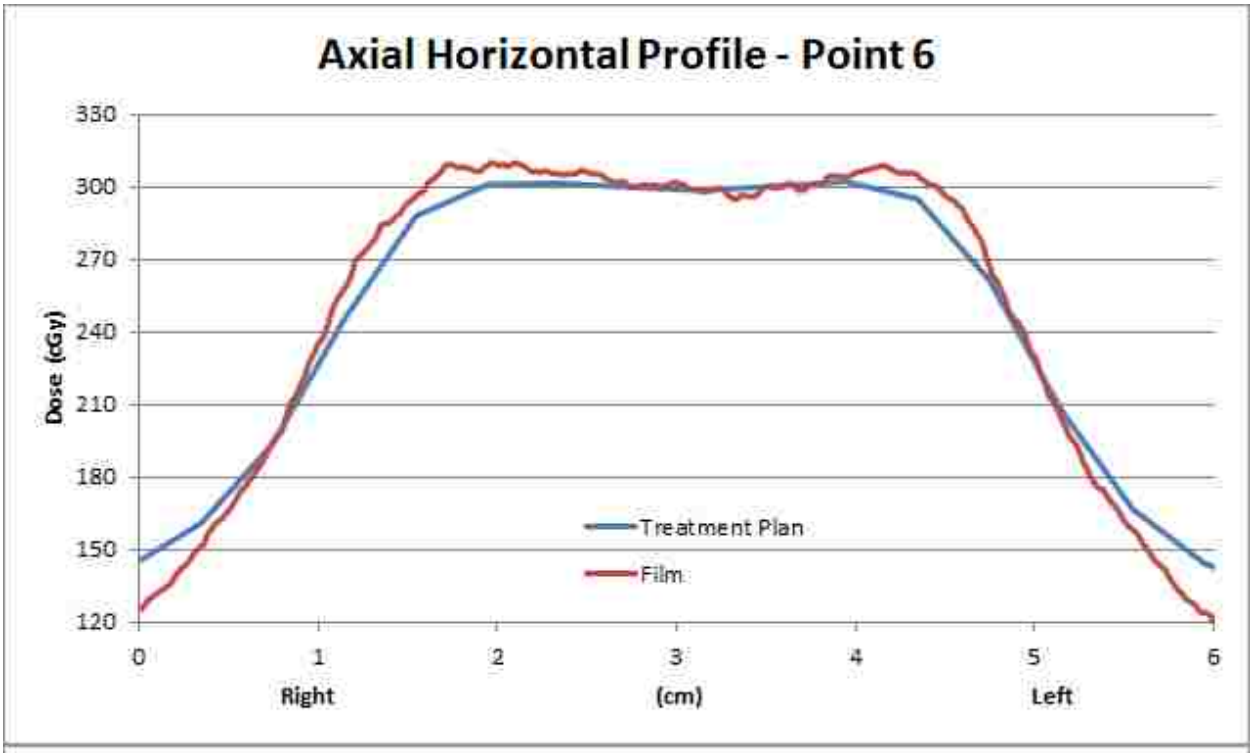

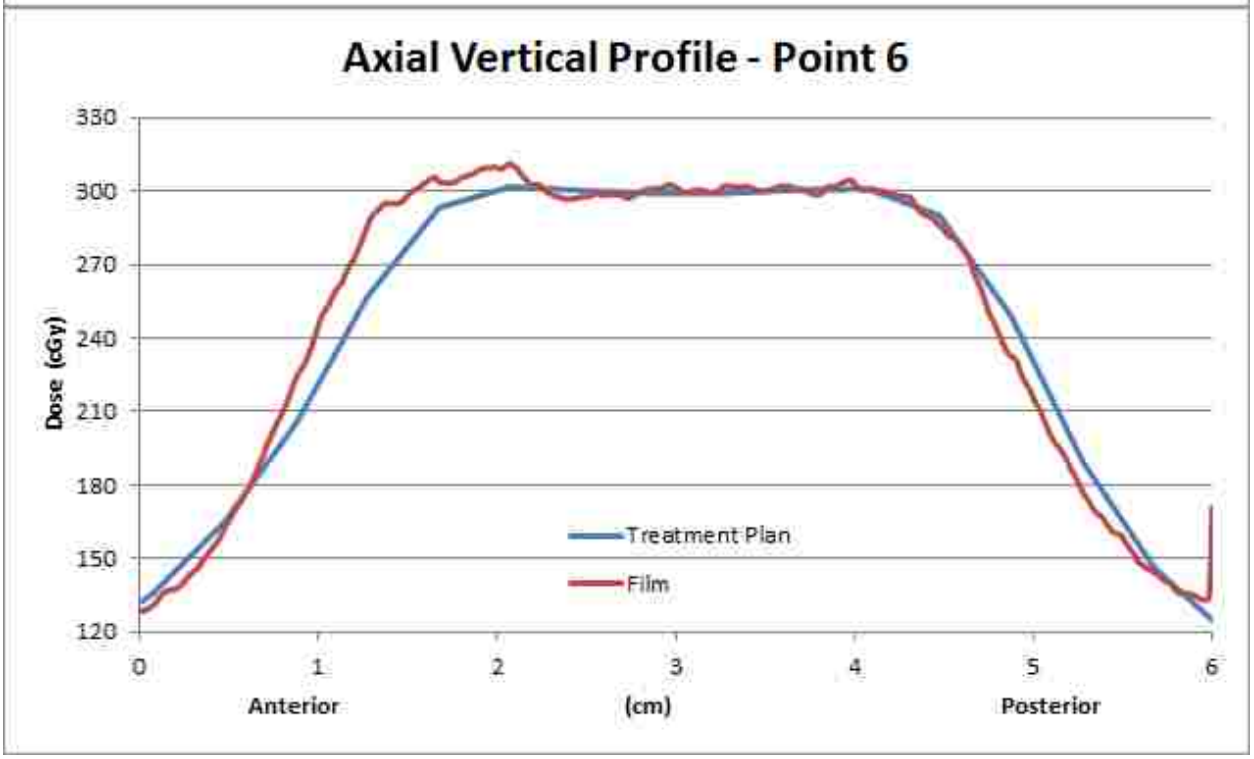

Figure A.40: Horizontal and vertical profiles for the axial image plane resulting from MV planar image guidance when the phantom was initially positioned at sample point 6.

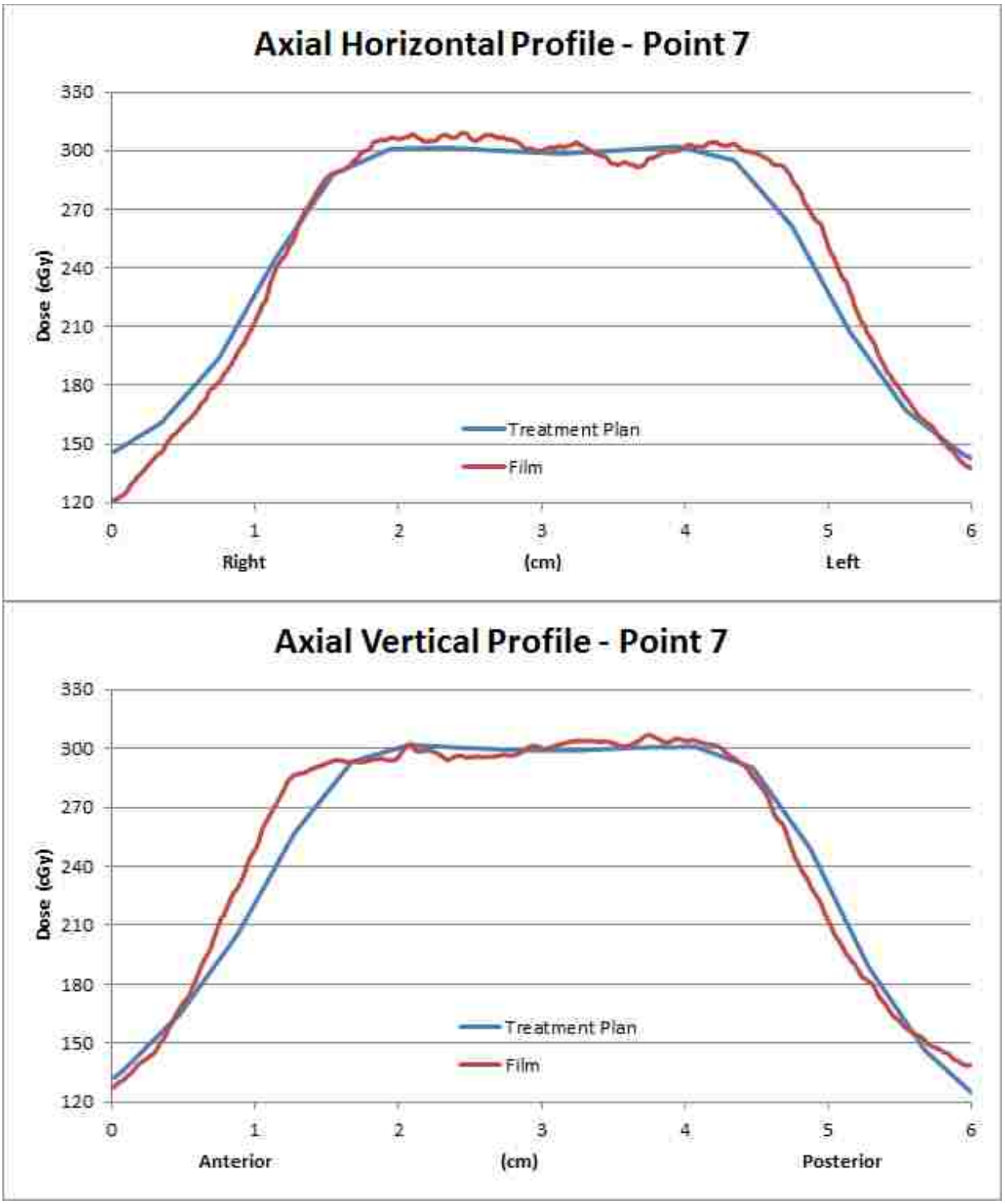

Figure A.41: Horizontal and vertical profiles for the axial image plane resulting from MV planar image guidance when the phantom was initially positioned at sample point 7.

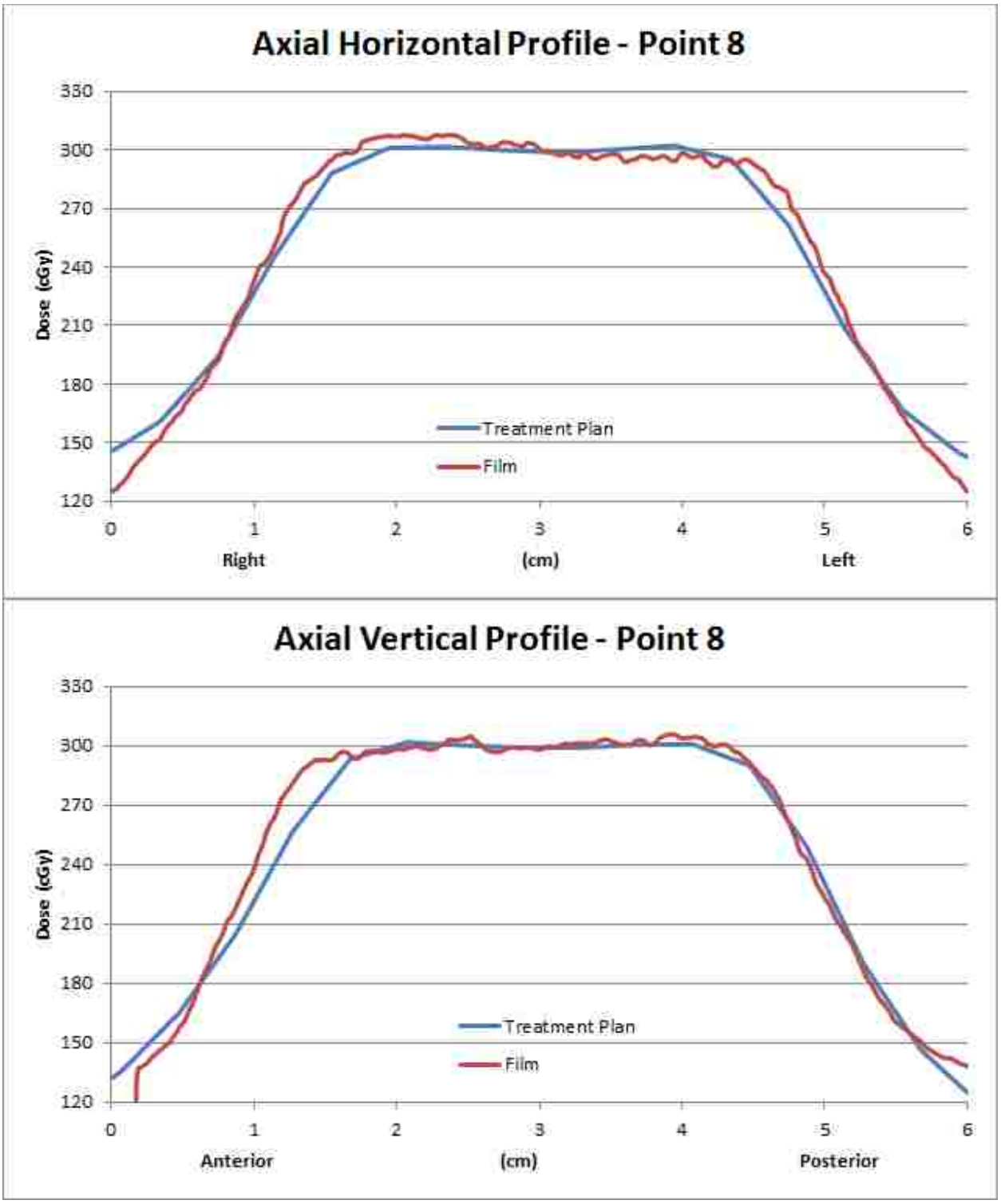

Figure A.42: Horizontal and vertical profiles for the axial image plane resulting from MV planar image guidance when the phantom was initially positioned at sample point 8.

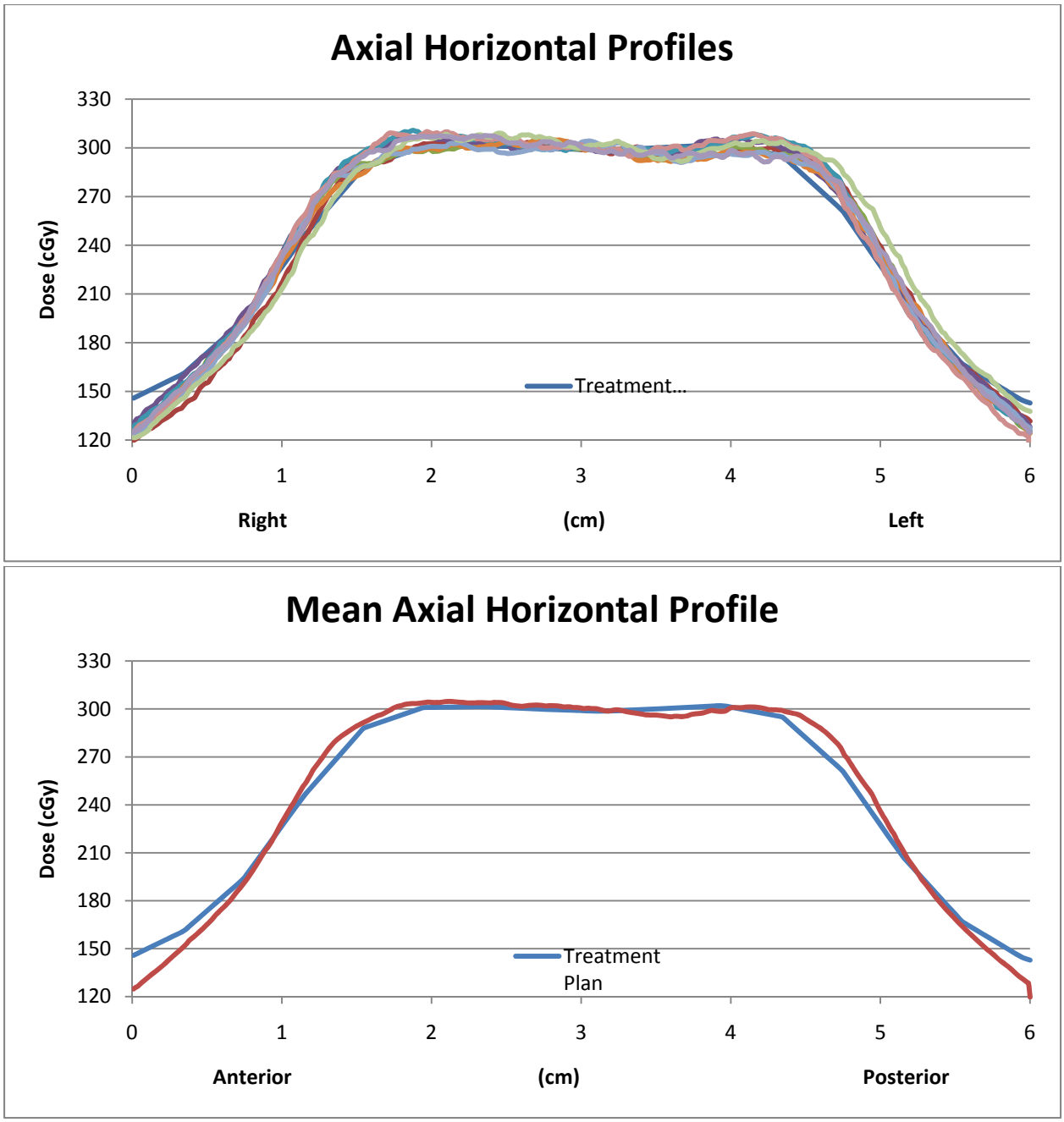

Figure A.43: (top) All horizontal profiles for the axial image plane resulting from MV planar image guidance. (bottom) Comparison of the mean axial horizontal profile with the profile from the treatment plan.

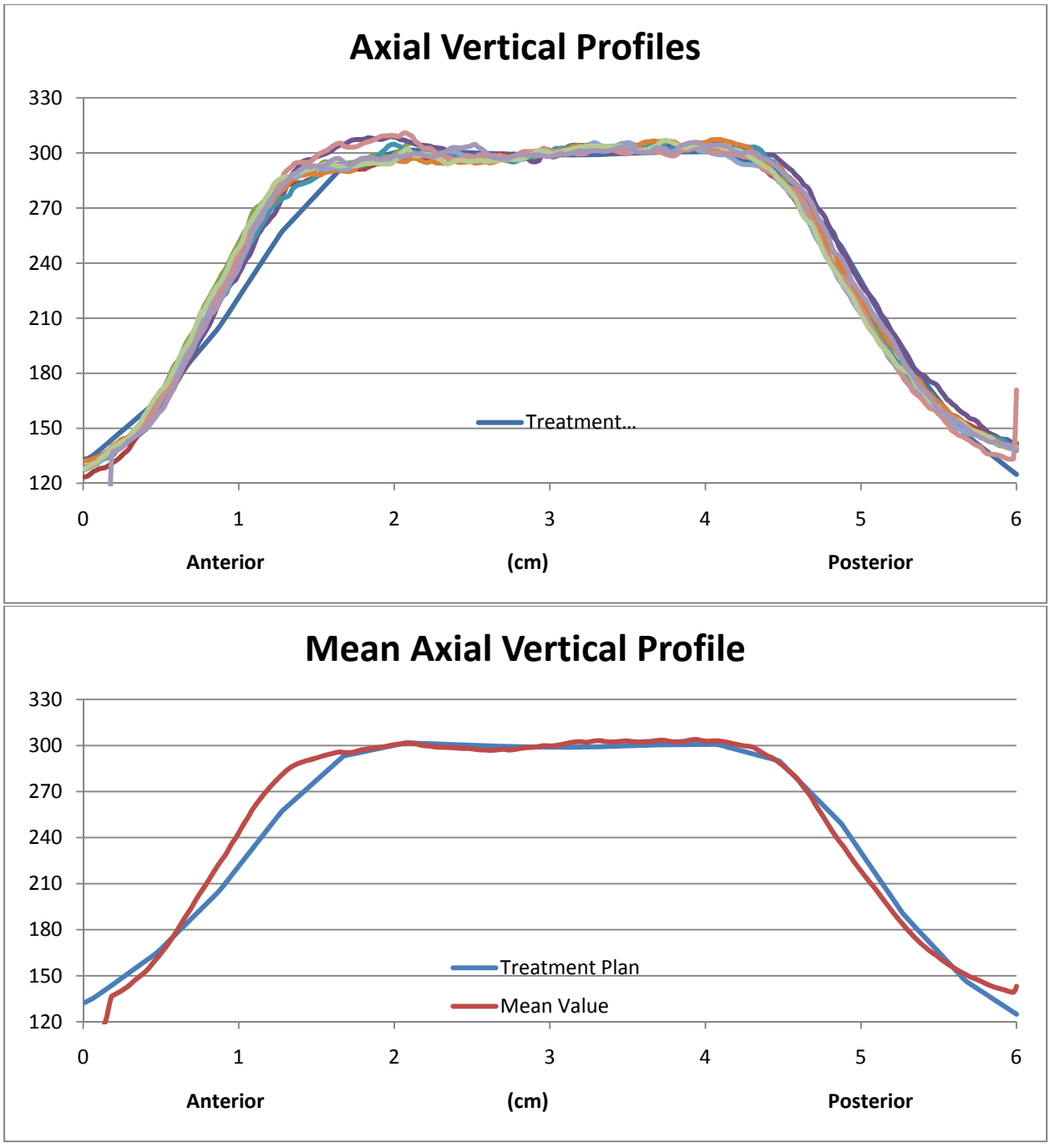

Figure A.44: (top) All vertical profiles for the axial image plane resulting from MV planar image guidance. (bottom) Comparison of the mean axial vertical profile with the profile from the treatment plan.

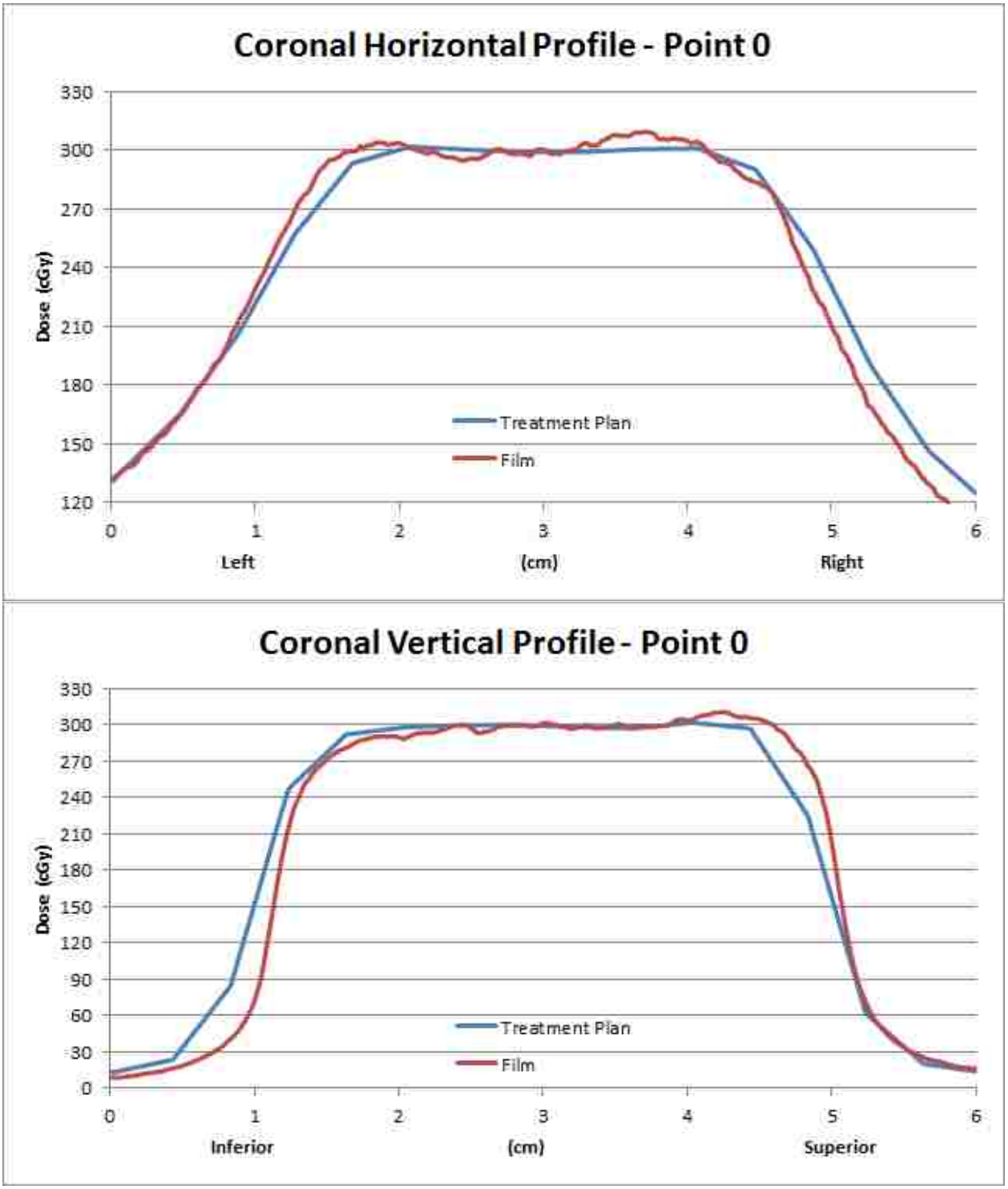

Figure A.45: Horizontal and vertical profiles for the coronal image plane resulting from MV planar image guidance when the phantom was initially positioned at sample point 0.

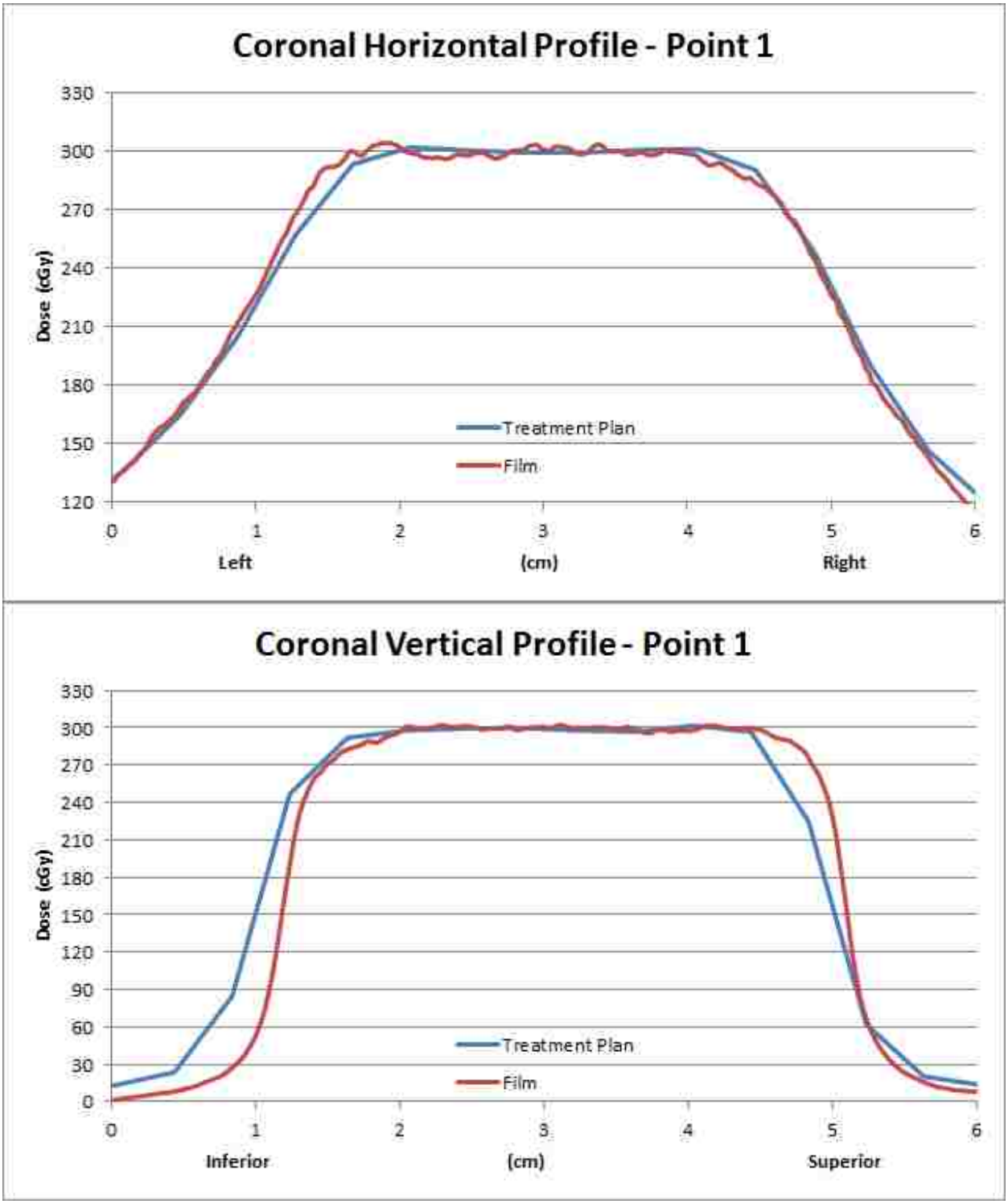

Figure A.46: Horizontal and vertical profiles for the coronal image plane resulting from MV planar image guidance when the phantom was initially positioned at sample point 1.

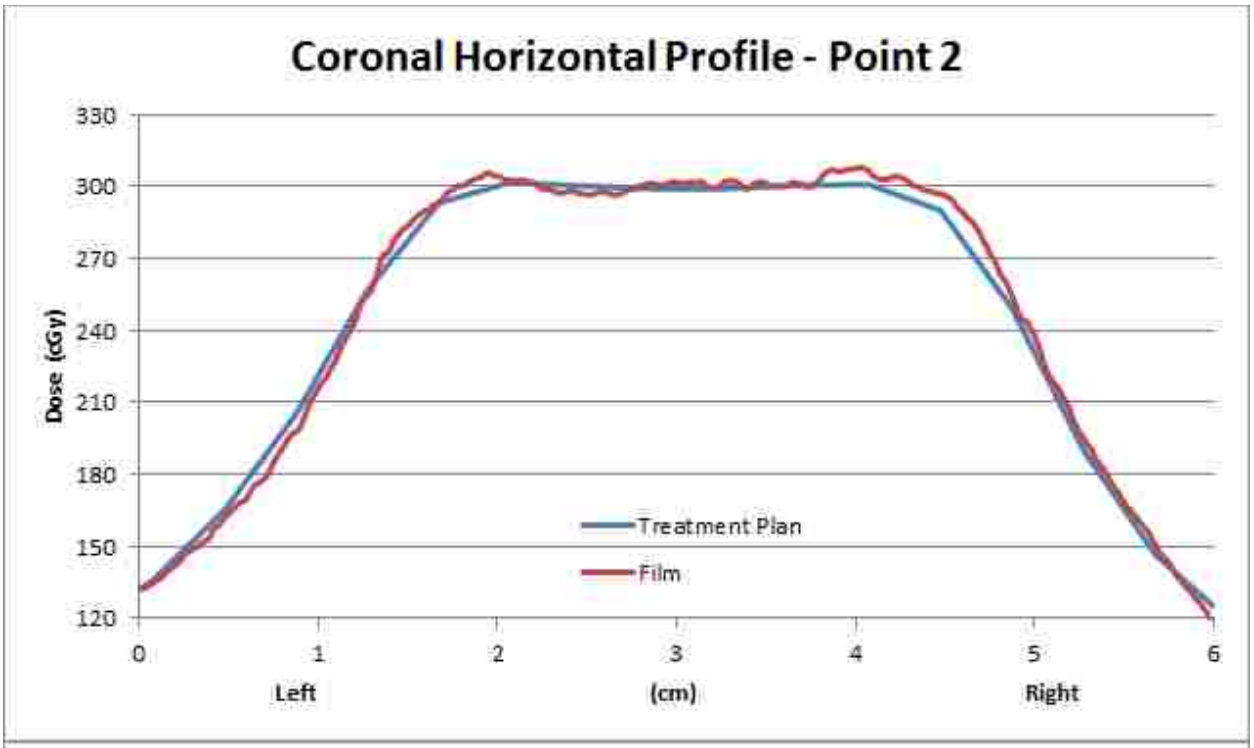

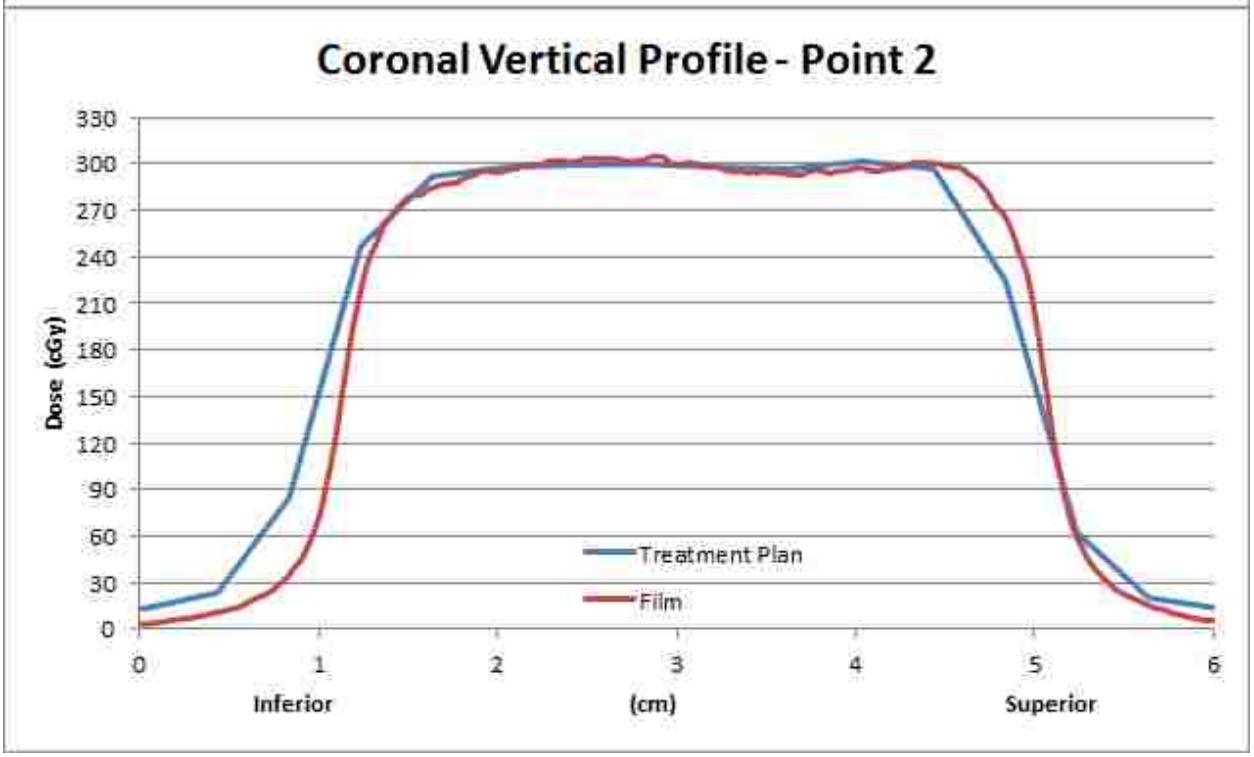

Figure A.47: Horizontal and vertical profiles for the coronal image plane resulting from MV planar image guidance when the phantom was initially positioned at sample point 2.

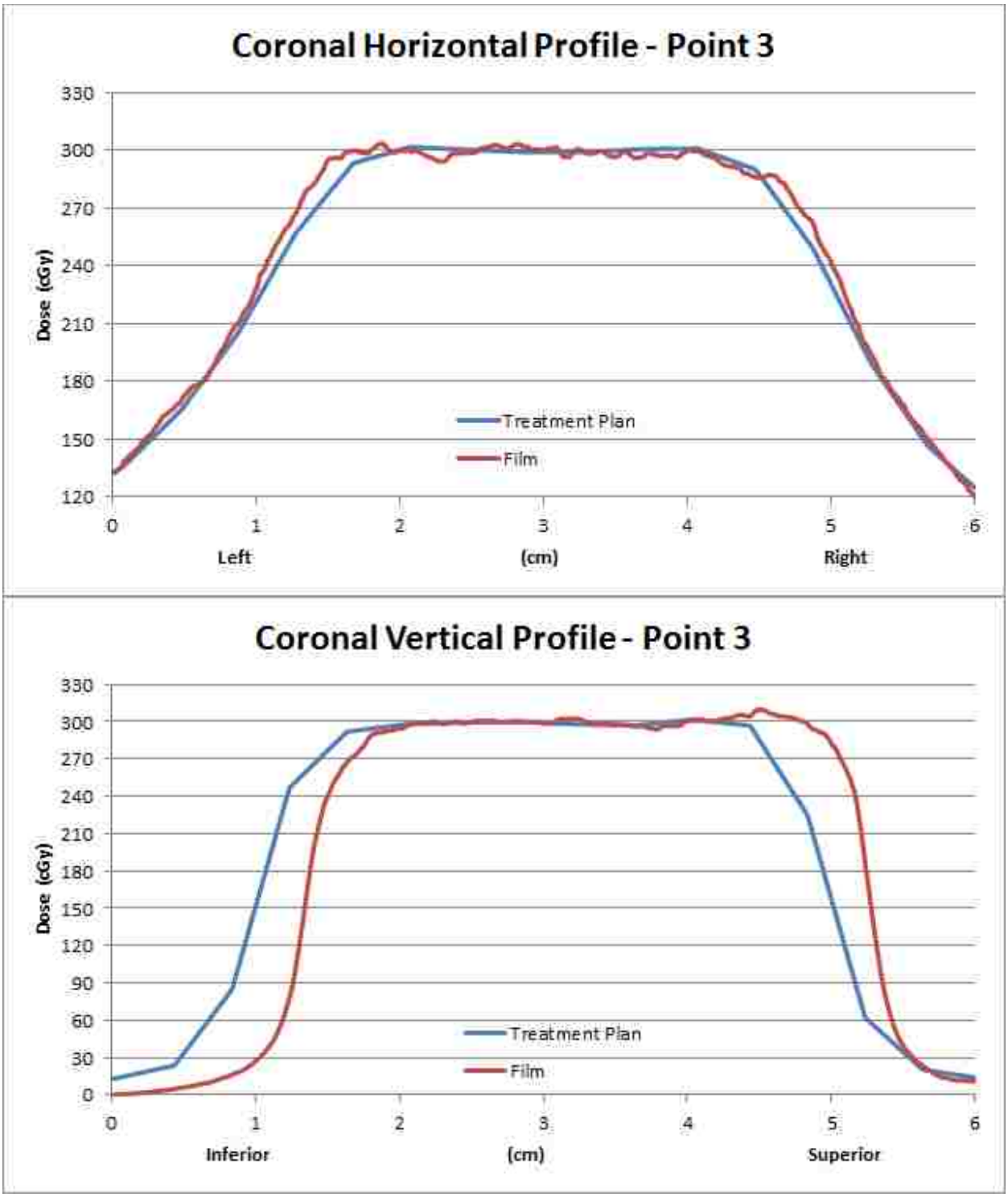

Figure A.48: Horizontal and vertical profiles for the coronal image plane resulting from MV planar image guidance when the phantom was initially positioned at sample point 3.

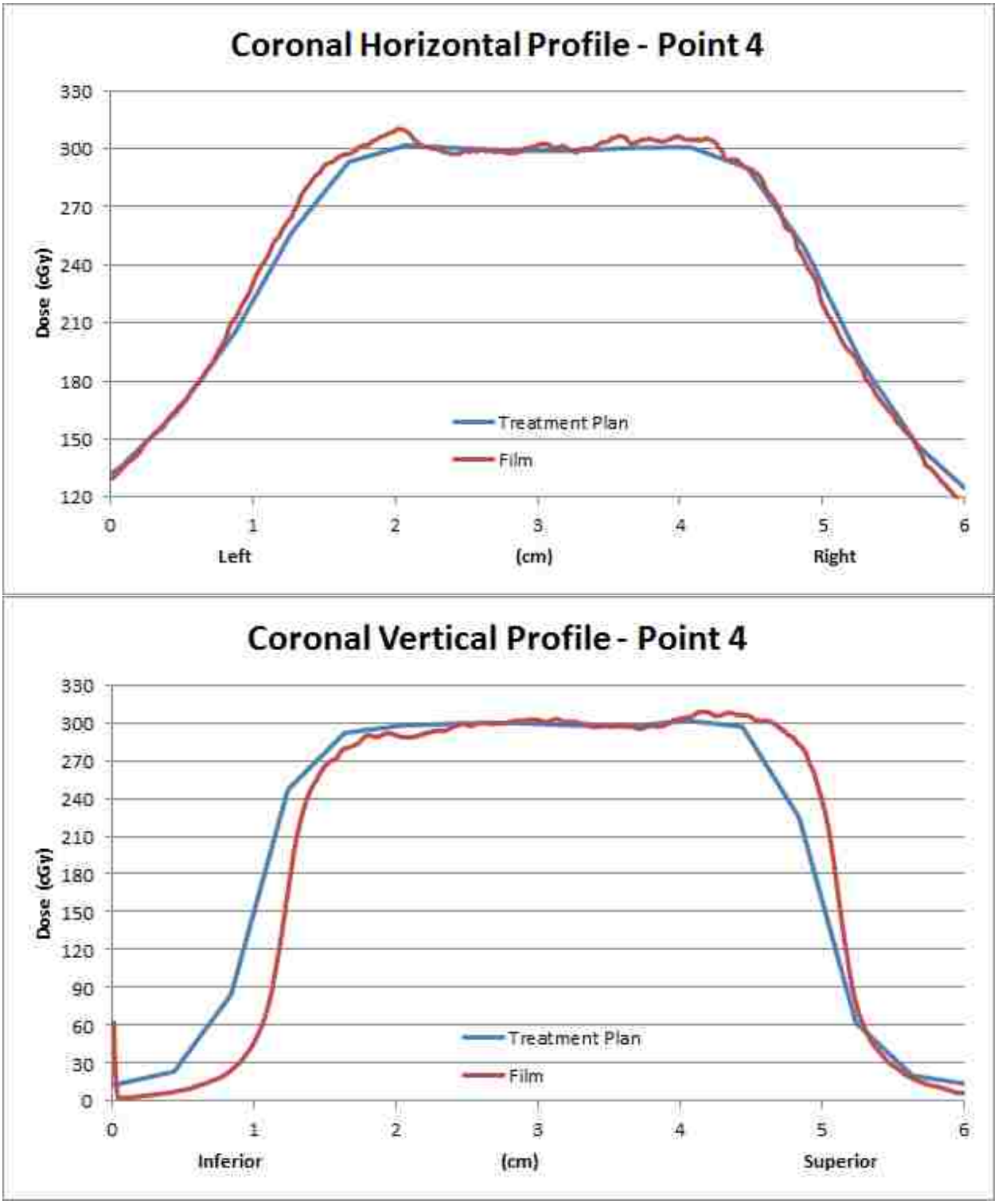

Figure A.49: Horizontal and vertical profiles for the coronal image plane resulting from MV planar image guidance when the phantom was initially positioned at sample point 4.

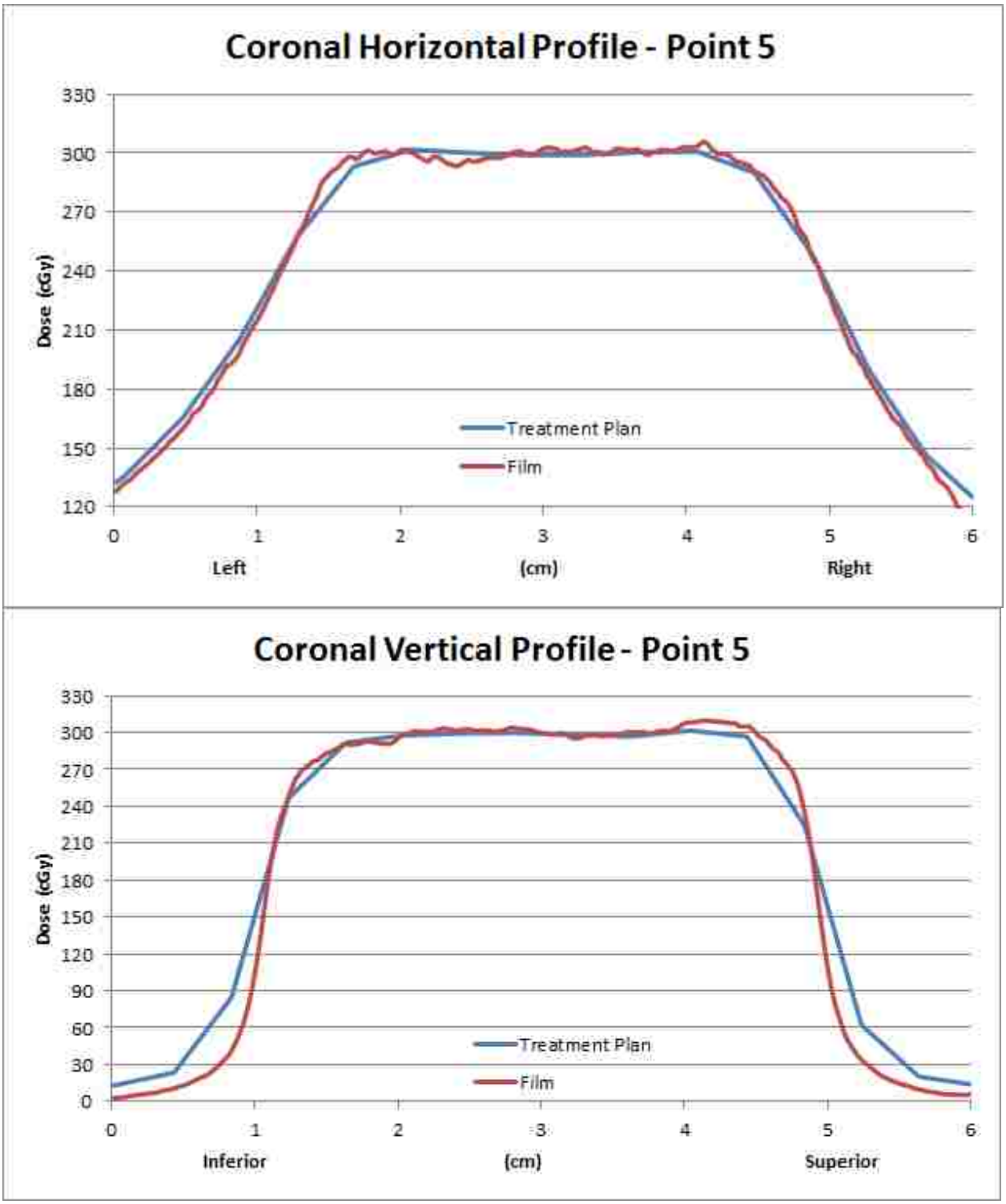

Figure A.50: Horizontal and vertical profiles for the coronal image plane resulting from MV planar image guidance when the phantom was initially positioned at sample point 5.

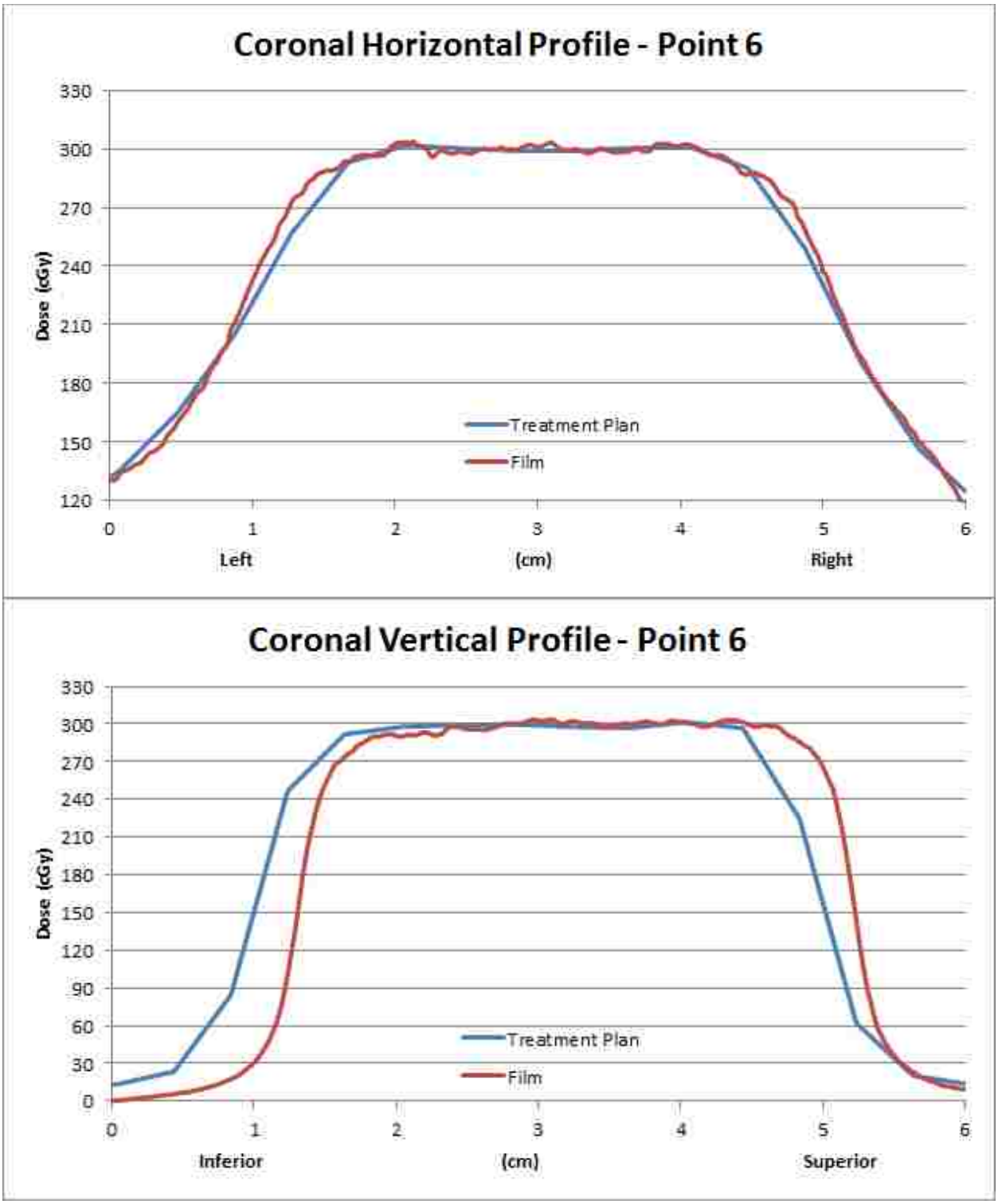

Figure A.51: Horizontal and vertical profiles for the coronal image plane resulting from MV planar image guidance when the phantom was initially positioned at sample point 6.

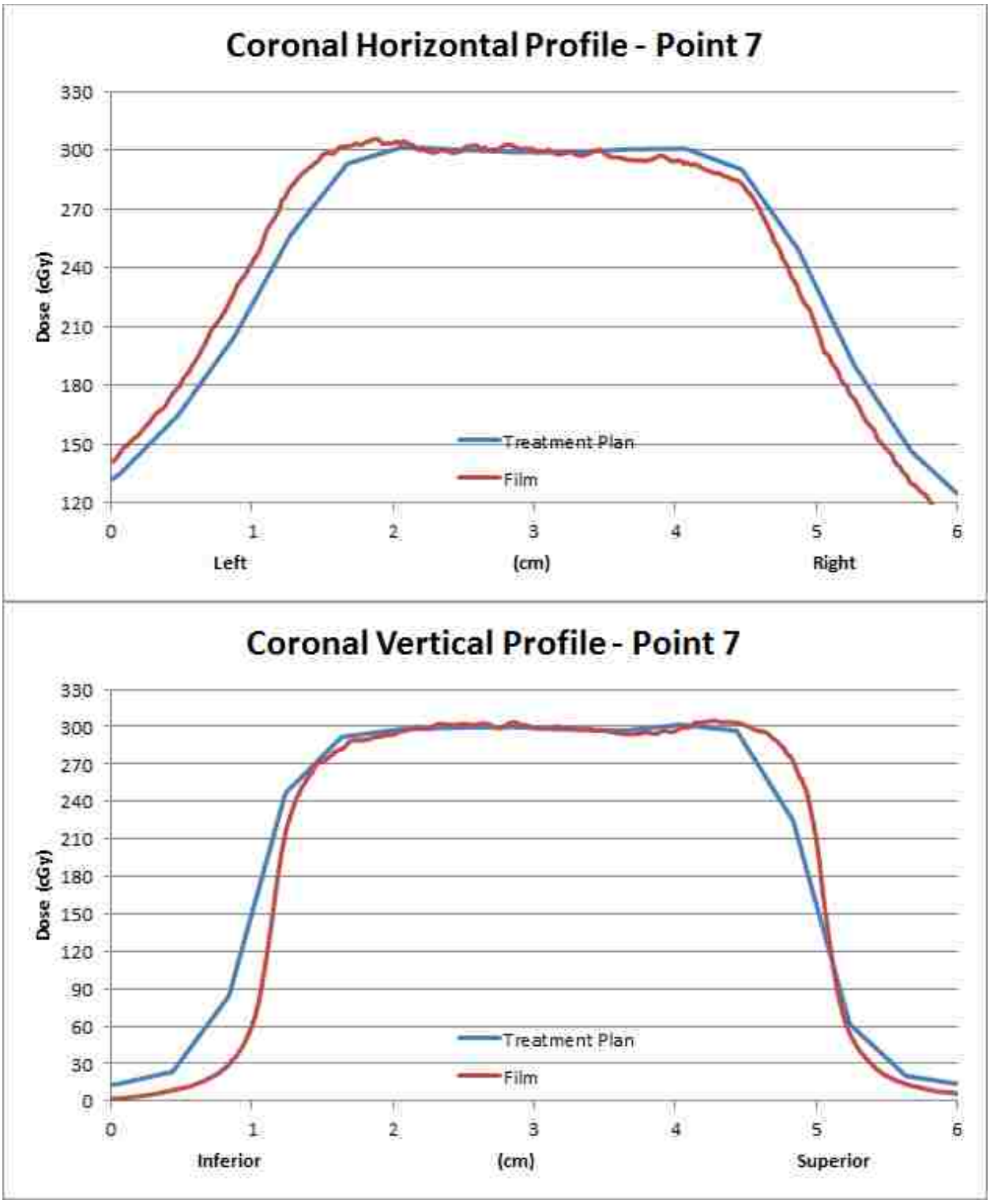

Figure A.52: Horizontal and vertical profiles for the coronal image plane resulting from MV planar image guidance when the phantom was initially positioned at sample point 7.

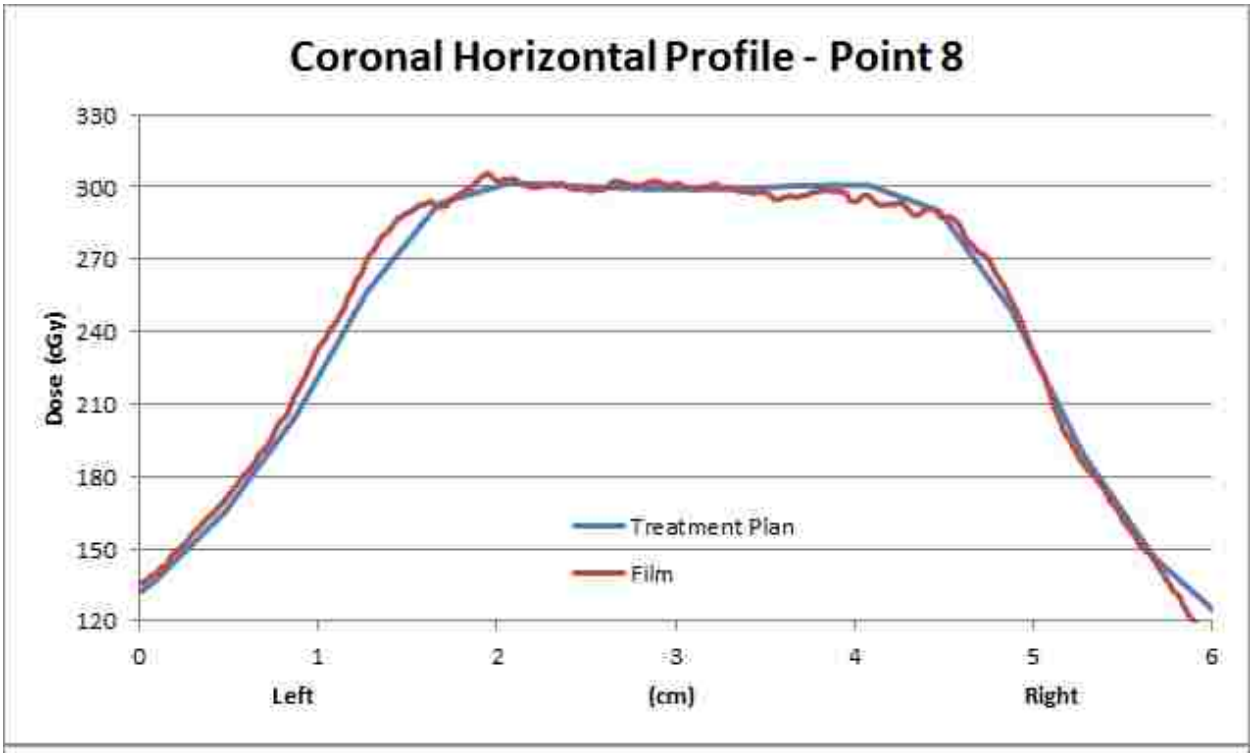

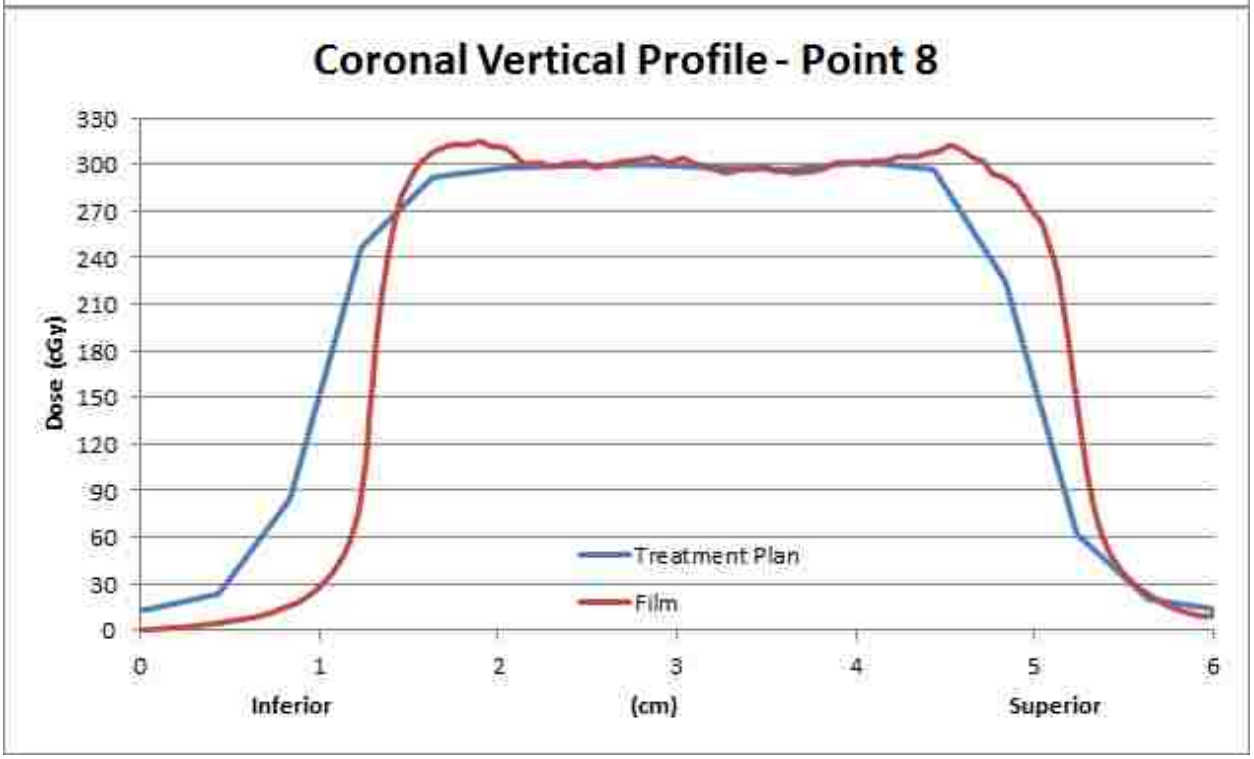

Figure A.53: Horizontal and vertical profiles for the coronal image plane resulting from MV planar image guidance when the phantom was initially positioned at sample point 8.

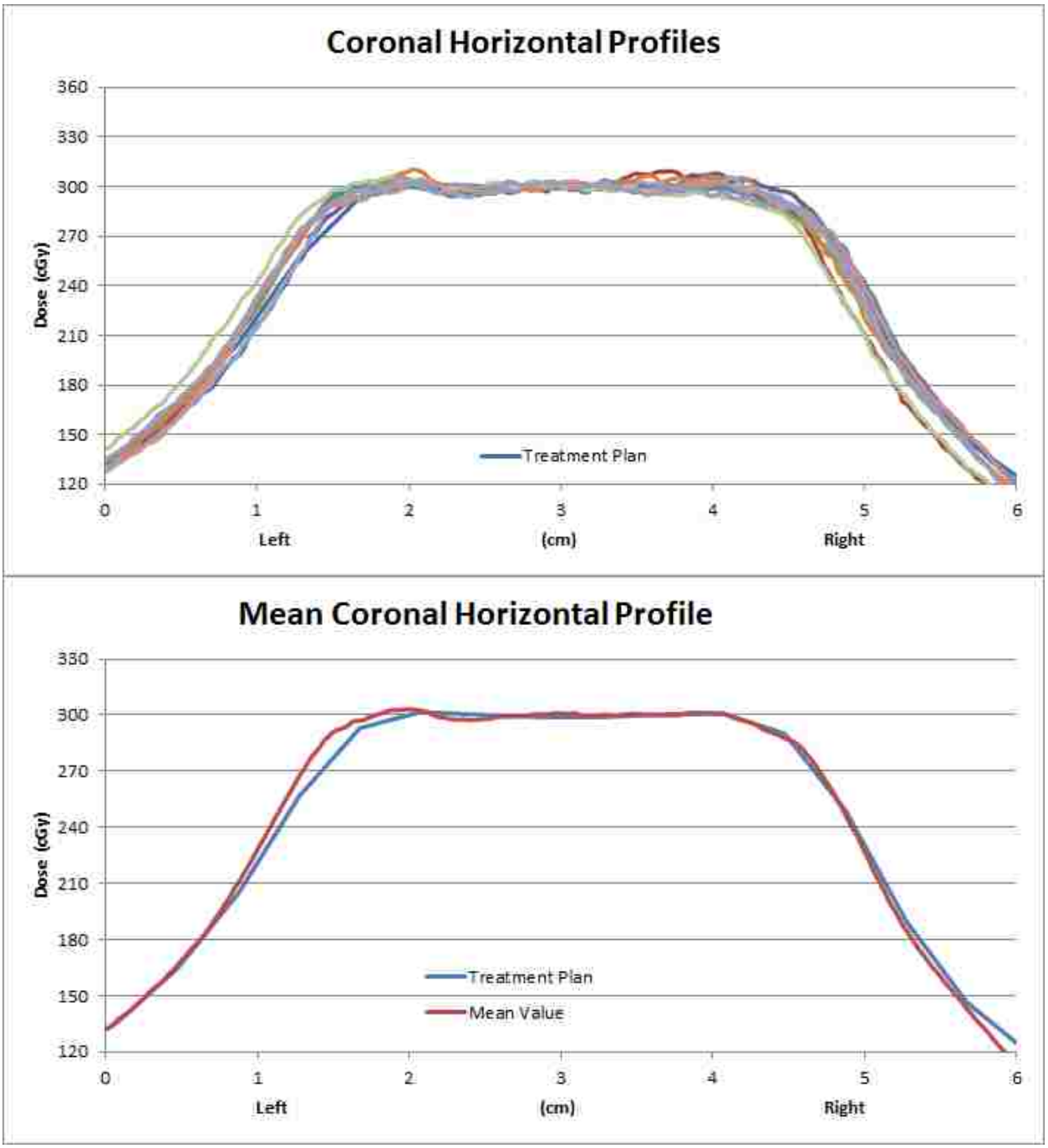

Figure A.54: (top) All horizontal profiles for the coronal image plane resulting from MV planar image guidance. (bottom) Comparison of the mean coronal horizontal profile with the profile from the treatment plan.

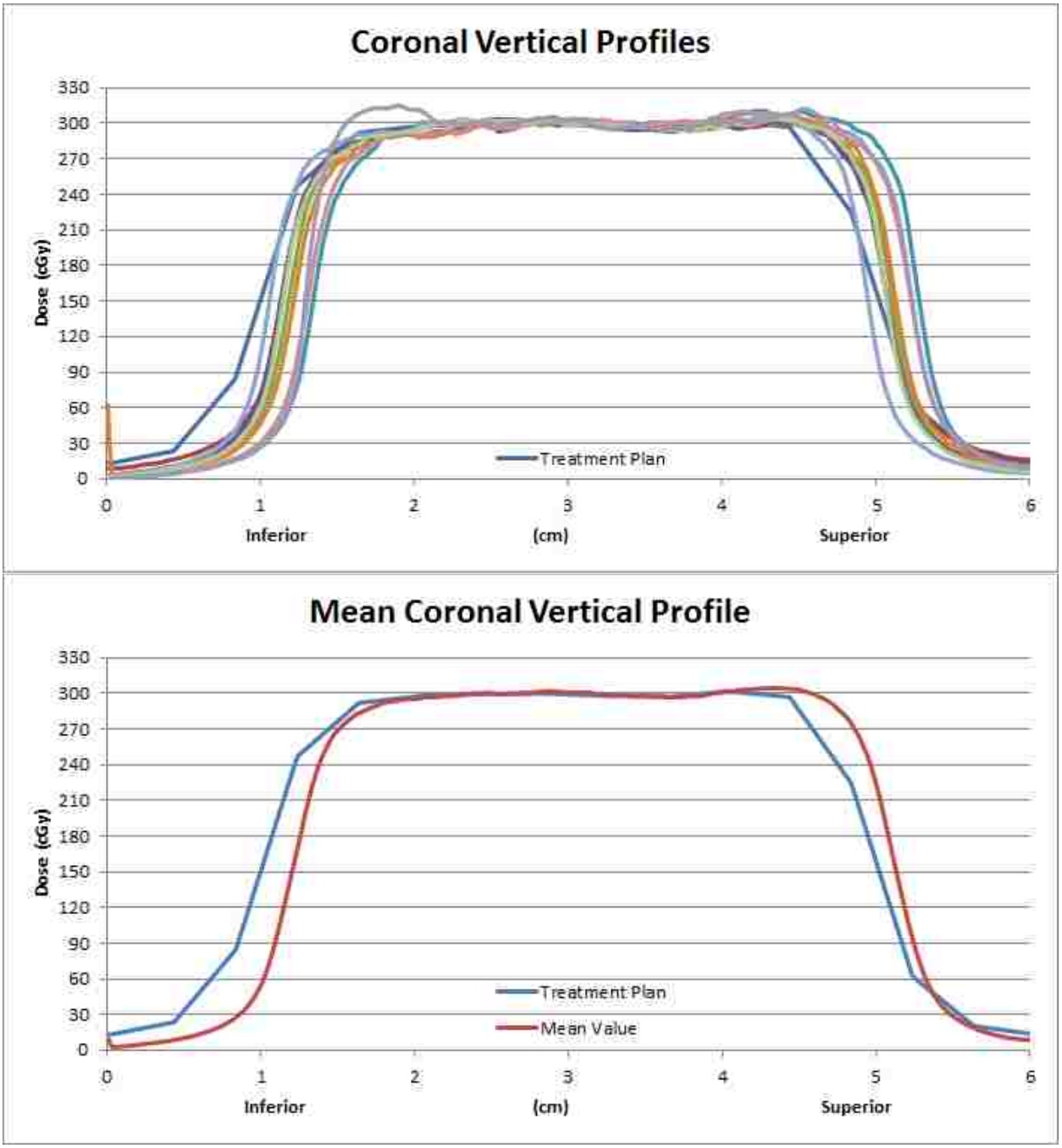

Figure A.55: (top) All vertical profiles for the coronal image plane resulting from MV planar image guidance. (bottom) Comparison of the mean coronal vertical profile with the profile from the treatment plan.

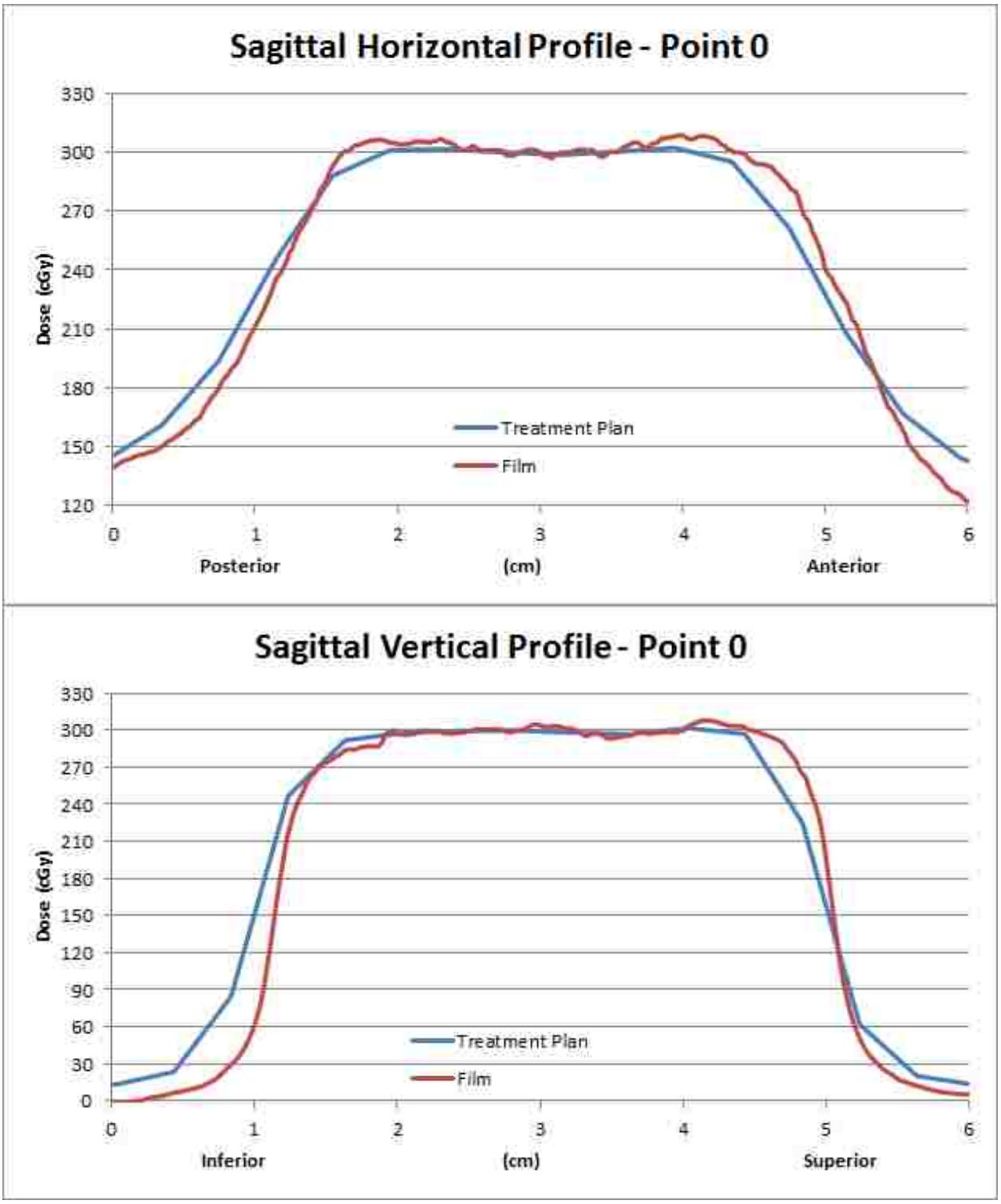

Figure A.56: Horizontal and vertical profiles for the sagittal image plane resulting from MV planar image guidance when the phantom was initially positioned at sample point 0.

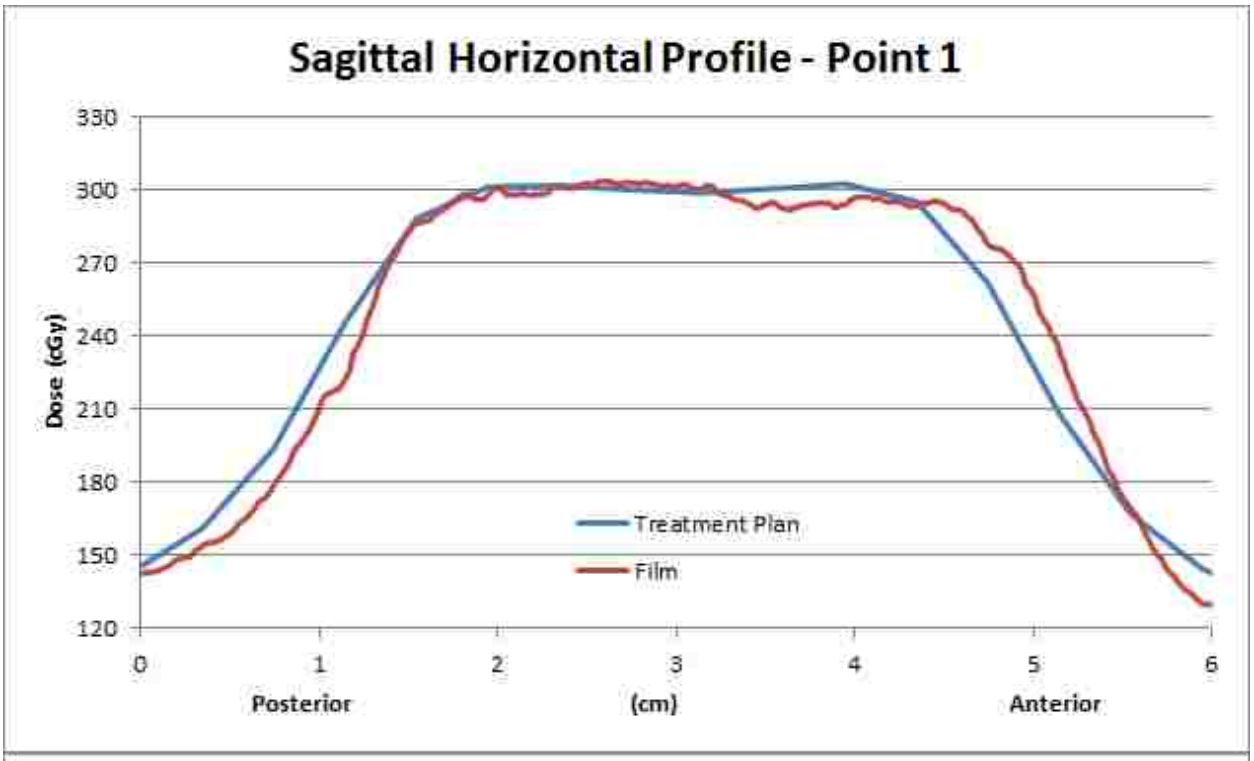

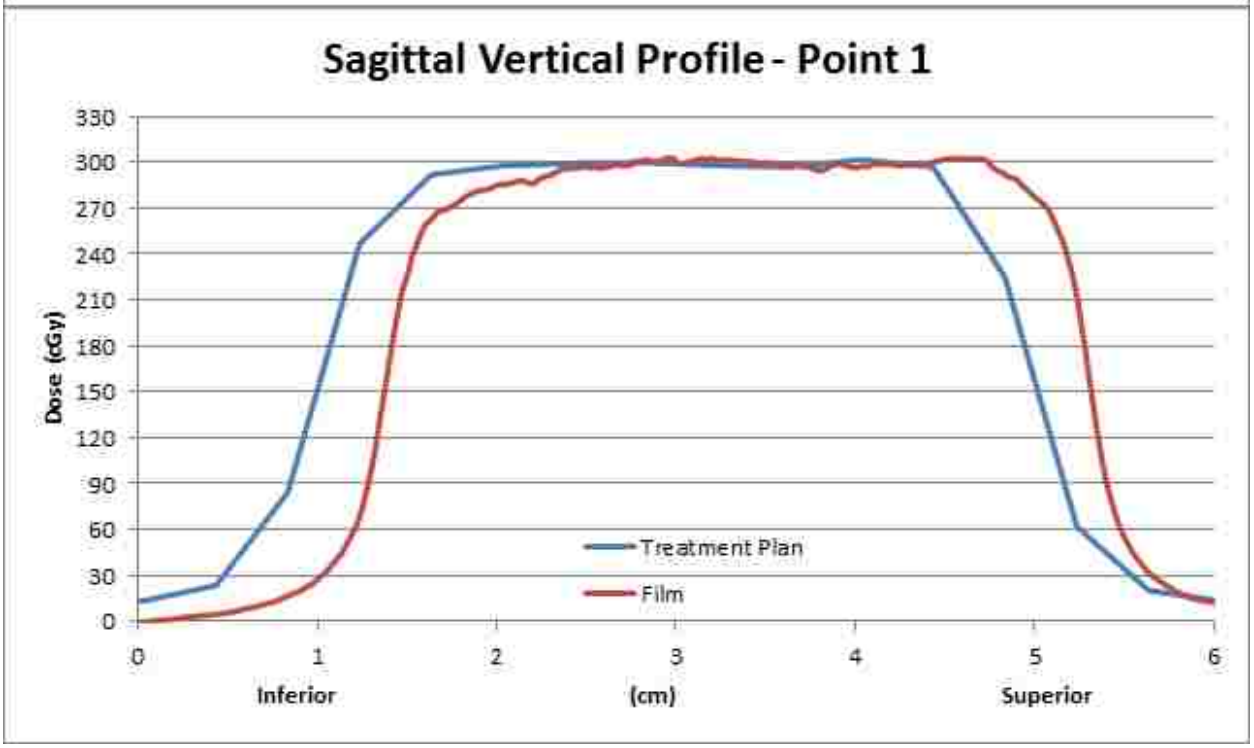

Figure A.57: Horizontal and vertical profiles for the sagittal image plane resulting from MV planar image guidance when the phantom was initially positioned at sample point 1.

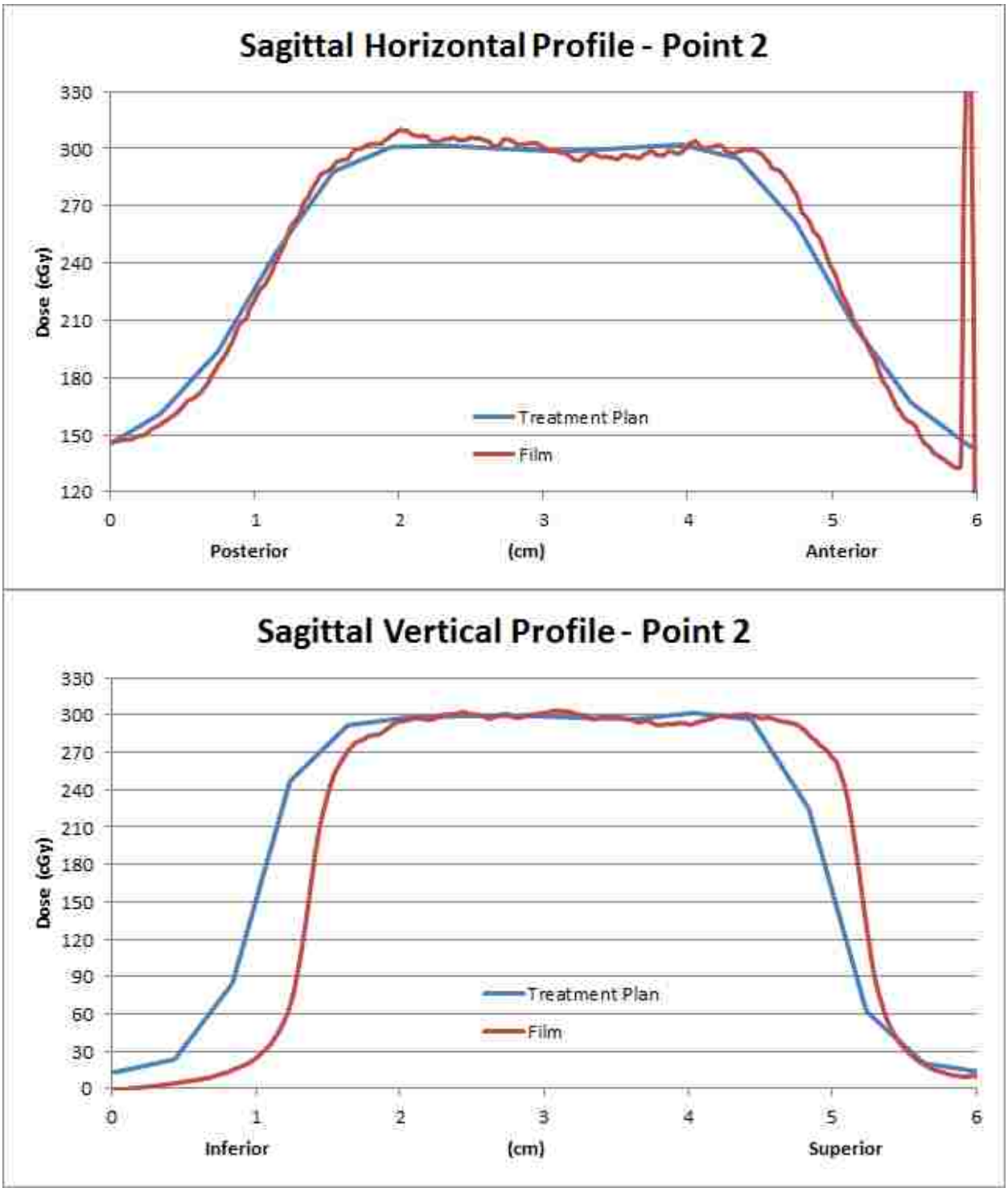

Figure A.58: Horizontal and vertical profiles for the sagittal image plane resulting from MV planar image guidance when the phantom was initially positioned at sample point 2.

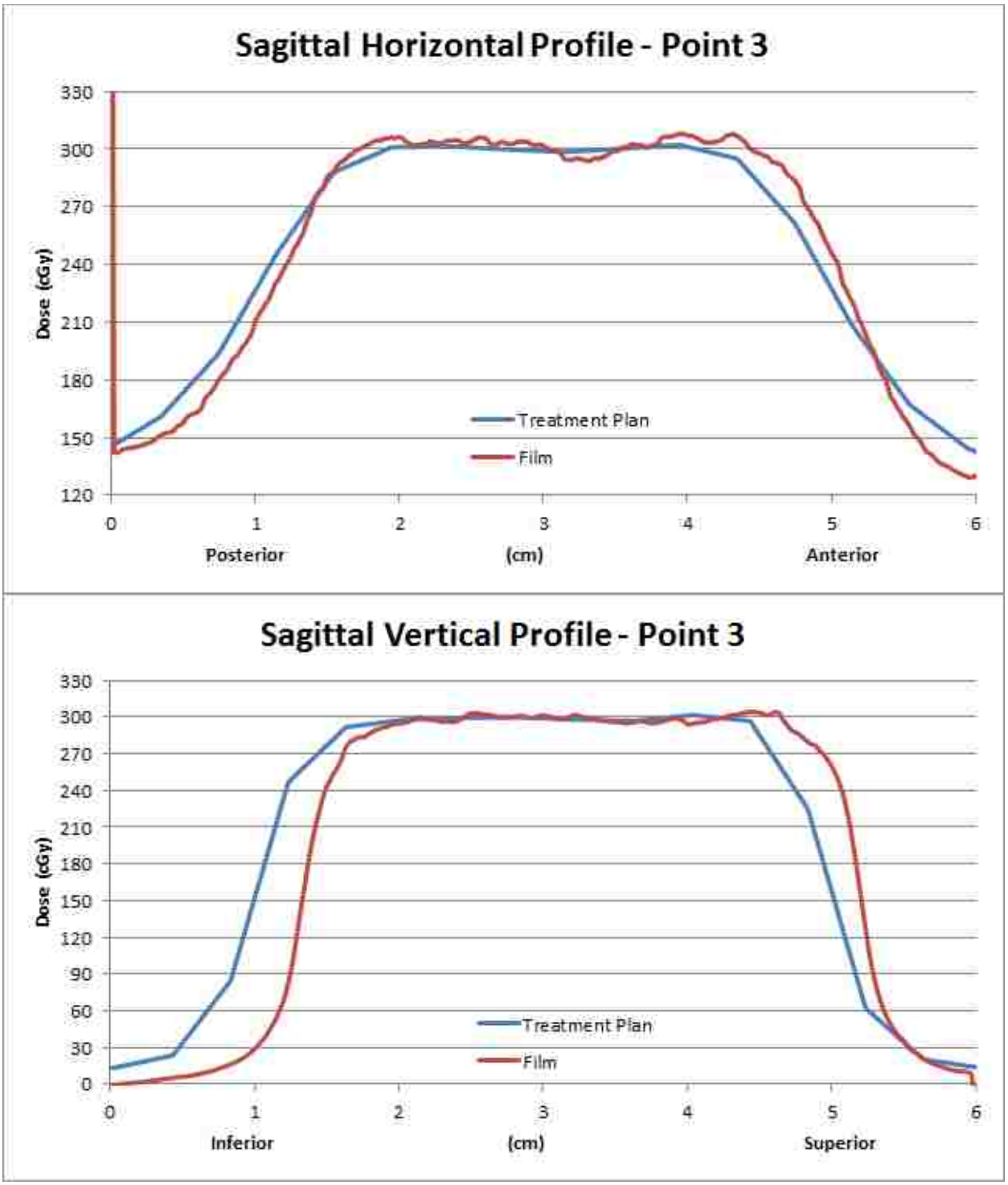

Figure A.59: Horizontal and vertical profiles for the sagittal image plane resulting from MV planar image guidance when the phantom was initially positioned at sample point 3.

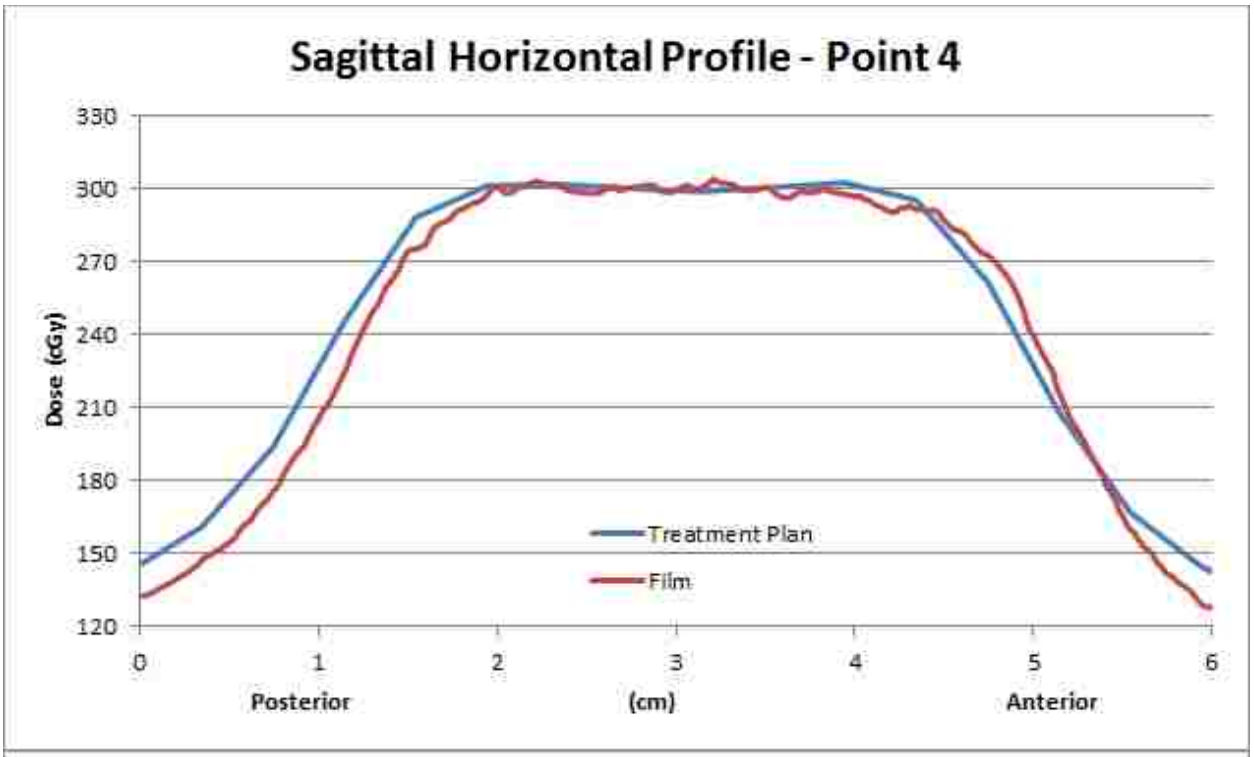

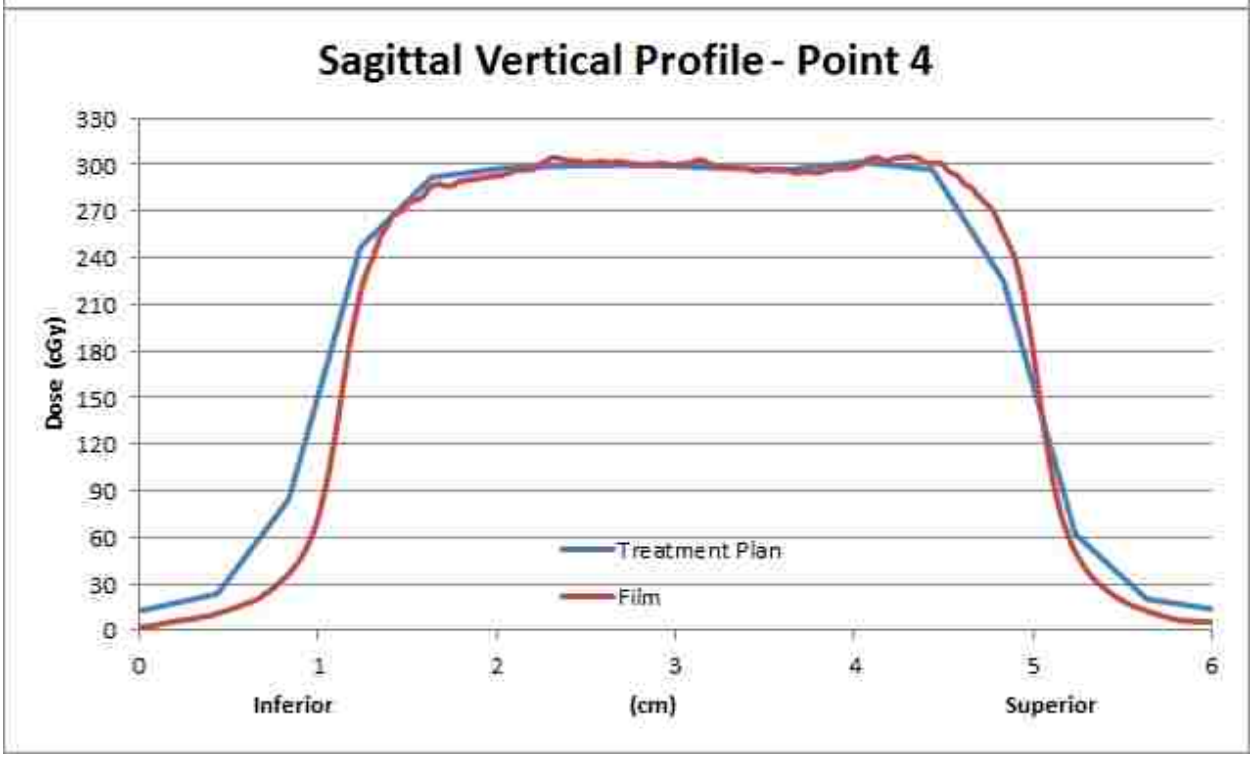

Figure A.60: Horizontal and vertical profiles for the sagittal image plane resulting from MV planar image guidance when the phantom was initially positioned at sample point 4.

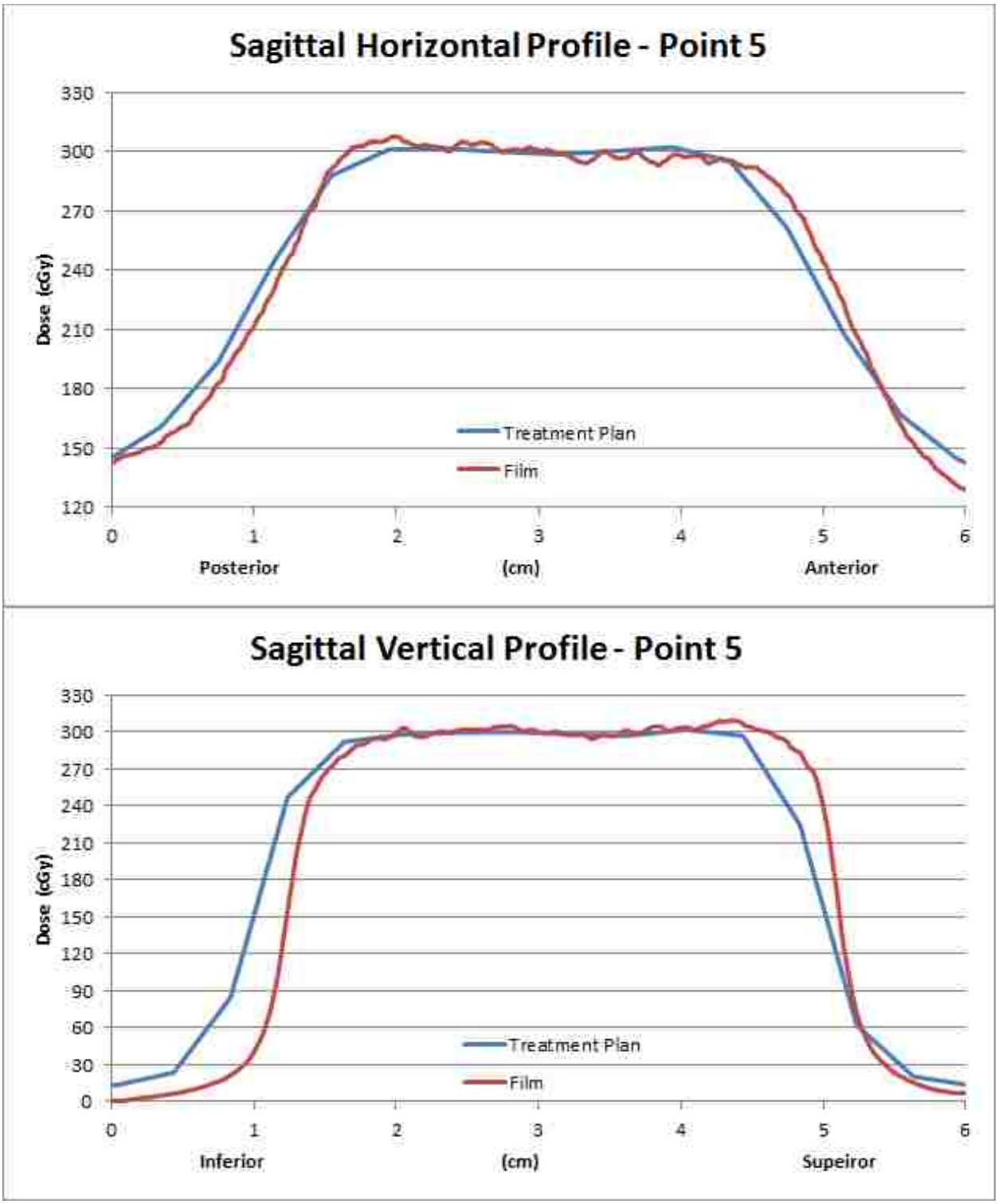

Figure A.61: Horizontal and vertical profiles for the sagittal image plane resulting from MV planar image guidance when the phantom was initially positioned at sample point 5.

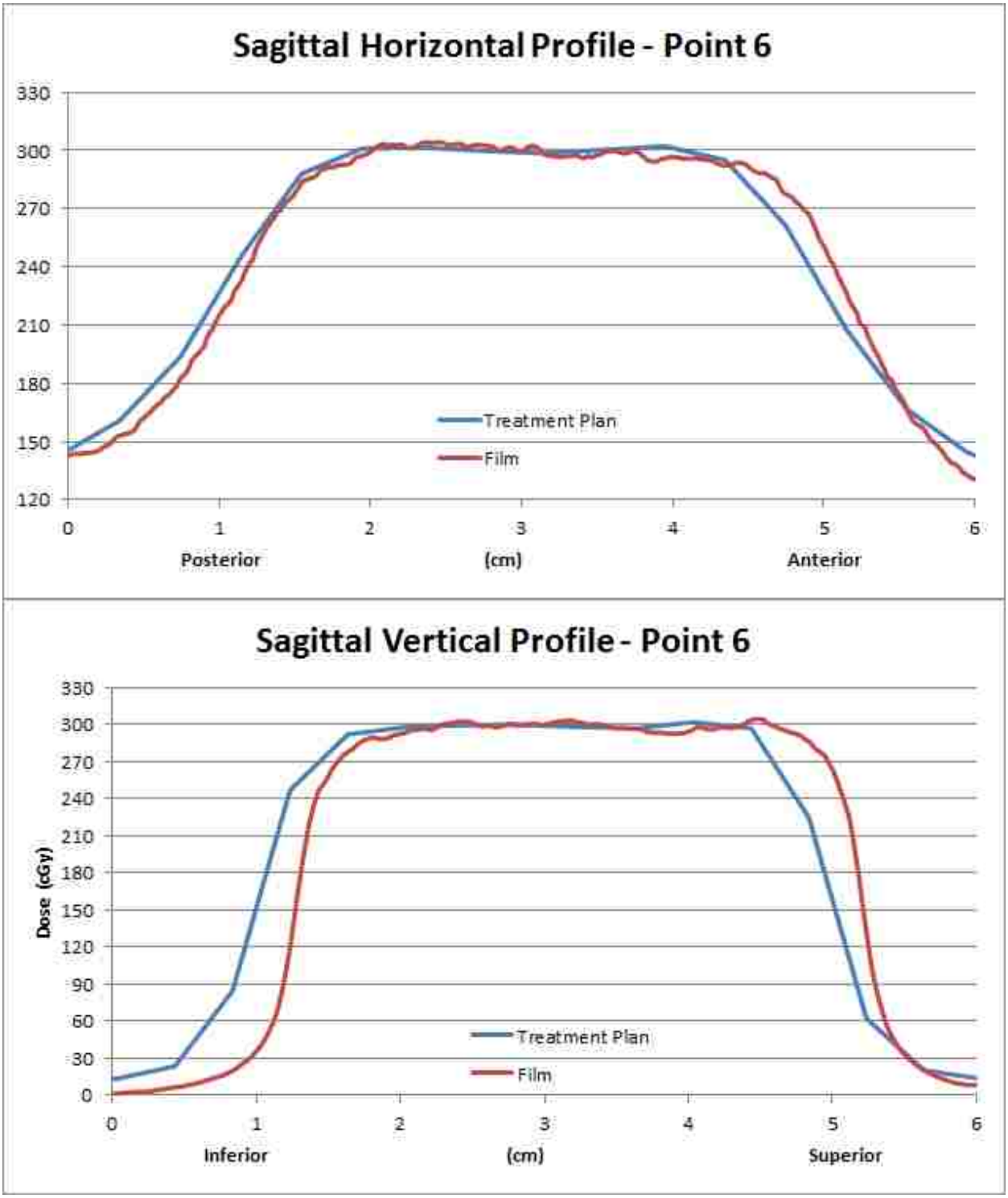

Figure A.62: Horizontal and vertical profiles for the sagittal image plane resulting from MV planar image guidance when the phantom was initially positioned at sample point 6.

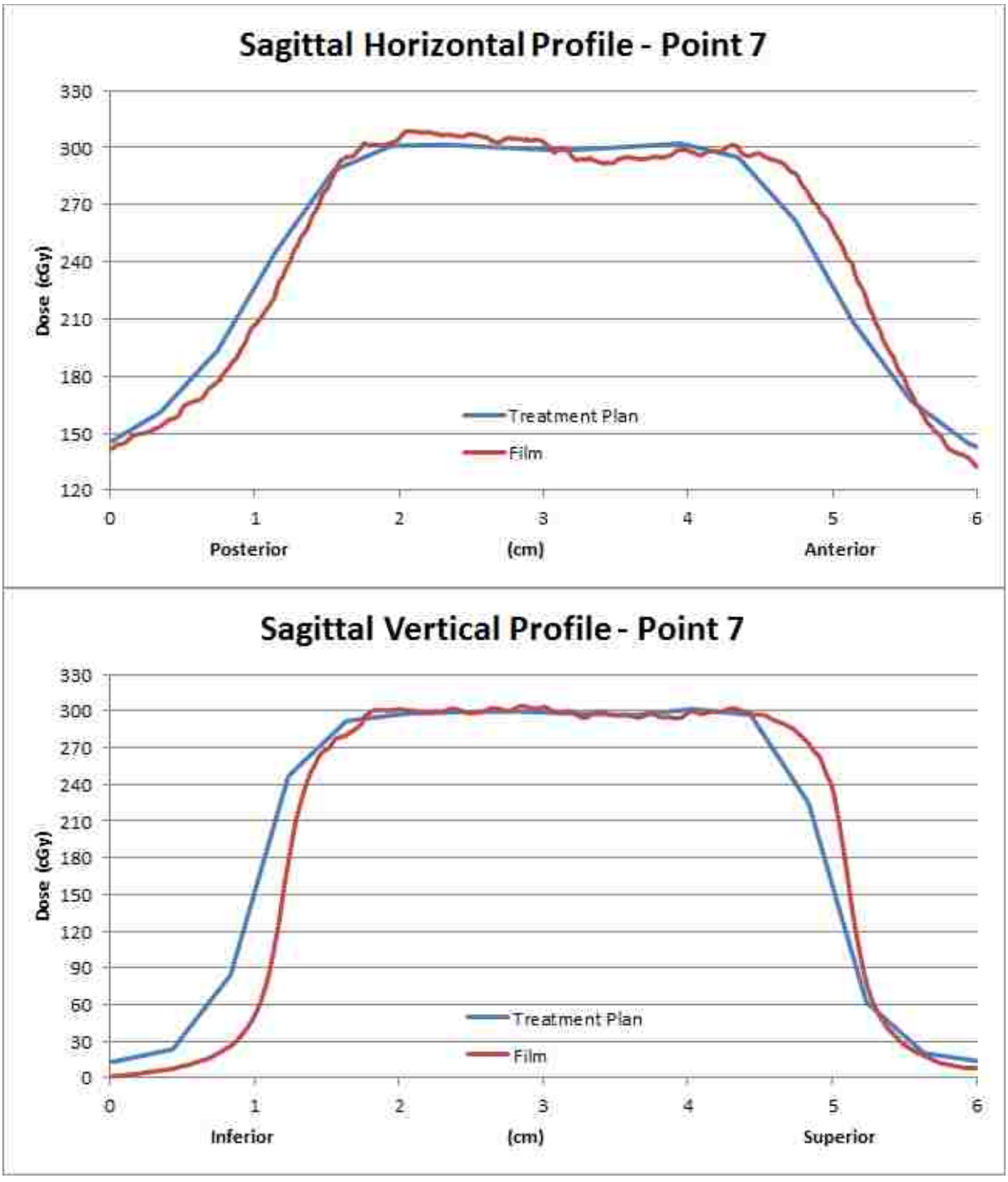

Figure A.63 Horizontal and vertical profiles for the sagittal image plane resulting from MV planar image guidance when the phantom was initially positioned at sample point 7.

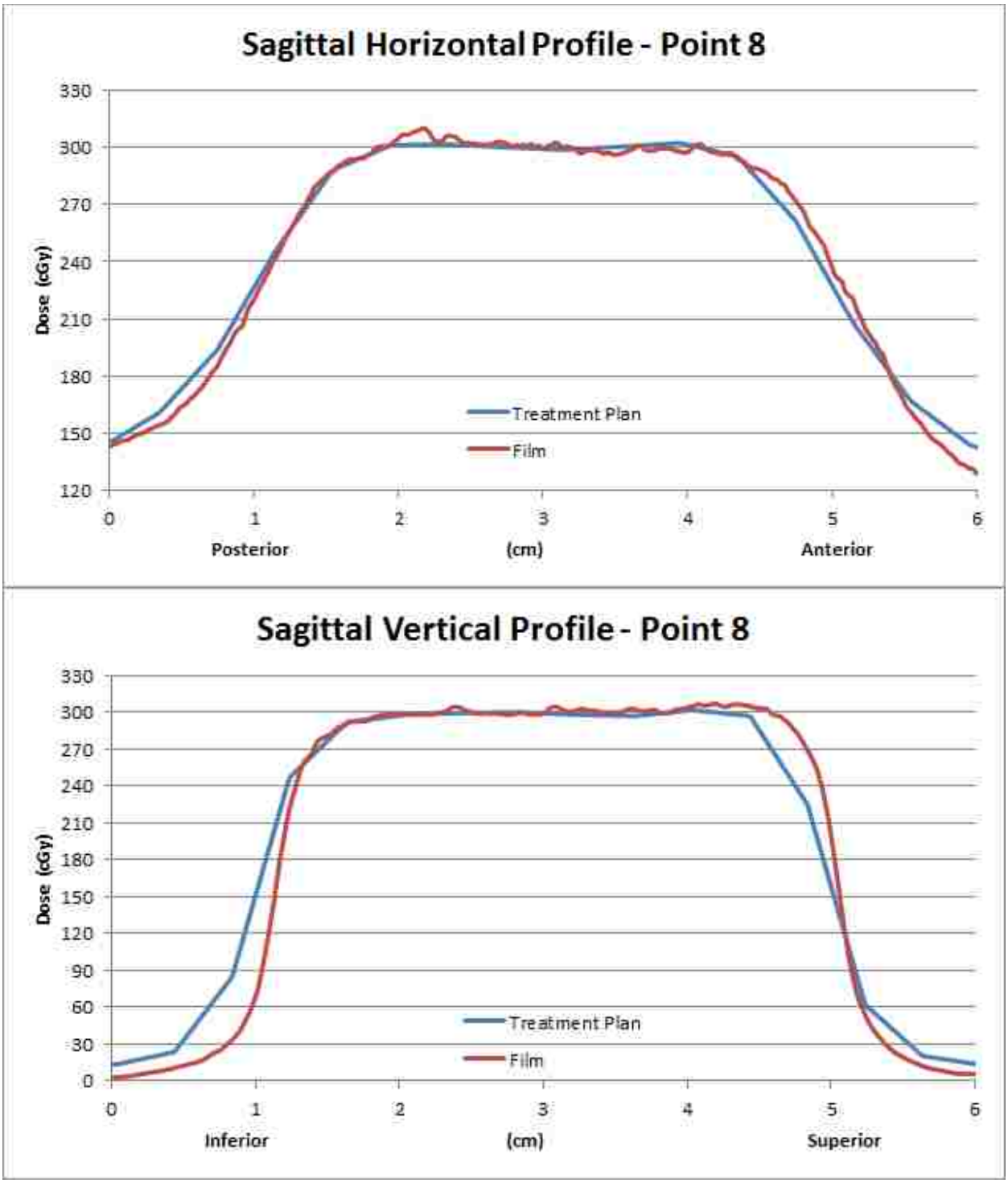

Figure A.64: Horizontal and vertical profiles for the sagittal image plane resulting from MV planar image guidance when the phantom was initially positioned at sample point 8.

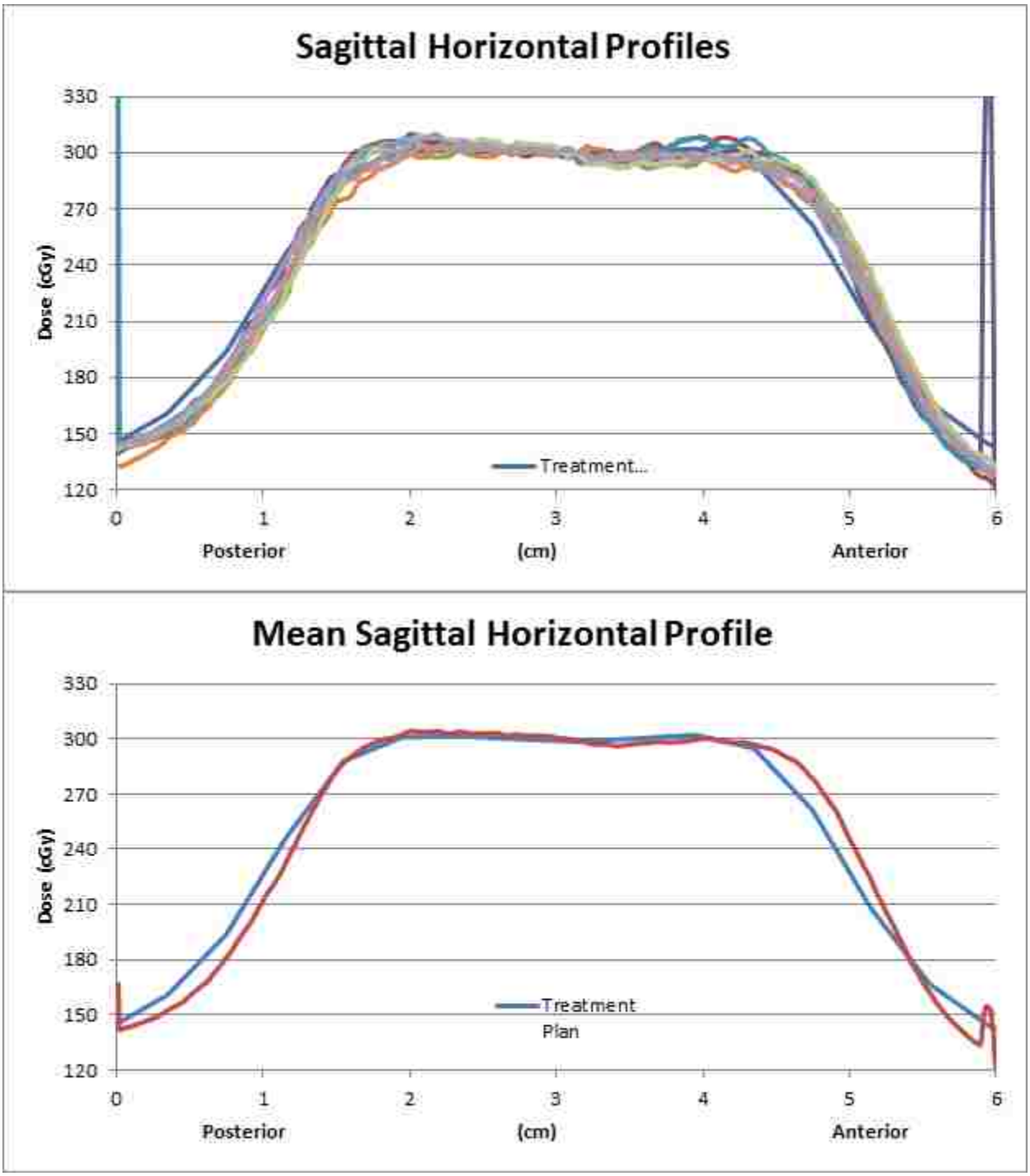

Figure A.65: (top) All horizontal profiles for the sagittal image plane resulting from MV planar image guidance. (bottom) Comparison of the mean sagittal horizontal profile with the profile from the treatment plan.

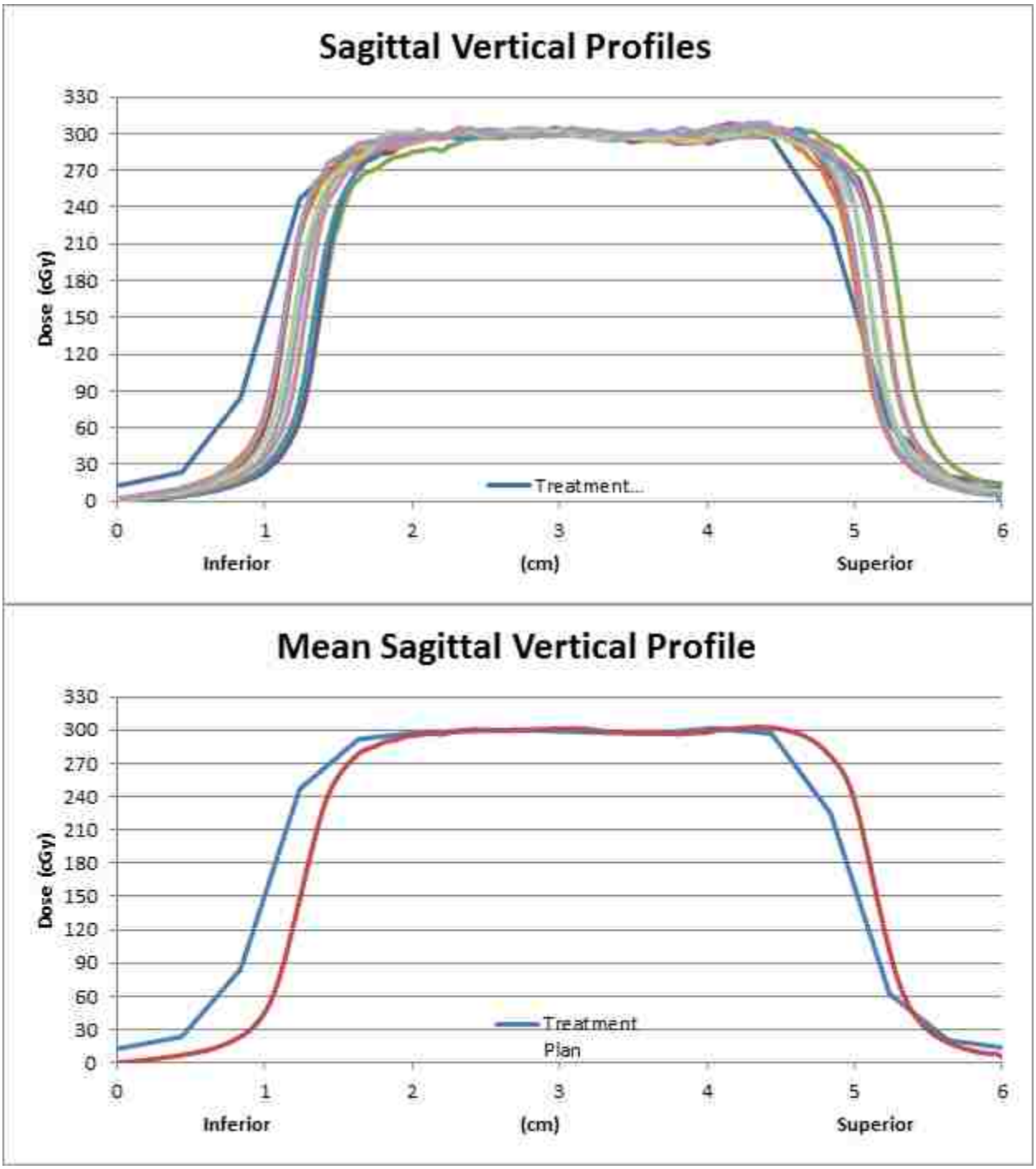

Figure A.66: (top) All vertical profiles for the sagittal image plane resulting from MV planar image guidance. (bottom) Comparison of the mean sagittal vertical profile with the profile from the treatment plan.

Table A.4: Data acquired from the first couch backlash test (3 cm intervals). Values in red indicate a discrepancy between the physical displacement and digital readout.

	LONGITUDINAL		LATERAL		VERTICAL	
Ruler (cm)	Digital (cm)	Difference (cm)	Digital (cm)	Difference (cm)	Digital (cm)	Difference (cm)
0	13.9		-22.4		17.1	
3	17.0	**3.1**	-19.4	3	14.1	3
6	20.0	3	-16.5	**2.9**	11.1	3
9	23.0	3	-13.4	**3.1**	8.1	3
12	26.0	3	-10.5	**2.9**	5.1	3
15	29.0	3	-7.5	3	2.1	3
18	32.0	3	-4.4	**3.1**	-0.9	3
21	35.0	3	-1.5	**2.9**	-4.0	**3.1**
24	38.0	3	1.5	3	-6.9	**2.9**
27	41.1	**3.1**	4.5	3	-9.9	3
30	44.1	3	7.5	3	-13.0	**3.1**
33	47.1	3	10.5	3	-16.0	3
36	50.1	3	13.5	3	-18.9	**2.9**
39	53.1	3	16.5	3	-21.9	3
42	56.1	3	19.5	3	-24.9	3
45	59.1	3	22.5	3	-27.9	3
Moving Reverse						
42	56.1	3	19.5	3	-24.9	3
39	53.1	3	16.5	3	-21.9	3
36	50.1	3	13.5	3	-19.0	**2.9**
33	47.1	3	10.5	3	-16.0	3
30	44.1	3	7.5	3	-13.0	3
27	41.1	3	4.5	3	-10.0	3
24	38.0	**3.1**	1.5	3	-6.9	**3.1**
21	35.0	3	-1.5	3	-4.0	**2.9**
18	32.0	3	-4.5	3	-1.0	3
15	29.0	3	-7.5	3	2.0	3
12	26.0	3	-10.5	3	5.1	**3.1**
9	23.0	3	-13.4	**2.9**	8.0	**2.9**
6	20.0	3	-16.5	**3.1**	11.0	3
3	17.0	3	-19.4	**2.9**	14.0	3
0	13.9	**3.1**	-22.4	3	17.1	**3.1**

Table A.5: Data acquired from the second couch backlash test (5 cm forward; 3 cm backward intervals). Values in red indicate a discrepancy between the physical displacement and digital readout.

	LONGITUDINAL		LATERAL		VERTICAL	
Ruler (cm)	Digital (cm)	Difference (cm)	Digital (cm)	Difference (cm)	Digital (cm)	Difference (cm)
0	90.1	-	-25.4	-	49.2	-
5	85.1	5	-20.5	**4.9**	44.1	**5.1**
2	88.1	3	-23.5	3	47.1	3
7	83.1	5	-18.5	5	42.1	5
4	86.1	3	-21.5	3	45.1	3
9	81.1	5	-16.5	5	40.1	5
6	84.1	3	-19.5	3	43.1	3
11	79.1	5	-14.5	5	38.1	5
8	82.1	3	-17.5	3	41.1	3
13	77.1	5	-12.5	5	36.1	5
10	80.1	3	-15.5	3	39.1	3
15	75.0	**5.1**	-10.5	5	34.1	5
12	78.0	3	-13.5	3	37.1	3
17	73.0	5	-8.5	5	32.2	**4.9**
14	76.1	**3.1**	-11.5	3	35.1	**2.9**
19	71.0	**5.1**	-6.5	5	30.1	5
16	74.0	3	-9.5	3	33.1	3
21	69.0	5	-4.5	5	28.1	5
18	72.0	3	-7.5	3	31.1	3
23	67.0	5	-2.5	5	26.1	5
20	70.0	3	-5.5	3	29.1	3
25	65.0	5	-0.5	5	24.1	5
22	68.0	3	-3.5	3	27.1	3
27	63.0	5	1.5	5	22.1	5
24	65.9	**2.9**	-1.5	3	25.1	3
29	60.9	5	3.5	5	20.1	5
26	64.0	**3.1**	0.5	3	23.1	3
31	59.0	5	5.5	5	18.1	5
28	62.0	3	2.5	3	21.1	3
33	57.0	5	7.5	5	16.1	5
30	60.0	3	4.5	3	19.1	3
35	55.0	5	9.5	5	14.1	5
32	57.9	**2.9**	6.5	3	17.1	3
37	52.9	5	11.5	5	12.1	5

34	56.0	**3.1**	8.5	3	15.1	3
39	50.9	**5.1**	13.5	5	10.1	5
36	53.9	3	10.5	3	13.1	3
41	48.0	**5.9**	15.5	5	8.1	5
38	51.9	**3.9**	12.5	3	11.1	3
43	46.9	5	17.4	**4.9**	6.1	5
40	49.9	3	14.5	**2.9**	9.1	3
45	44.9	5	19.5	5	4.2	**4.9**
42	47.9	3	16.4	**3.1**	7.1	**2.9**
47	42.9	5	21.4	5	2.1	5
44	45.8	**2.9**	18.5	**2.9**	5.1	3
49	40.9	**4.9**	23.5	5	0.1	5
46	43.9	3	20.5	3	3.1	3
51	38.8	**5.1**	25.4	**4.9**	-1.9	5
48	41.8	3	22.4	3	1.1	3
53	36.9	**4.9**	-	-	-3.9	5
50	39.9	3	-	-	-0.9	3
55	34.8	**5.1**	-	-	-5.9	5
52	37.8	3	-	-	-2.9	3
57	32.8	5	-	-	-7.9	5
54	35.8	3	-	-	-5.0	**2.9**
59	30.8	5	-	-	-9.9	**4.9**
56	33.8	3	-	-	-6.9	3
61	28.8	5	-	-	-11.9	5
58	31.8	3	-	-	-8.9	3
63	26.8	5	-	-	-13.9	5
60	29.8	3	-	-	-10.9	3
65	24.8	5	-	-	-15.9	5
62	27.8	3	-	-	-12.9	3
67	22.8	5	-	-	-17.9	5
64	25.8	3	-	-	-14.9	3
69	20.8	5	-	-	-19.9	5
66	23.8	3	-	-	-17.0	**2.9**
71	18.8	5	-	-	-21.9	**4.9**
68	21.7	**2.9**	-	-	-19.9	2
73	16.8	**4.9**	-	-	-23.9	4
70	19.8	3	-	-	-20.9	3
75	14.7	**5.1**	-	-	-26.0	**5.1**
72	17.7	3	-	-	-22.9	**3.1**
77	12.7	5	-	-	-27.9	5
74	15.7	3	-	-	-25.0	**2.9**

79	10.7	5		-	-		-29.9	**4.9**
76	13.7	3		-	-		-27.0	**2.9**
81	8.7	5		-	-		-32.0	5
78	11.7	3		-	-		-29.0	3
83	6.7	5		-	-		-33.9	**4.9**
80	9.7	3		-	-		-31.0	**2.9**
85	4.7	5		-	-		-35.9	**4.9**
82	7.7	3		-	-		-33.0	**2.9**
87	2.6	**5.1**		-	-		-37.9	**4.9**
84	5.7	**3.1**		-	-		-35.0	**2.9**
89	0.7	5		-	-		-39.9	**4.9**
86	3.7	3		-	-		-37.0	**2.9**
91	-	-		-	-		-41.9	**4.9**
88	-	-		-	-		-39.0	**2.9**

VITA

Matthew Sutton was born in Edison, New Jersey, on October 19, 1985, son of Michael Sutton and Nancy Kenney. Matt developed an appreciation for physics beginning in high school. After graduating from Neshaminy High School in 2004, he attended the Pennsylvania State University for four years where he majored in physics and minored in mathematics and bioengineering. It was during this time he developed an interest in how physics can be used in the medical profession. During his time at Penn State, he paid his way through college by working for Anheuser-Busch Entertainment Corporation. After graduating from Penn State, he was admitted into Louisiana State University's Master of Science program in medical physics and health physics. To further his knowledge of clinical medical physics, he has been accepted for a medical physics residency with Vassar Brothers – Health Quest in Poughkeepsie, NY.